Prediction of the Thermal Conductivity of Porous Foods

A thesis submitted in partial fulfilment
of the requirements for the degree of
Doctor of Philosophy in Food Engineering

Palmerston North, New Zealand

2002

James K. Carson

Abstract

A review of the food engineering literature exposed a paucity of information in the area of effective thermal conductivity prediction for porous foods. No useful guidelines were found that could advise a food engineer on the selection of appropriate effective thermal conductivity models for this application. The aims of this study were to increase the understanding in this area and to produce a general procedure for effective thermal conductivity prediction.

The specific focus of this study was the influence of porosity on thermal conduction and so the porous foods under consideration were assumed to contain small (<5mm), uniformly distributed void spaces filled with stagnant gas (either air or carbon dioxide), in order that convection and radiation effects could be neglected. It was also assumed that only bound water was present within foods so that moisture migration and its associated heat effects would not be an issue. Two basic classes of porous foods were identified: foods in which void spaces existed in the interstices of particulate foods were referred to as having "external porosity" and foods in which bubbles existed within a solid or liquid matrix were referred to as having "internal porosity".

Using a comparative method, thermal conductivity measurements were performed on food analogues comprised of expanded polystyrene (EPS) beads suspended in guar gel. Thermal conductivity data were produced that revealed a basic dependence of the relative effective thermal conductivity (k_e/k_1) on the porosity (v_2). The mean volume of the individual EPS beads used to simulate the air bubbles was varied between 10^{-6} and $4\text{x}10^{-3}$ of the total sample volume, but no significant dependence of k_e/k_1 on bead diameter was observed. Thermal conductivity measurements were also performed on samples containing squat aluminium cylinders suspended in guar gel. The results from these samples highlighted the significant influence of the component thermal conductivity on the uncertainties involved in effective thermal conductivity prediction.

Using a finite element software package, two-dimensional numerical models were constructed to simulate the measurement of effective thermal conductivity for theoretical material samples having different basic structures. These models allowed the relative significance of several structure-related variables to be examined. The results indicated that the status of the gaseous and solid/liquid components of porous foods, whether continuous or dispersed, and the degree to which pores (in the case of internal porosity) or particles (in the case of external porosity) were in contact with neighbouring pores or particles had a significant influence on the effective thermal conductivity. The sizes and shapes of the individual pores or particles were found to have only minor or negligible influence.

The predictions from two basic types of models were compared to the results from the physical experiments: those models that were functions of component thermal conductivity and volume fractions only (referred to as Type A models), and those that were functions of these two variables as well a third variable (referred to as Type B models). None of the Type A models provided accurate predictions for all the experimental data considered and it was concluded that, apart from certain scenarios, the use of Type B models was preferable. Of the Type B models considered, those that were based on isotropic physical models such as the Maxwell and Effective Medium Theory (EMT) based models, provided better predictions on average than those based on anisotropic physical models, such as the Krischer and Chaudhary-Bhandari models.

The analysis of the experiments and the results of the model evaluation exercise highlighted an important issue regarding the selection of appropriate effective thermal conductivity models: the effective thermal conductivity of the materials had a strong dependence on the optimum heat conduction pathway for a given structure. Hence an assessment of a material's structure should be performed in order to determine the optimum heat conduction pathway within that material.

Two basic optimal heat conduction pathways were identified. In the first scenario the continuous phase of the material has a higher thermal conductivity than the dispersed phase, as is the case with materials having internal porosity, and the optimum heat conduction pathway avoids the gas bubbles that comprise the dispersed phase. In the second scenario, the continuous phase has a lower thermal conductivity than the dispersed phase, as is the case with materials having external porosity, and the optimum heat conduction pathway passes through as many of the solid particles that comprise the dispersed phase as possible.

Previous workers have shown that the two forms of the Maxwell-Eucken model provided theoretical upper and lower limits of the effective thermal conductivity of isotropic materials. In this work, it was proposed that the effective thermal conductivities of materials having internal porosity are bounded by the Landauer-EMT model and the form of the Maxwell-Eucken model in which the continuous phase has a higher thermal conductivity than the dispersed phase. Similarly, it was proposed that the effective thermal conductivities of materials having external porosity are bounded by the Landauer-EMT model and the form of the Maxwell-Eucken model in which the continuous phase has a lower thermal conductivity than the dispersed phase.

The degree of contact between the pores or particles of the dispersed phase, which was related to the optimum conduction pathway, was identified as the variable having the most significant influence on a material's thermal conductivity, in terms of its position relative to thermal conductivity bounds. For this reason, effective thermal conductivity models for general applications should incorporate some measure of this variable. For isotropic, non-frozen foods, two new models based on the Maxwell and EMT structural models with structure-related parameters were proposed. An advantage of these models was that the values of the structure-related parameters had linear variation between the thermal conductivity bounds, unlike other models in the literature.

A simple, general procedure for predicting the effective thermal conductivity of isotropic non-frozen foods was proposed and tested on two types of cake. The predictions from the models recommended by the procedure for the cakes agreed with the experimental data to within ±10%, which would be sufficient for many food industry purposes.

It was recommended that further testing of the proposed thermal conductivity prediction procedure be performed to assess its accuracy and practicality. A need to improve the understanding of the relationship between the structure-related model parameter and the extent of contact between pores or particles was also identified.

Acknowledgements

First of all I would like to thank my supervisory team of Dr. David Tanner (chief), Dr. Simon Lovatt and Professor Andrew Cleland for the support, guidance and expert advice I have received while working for this degree. In addition, I would like to recognise the support of Professor Don Cleland and Associate Professor John Mawson who have provided supervisory-type assistance at various times. I would also like to acknowledge the assistance of the technical and support staff within the Institute of *Food, Nutrition and Human Health* at *Massey University.*

Thanks to the *Processing & Preservation Technology* team for 'adopting' me during my time at *AgResearch*, and I'd like to recognise assistance in various forms from Grant, Mark, Inge, Craig, Jim and Robert. I'd also like to thank Meg, Brian, Rachel and other *MIRINZ* staff for their help at various times.

I would like to thank my fellow post-grads at *Massey* for making the lab we all shared a constructive working environment, and also Mike, Stefan and John for sharing office space with me and for providing me with plenty of non-work-related conversation.

I am grateful for funding received from the *Foundation for Research, Science and Technology* through the Public Good Science Fund (Contract no. MRI 801).

Finally I'd like to thank my mother for proof-reading this thesis.

"It is certain that there is nothing more dangerous,
in philosophical investigations, than to take any thing for granted,
however unquestionable it may appear, till it has been proved by
direct and decisive experiment."

—Count Rumford (Benjamin Thompson)

"The heart of the discerning acquires knowledge;
the ears of the wise seek it out."

—Proverbs 18:15 (NIV)

Table of Contents

Chapter 1: Introduction

Introduction

The food industry relies heavily on thermal processing for the production and preservation of food products. A large field of study is concerned with the derivation of mathematical models of these thermal processes, models that may be used for the purposes of design, control and optimisation of the process.

A reliable model of a thermal process requires accurate thermal conductivity data. In practice, thermal conductivity data may be obtained from experimental measurements or thermal property data-bases, or alternatively, they may be predicted from effective thermal conductivity models. While the direct measurement of thermal conductivity is the ideal source of data, this is a complex task requiring special equipment, and hence this option may not always be feasible. By nature foods are complex materials and exhibit high degrees of variability in their thermal properties, and so the use of thermal conductivity data from literature data-bases introduces uncertainty. In addition, the range of food products available is so vast that data for many foods, particularly the more highly processed products, are simply not available. Hence the use of effective thermal conductivity models may often be the only practical option for determining a food's thermal conductivity.

Much of the study of the prediction of the thermal conductivity of food products has concentrated on its dependence on temperature and moisture content. While the dependence of thermal conductivity on the presence of a porous phase in a food product has been acknowledged, far less work has gone into studying the nature and extent of this dependence, with the consequence that it is unclear which effective conductivity models are most suitable. Since air or carbon dioxide may exist in appreciable amounts in a wide range of food products, there is a clear need to increase the current level of understanding as far as the prediction of the thermal conductivity of porous foods is concerned.

This work was funded by the *Foundation for Research, Science & Technology* (FRST) as Objective 2 of the **Refrigeration for Food Quality, Safety and Yield** programme (contract number MRI-801).

Objective Title: **Modelling the Thermal Conductivity of Foods**

Objective Statement: "A new and superior model of the effect of voidage on food product thermal conductivity, supplied in a usable form to the New Zealand food industry."

Chapter 2: Literature Review

2.1 Introduction

2.1.1 Objective

The aim of this review of the literature was to assess the present state of understanding of the effective thermal conductivity of porous food products and to identify areas requiring further investigation.

2.1.2 Scope and Outline

The specific focus of the present research was on the influence of gaseous components of foods (air and/or carbon dioxide) on thermal conductivity, and therefore other pertinent variables such as temperature and moisture content were only indirectly considered (see also Chapter 3).

The review was not limited to food engineering literature, since much of the fundamental work on effective conductivity models was concerned with electrical conductivity, and much of the thermal conductivity literature was concerned with inorganic materials.

The review was divided into four sections that aimed to:

1. provide a context for this study by highlighting the importance of accurate thermal conductivity data to the food industry
2. define effective thermal conductivity and introduce a selection of effective thermal conductivity models in common use
3. provide an overview of previous studies of the effective thermal conductivity of heterogeneous materials
4. summarise the review and identify needs for further work.

2.2 Thermal Process Modelling

2.2.1 Thermal Processing in the Food Industry

2.2.1.1 Applications of Thermal Processing

Thermal processing plays a major role in the food industry — almost all types of foods undergo thermal processing at some stage in the food chain. The benefits of thermal processing include:

- increasing the desirability and eating quality of the food
- extending the product's shelf-life
- extracting desirable ingredients from raw food materials
- inducing chemical reactions that convert a food material from one form to another
- a combination of any of these effects.

Fellows (2000) categorised thermal processes in the food industry as follows:

1. blanching and pasteurisation
2. heat sterilisation
3. evaporation and distillation
4. extrusion
5. dehydration (drying)
6. baking/roasting
7. frying
8. ohmic and microwave heating
9. chilling (cooling to the initial freezing temperature)
10. freezing (cooling below the initial freezing temperature)
11. freeze drying.

2.2.1.2 Design of Thermal Processing Equipment

Historically, the design of food processing units (e.g. ovens, dryers, refrigerators etc.) has largely been based on experience, but in more recent times analytical approaches have been employed (Thorne, 1992), in particular the implementation of design methods that have been used by chemical processing engineers (Fryer *et al.*, 1997, Brennan *et al.*, 1990, Hallström, 1988, Earle, 1966, Clarke, 1957). These methods are largely dependent on mathematical models that are usually derived from the physical laws that govern the process (e.g. mass and energy balances, reaction kinetics, thermodynamics, etc).

2.2.2 Mathematical Models of Thermal Processes

Mathematical models of thermal processes are typically collections of differential and algebraic equations. There are several different methods of solution of the model equations and the choice of solution will depend on the type of problem and the required accuracy.

2.2.2.1 Analytical Methods

Conduction is the simplest mode of heat transfer to describe mathematically and is often the only significant mode of heat transfer within a food product. Carslaw & Jaeger (1959) have provided analytical solutions to conduction equations for regular geometries with selected boundary conditions, both steady state and time-dependent. However, most food products do not have regular shapes and the analytical solution of the differential equations for irregular shapes can be difficult or impossible.

2.2.2.2 Semi-Analytical Methods

A thermal process such as chilling may be characterised by a general exponential decay curve after an initial time-lag regardless of the shape of the product. This observation has allowed the cooling curve for an individual product to be modelled by an analytical solution for a regularly shaped object with empirically derived shape and lag factors. For freezing, simplified models for moving boundary prediction can be adapted via shape factors. Several relatively simple chilling and freezing time prediction methods that used

these approaches have been devised and have proven effective (e.g. Fleming & Earle, 1967, Cleland & Earle, 1982a, 1982b, Lin *et al.*, 1996a, 1996b). However, such approaches are not suitable for more complex thermal processes involving composition changes and discontinuities in physical properties, or if convection is significant within the food product.

2.2.2.3 Empirical Methods

The literature contains many examples of empirical models of certain thermal processes. These models are typically based on measurements of process variables such as product temperature and moisture content etc. over time (e.g. Vélez-Ruiz & Sosa-Morales, 2001, Magee & McMinn, 2001). These empirical models have limited application and do not provide much insight into specific characteristics of a thermal process.

2.2.2.4 Numerical Methods

Numerical methods are capable of dealing with irregular shapes, fluid phases, different modes of heat transfer, most types of boundary conditions and variable physical properties. Numerical methods also have the potential to achieve the greatest accuracy (Cleland, 1990). The most common numerical methods are finite difference methods (refer to Crank, 1975, for description) and finite element methods (refer to Zienkiewicz, 1983, for description). With the advances in computing technology making the required computation achievable in practical amounts of time, numerical methods of solving the model equations have become more popular. Software packages are commercially available that allow the user to define the mathematical problem which is then solved by the computer. However, numerical methods are inherently more complex and cumbersome than most other methods, and in some situations simpler methods (e.g. the semi-analytical methods described in section 2.2.2.2) will prove to be as accurate for much less effort (Cleland & Earle, 1977).

2.2.3 Thermal Properties

Regardless of the method of solution used, the accuracy of any mathematical model of a thermal process is limited by, amongst other factors, the accuracy of data for physical properties such as density, specific heat capacity, thermal conductivity, latent heat of freezing, and latent heat of evaporation; properties which may vary during the thermal process. The number of physical properties that are required by the model depends on the situation. In some cases certain properties are irrelevant, while in other cases some properties may have negligible influence on the heat transfer process and hence may be ignored. But the majority of thermal process models (both steady-state and time-dependent) require thermal conductivity data.

Foods are heterogeneous materials made up of many chemical components in differing amounts. While data-bases of physical properties do exist for fresh and minimally processed foods such as fruits, vegetables, grains, cereals, meat, and dairy products (Mohsenin, 1980, Miles *et al.*, 1983, Rahman, 1995, *ASHRAE Handbook of Refrigeration*, 1998), it would be impossible to collate data-bases with properties of every single food product, especially since new food products are continually being developed. In the absence of measured physical property data, the best estimate of the property may be obtained from effective thermal property models.

For some properties (density, heat capacity, latent heat), an arithmetic mean of the component properties with weightings proportional to the amounts of the components is a sufficient estimate of the overall property. However this is usually not the case with thermal conductivity (*ASHRAE Handbook of Refrigeration*, 1998). Effective thermal conductivity models are discussed in Section 2.3.

2.2.4 Porous Foods

A diverse range of food products contain significant amounts of air or carbon dioxide on a volume basis, from minimally processed foods such as dried fruits and meat to highly processed foods such as starch-based, extruded snack-foods and dairy-based desserts.

2.2.4.1 Porosity

In engineering literature, the word "porosity" usually means the volume fraction of voidage within a material, i.e.:

$$porosity = \frac{volume\ of\ void\ space\ within\ material}{total\ volume\ of\ material}$$

(c.f. Eq. 3.3 of Rahman, 1995), and this definition of porosity will also be used in this thesis. However, its meaning is sometimes less explicit, and it may be used to refer to the presence of voids in general rather than specifically to the volume fraction of the voids. Terms such as "apparent porosity" and "bulk porosity" also appear in the literature. These terms are usually related to the means by which a measurement of porosity is performed (Rahman, 1995). Rahman (1995) outlines several methods that may be used to measure the porosity of food products.

Some food products contain little or no void space, while others, such as starch-based extrudates, may have porosities higher than 0.9 (Hicsasmaz & Clayton, 1992). Some types of food products may have a wide range of porosities. For example, Murakami & Okos (1989) reported porosities of whole milk powder between 0.45 and 0.83. The porosity of a food product may vary significantly during thermal processing. For example, cakes and bread rise during baking as a result of the increase in the volume of the air bubbles due to thermal expansion and/or the evolution of CO_2.

2.2.4.2 Internal and External Porosity

In some instances within the literature the word "porous" is used to describe materials in which void spaces exist in the interstices between loose or compacted grains or particles. Examples of foods that match this description include flour, corn meal, rice, shredded coconut, or any granular, flaked or powdered product. The word "porous" is also used to describe materials in which a solid/liquid matrix contains gas bubbles (also described as "pockets", "pores" or "cells") which may be either completely isolated (sometimes referred to as "closed pores"), connected to the surface of the matrix material (sometimes referred to as "open pores"), or interconnected with other bubbles (Hicsasmaz & Clayton, 1992). Examples of foods matching this description include ice cream, breads, dried fruit, and generally any food that is not in particulate form.

Since the presence of a gaseous phase affects the conduction of heat regardless of the structure of the material, both classes of material described above will be considered in this study. However, as will be explained in later chapters, it is valuable to retain a distinction between these two basic classes of porous foods and hence two types of porosity will be referred to. Void spaces that exist in the interstices of particulate foods will be referred to as "external porosity" and bubbles that exist within a solid or liquid matrix will be referred to as "internal porosity". This distinction is important because the optimal heat conduction pathways within a material are significantly affected by whether the porosity is internal or external.

It is possible that a food product may contain both internal and external porosity. For example, individual kernels of popcorn contain a significant amount of internal porosity once they have been popped, and a box of popcorn will have a significant amount of voidage between the kernels (external porosity).

2.2.4.3 Continuous and Dispersed Phases in Porous Materials

A number of effective conductivity models require the identification of a "continuous phase" and a "dispersed phase" (see Section 2.3). These models assume that one of the phases forms a matrix (continuous phase) around discrete particles or bubbles (referred to in general as "inclusions") that make up the dispersed phase. For materials with external

porosity, individual solid particles are surrounded by a gaseous matrix, and hence the gaseous component forms the continuous phase and the solid component forms the dispersed phase. For materials with internal porosity, individual gas bubbles are dispersed within a solid/liquid phase, and hence the gaseous component forms the dispersed phase.

2.2.4.4 Thermal conductivity of Major Food Components

Table 2.1 shows the thermal conductivities of food components at 0°C. Other than ice and air, the thermal conductivities of food components are of similar magnitude. As shown later, the ratio of the component thermal conductivities determines the possible range of the overall thermal conductivity of the material: the more dissimilar in magnitude the component thermal conductivities the wider the range. Therefore, the presence of air (or CO_2) has a significant influence on the overall thermal conductivity of the food.

	k/W m^{-1} K^{-1}
protein	0.18
fat	0.18
soluble carbohydrate	0.20
fibre	0.18
ash	0.33
liquid water	0.57
ice	2.2
air	0.024

Table 2.1: Thermal Conductivities of Food Components at 0 °C (taken from Holman, 1992, ASHRAE Handbook of Refrigeration, 1998)

2.3 Effective Thermal Conductivity Models

2.3.1 Thermal Conductivity Definitions

2.3.1.1 Thermal Conductivity and Conduction in Pure Materials

The rate of heat flow within a conducting medium, q (W), that results from a temperature gradient in the x-direction of Cartesian space, dT/dx (K m^{-1}), is directly proportional to that gradient and the cross-sectional area of heat flow A (m^2), in a relationship known as *Fourier's Law*:

$$q_c = -kA\frac{dT}{dx} \tag{2.1}$$

The proportionality constant k is known as the *thermal conductivity* of the medium through which the heat is transferred and the subscript c indicates that the heat transfer is by conduction only. The negative sign is inserted to ensure that the value of q_c is positive if the direction of heat flow is consistent with the Second Law of Thermodynamics (i.e. the heat flow is from hot to cold). The definition of thermal conductivity is taken from Fourier's Law:

$$k \equiv -\frac{q_c}{A(dT/dx)} \tag{2.2}$$

The *SI* units for thermal conductivity are W m^{-1} K^{-1}. For pure materials the thermal conductivity is dependent solely on temperature. This dependence is often adequately approximated by a linear function, or alternatively may be ignored if the temperature range in question is sufficiently narrow. (A description of thermal conduction at the microscopic level is given in Section 1-2 of Holman, 1992).

If an energy balance over an infinitesimally small isotropic volume is performed using Fourier's Law the following partial differential equation may be derived that describes the conduction of heat within that medium (Holman, 1992):

$$C(T)\frac{\partial T}{\partial t} = \frac{\partial}{\partial x}\left(k(T)\frac{\partial T}{\partial x}\right) + \frac{\partial}{\partial y}\left(k(T)\frac{\partial T}{\partial y}\right) + \frac{\partial}{\partial z}\left(k(T)\frac{\partial T}{\partial z}\right) \tag{2.3}$$

C is the volumetric heat capacity of the medium (J m^{-3} K^{-1}), t is time and, x, y and z are the rectangular co-ordinates in three-dimensional space. The derivation assumes that there is no heat generation or consumption within the material. Equation (2.3) is sometimes referred to as the *Diffusion Equation*. A more general form of Eq. (2.3) may be written that does not assume a rectangular coordinate system:

$$C(T)\frac{\partial T}{\partial t} = \nabla\left(k(T)\nabla T\right) \tag{2.4}$$

If k is not dependent on temperature and there is a steady heat flow, Eq. (2.4) is reduced to:

$$\nabla^2 T = 0 \tag{2.5}$$

which is known as *Laplace's Equation.*

2.3.1.2 Thermal Conductivity of Heterogeneous Materials – Effective Thermal Conductivity

For heterogeneous materials the thermal conductivity and volumetric heat capacity become dependent on the relative amounts of the components, and, in the case of the thermal conductivity, the spatial distribution of the components. The thermal diffusion equation for heterogeneous materials is significantly more complex than Eq. (2.4):

$$C(T, v_1, v_2, \ldots)\frac{\partial T}{\partial t} = \nabla\left(k(T, v_1, v_2, \ldots)\nabla T\right) \tag{2.6}$$

(v is the volume fraction of a component). In many situations, the geometric arrangements of the different components of a material are either unknown or too complicated to be described by analytic mathematical expressions. In these situations it is convenient to use *effective thermal properties*. The term "effective" is used to communicate the concept that the material is assumed to be homogeneous on a macroscopic scale, having a single conductivity k_e and volumetric heat capacity C_e. This allows the use of Eq. (2.4) for heterogeneous materials, rather than the more complicated Eq. (2.6).

The effective volumetric heat capacity may reasonably be represented by a weighted mean of the component volumetric heat capacities, although phase changes introduce complexities (see for example Schwartzberg, 1976). But due to its dependence on the spatial distribution of the components, the effective thermal conductivity is more difficult to model.

In some situations heat transfer by modes other than conduction may be significant in the fluid phase(s) of porous materials. Rather than treat these effects separately, it is often more convenient to use an apparent thermal conductivity, defined in the same way as true thermal conductivity (see Eq. 2.2), but calculated from the total heat flow rather than the conduction heat flow. Effective thermal conductivity models that incorporate radiation (e.g. Loeb, 1954), convection (e.g. Yagi &Kunii, 1957), and evaporation effects (e.g. Sakiyama & Yano, 1990) may be found in Appendix A.

2.3.2 Effective Thermal Conductivity Reviews

Studies of effective conductivity (both thermal and electrical) have been performed for many years and several reviews of the literature have been published. Selected reviews of effective thermal conductivity models are listed below, loosely divided into three categories:

1) particulates (such as soils and packed beds); Farouki, (1986), Cheng & Chin-Tsau (1998)

2) inorganic composite materials; Cheng & Vachon (1969), Progelhof *et al.*(1976)
3) foods; Murakami & Okos (1989), Rahman (1995)

Many of the models have been derived for specific applications and cannot easily be applied to general situations. Some, however, have general applicability and occur frequently in the literature. A selection of commonly cited models is discussed in subsequent sections. Appendix A contains a more comprehensive list of effective thermal conductivity models, although it is by no means a complete list since new effective thermal conductivity models continue to appear (e.g. Slavin *et al.*, 2000). Unless otherwise specified, the subscript '1' refers to the continuous phase, and the subscript '2' refers to the discontinuous (dispersed) phase (in many models this distinction between components is not necessary).

2.3.3 Series/Parallel based Effective Thermal Conductivity Models

2.3.3.1 Series, Parallel and Geometric Models

The two simplest effective thermal conductivity (k_e) models are the Series and Parallel models, shown below for a two-component material:

Series Model:
$$k_e = \frac{1}{(1-v_2)/k_1 + v_2/k_2} \tag{2.7}$$

Parallel Model
$$k_e = (1-v_2)k_1 + v_2 k_2 \tag{2.8}$$

(The Series model is sometimes referred to as the Perpendicular model). As their titles suggest, the Series model assumes that the heat flows through all the components of the material in series and the Parallel model assumes that the heat flows through the components of the material in parallel, by analogy to the calculation of the total resistance in an electrical circuit by Ohm's law. While these physical models are simplistic, they do provide theoretical minimum and maximum bounds for the effective thermal

conductivity of a material of known component thermal conductivities and volume fractions, so long as the heat transfer is by conduction only (Bart, 1994).

Inspection of Eqs. (2.7) and (2.8) reveals that the Series and Parallel models are simply the weighted harmonic and arithmetic means of the component thermal conductivities respectively. Lichteneker (cited in Woodside and Messmer, 1961a) proposed a simple intermediate to the Series and Parallel models which is the weighted geometric mean of the component conductivities:

$$k_e = k_1^{(1-v_2)} k_2^{v_2} \tag{2.9}$$

Equation (2.9) is usually referred to as the Geometric model.

2.3.3.2 Krischer's Model

Krischer (1963) (cited in English in Keey, 1972) derived a simple model for dry porous materials:

$$\frac{1}{k_e} = \frac{1-f_K}{(1-v_2)k_1 + v_2 k_2} + f_K\left(\frac{1-v_2}{k_1} + \frac{v_2}{k_2}\right) \tag{2.10}$$

Krischer's model is the weighted harmonic mean of the predictions of the Series and Parallel models. Keey (1972) suggested typical f_K-values of 0.2 and 0.25, while Lin *et al.* (1997) suggested a mean f_K-value of 0.16 for porous food products. An f_K-value of 0 reduces Eq. (2.10) to the Parallel model and an f_K-value of 1.0 reduces Eq. (2.10) to the Series model.

2.3.3.3 Chaudhary-Bhandari Model

Chaudhary and Bhandari (1968) proposed a model for predicting the thermal conductivity of partially saturated calcareous sandstone:

$$k_e = [(1-v_2)k_1 + v_2 k_2]^{f_{CB}} \left(\frac{1-v_2}{k_1} + \frac{v_2}{k_2} \right)^{(1-f_{CB})} \quad (2.11)$$

Eq. (2.11) is a weighted geometric mean of the predictions of the Series and Parallel models, where f_{CB} is an empirically determined weighting parameter. Predictions from Eq. (2.11) were plotted against experimental results obtained by Sugawara (1961). For porosities ranging between 0.145 and 0.326, the f_{CB} parameter values were between 0.8 and 0.9.

2.3.3.4 Herminge, Renaud, Rahman-Potluri-Varamit Models

Herminge (1961), Renaud *et al.* (1992), and Rahman *et al.* (1991) (all cited in Rahman, 1995) also proposed models that were simple combinations of the Series and Parallel models, however they have not been used as extensively the Krischer and Chaudhary-Bhandari models. (See Appendix A for the model equations).

2.3.3.5 Tsao and Cheng-Vachon Models

Tsao (1961) proposed a more elaborate combination of the Series and Parallel models as an effective thermal conductivity model. The derivation assumed that a unit cube of heterogeneous material could be sliced into infinitesimally thin pieces and then re-constituted in such a way that each phase was accumulated into separate regions of the unit cube (see diagrams in Tsao, 1961). This assumption was based on the fact that the Series and Parallel models do not require specification of the sequence in which the components are positioned with respect to the heat flow, but only the orientation (parallel or transverse to the direction of heat flow). The rearranged distribution of the porous phase was modelled by a normal distribution. The effective thermal conductivity was a function of this porosity distribution with the mean and standard deviation of the normal distribution serving as parameters that were dependent on the material being modelled.

Cheng and Vachon (1969) modified Tsao's model by assuming that the porous phase could be modelled by a parabolic distribution instead of a normal distribution, the parameters of which could be related to the amount of the porous phase:

$$\frac{1}{k_e} = \frac{2\tan^{-1}\left(\frac{\Psi_1}{2}\sqrt{\frac{\Psi_2(k_1-k_2)}{k_1+\Psi_1(k_2-k_1)}}\right)}{\sqrt{\Psi_2(k_2-k_1)[k_1+\Psi_1(k_2-k_1)]}} + \frac{1-\Psi_1}{k_1} \qquad (2.12)$$

where: $\Psi_1 = \sqrt{3v_2/2}$ and $\Psi_2 = -4\sqrt{2/(3v_2)}$

The presence of the arctangent function in Eq. (2.12) means that the model does not provide predictions for all values of v_2.

2.3.3.6 Russell's Model

Russell (1935) derived an effective thermal conductivity model from a physical model of cubic voids in a continuous, grid-like matrix (see Russell, 1935, for diagram). The regular arrangement of the physical model meant that it could be viewed as a network of resistors in series and parallel, and an expression for the effective thermal conductivity was derived by applying Ohm's law to the network:

$$k_e = k_1\left[\frac{v_2^{2/3} + \frac{k_1}{k_2}(1-v_2^{2/3})}{v_2^{2/3} - v_2 + \frac{k_1}{k_2}(1+v_2-v_2^{2/3})}\right] \qquad (2.13)$$

(Note: Russell recommended that this model should be used to examine and explain phenomena related to effective thermal conductivity rather than being used to predict the thermal conductivities of real materials.)

2.3.4 Maxwell-Based Effective Thermal Conductivity Models

2.3.4.1 Maxwell's Work on Conduction in Heterogeneous Media

In the third edition of *A Treatise on Electricity and Magnetism* (originally published in 1892, reprinted in 1954), Maxwell devoted a chapter to electrical conduction through heterogeneous media. He considered the scenario of a sphere of conductivity k_s contained

within a medium of conductivity k_m. Expressing his analysis in terms of thermal conduction, when the sphere and its containing medium were subjected to a steady state external temperature gradient, the temperature field outside the sphere (T_m) was calculated from Eq. (2.14):

$$T_m = br\cos\theta - bR^3 \frac{k_s - k_m}{k_s + 2k_m} \frac{\cos\theta}{r^2} \tag{2.14}$$

where r and θ are polar coordinates (with the centre of the sphere as the coordinate origin), R is the diameter of the sphere (m) and b is the magnitude of the temperature gradient (K m^{-1}). The temperature field within the sphere (T_s) was calculated from Eq. (2.15):

$$T_s = b\frac{3k_m}{k_s + k_m} r\cos\theta \tag{2.15}$$

(refer to Appendix B for a rigorous derivation of Eqs. 2.14 and 2.15).

He then considered the case of n small spheres of radius R_2 contained within a larger sphere of radius R_1 whose distances of separation where significantly greater than R_2 (in order that the local distortions to the temperature field caused by individual spheres did not influence the temperature field surrounding a neighbouring sphere). The volume fraction (v_2) of the small spheres was given by:

$$v_2 = n\frac{R_2^3}{R_1^3} \tag{2.16}$$

The temperature field a significant distance from the centre of the containing sphere was determined from Eq. (2.17):

$$T_m = br\cos\theta - bv_2 R_1^3 \frac{k_2 - k_1}{k_2 + 2k_1} \frac{\cos\theta}{r^2} \tag{2.17}$$

Maxwell then considered the situation if the larger sphere had been filled with a material of conductivity k_e (making the assumption that heterogeneous materials may be treated as being effectively homogeneous on a macroscopic scale, see Section 2.3.1.2):

$$T_m = br\cos\theta + bR_1^3 \frac{k_e - k_1}{k_e + 2k_1} \frac{\cos\theta}{r^2} \tag{2.18}$$

In order for the two expressions (Eqs. 2.17 and 2.18) to produce the same result:

$$\frac{k_e - k_1}{k_e + 2k_1} = v_2 \frac{k_2 - k_1}{k_2 + 2k_1} \tag{2.19}$$

It may be of interest to note that Eq. (2.19) is equivalent to equations for other properties of heterogeneous materials, such as Poisson's theory for induced magnetism, the Clausius-Mossotti theory for dielectric constants, and the Lorenz-Lorentz theory for refractive indices (Fricke, 1924). By rearrangement:

$$k_e = k_1 \frac{2k_1 + k_2 - 2(k_1 - k_2)v_2}{2k_1 + k_2 + (k_1 - k_2)v_2} \tag{2.20}$$

Equation (2.20) is usually referred to as the Maxwell-Eucken equation after Eucken who first applied Maxwell's model to a thermal situation (Eucken, 1940). It is important to note that the Maxwell-Eucken model requires the distinction between the components, one being the dispersed phase and the other being the continuous phase. Equation (2.21) gives the predictions if k_1 becomes the dispersed phase and k_2 the continuous phase:

$$k_e = k_2 \frac{2k_2 + k_1 - 2(k_2 - k_1)(1 - v_2)}{2k_2 + k_1 + (k_2 - k_1)(1 - v_2)} \tag{2.21}$$

(Note: the derivation in Maxwell, 1954, is in terms of specific resistances, the reciprocal of conductivity. Also, Maxwell labelled the small spheres as component 1 and the large

sphere as component 2, the reverse of what is shown above. Hence there are slight differences in the appearance of the equations and also the final result between Maxwell's derivation and the derivation shown here, but it can be shown that Eq. 2.20 is equivalent to Eq. 17 of p. 440 of Maxwell, 1954. The difference in terminology here ensures consistency with the rest of this text).

2.3.4.2 Hamilton's Modification of the Maxwell-Eucken Model

Following an approach used by Fricke (1924), Hamilton (Hamilton & Crosser, 1962) modified the Maxwell-Eucken model to allow for non-spherical inclusions in the continuous medium:

$$k_e = k_1 \frac{(n-1)k_1 + k_2 - (n-1)(k_1 - k_2)v_2}{(n-1)k_1 + k_2 + (k_1 - k_2)v_2} \tag{2.22}$$

The parameter n is a shape factor related to the sphericity of the inclusions with an n-value of 3 corresponding to a perfect sphere, in which case Eq. (2.22) reduces to Eq. (2.20). However, the n-value may also be used to fit the model to experimental thermal conductivity data. The basic shape of the Maxwell-Hamilton model remains the same as that of the Maxwell-Eucken model for the majority of n-values. If n has a value of 1, Eq. (2.22) reduces to the Series model and if n has a value of ∞ Eq. (2.22) reduces to the Parallel model.

2.3.4.3 Levy's Model

Levy (1981) proposed a model that used algebraic manipulation to force the two forms of the Maxwell-Eucken model (Eqs. 2.20 and 2.21) to produce the same result. This was achieved by replacing the volume fraction term (v) in the Maxwell-Eucken equations by a new function F:

$$F = \frac{2/\Lambda - 1 + 2v - \sqrt{(2/\Lambda - 1 + 2v)^2 - 8v/\Lambda}}{2} \tag{2.23}$$

where:

$$\Lambda = \frac{(k_1 - k_2)^2}{(k_1 + k_2)^2 + k_1 k_2 / 2} \tag{2.24}$$

Levy's adjustment to the Maxwell-Eucken model had no physical basis, and the shape of the model had a different characteristic to that of the Maxwell-Eucken model. Levy's model did not make a distinction between the component phases.

2.3.5 Effective Medium Theory Models

The Effective Medium Theory (EMT), also known as the Effective Medium Approximation, is closely related to Percolation Theory (Hammersley, 1983, Zallen, 1983). Percolation Theory is a statistical approach that has often been used to model the conductivity of random mixtures of component materials, particularly when one component has a much higher conductivity than the other component (Kirkpatrick, 1973, Davis, 1975). The EMT assumes that the net influence on the overall temperature gradient caused by the local distortions from each individual particle is zero when averaged over a sufficiently large volume, which means that each particle in the mixture behaves as though it were totally surrounded by material that has the overall properties of the mixture.

2.3.5.1 Landauer's Model

Landauer (1952) derived a model for predicting the electrical conductivity of alloys:

$$\sum_i v_i \frac{k_i - k_e}{k_i + 2k_e} = 0 \tag{2.25}$$

For two components Eq. (2.25) may be rearranged to be explicit in terms of k_e:

$$k_e = \tfrac{1}{4}\left((3v_2 - 1)k_2 + [3(1 - v_2) - 1]k_1 + \sqrt{[(3v_2 - 1)k_2 + (3\{1 - v_2\} - 1)k_1]^2 + 8k_1 k_2}\right) \tag{2.26}$$

When the k_e predictions of Landauer's model are plotted as a function of v_2 the plot displays the Percolation characteristic, having a linear segment at either end of the porosity range connected by a pronounced curve that becomes a genuine cusp as the ratio k_1/k_2 is increased.

Equation (2.25) may be arrived at by different lines of reasoning. The derivation shown in Davis *et al.* (1975) follows the same derivation as that for Maxwell's model (see Section 2.3.4.1 and Appendix B) up to the stage where Eqs. (2.14) and (2.15) are derived, at which point the EMT makes different assumptions from the Maxwell model. The similarity between the two models is clear (compare Eq. 2.25 with Eq. 2.19). However, by assuming a totally random arrangement of component materials, Landauer's EMT model did not make a distinction between the components.

2.3.5.2 Kirkpatrick's Model

Kirkpatrick (1973), in a study of the conduction of networks of resistors, derived a modified form of Landauer's original EMT equation:

$$(1-v_2)\frac{k_1-k_e}{k_1+(Z/2-1)k_e}+v_2\frac{k_2-k_e}{k_2+(Z/2-1)k_e}=0 \qquad (2.27)$$

The parameter Z, called the *coordination number*, was the number of neighbouring resistors to which each individual resistor in the network was connected. The networks were arranged in regular square and cubic lattices and Z was therefore dependent on the number of dimensions being considered, $Z = 4$ for two dimensions and $Z = 6$ for three dimensions. Equation (2.27) reduces to Eq. (2.25) for the three-dimensional case. As with Hamilton's modification of Maxwell's model, the Z parameter in Kirkpatrick's model may be used to fit the model to experimental data. Kirkpatrick's model reduces to the Series and Parallel models when $Z = 2$ and ∞ respectively. Kirkpatrick's model retained the same basic shape as Landauer's model as the Z parameter was varied.

2.3.6 Models Specifically for Food Products

2.3.6.1 Empirical Models

Empirical thermal conductivity models are available in the literature for selected foods and food components. A large number of empirical models are linear functions of temperature and moisture content (Mohsenin, 1980, Miles *et al.*, 1983, Rahman, 1995 provide reviews). These linear correlations are limited by the range of moisture content to which they may be applied. Some workers have used polynomial and exponential correlations in order to allow wider ranges of applicability (e.g. Lozano *et al.* 1979, Mattea *et al.*, 1989, Rahman & Potluri, 1990). Some models also contain a porosity term in the correlation (e.g. Vagenas *et al.*, 1990, Rahman, 1992, Rahman *et al.*, 1997). Empirical models require extensive thermal conductivity measurements, and yet, due to variations in the correlation constants (not only from the different types of foods, but also from variety, harvesting time and harvesting location), have very limited applications. Very few thermal conductivity correlations are available in the literature for highly processed foods.

2.3.6.2 Kopelman's Models

Kopelman (cited in *ASHRAE Handbook of Refrigeration*, 1998) derived effective thermal conductivity models that attempted to account for different food structures:

a) Isotropic material with k_1 greater than k_2:

$$k_e = k_1\left[\frac{1-v_2^{2/3}(1-k_2/k_1)}{1-v_2^{2/3}(1-k_2/k_1)(1-v_2^{1/3})}\right] \tag{2.28}$$

Equation (2.28) is mathematically equivalent to Russell's model (Eq. 2.13). Rahman (1995) suggested that, since water has a higher thermal conductivity than other food components (see Table 2.1), Eq. (2.28) is most applicable for high moisture content foods, when water forms a continuous phase.

b) For isotropic materials in which k_1 is much greater than k_2 Eq. (2.28) may be approximated by:

$$k_e = k_1\left[\frac{1-v_2^{2/3}}{1-v_2^{2/3}(1-v_2^{1/3})}\right] \tag{2.29}$$

c) For anisotropic materials with heat flow parallel to fibres:

$$k_e = k_1\left[1-v_2\left(1-\frac{k_2}{k_1}\right)\right] \tag{2.30}$$

d) For anisotropic materials with heat flow in series with fibres:

$$k_e = k_1\left[\frac{1-\left(\frac{v_2^{1/2}}{1-k_2/k_1}\right)}{1-\left(\frac{v_2^{1/2}}{1-k_2/k_1}\right)(1-v_2^{1/2})}\right] \tag{2.31}$$

2.3.6.3 Murakami & Okos Model

Murakami & Okos (1989) modified Krischer's model (Eq. 2.10) with the aim of relating the f_K parameter to the moisture content and porosity of food products. Based on a regression analysis of thermal conductivity data from the literature, the new parameter f_{MO} was given by:

$$f_{MO} = \sum_{j=0}^{3}\left[\left(\sum_{l=0}^{3} B_{jl}\Gamma_j^l\right)(v_2-0.4)^j\right] \tag{2.32}$$

where B values were regression constants and Γ_j-values were adjustable parameters.

2.3.6.4 Hill, Leitman & Sunderland Model for Meat

Hill *et al.* (1967) derived a model for the effective thermal conductivity of fresh and frozen meat. The model assumed that heat was conducted through the meat by three parallel pathways: through the meat fibre, through the aqueous phase, and through the meat fibre and aqueous phase in series (see Figs. 2 and 3 of Hill *et al.*, 1967). The following equation was derived:

$$k_e = k_2(2\Phi - \Phi^2) + k_1(1 - 4\Phi + 3\Phi^2) + \frac{8k_1k_2(\Phi - \Phi^2)}{k_1\Phi + k_2(4 - \Phi)} \tag{2.33}$$

$$\Phi = 2 - \sqrt{4 - 2v_2}$$

In Eq. (2.33) component 2 refers to the meat fibres and component 1 refers to the aqueous phase.

2.3.7 Multi-Component Systems

Of the models listed above for 2-component systems, the Series, Parallel, Geometric, Krischer, Chaudhary-Bhandari, Landauer-EMT and Kirkpatrick-EMT models may all be extended to multi-component systems. While the Maxwell-Eucken model cannot be used for multi-component systems, Hamilton (cited in Cheng & Vachon, 1969) derived a multi-component form of Eq. (2.22):

$$k_e = k_1\left[\frac{1 - \sum_{i=2}^{m} \frac{v_i(n_i - 1)(k_1 - k_i)}{k_i + (n_i - 1)k_i}}{1 + \sum_{i=2}^{m} \frac{v_i(k_1 - k_i)}{k_i + (n_i - 1)k_i}}\right] \tag{2.34}$$

where m is the number of components, and the subscript i refers to the ith component.

In some situations materials are separated into different phases rather than into individual chemical components, which then allows for the use of two-component models Alternatively, 2-component models may be used in successive stages (examples of these methods of dealing with multi-components systems may be found in Murakami & Okos, 1989, and Krach & Advani, 1996).

2.3.8 Plots of Thermal Conductivity Predictions

Figure 2.1 shows plots of the predictions of eleven models over the entire range of volume fractions of a two component material with $k_1/k_2 = 20$ (which is similar to that of an unfrozen, high water-content food product containing air).

Other than the Krischer and Chaudhary-Bhandari models, the models plotted in Fig. 2.1 are functions of component volume fractions and conductivities only, and the assumed physical structure is accounted for by the mathematical relationships between these variables. The values for the f parameters in the Krischer and Chaudhary-Bhandari plots were taken from recommendations in the literature.

The fact that Fig. 2.2 has the appearance of a maze of railway tracks at a shunting yard indicates that the differences between the models are substantial, and that physical structure has a significant influence on thermal conductivity. Not only do the models lie in different regions on the graph, but there are also clear differences between the basic shapes of the plots.

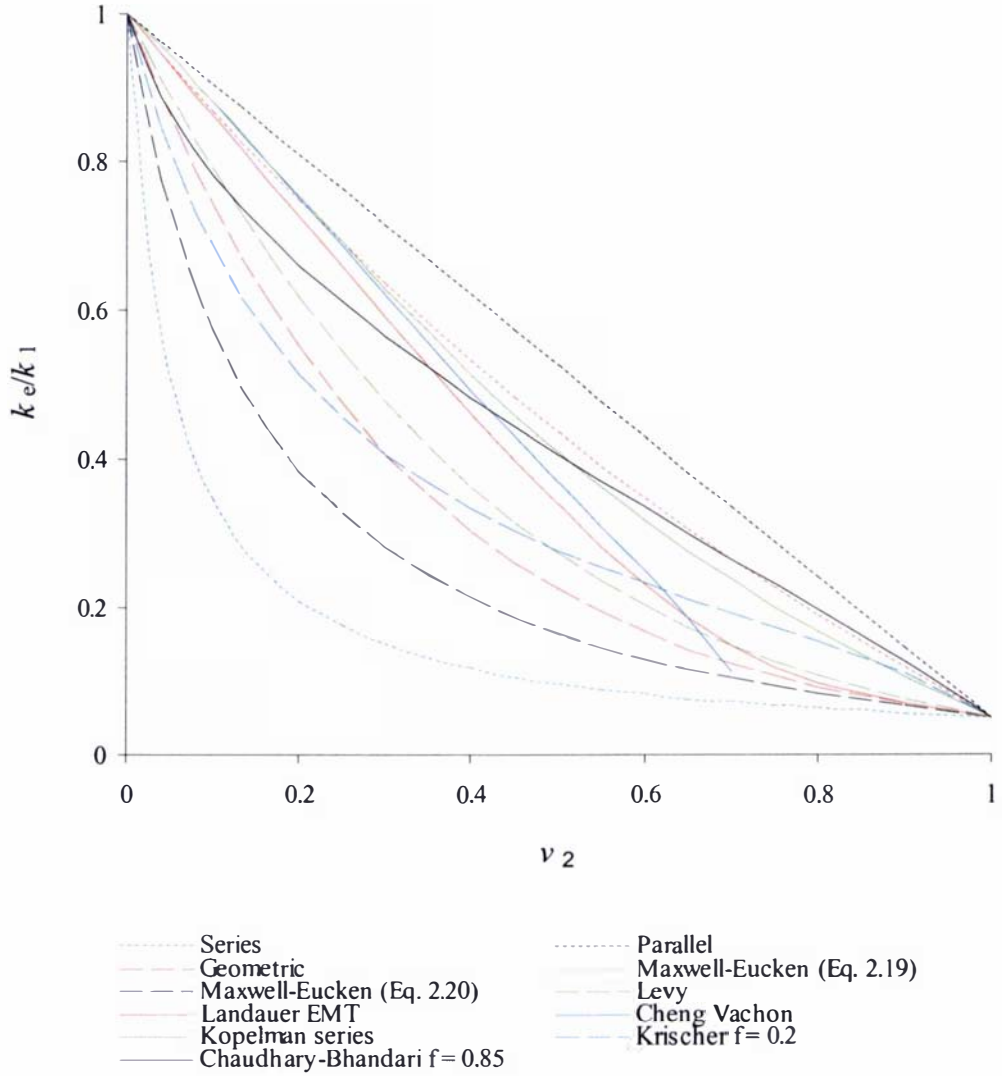

Figure 2.1: Plots of Selected Effective Thermal Conductivity Models, $k_1/k_2 = 20$

2.3.9 Thermal Conductivity Bounds

The Series and Parallel models were first proposed as thermal conductivity bounds by Weiner (cited in Bart, 1994). Figure 2.1 shows that the predictions from all the other models plotted lie within the region bounded above and below by the Parallel and Series models respectively. In fact, as mentioned in Section 2.3.3, the Series and Parallel models represent the bounds of thermal conductivity regardless of material structure, provided conduction is the only mechanism of heat transfer involved (Bart, 1994).

Hashin & Shtrikman (1962) derived bounds for the effective conductivity of isotropic materials:

$$k_e = k_1 + \frac{v_2}{\frac{1}{k_2 - k_1} + \frac{(1 - v_2)}{3k_1}} \tag{2.35}$$

$$k_e = k_2 + \frac{(1 - v_2)}{\frac{1}{k_1 - k_2} + \frac{v_2}{3k_2}} \tag{2.36}$$

(It turns out that Eqs. (2.35) and (2.36) are mathematically equivalent to the Maxwell-Eucken equations (2.20) and (2.21), although derived by a different line of reasoning and for different purposes). The Hashin-Shtrikman bounds always lie within the Wiener bounds (Bart, 1994).

Thermal conductivity bounds are useful because they can clearly demonstrate the level of uncertainty in effective thermal conductivity predictions that may be expected for a given system. Figures 2.2a to 2.2d show the Wiener bounds (i.e. Series and Parallel models) and Hashin-Shtrikman bounds for four different food types: Fig. 2.2a shows the bounds for a dry, non-porous food (k_1/k_2 = 1.2); Fig 2.2b shows the bounds for a non-porous, non-frozen food (k_1/k_2 = 3); Fig 2.2c shows the bounds for a porous, non-frozen food (k_1/k_2 = 20); Fig 2.2d shows the bounds for a porous, frozen food (k_1/k_2 = 100). The conclusion to be drawn from Figs. 2.2a-2.2d is clear: the more dissimilar the component thermal conductivities, the wider the envelope between the upper and lower thermal conductivity bounds, and the greater potential for uncertainty involved in effective thermal conductivity prediction.

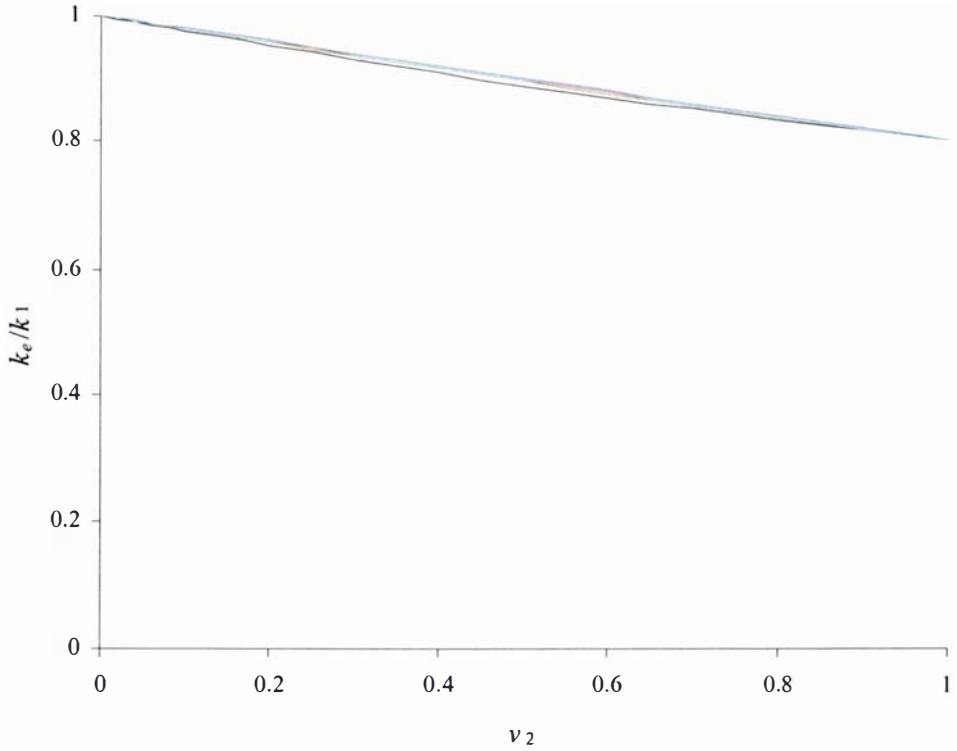

Figure 2.2a: Upper and lower Wiener bounds (blue and black lines), and upper and lower Hashin-Shtrikman bounds (red and green lines) for typical dry, non-porous food ($k_1/k_2 = 1.2$)

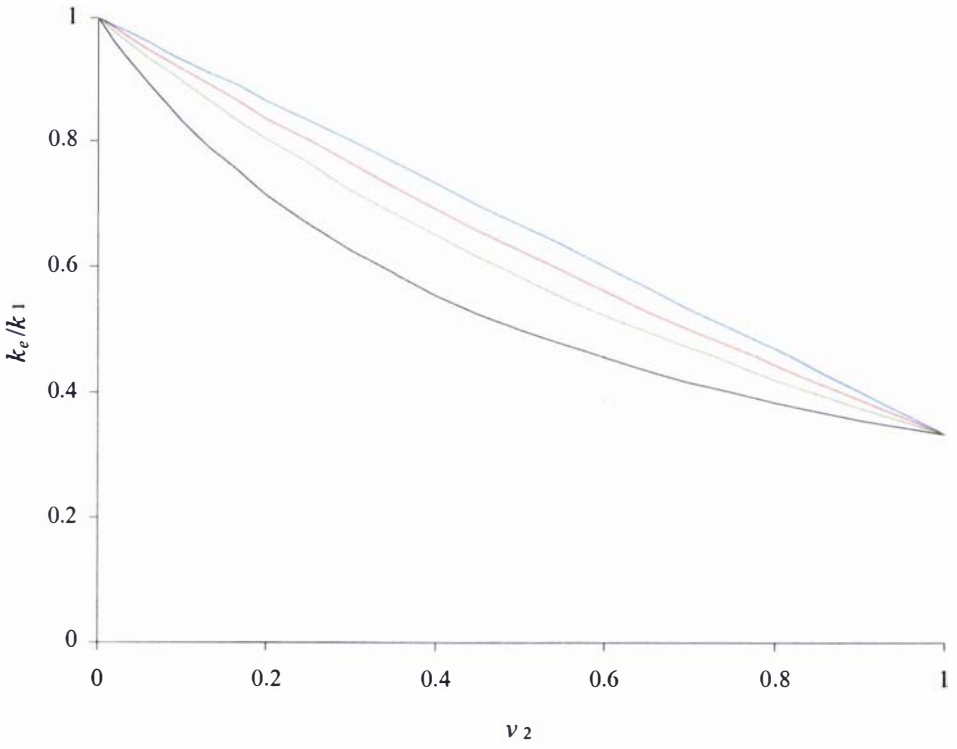

Figure 2.2b: Upper and lower Wiener bounds (blue and black lines), and upper and lower Hashin-Shtrikman bounds (red and green lines) for typical non-porous, non-frozen food ($k_1/k_2 = 3$)

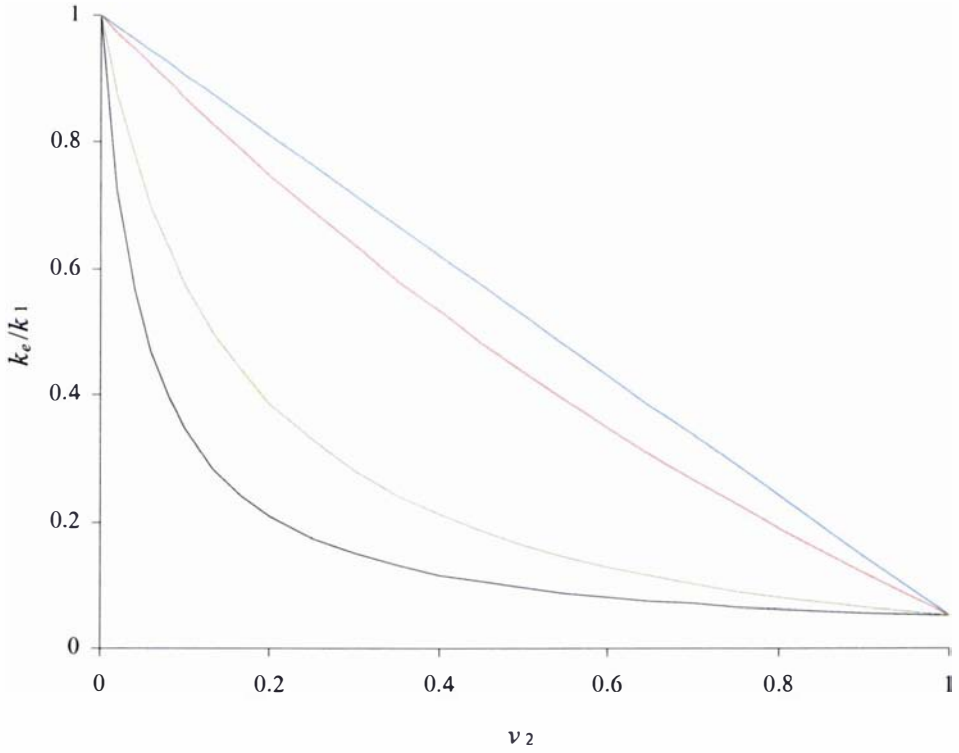

Figure 2.2c: Upper and lower Wiener bounds (blue and black lines), and upper and lower Hashin-Shtrikman bounds (red and green lines) for typical porous, non-frozen food ($k_1/k_2 = 20$)

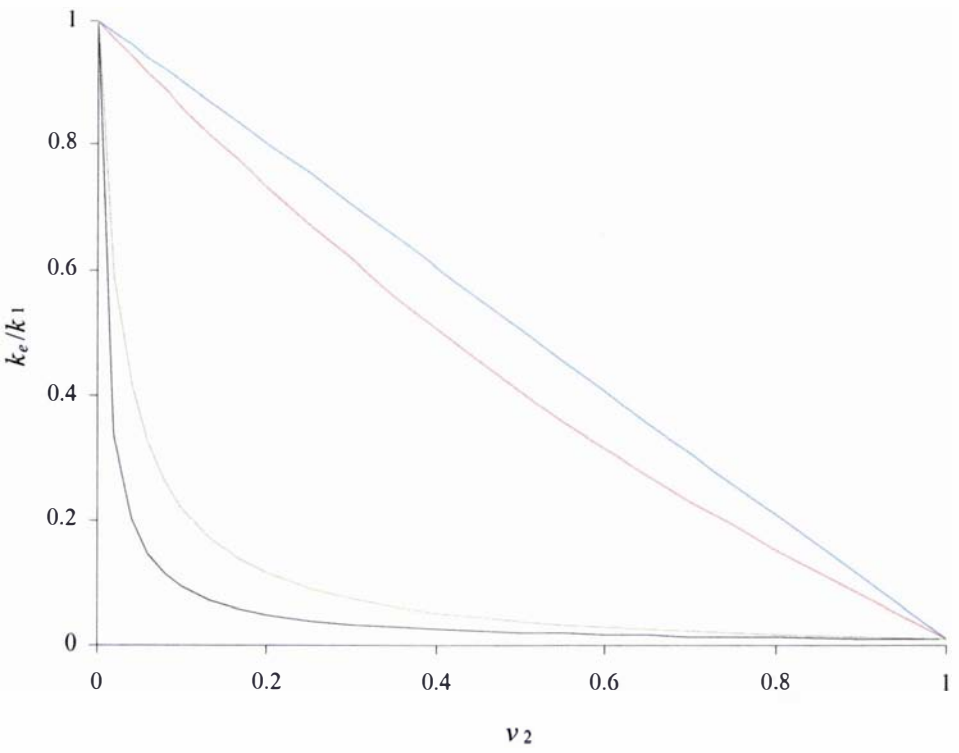

Figure2.2d: Upper and lower Wiener bounds (blue and black lines), and upper and lower Hashin-Shtrikman bounds (red and green lines) for typical frozen, porous food ($k_1/k_2 = 100$)

2.4 Effective Thermal Conductivity Studies

2.4.1 Studies of Factors that have Potential to Influence Effective Thermal Conductivity

2.4.1.1 Russell (1935)

In a study on the thermal conductivity of porous insulating bricks Russell (1935) identified the size, shape and distribution of the pores as having potential to influence the effective thermal conductivity of the brick. Using his effective thermal conductivity model (Eq. 2.13) he calculated the effective thermal conductivities for idealised material structures over a range of volume fractions and component thermal conductivities. He divided the insulating bricks into two classes: those that had internal air "pockets", and those where voids existed between granules (external voids). He concluded that for a given porosity and component thermal conductivity a granular brick (external voids) would have a lower conductivity than a brick containing cellular pores (internal voids). He also concluded that if the size of the pore was uniform then the pore size should have no influence on the thermal conductivity, so long as the pores were small enough that convection and radiation effects were negligible. For spherical pores he concluded that the size distribution of the pores had no effect either. Radiation was seen as having potential significance at high temperatures in larger pores (greater than ¼ inch, 6.35mm), and for bricks with high permeability convection could also become significant.

2.4.1.2 Francl & Kingery (1954)

In an investigation on the effect of porosity on the thermal conductivity of ceramics, Francl & Kingery (1954) stated that the size, shape and orientation of pores within a ceramic had potential to influence the effective thermal conductivity of the ceramic. They performed thermal conductivity measurements on samples of alumina that contained regular arrangements of spherical and cylindrical pores. The result revealed that, as expected, the samples containing cylindrical pores exhibited highly anisotropic

characteristics. The size of the pores was found to be significant only at higher temperatures (above 500°C) when radiation became significant.

2.4.1.3 Yagi & Kunii (1957)

Yagi & Kunii (1957) analysed the different heat transfer pathways within packed beds in order to derive models for predicting the effective thermal conductivity. In the absence of fluid flow the significant pathways were defined as:

- conduction within the solid particle
- conduction through the surface of contact between neighbouring particles
- radiation from the surface of a particle to its neighbours
- radiation between neighbouring voids.

The heat flows through these basic heat transfer pathways were combined either in series or parallel (see Fig. 4 of Yagi & Kunii, 1957) so that expressions for the effective thermal conductivities of different scenarios could be determined (different forms of Yagi & Kunii's model are shown in Appendix A). Kunii & Smith (1960) later applied a similar analysis to porous rocks (consolidated sands).

2.4.1.4 Hamilton & Crosser (1962)

Hamilton & Crosser (1962) performed thermal conductivity measurements on suspensions of different shapes of particles (spheres, cubes, cylinders, parallelepipeds, and discs) of two different materials (aluminium and balsa wood) suspended in *Silastic*® RTV-502 rubber. The volume fractions of the dispersed phase varied between 0 and 0.27. They found that the shape of the particles was influential for the aluminium suspensions but not for the balsa suspensions. These results suggested that the conductivity of the dispersed phase had to be significantly higher than the conductivity of the continuous phase in order for the shape of the particles to become significant.

A sphericity factor was proposed that allowed equations that assumed spherical inclusions, such as the Maxwell-Eucken model, to be used for non-spherical shapes. The sphericity factor was related to the ratio of the surface area of the particle to the surface

area of a sphere having the same volume as that particle. In the Maxwell-Hamilton model (Eq. 2.22) the sphericity was accounted for by the *n* parameter.

It was emphasised that the thermal conductivity of a composite of two materials with significantly different component thermal conductivities varied greatly, depending on which phase was continuous and which was discontinuous. It was also pointed out however, that in some practical situations the distinction between the component phases was not obvious, especially when the inclusions of the apparent dispersed phase came into contact with neighbours.

2.4.1.5 Brailsford & Major (1964)

Brailsford & Major (1964) were concerned with the prediction of the thermal conductivity of multi-phase materials, using porous sandstone as a case study. They considered five models in their investigation, the Series model (Eq. 2.7), Parallel model (Eq. 2.8), both forms of the Maxwell-Eucken model (Eqs. 2.20 and 2.21) and the Landauer-EMT model (Eq. 2.26). The Series and Parallel models were chosen since they predicted the maximum and minimum bounds of the effective thermal conductivity (Wiener bounds) and the Maxwell-Eucken model was chosen because it distinguished between the components, one being continuous and the other being dispersed. The Landauer-EMT model was chosen as an 'average' model because both components were treated equally, and the predictions of the model always lay between the predictions of the two forms of the Maxwell-Eucken model. They found that the conductivity of the sandstone was not predicted with sufficient accuracy by any of the five models considered; however a good fit was produced by modifying the Maxwell-Eucken model with the introduction of an adjustable parameter.

2.4.1.6 Cheng & Vachon (1969)

Cheng & Vachon (1969) performed a theoretical study on the effective thermal conductivity of two and three phase solid heterogeneous mixtures. The study built on previous work by Maxwell, Fricke, Tsao, and Hamilton. Hamilton (cited in Cheng & Vachon, 1969) had divided heterogeneous materials into four groups according to the

magnitude of the ratio of component thermal conductivities and which component (continuous or dispersed) had the higher thermal conductivity:

1. $k_1/k_2 > 100$
2. $k_2/k_1 > 100$
3. $1 < k_1/k_2 < 100$
4. $1 < k_2/k_1 < 100$.

Cheng & Vachon's work focused on the 2nd group of materials (i.e. those where the thermal conductivity of the discontinuous phase was more than 100 times greater than the thermal conductivity of the continuous phase), which, based on Hamilton's conclusions, were the least suited to predictions from Maxwell-based models. They modified Tsao's approach to come up with a new model (Eq. 2.12).

2.4.1.7 Fidelle & Kirk (1971)

In a study of effective thermal conductivity models for particulate composites, Fidelle & Kirk (1971) examined the issue of whether it was valid to assume uni-directional heat flow or whether it was necessary to consider tri-directional heat flow. They also examined the influence of particle size on effective thermal conductivity. They concluded that the assumption of uni-directional heat flow was not a severe limitation and that the size of the particles was not significant unless the diameter of the particle was greater than 1/10 the diameter of the overall system, in the direction of the heat flow. They also observed that relatively large changes in the thermal conductivity of the particulate phase did not significantly affect the effective thermal conductivity for a given continuous (fluid) phase.

2.4.1.8 Progelhof, Throne & Reutsch (1976)

Progelhof *et al.* (1976) reviewed 35 effective thermal conductivity models and evaluated their predictions for the thermal conductivity of polymer composites against experimental data in the literature. They found that no single model provided accurate predictions for all of the composites they considered.

2.4.1.9 Nozad, Carbonell & Whitaker (1985)

Nozad *et al.* (1985) derived a theoretical model for heat conduction in two-phase particulate systems and compared the predictions of the model to experimental results.

The model contained an empirically determined parameter that related the particle-to-particle contact area to the overall surface area of a particle. The model worked well for systems where the component thermal conductivity ratio was less than 100 but did not work as well when the component thermal conductivity ratio was increased beyond 100. The issue of accounting for particle-particle contact was identified as being of key importance in the accuracy of predictive models for particulate systems.

2.4.1.10 Farouki (1986)

Farouki (1986) reviewed and evaluated several models for predicting the thermal conductivity of soils. The accuracy of the models depended on the type and condition of soil being considered: whether it was frozen or unfrozen, the degree of saturation, the coarseness of the grains, and the quartz content of the soil. No single model gave accurate predictions for all soils under all conditions.

2.4.1.11 Tanaka & Chisaka (1991)

Tanaka & Chisaka (1991) derived a model for the effective thermal conductivity of gas and solid mixtures (such as dry, packed beds). Their model was based on a simple geometric structure, and the degree of particle-to-particle contact was related to the void fraction (unlike the approach of Nozad *et al.*, 1985, who determined the particle contact empirically). The model required that the discontinuous phase (whether solid or gaseous) be specified and hence, similar to the Maxwell-Eucken model, the model had two different equations, depending on whether the solid phase was continuous or discontinuous. The model was applied to systems with discontinuous solid phases and provided similar predictions to the model proposed by Kunii (Kunii & Smith, 1960, see also Section 2.4.1.3).

2.4.1.12 Every, Tzou, Hasselman & Raj (1992)

In a study on the effective thermal conductivity of zinc-sulphide/diamond composites Every *et al.* (1992) discovered that the overall thermal conductivity was increased by large particles of diamond, but decreased by small particles of diamond.

2.4.1.13 Krach & Advani (1996)

Krach & Advani (1996) set up finite element models to investigate the effect of air voids on the effective thermal conductivity of carbon/carbon-fibre composites. They considered spherical, oval and crack-shaped voids both parallel and perpendicular to the fibre, in increments of 5% up to a total void volume of 25%. They observed a small dependence of the effective thermal conductivity on the void shape but no dependence on the size of the voids.

2.4.2 Studies on the Effective Thermal Conductivity of Porous Food Products

2.4.2.1 Murakami &Okos (1989)

Murakami & Okos (1989) performed a study on the effective thermal conductivity of un-frozen, porous food products. They had observed that there was no general model that was suitable for predicting the thermal conductivity of porous foods and noted that this was, in part, due to the inherently variable nature of the structures of porous foods. They used thermal conductivity data for selected powdered and granular food products to evaluate the accuracy of nine effective thermal conductivity equations. The equations that were evaluated included:

- Series model, Eq. (2.7)
- Parallel model, Eq. (2.8)
- Krischer's model, Eq. (2.10)
- Chaudhary-Bhandari model, Eq. (2.11)
- both forms of the Maxwell-Eucken model, Eqs. (2.20) and (2.21) (note that the equation referred to in Table 2 of Murakami and Okos, 1989, as the "Fluid-continuous" model is identical in form to the Maxwell-Eucken equation in the same table, Eq. 2.20 but with different designations of which component of the food is the continuous phase, while the "Solid-continuous" model is equivalent to Eq. 2.21, see Brailsford and Major, 1964)

- Landauer's EMT model Eq. (2.26) (referred to as the "Random Distribution" model in Murakami and Okos, 1989, but is equivalent to Landauer's model, see Brailsford and Major, 1964)
- Kopelman's isotropic model, Eq. (2.28).

The thermal conductivity data for the foods were taken from the literature and from measurements performed by the authors using the thermal conductivity probe method. The moisture contents of the foods considered ranged between 0 and 39% on a weight basis and the porosities ranged between 0.08 and 0.83. Because some of the predictive models considered were for two-component systems only, the chemical components (i.e. water, fat, protein, soluble carbohydrate, fibre, ash and air) were considered to be part of either a continuous phase or a discontinuous phase. The conductivities of each phase were calculated from the conductivities of the components within that phase using either the Series or Parallel models.

None of the predictive models were found to provide accurate predictions for all types of foods over a range of porosities and moisture contents. However, all the measured data were found to lie within the bounds of the Series and Parallel model predictions and based on this observation it was suggested that models that were combinations of the Series and Parallel models (e.g. the Krischer and Chaudhary-Bhandari models) would provide good predictions. A new model was proposed based on Krischer's model, in which the f parameter was related to the moisture content and porosity of the food product by using a regression analysis of some of the thermal conductivity data (as described in Section 2.2.6.3). Some of the thermal conductivity data collated by the authors were not used in the regression analysis since their reliability was questioned.

For the range of powdered foods and compositions considered, the new model provided better thermal conductivity predictions for powders than any of the other models examined, although some of the individual errors were as high as 28%. The model did not provide good predictions for foods consisting of large grains (such as rice, corn grains and shredded coconut). Foods with internal pores were not considered.

In deriving their model the authors acknowledged that, for the sake of simplicity, certain important factors relating to porous phase had not been considered. These factors included the pore size, particle size distribution and the degree of particle-particle contact.

2.4.2.2 Sakiyama & Yano (1990)

Sakiyama & Yano (1990) performed conductivity measurements at two different temperatures on air-impregnated gels using a method that enabled the moisture and air contents of the gels to be varied independently of each other. The experimental results were compared to predictions from the Parallel model (Eq. 2.8) and the Maxwell-Eucken model (Eq. 2.19). Some of the experimental conductivity values for the high water content gels at the higher temperature (40°C) were higher than the theoretical limit imposed by the Parallel model. It was suggested that, in these instances, evaporative heat transfer effects, from water diffusion across the pores, were being measured along with conduction. A modified form of the Maxwell-Eucken equation was proposed to account for the evaporative heat transfer effects and was tested in a later study (Sakiyama *et al.* 1999).

2.4.2.3 Lin (1994)

In the course of studying the prediction of chilling times of food products, Lin had observed that no systematic experimentally-based study of the effect of air voids on chilling rates could be found in the literature (Lin, 1994). In order to shed some light on the subject some simple experiments were performed. Plastic containers filled with diced and grated cheddar cheese were cooled and the thermal conductivity was back-calculated from the temperature-time data. The void fraction (porosity) within these containers was varied between (0 and 0.5), and the size of the voids was also varied. The results were compared to predictions from eight thermal conductivity models:

- Series model, Eq. (2.7)
- Parallel model, Eq. (2.8)
- Krischer's model, Eq. (2.10)
- Maxwell-Eucken model, Eq. (2.20)
- Levy's model, Eqs. (2.20) and (2.23)

- Landauer's EMT model Eq. (2.25)
- Kopelman's isotropic model, Eq. (2.28)
- Hill *et al.*'s model, Eq. (2.32).

Levy's model and Krischer's model with an f parameter of 0.16 were found to give the best predictions. No significant dependence of effective thermal conductivity on void size was observed. However the uncertainty involved in the thermal conductivity measurements was high, and the uniformity of the distribution of the pores could not be guaranteed.

2.4.2.4 Empirical Studies of the Effective Thermal Conductivity

A number of empirical studies of the effective thermal conductivity of bakery products have been performed (e.g. Unklesbay *et al.*, 1981, Zanoni *et al.*, 1995, Baik *et al.* 1999). The typical approach has been to record how the porosity (or bulk density) and thermal conductivity varied during the baking process in order to derive an empirical thermal conductivity correlation as a function of porosity, temperature and moisture content. As with other purely empirical studies, the application of the results would be limited to situations closely resembling the original situation that was used to derive the model.

2.5 Summary of Literature Review

- Accurate thermal conductivity data is of vital importance to the understanding and design of industrial thermal processes.
- Effective thermal conductivity models must be used when reliable thermal conductivity data are unavailable.
- Porous foods pose greater difficulties for thermal conductivity predictions than non-porous foods because of the significant influence air has on the food's structure, and because the thermal conductivity of air is so much lower than that of other food components.

- The thermal conductivity literature contains a myriad of thermal conductivity models that have been proposed for many different applications — the fact that new models are still being derived indicates that the existing effective thermal conductivity knowledge is far from complete.
- Reviewers who have performed model validation exercises have concluded that no single model may be relied upon for accurate thermal conductivity predictions for all types of heterogeneous materials (Pregelhof *et al.*, 1976, Murakami & Okos, 1989, Farouki, 1986), and it is clear that the task of predicting effective thermal conductivities requires consideration of the material and thermal process(es) involved.
- Several important factors that must be considered in the selection of an appropriate model include:
  1. the relative magnitudes of the component thermal conductivities
  2. material composition
  3. material structure
  4. the temperature(s) involved in the thermal process
  5. the presence of fluid flow.
- From a thermal conductivity perspective porous material structures may be grouped as shown in Fig. 2.3:

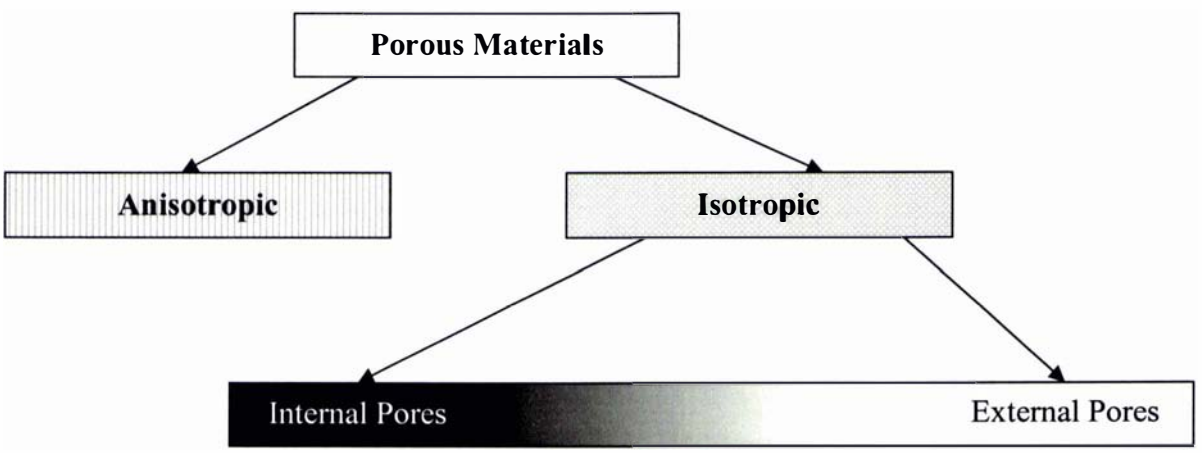

Figure 2.3: Classification of Porous Materials

- For anisotropic materials the orientation of the material components with respect to heat flow has a critical influence on the effective thermal conductivity.
- For isotropic materials the size, shape, distribution and contact/interaction of the pores (or particles) have potential to influence the effective thermal conductivity.
- The continuous phase of a material has a greater influence on thermal conductivity than the discontinuous phase, although for some materials it is difficult to distinguish which component is which.
- The study of the effective thermal conductivity of porous foods has not received much attention and it is unclear which models should be used for the prediction of effective thermal conductivities of porous food systems (refer to Fig. 2.2).

Chapter 3: Preliminary Considerations

Preliminary Considerations

From the food engineering texts encountered in the literature review, a general observation was that sections devoted to the prediction of effective thermal conductivity of foods typically provided a list of effective thermal conductivity models, but little in the way of guidelines about the suitability of the models for different applications. The literature did not appear to contain any clear guidelines for selecting appropriate model(s) for the prediction of the effective thermal conductivity of porous foods.

Murakami & Okos (1989), Sakiyama & Yano (1990), and Lin (1994) all identified a need to increase the understanding of the influence of porosity on the thermal conductivity of a food product. The study performed by Murakami & Okos was, perhaps, the most extensive study to date on the effective thermal conductivity of porous foods. However, as the authors themselves pointed out, the model produced by the study did not work well on foods for which experimental data was not included in the data-regression exercise. The data-regression approach used in deriving their thermal conductivity model did not provide much insight into the relative influences of different porosity-related variables since the regression constants used in the model could not easily be related to physical quantities.

By isolating and examining the influence of the void fraction and the void size on thermal conductivity, the study performed by Lin adopted a more systematic approach to porosity than that of Murakami & Okos. However, Lin's study was relatively restricted, being a side issue to the main focus of his work, and the uncertainties involved in the measurements were high. Both studies were concerned with external voids, and, according to the literature, the results in terms of model recommendations were not necessarily applicable to foods with internal voids due to the difference in the relative contributions effective thermal conductivity of the continuous and discontinuous phases (see Section 2.3). Krischer's model (Eq. 2.10) was attractive to Murakami & Okos and Lin because of the adjustable parameter that allowed the model to be fitted to data anywhere within the Wiener bounds (i.e. the Series and Parallel models, refer to Section 2.3.8).

Neither study, however, considered other models with adjustable parameters, and it was unclear whether the data followed the basic shape of the Krischer model or whether a different model with an adjustable parameter might fit the results better over a range of volume fractions.

The study performed by Sakiyama & Yano (1990) was concerned with internal voids (pores), and the method of experimentation and analysis that was employed made it easy to examine the various factors that influenced the thermal conductivity (particularly the graphical display of results and the ability to vary moisture content and porosity independently). However, the void phase was characterised by its volume fraction only, and the literature has indicated that the volume fraction alone will not necessarily account for the influence of the void phase on the thermal conductivity. In addition, the number of experimental data points was less than would be desirable for the purposes of model evaluation.

Missing from previous work was a systematic study of the porosity related variables that have been identified in the literature as having the potential to influence the thermal conductivity, and an extensive and reliable experimental data-set of thermal conductivities over a range of porosity in a form that was convenient for evaluating effective thermal conductivity models. There was also a need for a clear set of guidelines for selecting appropriate effective thermal conductivity models for particular applications.

Therefore the objectives of this study were:

1) to set up an experimental apparatus that allowed thermal conductivities of experimental samples to be measured, and to prepare samples of food analogues that had accurately controlled component volume fractions
2) to vary the porosity, mean pore size, and component thermal conductivity ratio of the food analogue samples in order to examine the influence each variable has on the effective thermal conductivity
3) to set up numerical models to simulate different food structures, and to examine the influences of porosity, pore size, pore shape, and pore/particle contact in

order to examine the influence each variable has on the effective thermal conductivity, and to determine which variables are most significant

4) to evaluate models from the literature based on the results of the experiments and the numerical simulations

5) to propose a generalised framework for the analysis of heat conduction in heterogeneous materials

6) to propose general guidelines for the selection of the most suitable effective thermal conductivity models for foods, in particular foods containing significant porosity

7) to test the conclusions drawn from the model validation exercise on real food systems.

Since the primary focus of this study was the influence of a gaseous phase (whether internal or external) on thermal conduction, the foods and food analogues involved in the experiments were considered to be two-phase systems composed of a gaseous phase and a condensed phase (i.e. a solid, a liquid or a solid/liquid mixture), and experiments were planned with the aim of minimising possible heat transfer by modes other than conduction. It was assumed that void spaces within foods are small (<5mm), that temperatures involved are low (<25°C) and that only bound moisture exists within the food product, in order that conduction is the only significant mode of heat transfer. The study was limited to the investigation of porous foods that are isotropic on a macroscopic scale.

Heat transfer by convection and radiation and as a result of moisture migration may be significant in porous foods, particularly as the temperature is increased. In addition, anisotropy and ice formation will also have significant effects on the heat transfer within porous foods. However, full consideration for each possible heat transfer effect other than conduction was beyond the scope of this work, although a brief discussion of the significance of these issues is made in Section 7.5 of Chapter 7.

Chapter 4: Experimental Data Collection

4.1 Introduction

4.1.1 Objectives

The aim of the experiments described in this chapter was to produce thermal conductivity data that could be used to evaluate effective thermal conductivity models. The experiments also examined the influences of porosity, mean pore size, and component thermal conductivities on effective thermal conductivity.

4.1.2 Experimental Strategy

Of the studies on the thermal conductivities of porous foods undertaken previously (see Section 2.4.2 of Chapter 2), the work of Sakiyama & Yano (1990) stood out because their approach allowed a systematic investigation of the effects of individual variables (moisture content and porosity) on the thermal conductivity. A similar approach was adopted in this study to examine the relative influences of certain porosity-related variables. Since the emphasis of these experiments was on the effect of porosity on the thermal conductivity (as distinct from other food components), it was convenient for the experimental samples to be considered as two-component materials comprised of a gasous phase and a condensed phase.

4.1.3 Experimental Materials

Real foods are not well suited to the manipulations of structure and composition that were desirable for the type of experiments being performed in this study. Because of the versatility they offer, food analogues, which are materials having similar properties to those of real foods, have often been used in heat transfer experiments (including Sakiyama & Yano, 1990). Due to the importance of the component thermal conductivity ratio to the prediction of effective thermal conductivity, as was discussed in Sections 2.3.9

and 2.4.1 of Chapter 2, a food analogue for these experiments required component thermal conductivities as close as possible to the real food components being considered.

The porous foods that were the focus of this study were modelled by suspensions of expanded polystyrene (EPS) beads in gels made from guar gum. The use of EPS beads made it possible to vary the volume fraction of the 'gasous' phase and also allowed the mean 'pore' size to be varied in a controlled manner. Guar gum is a polysaccharide which is extracted from the guar plant. It is used extensively in the food industry as a thickener or emulsifier in a wide range of products including ice-cream, frozen desserts, salad dressings, sauces and pet foods (Kirk-Othmer, 1994). It was chosen as a gelling agent because it formed a very firm gel with the addition of trace amounts of borax, and could be prepared at room temperature, unlike many other gelling agents such as agar. The guar gels had similar properties to water (see Table 4.1), which has the highest thermal conductivity of the major food components. This mixture had the highest component thermal conductivity ratio that would be encountered with non-frozen foods, and hence represented a worst case scenario, in the sense that the thermal conductivity bounds described in Section 2.3.9 of Chapter 2 were furthest apart, and hence the uncertainty involved in the thermal conductivity predictions is greatest.

Experiments were also performed on samples containing squat aluminium cylinders suspended in guar gel. While this mixture was not analogous to any food product, it provided a contrast to the EPS/guar-gel samples in that the thermal conductivity of the dispersed phase was higher than the conductivity of the continuous phase. These experiments were performed in order to examine the relative contributions of the continuous and dispersed phases to the overall thermal conductivity of a material.

4.2 Thermal Conductivity Measurement

4.2.1 Measurement Techniques

The thermal conductivity of a material may be measured by a number of methods that can be divided into two categories: steady state methods, and transient methods. The measurements may be comparative (i.e. relative to a material of known conductivity) or absolute. The choice of measurement technique is often determined by the material for which measurements are required. Thermal conductivity measurement methods that have been used for food materials have been reviewed by Nesvadba (1982), Murakami & Okos (1989) and Rahman (1995). Selected commonly used methods are discussed briefly below.

4.2.1.1 Steady State Methods

Steady state methods use apparatus that are constructed in such a way that measurements are made according to a direct application of Eq. (2.2), i.e. a constant heat flow between two constant temperatures is imposed over a known heat transfer area across a sample of known thickness. This method allows for the most direct thermal conductivity measurements since only the fundamental quantities from Eq. (2.2) are involved, and hence these methods have the potential for high accuracy. However, steady-state apparatus require lengthy equilibration periods (several hours) and the thickness of the measurement samples must be very small by comparison with the dimensions of the area of heat flow (in order to minimise edge effects), which is often highly impractical with food products. As a result, steady state techniques are not usually the preferred measurement choice for food products (Rahman, 1995), although devices such as the guarded hot-plate have been used (e.g., Pham & Willix, 1989).

4.2.1.2 Transient Methods

A method developed by Fitch (cited in Nesvadba, 1982), has been used to measure thermal conductivities, often of low conductivity materials. A material sample is sandwiched between a heat source and a heat sink, one side of which is kept at constant

temperature while the time-temperature history of the other side is recorded. The method is sometimes referred to as quasi-steady state because it is assumed that a steady temperature profile has been developed in the sample, which is unlikely in reality. The original Fitch apparatus has been modified and developed several times, and has been used for a number of different foods (Rahman, 1995). However, the shape of the samples for the Fitch-type apparatus is constrained, being required either to fill a cavity or fit between two plates, depending on the exact design of the apparatus. This constraint limits the suitability of the Fitch apparatus for some applications.

Another commonly used transient method is the line heat-source method, also known as the thermal conductivity probe (Murakami & Okos, 1989). In this method a heat source (i.e. the probe) is introduced into a sample which is a much larger body (assumed to be infinite). The temperature change of the probe that results from a constant rate of heating is recorded. The rate of temperature change is proportional to the thermal conductivity of the sample. The fact that the conductivity probe does not have to surround the test material makes it attractive for irregularly shaped objects. Rahman (1995) states that the line-source method is the most commonly used device for measuring the thermal conductivity of biological materials, including foods. However, the conductivity probe makes local measurements rather than overall measurements, and hence the measurements may be sensitive to the position of the probe within a non-homogeneous sample.

4.2.2 Method of Measurement Employed in this Study

By comparison with most thermal conductivity measurement samples, the food analogue samples that were used for these experiments were necessarily large in order to ensure that the distribution of the EPS beads, which were dispersed randomly in the guar-gel, would be uniform. The size of the samples precluded the use of steady state methods or the Fitch apparatus. The conductivity probe was not suitable because of the likelihood that local measurements might differ significantly from overall measurements.

Instead a comparative method was used that involved the cooling of two spheres side by side in a well-stirred ice/water bath (see Fig. 4.2 for a diagram of the set-up). One sphere contained the test material (suspension of EPS beads in guar-gel) and the other contained a reference material of known thermal conductivity (guar-gel). The thermal conductivities of the samples were back-calculated from the temperature-time data of the cooling spheres. The use of spherical sample containers avoided the undesirable edge effects that are associated with other geometries, and allowed for uni-dimensional heat transfer calculations.

A disadvantage of using a non-steady state method was that the temperature dependence of the thermal conductivities of the materials involved was not determined, and instead temperature-averaged conductivity values were measured. The temperature dependencies of the components of the material investigated in this study were linear in the range investigated, increasing as the temperature was increased (see Appendix C). Since the temperature dependencies of the conductivities of the components were increasing in the same direction and the measurement technique was comparative, the effect of this linear dependence was minimised, and hence no corrections for the temperature variations were made in the calculations. The samples were cooled from approximately 20°C to approximately 1°C and so, due to the linear temperature dependence of the materials, the midpoint value (i.e. 10°C) was a representative temperature and all physical property data required in the calculations were taken at this temperature (see Table 4.1).

4.2.2.1 Theoretical Basis of the Measurement Technique

The method was based on the analytical solution for the centre temperature of a sphere being cooled with convection boundary conditions as described by Eq. (4.1):

$$\frac{T-T_\infty}{T_0-T_\infty}=\sum_{i=1}^{\infty}\frac{2Bi\left(\beta_i^2+(Bi+1)^2\right)\sin\beta_i}{\beta_i\left(\beta_i^2+(Bi+1)^2\right)}\exp(-\beta_i^2 Fo) \qquad (4.1)$$

Fo is known as the Fourier Number and may be thought of as a dimensionless time variable (see Eq. 4.6), *Bi* is known as the Biot Number, and β coefficients are the roots of the transcendental equation:

$$\beta_i \cot \beta_i - (Bi + 1) = 0 \tag{4.2}$$

The Biot Number is the ratio of the external heat transfer resistance (convection) to the internal heat transfer resistance (conduction):

$$Bi = \frac{hR}{k} \tag{4.3}$$

where h is the film heat transfer coefficient, R is the radius of the sample container, and k is the thermal conductivity of the sample.

It has been shown (Appendix C of Holman, 1992) that for $Fo > 0.2$ the infinite series in Eq. (4.1) may be approximated by the first term alone with an error of less than 1%, hence:

$$\frac{T - T_\infty}{T_0 - T_\infty} \approx f_1(Bi, \beta_1) \exp(-\beta_1^2 Fo) \tag{4.4}$$

When the temperature-time histories of the cooling spheres were plotted on a logarithmic scale, the linear portion of the graph could be fitted by:

$$\ln\left(\frac{T - T_\infty}{T_0 - T_\infty}\right) = \ln Y = B - \sigma t \tag{4.5}$$

where σ was the slope of the linear portion of the graph. The quantity Y is sometimes called the *fractional unaccomplished temperature change*. By comparing (4.4) with (4.5):

$$\sigma = \frac{k\beta_1^2}{\rho c R^2} \tag{4.6}$$

given that:

$$Fo = \frac{kt}{\rho c R^2} \tag{4.7}$$

Eq. (4.6) may be rearranged to give:

$$k = \frac{\sigma \rho c R^2}{\beta_1^2} \tag{4.8}$$

Because the measurement of the thermal conductivity of the test sample (k_e) was relative to that of the control sample (k_c) it was convenient to perform the calculations for the two spheres relative to each other:

$$\frac{k_e}{k_c} = \frac{\sigma_e}{\sigma_c}\frac{\rho_e}{\rho_c}\frac{c_e}{c_c}\frac{R_e^2}{R_c^2}\frac{\beta_c^2}{\beta_e^2} \tag{4.9}$$

Hence the relative effective thermal conductivity (k_e/k_c) measured by this technique was the product of five ratios. The β coefficient was a function of Bi which was in turn a function of k and so the calculation of k_e/k_c was performed iteratively. Other than c_e, all the variables in Eq. (4.9) were measured. Due to the impracticality of performing specific heat capacity measurements for each test sample, c_e was calculated from the weighted mean of the specific heats of the components according to Eq. (4.10):

$$c_e = \sum_i \frac{v_i \rho_i}{\rho_e} c_i \tag{4.10}$$

where the subscript i referred to the individual components of the material.

4.3 Apparatus and Procedure

4.3.1 Apparatus

4.3.1.1 Sample Containers

The sample containers were comprised of two flanged hemispheres that were spun from 2 mm thick aluminium (see Fig. 4.1). Two sample container sizes were used; the larger containers had inside radii of approximately 101 mm and the smaller containers had radii of approximately 75 mm (see Appendix C). The hemispheres were sealed together, with silicone RTV sealant, and, in the case of the larger spheres, were held together by bolts and nuts.

4.3.1.2 Temperature Measurement

The samples' temperatures were measured by copper-constantan (T-type) 0.5 mm gauge thermocouples placed at the centres of the containers.

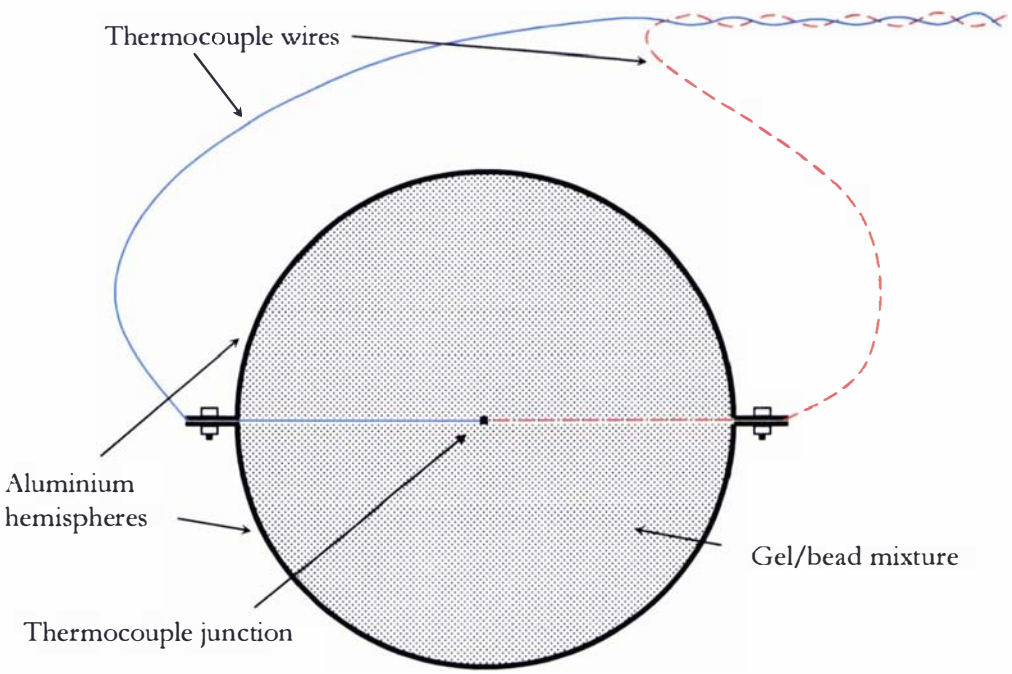

Figure 4.1: Sample Containers and Thermocouple Placement

The readings were logged by a *Hewlett Packard*™ 3497a Data Acquisition Unit. The two thermocouple wires were attached at the tips and were held in place by tension in such a way that the junction lay at the centre of the sphere (see Fig. 4.1).

4.3.1.3 Ice/Water Bath

The bath was 800 mm long by 715 mm wide and 500 mm deep. A gauze screen partitioned the ice section from the rest of the bath (see Fig. 4.2). A small pump (0.4 -1.3 m^3/hour) recirculated the water over the ice. The bath was well mixed to ensure a uniform temperature distribution throughout the bath and to provide high heat transfer coefficients at the surface of the sample containers.

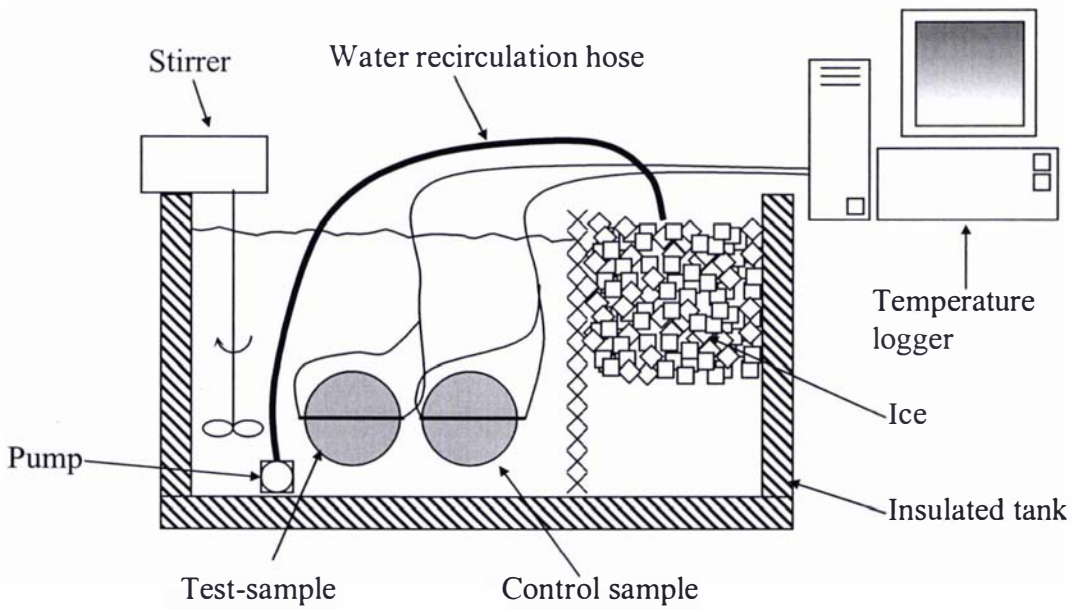

Figure 4.2: Experimental Apparatus

4.3.1.4 Measurement of Heat Transfer Coefficients

Heat transfer coefficients within the bath were measured with the aid of a 37.7 mm diameter copper sphere. The copper sphere was cooled in the bath while a thermocouple placed at its centre recorded the temperature, and the heat transfer coefficient was determined from the temperature-time data according to Eq. (4.11):

$$\frac{T - T_\infty}{T_0 - T_\infty} = \exp\left(-\frac{hAt}{mc}\right) \tag{4.11}$$

where m was the mass of the copper sphere, c was the specific heat capacity of copper, A was the surface area of the sphere and h was the heat transfer coefficient. Equation (4.11) was suitable as an approximation of Eq. (4.1) because the thermal conductivity of copper was high (375 W m^{-1} K^{-1}) and hence Bi was low (i.e. the resistance to heat transfer was limited by the convection from the surface of the sphere to the bath, rather than conduction from the centre of the sphere to the surface). This method allowed heat transfer coefficient measurements to be made anywhere within the bath. The heat transfer coefficients measured by this technique varied between 1100 and 2000 W m^{-2} K^{-1} depending on the position within the bath.

Since the copper sphere had a smoother surface and a smaller diameter than the aluminium sample containers, the heat transfer coefficients at the surface of the aluminium sample containers would not necessarily be the same as those measured by the copper sphere, although it would be reasonable to assume that they would be of similar magnitude. Since the h measurements obtained by the copper sphere were of sufficient magnitude that it could be assumed that the resistance to convection heat transfer from the surface of the sample containers was negligible by comparison with the resistance to conduction through the sample materials, relatively large fluctuations in the surface heat transfer coefficient ($\pm$200 W m^{-1} K^{-1}) would have had negligible influence on the cooling rates of the sample. This point is explained further in the uncertainty analysis (see Section 4.4.1.2).

4.3.2 Experimental Datasets

Table 4.1 shows the relevant thermal properties of the materials involved (see also Appendix C). Four different experimental datasets were collected from different types of samples:

- ***Dataset 1***: 2 mm EPS beads in guar-gel contained in 101 mm radius aluminium spheres
- ***Dataset 2***: 6.5 mm EPS beads in guar-gel contained in 75 mm radius aluminium spheres
- ***Dataset 3***: 25 mm EPS beads in guar-gel contained in 75 mm radius aluminium spheres
- ***Dataset 4***: 6.5mm diameter, 6mm length aluminium cylinders in guar-gel contained in 75 mm radius aluminium spheres

	k/(W m^{-1} K^{-1})	ρ/(kg m^{-3})	c/(kJ kg^{-1} K^{-1})
Guar-gel	0.60[a]	1010[a]	4.15[a]
Air	0.025[b]	1.24[b]	1.006[b]
2mm EPS	0.035[c]	35.4[a]	1.21[b]
6.5mm EPS	0.037[c]	16.7[a]	1.21[b]
25mm EPS	0.035[c]	33.2[a]	1.21[b]
Al cylinders	209[c]	2680[a]	0.896[b]

[a]measured by author [b]taken from the literature [c]manufacturer's data

Table 4.1: Physical properties at a midpoint temperature value of 10°C of materials used in experiments (refer to Appendix C for more detail)

4.3.3 Sample Preparation

4.3.3.1 Samples Containing 2 mm and 6.5 mm EPS beads

The guar-gel contained 4% guar powder (mass basis), obtained from *Germantown International Limited*, 0.04% borax ($Na_2B_4O_7 \cdot 10H_2O$) with the remaining amount being

water. The samples were prepared in a bowl with a whisk-type agitator (*Kenwood Chef Excel*™ houschold cake mixer). The borax was dissolved in the water before the guar powder was added, since it was observed that the gels produced from the simultaneous solution of the borax and guar powder did not always set properly.

Once all the guar powder had been mixed into the water, a small quantity of EPS beads was added to the mixture. At first the beads floated on top of the mixture, but as the gel became thicker, the beads began to submerge and disperse throughout the mixture. More beads were slowly added to the mixture while under constant agitation. Once all the beads had been added, agitation was performed by hand, since this achieved a better mixing motion for that particular step of the process than could be achieved by the whisk agitator. Once the gel had set sufficiently, the mixture was transferred to the sample containers.

The mixing process in the preparation of these samples required a certain degree of judgment to determine the appropriate times to add the beads and to transfer the mixture to the sample containers, but this was developed with practice. The uniformity of the distribution of the EPS in the food analogues containing 2 mm beads was tested by removing samples from different parts of the mixing vessel and determining the mass fraction of EPS beads in the different samples. The standard deviation of the mass fraction of EPS beads in 5 samples was within 2% of the mean value of 0.00804, which was deemed an acceptable degree of uniformity. In addition, the samples were examined when the experimental run had been completed to visually assess the uniformity of the distribution. In some samples, the gel had not been allowed sufficient time to set and the EPS beads had floated to one end of the sphere. Data collected from such samples were rejected. The samples containing the 6.5 mm beads were mixed in the same vessel using the same agitator as the 2 mm beads and so it was assumed that the same degree of uniformity was achieved. The 6.5 mm bead samples were also subjected to a visual assessment of uniformity on completion of each run.

4.3.3.2 Samples Containing 25 mm EPS balls

Due to the size of the 25 mm EPS balls it was not possible to use the same preparation method that was used for the samples containing 2 mm beads and the 6.5 mm beads. Instead the gel ingredients were mixed without the EPS and the mixture was allowed to set partially, before the EPS balls were placed in the gel by hand. This procedure involved an element of trial and error in order to time the addition of the beads so that the beads did not float, but before the gel was too firm. Because the number of beads involved was relatively small (between 14 and 126, depending on the desired porosity) it was difficult to guarantee a uniform distribution by a random mixing process, however the deliberate positioning of the beads with even spacings between neighbours approximated a uniform distribution.

4.3.3.3Samples Containing Aluminium cylinders

The samples containing aluminium cylinders required a similar preparation approach to that used for the 25 mm EPS balls because the timing of the addition of the aluminium to the gel was critical in order to achieve suspension. Again, the process involved some trial and error.

4.3.3.4 Control Samples

The control spheres for all the experiments contained guar-gel with the same ingredient proportions as were used in the test samples (Section 4.3.3.1). For the control samples the gel mixture was poured into the sample containers while still in the liquid state, to allow for good thermal contact of the gel to the surface of the container.

4.3.4 Procedure

The samples were allowed to reach thermal equilibrium overnight before being placed in the stirred water bath and cooled from approximately 20 °C to approximately 1 °C. The bath temperature was measured by a T-type thermocouple (copper/constantan) and was recorded at regular time intervals, along with the sample temperatures. The larger sample containers (101 mm radius) were cooled for approximately 8 hours, while the smaller

sample containers (75 mm radius) were cooled for approximately 3½ hours. There was room in the bath for two of the larger sample containers only; however there was room for three of the smaller sample containers (two test samples and one control sample), and hence two measurements could be performed per experimental run.

The ice/water bath was sufficiently agitated that the *Bi* values were high (150 – 800) for the EPS/guar-gel experiments and hence variations in heat transfer coefficient were not significant for these samples. For this reason heat transfer coefficient measurements were made for selected runs only, for samples containing EPS. However, *Bi* was lower (13 – 140) for the aluminium/guar-gel experiments, hence variations in the heat transfer coefficient were more significant and heat transfer coefficient measurements were performed for each run. The heat transfer coefficient was measured in five different locations around the sample containers, and the average value was used in calculations.

4.3.5 Calculations

Two quantities were calculated from the measurements that were performed: the relative effective thermal conductivity (k_e/k_c) and the volume fraction of the dispersed phase (v_2, the EPS or aluminium). The relative effective thermal conductivity was calculated from Eq (4.9) as described in Section 4.2.2. Unfortunately it was impossible to prepare the test samples containing EPS without the entrainment of a certain amount of air. While the quantity of EPS beads added to the mixture could be controlled, the amount of air that was entrained depended on the mixing process itself and varied from sample to sample. The volume fractions were calculated from the densities of the components and the final density of the sample itself as follows, starting with a mass balance of the components in the sample container:

$$m_e = m_{air} + m_{EPS} + m_{gel} \tag{4.12}$$

where m was the mass of the component. Substituting $m = \rho V$ into Eq. (4.12):

$$\rho_e V_e = \rho_{air} V_{air} + \rho_{EPS} V_{EPS} + \rho_{gel} V_{gel} \tag{4.13}$$

It was assumed that the densities of the components were the same before and after they were combined in the sample, i.e.:

$$V_e = V_{air} + V_{EPS} + V_{gel} \tag{4.14}$$

and:

$$v_i = V_i / V_e \tag{4.15}$$

Equation (4.13) and Eq. (4.14) were divided by V_e which gave:

$$\rho_e = \rho_{air} v_{air} + \rho_{EPS} v_{EPS} + \rho_{gel} v_{gel} \tag{4.16}$$

and

$$1 = v_{air} + v_{EPS} + v_{gel} \tag{4.17}$$

In order to determine the component volume fractions, one more independent equation was required. Relying on the assumption expressed earlier:

$$\frac{V_{EPS}}{V_{gel}} = \frac{v_{EPS}}{v_{gel}} = \varphi \tag{4.18}$$

where φ was constant having been set in the preparation of the test sample. Rearranging Eq. (4.17) and Eq. (4.18) and substituting Eq. (4.18) into Eq. (4.17) gave:

$$v_{air} = 1 - \varphi v_{gel} - v_{gel} \tag{4.19}$$

Substituting Eq. (4.18) into Eq. (4.16) gave:

$$\rho_e = \rho_{air} v_{air} + \rho_{EPS} \varphi v_{gel} + \rho_{gel} v_{gel} \tag{4.20}$$

Using (4.19) to eliminate v_{air} in (4.20) and rearranging for v_{gel}:

$$v_{gel} = \frac{\rho_e - \rho_{air}}{\rho_{EPS}\varphi + \rho_{gel} - \rho_{air}(1+\varphi)} \tag{4.21}$$

v_{air} and v_{EPS} were then calculated from Eq. (4.18) and (4.19). The effective density of the sample (ρ_e) predicted by Eq. (4.16) could be compared against the measured ρ_e values, which provided a means of validating the assumptions made in calculating the values of v_{gel}, v_{air} and v_{EPS} . The discrepancies between the measured and predicted values ρ_e were less than 1%, which suggested that Eqs. (4.21), (4.18) and (4.19) provided sufficiently reliable calculations of the component volume fraction. The volume fractions of the samples containing the aluminium cylinders were calculated in a similar way.

4.4 Results

4.4.1 Uncertainty Analysis

Nesvadba (1982) provided a checklist of possible sources of systematic and random error in thermal conductivity measurements. The items on the list that were relevant to the method used in this work are discussed below.

4.4.1.1 Potential Sources of Systematic Error

Distortion of Temperature Field by Temperature Sensor: The position of the sensor was not moved during the experimental run and any distortion to the temperature field caused by the presence of the sensor was therefore constant throughout the run. The thermocouple wires that were used were 0.5 mm in diameter, and because the wires were attached end-to-end rather than wound together (refer to Fig. 4.1), the maximum

thickness of the wire (including insulation) was approximately 2 mm. The volume occupied by the sensor was negligible by comparison with the sample volume and the radial area occupied by the sensor wires was negligible by comparison with the heat transfer area in the radial dimension. Hence any distortion to the temperature field would affect only a small proportion of the sample and influence only a small proportion of the heat transfer area. It was assumed that negligible error was introduced by the distortion to the temperature field caused by the presence of the temperature sensor.

Conduction Losses through Temperature Sensor: The high thermal conductivity of the thermocouples (385 W m^{-1} K^{-1} for copper, 23 W m^{-1} K^{-1} for constantan) meant that there would undoubtedly have been some conduction losses through the thermocouple wires. However, the cross-sectional area of the wires was approximately 2 x 10^{-7} m^2 per wire, and negligible compared to the total surface areas of the sample containers (approximately 1.3 x 10^{-1} m^2 and 7 x 10^{-2} m^2). Hence, even with their high thermal conductivities, any heat 'leakage' down the thermocouple wires would have been negligible by comparison with the overall heat flow from the samples.

Assumption of Uniform Heat Transfer Rate from Surface of Sample Container: Although the heat transfer coefficient at the surface of the sample containers was not necessarily uniform, the high thermal conductivity of the aluminium containers meant that temperature variation across the container surface would have been small.. In any case, the time required for the container walls to reach the uniform temperature of the bath would have been negligible by comparison with the cooling time of the samples, and so this assumption would introduce negligible uncertainty to the calculations.

Temperature Sensor Calibration: Since temperature differences were used in all the calculations, it was only essential that thermocouples were calibrated relative to each other, since any deviation from absolute temperature would cancel itself. The agreement between thermocouples was, on average, within 0.02°C at 0°C, and hence no adjustments to the readings were made.

Assumption of Uniformity of Temperature within Ice/Water Bath: Thermocouples were placed at different positions within the bath in order to test this assumption. The readings were all within 0.1 °C of each other (cf. average discrepancy in calibration of thermocouples of 0.02 °C).

Cooling Curves Approximated by Straight Lines: It is well known that the transient cooling of an object by convection at its surface follows a first order exponential decay after an initial lag period, which produces a linear trend in the $\ln Y$ vs t plot. In fact, the occurrence of a non-linear trend in the $\ln Y$ vs t plot was used as a basis to reject the results of that experimental run. However, the choice of a $\ln Y$ value of -0.5 as the threshold beyond which linearity was assumed (see Section 4.4.2), was based on visual assessments of the curves and had no theoretical justification. Since the thermal conductivity of the sample was not known, it was not practical to use a value of Fo as a threshold, as recommended in Holman, 1992 (see section 4.2.2.1). Systematic error might have been introduced by the use of $\ln Y = -0.5$ as a threshold rather than a different $\ln Y$ value.

In order to test this potential source of error, the slopes of a typical cooling curve were calculated based on data below $\ln Y = -0.5$, data below $\ln Y = -1$, data below $\ln Y = -1.5$ and data below $\ln Y = -2$. The standard deviation of the calculated slopes was less than 1% of the mean value. The threshold of $\ln Y = -0.5$ was used for both the test sample and the control sample, and since the important result was the ratio of these slopes, any systematic error would largely have cancelled itself. Hence it was unlikely that the use of $\ln Y = -0.5$ as a linearity threshold would have contributed significant error.

4.4.1.2 Potential Sources of Random Error and Precision of Measurements

Uniformity of Initial Temperature Profile of Sample: The required cooling time in the ice/water bath for the larger sample containers was approximately 8 hours, and the cooling time for the smaller containers was approximately 3½ hours. The samples were prepared at room temperature and left overnight (i.e. >12 hours), either in a stirred water bath (in the case of the larger sample containers) or a temperature controlled room in front of an air conditioner vent (in the case of the smaller sample containers). It was

assumed that these conditions would have been sufficient for the samples to reach thermal equilibrium.

Thermal Contact between Sample and Sensor: The guar-gel adhered well to the thermocouple and the samples were prepared in such a way that the thermocouple was packed tightly. Temperature changes during the experiment were slow by comparison with the response time of the thermocouple, so this issue was unlikely to have introduced significant error.

Position of Temperature Sensor: In the calculations described in Section 4.2.2, it was assumed that the thermocouple was positioned at the exact centre of the sphere. However the quantity of interest from the temperature-time data of the experiments was the gradient of the cooling curve rather than the ordinate intercept (refer to Eq. 4.5) and this gradient was, theoretically, independent of the position sensor, so long as it was in contact with the sample material. Therefore small differences in the placement of the sensor near the centre of the sample were unlikely to have had any effect.

Instrumentation: Electronic equipment is susceptible to electromagnetic interference from other electronic devices. Some 'spikes' were observed in the temperature data that was logged, although the cause was unclear. However these spikes in the data were easy to identify, having consistent numerical values that were much greater than the temperatures involved. The frequency of temperature recording was sufficient that these spikes could be removed without losing the shape of the temperature-time curve.

Precision of Density measurements: The density ratio (ρ_e/ρ_c) was measured by weighing the samples in their containers whose volumes were known. The precision of these measurements was estimated as being within 1%.

Precision of the Slope of the Cooling Curve measurements: Since all test samples were cooled alongside a reference sample containing guar-gel, a measurement of σ_c was made each run. The standard deviation in the measurements of σ_c was 2%. Replicate measurements were made for approximately half the samples tested. The discrepancies

between the σ_e values for the replicate measurements in Dataset 1 were all 2% or less but were as high as 3% for some samples in Dataset 2, and 5% for some samples in Dataset 3. Hence a precision in σ_e/σ_c of 2% was estimated for Dataset 1, 3% in Dataset 2 and 5% in Dataset 3. The discrepancies between replicate σ_c values for Dataset 4 (aluminium/gel) were as high as 8% in two measurements, however the majority were 4% or less.

Sample Container Radius measurement: The container radius ratios (R_e^2/R_c^2) for the 101 mm diameter containers used in Dataset 1 were less than 0.5% different from unity. The radius ratio of the 75 mm containers used in Datasets 2, 3 and 4 varied between 0.5 and 4% different from unity, depending on the particular containers used in the measurement. Since the contribution of R_e^2/R_c^2 to the calculation of (k_e/k_c) was minor, any uncertainty in the measurement was considered negligible.

Precision of Beta Coefficient calculation: Based on an average surface heat transfer coefficient of 1200 W m^{-2} K^{-1} the Biot Numbers involved in the Datasets 1 to 3 (EPS/guar-gel) were estimated as ranging between 150 and 800 depending on the size of the sample container and the composition of the sample. Figure 4.3 shows the dependence of the β values on Bi according to Eq. (4.2). It is clear from Fig. 4.3 that the experiments were performed in a region where the β values had a very minor dependence on changes in Bi and were close to the limiting value of π. Hence β_c^2/β_e^2 for the EPS/guar-gel mixtures was always close to unity and the uncertainty in the measurement of this ratio was considered negligible for the EPS/guar-gel samples.

For Dataset 4, Bi values as low as 13 were encountered. From Fig. 4.3 it is clear that the dependence of β_1 on Bi is significant in this region of the curve. The sensitivity of β_1 to changes in Bi is indicated by the numerical value of $\mathrm{d}\,\beta_1/\mathrm{d}Bi$, which is the gradient of the plot shown in Fig. 4.3. For a Bi value of 13, the numerical value of $\mathrm{d}\,\beta_1/\mathrm{d}Bi$ was 0.6% of the numerical value of β_1. Hence 0.6% was used as an estimate of the precision of the β values involved in the calculations of the aluminium/gel experiments.

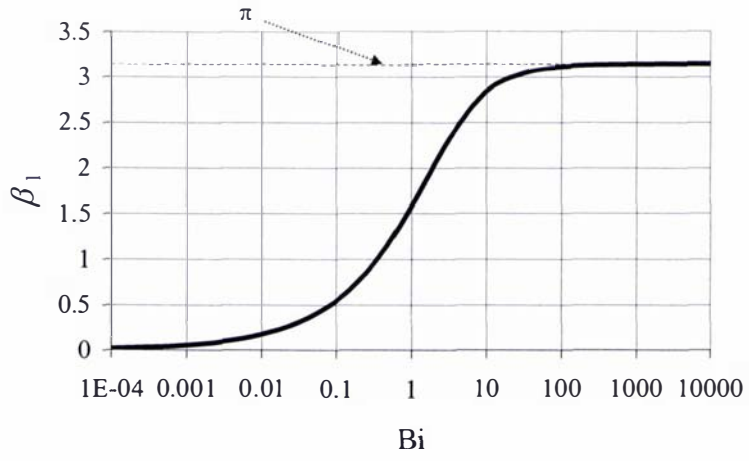

Figure 4.3: Variation of β_1 with Bi according to Equation 4.2

Specific Heat Capacity: Since the specific heat capacity of the guar-gel (similar to that of water) was so much greater than that of air and EPS, $c_e \approx c_c$ and it was expected that c_e/c_c of the EPS/guar-gel samples would remain close to unity. At the highest porosity of any of the measurements performed, the value of c_e/c_c as determined by Eq. (4.10) was 3.5% different from unity, with the majority of values being 2% or less. Since this ratio only made a minor contribution to the calculation of k_e/k_c it was unlikely that any uncertainty (such as the uncertainty associated with the assumption made by Eq. 4.10) in c_e/c_c contributed more than 1% to the overall uncertainty of the EPS/guar-gel results.

Unlike the EPS, the specific heat capacity of the aluminium cylinders was not negligible by comparison to the specific heat of the guar-gel and so the term c_e/c_c had a significant influence on the k_e/k_c calculation. As with the EPS/guar-gel samples, c_e was calculated from Eq. (4.10) based on the densities and specific heats of the sample components. The uncertainties involved in these quantities were comparatively low (1% or less), and so, based on these uncertainties alone, the uncertainty in c_e would not be great. There was also a degree of uncertainty associated with the use of Eq. (4.10), although it was difficult to arrive at a numerical estimate of this uncertainty. The use of Eq. (4.10) for non-frozen

foods has been recommended by previous workers (*ASHRAE Handbook of Refrigeration*, 1998, Rahman, 1995) and it was assumed therefore that it did not introduce a significant amount of uncertainty above the uncertainty involved in the physical quantities.

Volume Fraction: The v_2 values were determined from the densities of the test samples as well as the relative amounts of the non-air ingredients used in preparing the test samples. The estimated precision of these measurements was approximately 1%.

Numerical Estimate of Random Error in Results: Table 4.2 shows a summary of the predicted uncertainty due to random error, based on the individual uncertainties of the quantities involved in the plots of k_e/k_c vs. v_2 (see Eqs. 4.9 and 4.21). The root mean square of the estimated error for each individual variable was used as a measure of the combined error.

	ρ_e/ρ_c	σ_e/σ_c	β_c^2/β_e^2	R_e^2/R_c^2	c_e/c_c	v_2	*Combined error (%)*
Dataset 1	1	2	0	0	1	1	**2.6**
Dataset 2	1	3	0	0	1	1	**3.5**
Dataset 3	1	4	0	0	1	1	**4.4**
Dataset 4	1	8	0.6	0	2	1	**8.4**

Table 4.2: Predicted percentage random error in experimental results

4.4.1.3 Overall Estimate of Uncertainty

The random error associated with experimental measurements may be determined from the scatter in the data. Since the true functional relationship between k_e/k_c and v_2 was unknown, the scatter could only be estimated by assuming a relationship between these variables. This was achieved by fitting a polynomial function to the experimental data and then measuring the scatter about the fitted line. Table 4.3 shows comparisons of the estimated scatter in each dataset, by assuming two different models for each set of data.

	Linear	Quadratic	Cubic	Quartic
Dataset 1	1.8%	1.0%		
Dataset 2	2.6%	2.2%		
Dataset 3	2.7%	1.8%		
Dataset 4			7.1%	4.6%

Table 4.3: Estimated scatter in the experimental results

The uncertainties shown in Table 4.3 are slightly lower than those shown in Table 4.2 but are of similar magnitudes, and hence are in relative agreement.

The systematic error from the potential sources discussed in section 4.4.1.1 was negligible by comparison with the random error and hence would have had little effect on the overall uncertainty by comparison with the random error. Therefore the random error was used as an estimate of the overall uncertainty in the experimental results.

4.4.2 Typical Temperature-Time History of Cooling Samples

Figure 4.3 shows a typical temperature-time curve for the cooling of the test and control samples, plotted as the natural logarithm of the fractional unaccomplished temperature change ($\ln Y$) as a function of time (t) (see Eq. 4.5). The linear best-fit lines were plotted for data values below $\ln Y = -0.5$.

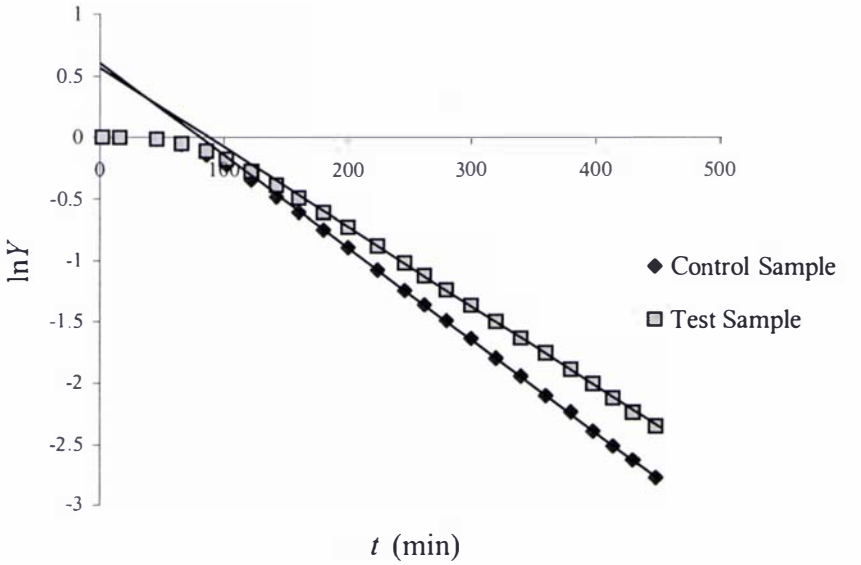

Figure 4.4: Typical temperature-time history of cooling spheres

4.4.3 Expanded Polystyrene/Guar-gel Results

The samples were treated as three-component mixtures when the k_e/k_c values were calculated because the densities of air and EPS or aluminium were sufficiently different that an unacceptable degree of error would have been introduced if they had not been treated separately. However, since the thermal conductivities of air and EPS were similar these two components were treated as a single phase (the void phase, v_2) when the results were plotted graphically. The samples containing aluminium were also treated as three-component mixtures in the calculations, but were treated as two-component mixtures when the results were plotted graphically, aluminium as one phase, and the guar-gel/air mixture as the continuous phase. The results are plotted along with the Wiener bounds (see Section 2.3.9 of Chapter 2).

4.4.3.1 Experimental Results for Dataset 1

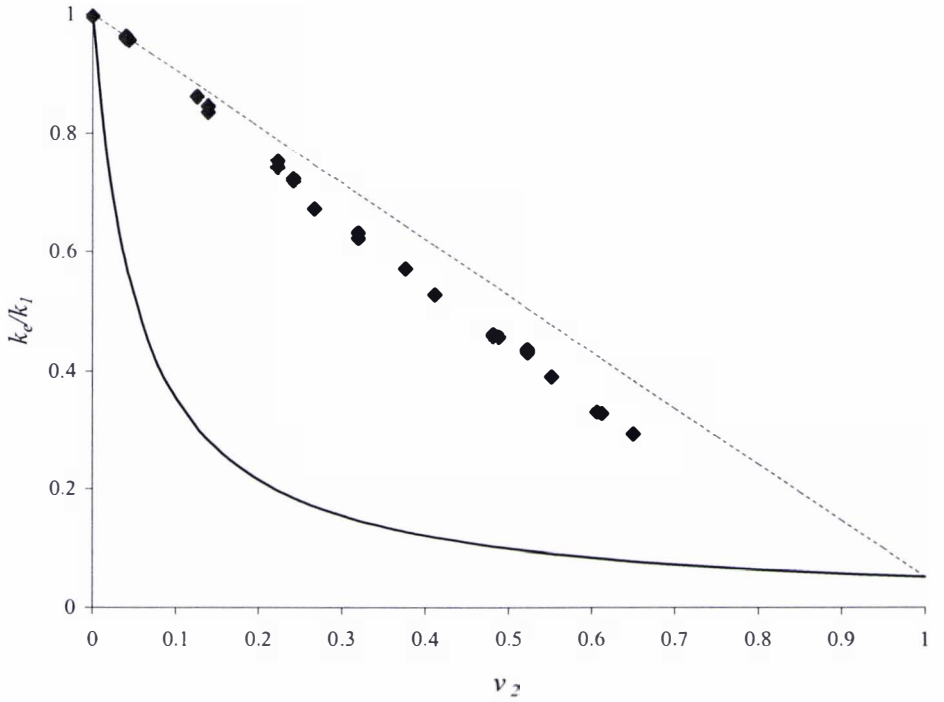

Figure 4.5: Results from 2mm EPS beads and guar-gel samples (points) plotted with theoretical limits to effective thermal conductivity provided by the Wiener bounds (solid and dashed lines)

v_2	k_e/k_c (k_e/k_1)		
	Replicate 1	Replicate 2	Replicate 3
0.000	0.996	0.997	
0.040	0.959	0.963	
0.043	0.956		
0.125	0.861		
0.139	0.836	0.846	
0.222	0.744	0.755	0.742
0.242	0.722	0.725	0.725
0.267	0.674		
0.319	0.625	0.634	
0.376	0.572		
0.412	0.529		
0.481	0.464	0.461	
0.488	0.460		
0.523	0.432	0.438	
0.551	0.392		
0.606	0.332		
0.612	0.329		
0.650	0.296	0.295	

Table 4.4: Numerical results from 2 mm EPS beads in guar-gel

4.4.3.2 Experimental Results for Dataset 2

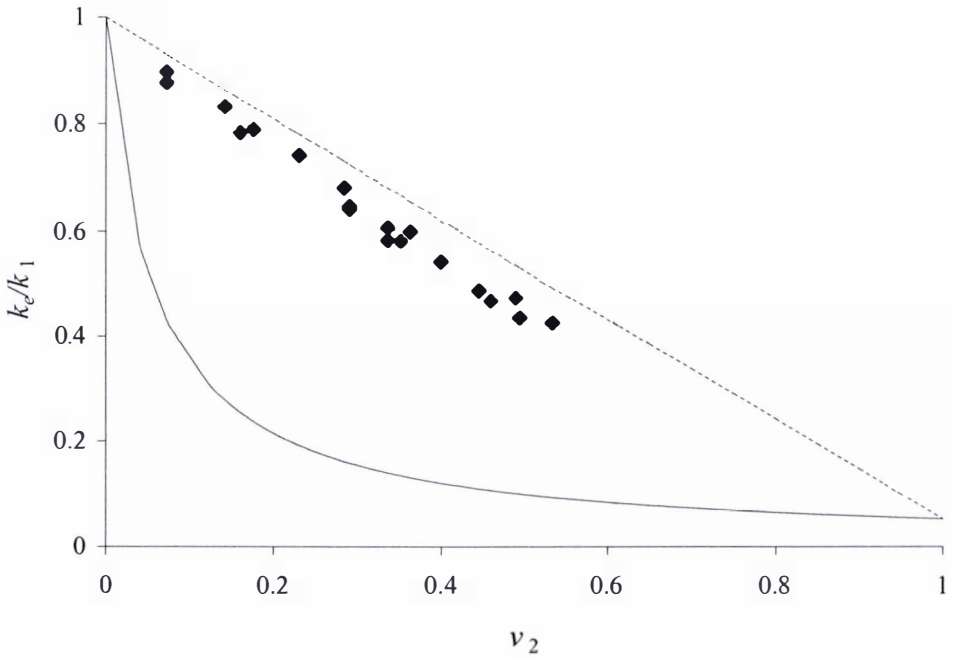

Figure 4.6: Results from 6.5mm EPS beads and guar-gel samples (points) plotted with theoretical limits to effective thermal conductivity provided by the Wiener bounds (solid and dashed lines)

v_2	k_e/k_c (k_e/k_1)	
	Replicate 1	Replicate 2
0.073	0.879	0.898
0.143	0.833	
0.161	0.784	
0.177	0.790	
0.231	0.742	
0.285	0.681	
0.291	0.641	0.646
0.337	0.607	0.584
0.352	0.582	
0.364	0.599	
0.400	0.541	
0.446	0.487	0.486
0.460	0.467	
0.490	0.474	
0.496	0.434	
0.535	0.425	

Table 4.5: Numerical results from 6.5 mm EPS beads in guar-gel

4.4.3.3 Experimental Results for Dataset 3

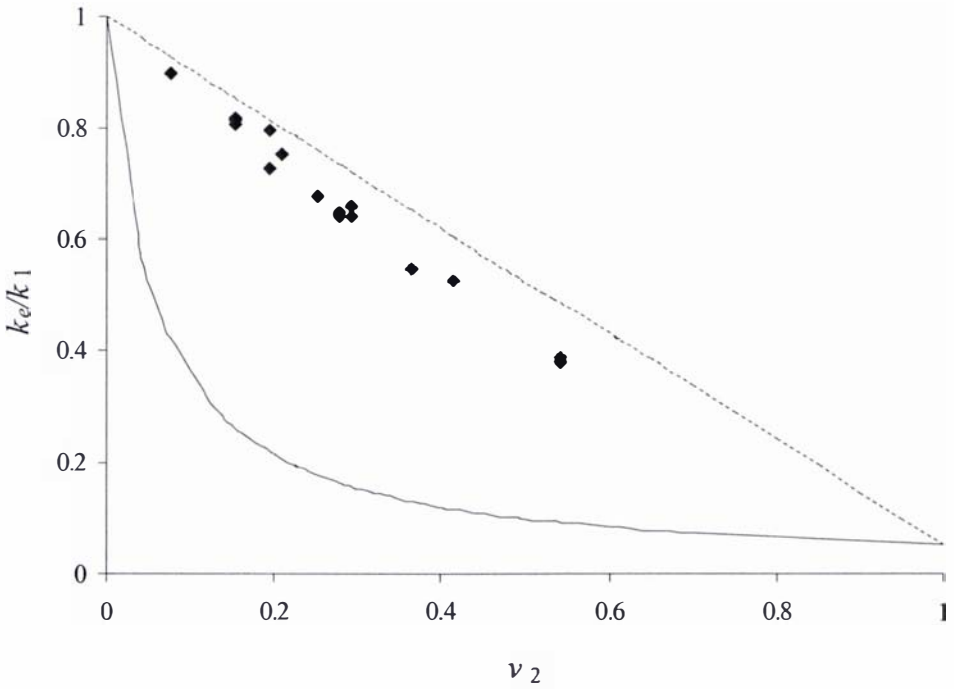

Figure 4.7: Results from 25mm EPS balls and guar-gel samples (points) plotted with theoretical limits to effective thermal conductivity provided by the Wiener bounds (solid and dashed lines)

v_2	k_e/k_c (k_e/k_1)	
	Replicate 1	Replicate 2
0.076	0.900	0.900
0.154	0.817	
0.154	0.818	0.806
0.194	0.796	0.730
0.210	0.755	
0.251	0.678	
0.280	0.640	0.649
0.294	0.658	0.641
0.364	0.546	
0.415	0.527	
0.543	0.377	0.383

Table 4.6: Numerical results from 25 mm EPS balls in guar-gel

4.4.3.4 Comparison of Experimental Results for Datasets 1, 2 and 3

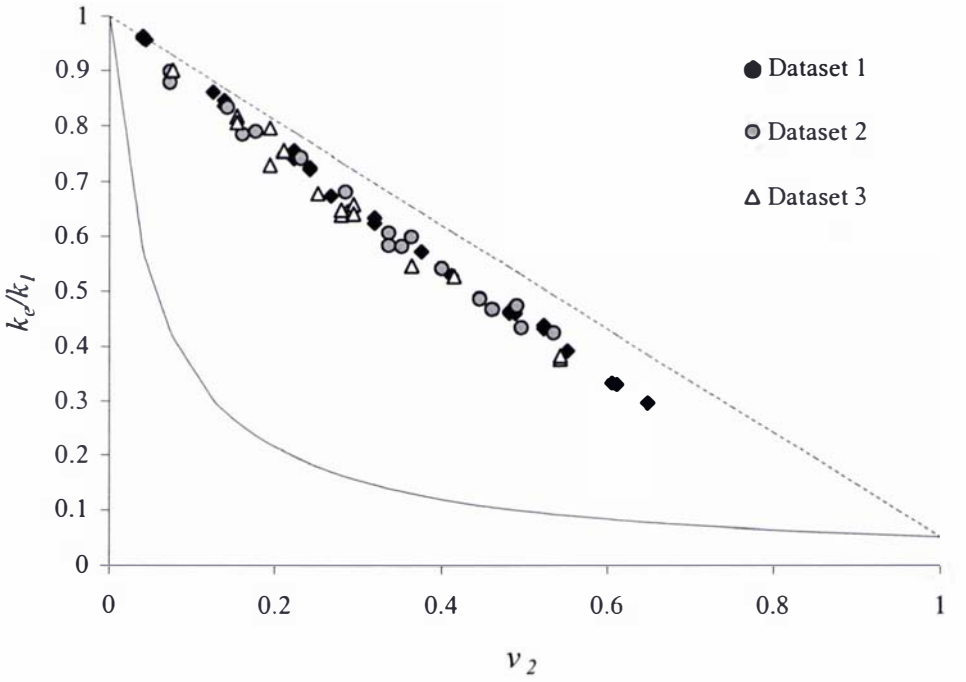

Figure 4.8: Combined results from EPS guar-gel samples plotted with theoretical limits to effective thermal conductivity provided by the Wiener bounds (solid and dashed lines)

4.4.3.5 Analysis of Variance Tests

Analysis of Variance (ANOVA) tests were performed in order to determine whether there was any significant difference between Datasets 1 to 3 and hence whether there was a dependence of the effective thermal conductivity on the mean size of the voids. The variable that was tested was the deviation of the thermal conductivity data from a linear best-fit model. When single factor ANOVA tests were performed, the results suggested that there was a significant difference between the results from Dataset 1 and the results from each of Datasets 2 and 3, however there did not appear to be any difference between the results from Datasets 2 and 3 at the 5% level of significance (the results of the ANOVA tests may be seen in Appendix D).

4.4.4 Aluminum/Guar-Gel Results

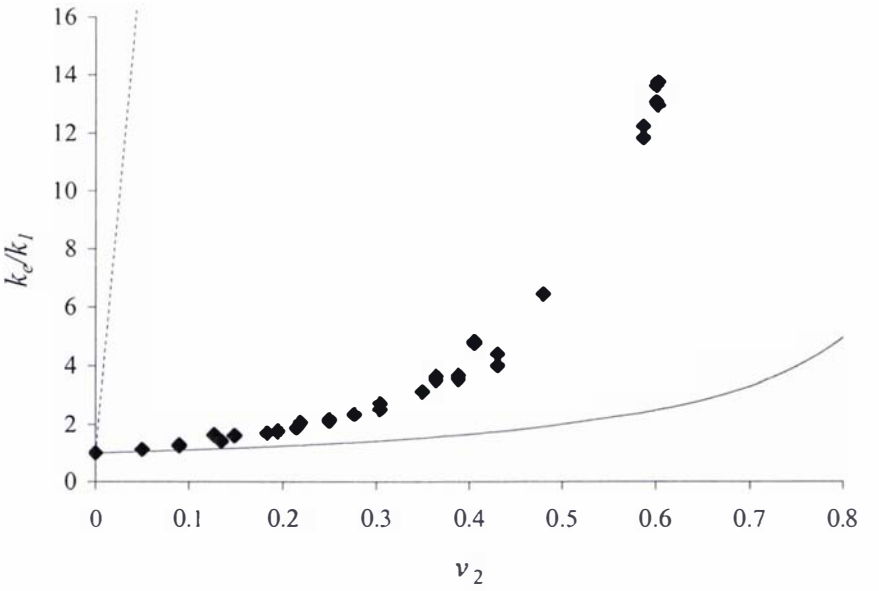

Figure 4.9: Results from samples containing aluminium cylinders and guar-gel (points) plotted with theoretical limits to effective thermal conductivity provided by the Wiener bounds (solid and dashed lines)

v_2	k_e/k_c (k_e/k_1)	
	Replicate 1	Replicate 2
0.050	1.12	1.12
0.090	1.29	1.25
0.127	1.62	1.64
0.135	1.42	1.41
0.148	1.61	
0.183	1.67	
0.195	1.72	
0.214	1.85	
0.219	2.05	
0.249	2.14	2.09
0.276	2.32	
0.304	2.50	2.70
0.349	3.13	
0.365	3.63	3.52
0.388	3.55	3.67
0.405	4.81	4.73
0.431	4.01	4.40
0.480	6.41	
0.587	11.82	12.22
0.601	13.63	13.06
0.603	12.96	13.76

Table 4.7: Numerical results from aluminium cylinders in guar-gel

4.5 Discussion

4.5.1 Effectiveness of the Thermal Conductivity Measurement Procedure

The procedure used was suitable for making comparative thermal conductivity measurements since the scatter in the results for the EPS/guar-gel samples in particular was similar to that expected for data measured by other commonly used types of apparatus (e.g. see Pham & Willix, 1989). The use of EPS, the relatively low temperatures involved (0 to 20°C), and the low temperature gradients minimised the possibility of significant heat transfer by radiation, natural convection and evaporation within the voids (as was encountered by Sakiyama & Yano, 1990), even given the presence of a significant amount of air.

4.5.2 Effectiveness of the Guar-gel/EPS Bead Mixture as a Food Analogue

As stated above, the test samples contained both air and EPS, which was unavoidable. The amount of air relative to the amount of EPS was greatest at low porosities and decreased as the porosity increased. The probability that randomly dispersed pores would come into contact with other pores would have increased as the volume fraction of pores was increased, and therefore interaction between pores would have been more significant in the experiments with higher porosities when EPS was the dominant pore material. A limitation of the use of EPS beads to represent air was that the individual EPS 'pores' could not interconnect to the same extent as real air, which may have affected the heat transfer pathways. The continuous phase has a more dominant influence on the overall heat transfer than the dispersed phase (Russell, 1935), and because the contact between the EPS beads, which were effectively rigid, was limited, the use of EPS beads meant there was a definite dispersed phase and a definite continuous phase. With air alone, it may have been possible to have both phases (the gel and the pores) essentially continuous at higher porosities, since the contact between air bubbles would not have been as

constrained. For these reasons the results from the EPS/guar-gel experiments would not be expected to model all types of porous foods.

4.5.3 The Effect of Void Size

The size of the EPS beads relative to the size of the sample container was varied between 10^{-6} and $4x10^{-3}$ (volume basis) in Datasets 1 to 3. The results suggested a minor dependence of k_e/k_c on the bead size, with k_e/k_c decreasing as the relative bead size was increased at a given porosity. Because the ANOVA tests did not show a difference between the results from Datasets 2 and 3 it appeared that any effect caused by the size of the voids was of a similar magnitude to the experimental uncertainty. The dependence of k_e/k_c on pore size may itself have been related to the component thermal conductivity ratio but it seemed reasonable to conclude that for a thermal conductivity ratio of approximately 20, as was the case with guar-gel and EPS/air mixture, the effect of pore size was minimal.

The fact that the void phase contained both air and EPS meant that there was a much greater range of pore sizes than there would have been with EPS beads alone, which was not ideal. Most of the air bubbles were smaller than the smallest beads, but occasionally some air pockets as large as 10mm in diameter were observed. Because the dependence of the effective thermal conductivity on bead size appears to have been minor this was not considered to be a serious issue.

4.5.4 Aluminium/Gel Mixtures

Figure 4.9 highlighted the influence of the component thermal conductivity ratio on the uncertainty involved in effective thermal conductivity prediction. With a component thermal conductivity ratio of approximately 350, the region between the Wiener bounds was vast. The results appeared to follow the percolation characteristic (see Section 2.3.5 of Chapter 2) with a relatively minor dependence of effective thermal conductivity on the

volume fraction at low values of v_2 but with a strong dependence beyond a v_2 value of about 0.4.

4.6 Conclusion

The experimental procedure and results described in this chapter have fulfilled the first two objectives listed in Chapter 3. The EPS/guar-gel mixture was not an ideal food analogue, since entrainment of air was significant, but the method still provided a set of data that was better than any of the previous data for porous foods for the purposes of model evaluation. Even with the entrained air, the small size of the bubbles and the low temperatures involved meant that heat transfer by modes other than conduction, which were encountered by Lin (1994) and Sakiyama & Yano (1990), would have been negligible (see Progelhof *et al.*, 1976, and Russell, 1935). The scatter in the results was much lower than the scatter in Lin's data, and the dataset was much larger than that of Sakiyama & Yano.

The data were of sufficient precision and over a sufficient v_2 range that the k_e/k_c (k_e/k_1) vs. v_2 trend was clear, as shown in Figs. 4.5 to 4.9. This would allow comparisons between the characteristic shapes of the data and effective thermal conductivity models, which would assist in the identification of models that are suitable over a range of v_2 values, rather than those that only provide good predictions for some portions of the v_2 range (see Section 2.3.8 of Chapter 2).

Chapter 5: Numerical Simulations

5.1 Introduction

5.1.1 Objectives

The aim of the numerical analysis described in this chapter was to add to the experimental work described in Chapter 4 by providing data that could be used to evaluate effective thermal conductivity models. The numerical simulations provided the opportunity for greater flexibility than the physical experiments for examining the relative effects of certain variables identified in the literature as having potential to influence the effective thermal conductivity.

5.1.2 Relevant Structure-Related Variables

Variables relating to the structure of the food that have been identified as having potential to influence the effective thermal conductivity include: the spatial distribution of the pores, pore shape, relative pore size, pore orientation, and any interaction (contact and/or coalescence) between neighbouring pores (refer to Sections 2.3 and 2.4 of Chapter 2).

5.1.2.1 Spatial Distribution of Pores

It is obvious that the spatial distribution of the components of a material has an influence on the conduction of heat. The scope of this study was limited to random and approximately uniform distributions of component materials, which is the assumed distribution of most effective thermal conductivity models and is also a realistic representation of many food materials.

5.1.2.2 Individual Pore Size

In general, experimental studies, including the experiments described in Chapter 4, have reported the effect of the size of individual pores as being small or negligible for conductivity ratios and conditions that would typically be involved in food products and processes. However, the size of the inclusions of the dispersed phase has been found to

influence internal heat transfer in some composite materials when the thermal conductivity of the dispersed phase was much greater than the conductivity of the continuous phase, and at high temperatures (above 500°C) when radiation was significant (Every *et al.*, 1992).

The results of the experiments performed as described in Chapter 4 indicated a minor dependence of the effective thermal conductivity on relative pore size, with the effective thermal conductivity decreasing as the relative pore size was increased, but the difference was of a similar magnitude to the uncertainty in the results (2-5%). Since the literature suggested that there should be no dependence of thermal conductivity on pore size under these conditions, there was an incentive to corroborate the experimental results with numerical simulations.

5.1.2.3 Individual Pore Shape

The shapes of pores that exist within a food product are dependent largely on the physico-chemical properties of the food and the manufacturing process, although post-production handling may also have effects (Niranjan, 1999). Pores within foods are most commonly isometric, and foods manufactured from viscous fluids by processes that involve low Reynolds numbers are likely to contain pores that are essentially spherical.

The experiments performed by Hamilton & Crosser (1962) suggested that if the continuous phase of a heterogeneous material had a higher thermal conductivity than the dispersed phase, the shapes of the inclusions of the dispersed phase would have no influence on the thermal conductivity, and hence the shape of internal pores in a food product would not be expected to affect the thermal conductivity. However, their experiments were only performed for two different volume fractions of the dispersed phase (0.15 and 0.27) and so there was an incentive to perform simulations over a wider range of volume fractions, particularly dispersed-phase volume fractions greater than 0.27, in a thermal conductivity range that was similar to that of porous foods.

5.1.2.4 Pore Orientation

The orientation of non-isometric pores has the potential to cause pronounced anisotropy. However, the orientation of non-isometric pores in many foods is likely to be random, and hence will approach isotropy on a macroscopic scale. As mentioned previously, this study was limited to materials that could be considered to be isotropic.

5.1.2.5 Pore Interaction

According to the literature, the degree to which individual inclusions (pores or particles) of a dispersed phase come into contact with neighbouring inclusions has a significant influence on the overall thermal conductivity (see Section 2.3 of Chapter 2). The degree of contact between neighbouring inclusions is often assumed, directly or indirectly, in the derivation of effective thermal conductivity models. For example, models that require one component to be continuous and the other to be dispersed implicitly assume a different degree of contact to models that do not make distinctions between the component phases. There was a clear incentive to examine the effect these assumptions of pore interaction have on the overall effective thermal conductivity.

5.1.3 Choice of Numerical Method

The use of numerical simulations to study effective thermal and electrical conductivity is common and several different numerical methods have been employed, including finite difference methods (e.g. Davies & Fryer, 2001), finite element methods (e.g. Krach & Advani, 1996), and boundary element methods (e.g. Baltz & Ingber, 1997). Finite difference methods have the potential for simplicity and lower computing requirements than finite element methods. Finite element methods have the advantage that the discretisation process is not constrained by regular node positioning, and so they are more suitable to irregular geometries and spatially variable properties and conditions. Boundary element methods may be thought of as a special class of finite element methods.

Initially both finite element and finite difference methods were employed in this study. However, it was discovered that the level of complexity that was required in the development of reliable finite difference models nullified the potential advantage of simplicity they might otherwise have had over finite element models, as explained in Appendix E. Accordingly, only the results from the simulations by finite element methods are considered in this chapter.

Ideally the simulations would have been performed in three dimensions. However, neither the computer software nor the required computing power was available to perform the type of three-dimensional finite element simulations required, and so two-dimensional simulations were performed.

5.1.4 Basic Principles of the Finite Element Method

A general description of finite element methods applied to a thermal context may be found in Cleland (1990). Briefly, the method involves the division of the region of interest into a number of discrete elements with temperature nodes on the element boundaries and sometimes (in the case of non-linear elements) inside the elements. The temperature at each node is related to its neighbours' temperatures by a differential equation, and the equations of all the nodes are solved simultaneously and implicitly. The size and positioning of the elements may be chosen to optimise the solution procedure. Typically this involves reducing the element size (hence increasing the number of elements) wherever steep temperature gradients exist (i.e. near discontinuities in thermal properties and conditions), and vice versa in regions of flat temperature gradients.

5.2 Method

5.2.1 Modelling Strategy

The finite element (FE) models were set up to simulate a two dimensional steady state thermal conductivity measurement apparatus. This theoretical measurement device comprised an FE grid with two perfectly insulated sides and two sides held at constant temperature, T_{hot} and T_{cold} (see Figure 5.1). The finite element grid area was divided into regions of different conductivity corresponding to the different components (k_1 and k_2) of a theoretical test sample.

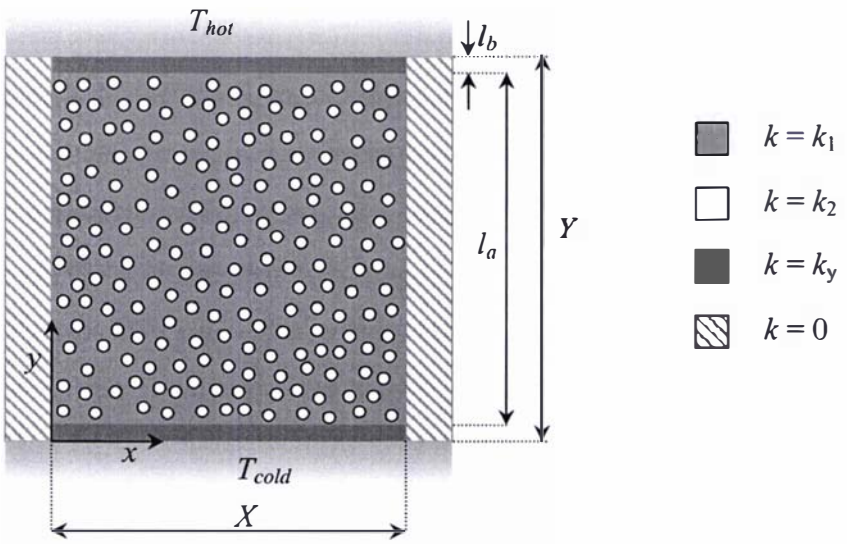

Figure 5.1: Theoretical thermal conductivity measurement device used in numerical simulations

A third material of conductivity k_y was positioned at both the hot and cold ends of the theoretical test sample to allow energy balances to be performed in regions of constant thermal conductivity (therefore $X \neq Y, X = l_a$).

The conduction within the FE grid area was governed by the following form of Laplace's Equation:

$$\frac{\partial}{\partial x}\left(k(x,y)\frac{\partial T}{\partial x}\right)+\frac{\partial}{\partial y}\left(k(x,y)\frac{\partial T}{\partial y}\right)=0 \tag{5.1}$$

The relevant external boundary conditions are shown below (the coordinate origin is in the bottom left hand corner of the grid shown in Fig. 5.1).

At the insulated boundaries:

$$\left.\frac{dT}{dx}\right|_{x=0}=0 \tag{5.2}$$

$$\left.\frac{dT}{dx}\right|_{x=X}=0 \tag{5.3}$$

At the constant temperature boundaries:

$$T|_{y=0}=T_{cold} \tag{5.4}$$

$$T|_{y=Y}=T_{hot} \tag{5.5}$$

Once the nodal equations were solved, the temperature distribution over the FE grid was known and so it was possible to perform energy balances over a thin slice (Δy) of the FE grid at both the hot and cold ends:

$$Q_{cold}=k_y X\frac{(T_{cold+\Delta y}-T_{cold})}{\Delta y} \tag{5.6}$$

$$Q_{hot} = k_y X \frac{(T_{hot} - T_{hot-\Delta y})}{\Delta y} \tag{5.7}$$

Under steady state conditions Q_{hot} and Q_{cold} should be equal in value, and this requirement was used as a check on the convergence of the solution. Once the heat flow had been determined the overall conductivity between the hot and cold ends (including the theoretical test sample and two end zones) was calculated from Eq. (5.8):

$$k_g = \frac{Q_{hot} Y}{X(T_{hot} - T_{cold})} \tag{5.8}$$

where Y was the total distance through which the heat was transferred (see Fig. 5.1). The heat was transferred in series through the hot end zone, the theoretical test material, and the cold end zone, hence the effective thermal conductivity, k_e, of the test material was:

$$k_e = \frac{l_a}{\frac{Y}{k_g} - \frac{2l_b}{k_y}} \tag{5.9}$$

5.2.2 *PDEase2D™* Software Package

The finite element simulations were performed using Version 2.6.1c of the *PDEase2D™* software package (Macsyma Inc., Arlington MA). The *PDEase2D™* program automatically constructed a finite element grid based on the governing partial differential equation, the geometric boundaries of the different regions, and the boundary conditions that were specified. Figure 5.2 shows an example of a *PDEase2D™* input script, Fig. 5.3 shows the finite element grid that was constructed from those input data, and Figs. 5.4 and 5.5 show selected forms of the results display that were available. Numerical results were output to a text file for further processing in a spreadsheet. *PDEase2D™* used the *Galerkin* finite element method.

```
Title
        "Steady state heat flow in a two material object"
Select
    errlim=1e-4                                  (sets calculation error limit)
Variables
    Temp(range=0,20)                             (specifies simulation variable)
Definitions
     k
     h                                           (specifies thermal properties
     Ta                                           and external conditions)
     Th
     Tc
Equation
     dx(-k*dx(temp))+dy(-k*dy(temp))=0           (governing partial differential
                                                  equation, Eq. 5.1)
Boundaries
 Region 1
   k=0.6
   h=0.0000001
   Th=20
   Ta=10
   Tc=1
   natural(temp)=h*(Ta-temp)                     (defines geometric boundaries
   start (0,0)                                    boundary conditions and thermal
   line to (1,0)                                  properties within Regions 1 and 2)
   value(temp)=Tc
   line to (1,1)
   natural(temp)=h*(Ta-temp)
   line to (0,1)
   value(temp)=Th
   line to (0,0)
   finish
 Region 2
   k=0.03
   start (0.5,0.3)
   arc(center=0.5,0.5) angle=360
   finish

Plots
   grid(x,y)                                     (draws a plot of the FE grid, see Fig. 5.3)
   contour(temp)                                 (draws a temperature contour plot see Fig. 5.4)
   surface(temp)                                 (draws a temperature surface, see Fig. 5.5)

End
```

Figure 5.2: Sample program script for *PDEase2D™*

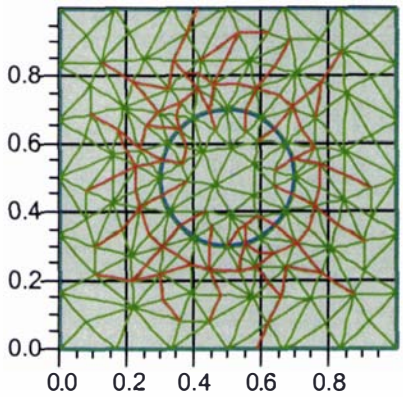

Figure 5.3: Finite element grid developed by *PDEase2D* ™ for the input script shown in Fig. 5.2

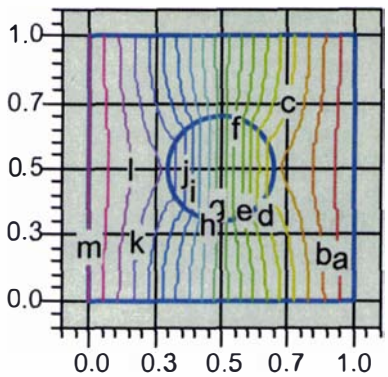

Figure 5.4: Simulation results in the form of temperature contours (isotherms) for the inputs shown in Fig. 5.2

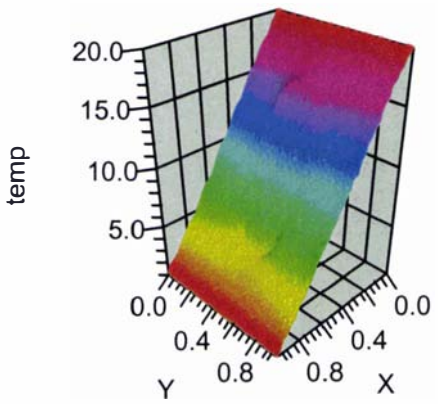

Figure 5.5: Simulation results in the form of a temperature surface for the inputs shown in Fig. 5.2

The number and position of elements was automatically adjusted by *PDEase2D™* throughout the simulation. An initial grid of nodes was set up and the program attempted to solve the nodal equations. If the sensitivity of the initial grid was insufficient to converge at a solution within the specified error limit of 10^{-4}, the program increased the number of elements so that the grid was finer, particularly where sharp temperature gradients were encountered, and another attempt at convergence was made. The process was repeated until the grid was fine enough to achieve a solution. For the simulations involved in this study, *PDEase2D™* required between 2 and 7 attempts per simulation to arrive at a satisfactory solution.

5.2.3 Numerical Simulation Datasets

5.2.3.1 ***Simulation 1****: Effect of Pore Size*

In order to examine the effect of pore size on the effective thermal conductivity, circles of conductivity k_2 were plotted in a continuous phase of k_1 (see Fig. 5.6 for a diagram of the FE grid regions). The positioning of the circles was determined with the use of random

numbers that assigned the coordinates of the centre of the circle. Since the positioning of each circle was required as a separate statement in the *PDEase2D™* input script (see an example of the description of a circle Fig. 5.2 under the heading "Region 2"), and as many as 145 circles were involved, a *QBASIC™* program was written that used a FOR-NEXT loop to perform this repetitive task. The output of the BASIC program was in the form of a text file that could be 'cut' and 'pasted' straight into the *PDEase2D™* input script. The random numbers that were used for the circle coordinates were first passed through filters to ensure that they did not intersect the external boundaries nor cause contact with any neighbouring pores (a printout of the *QBASIC™* program *PLOTC.BAS* that was used to plot the circles may be found in Appendix F).

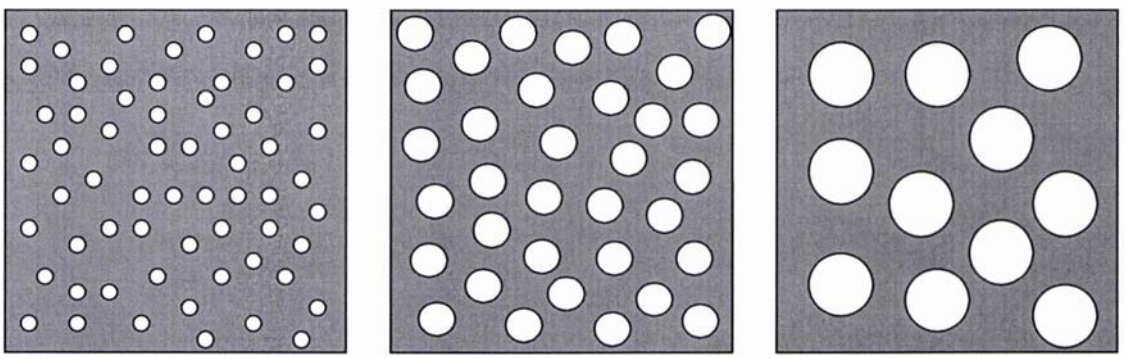

Figure 5.6: Diagrams (not to scale) of Finite Element grids used to examine the influence of pore size on the effective thermal conductivity (grey area = k_1, white area = k_2)

The radii (R) of the individual circles were varied between $0.003X$ and $0.12X$ (where X was the width of the FE grid area, see Fig. 5.1). The volume fraction of the dispersed phase (v_2) was varied between 0 and 0.5.

5.2.3.2 ***Simulation 2****: Effect of Pore Shape*

In order to examine the effect of non-circular pores on the effective thermal conductivity, simulations were performed on FE grids containing square and rectangular inclusions

similar to those containing circles (see Fig. 5.7). The individual pores of all three shapes were of a similar size (each individual inclusion occupied approximately 5 x 10^{-3} of the total grid area). The positions of the square inclusions were determined by random number in a similar manner to the circular inclusions, using the *QBASIC™* program *PLOTSq.BAS* (see Appendix F). The rectangular pores had aspect ratios of 2:1 and their alignments were alternated between parallel to, and transverse to the direction of heat flow in order to approximate a random orientation (see Fig. 5.7). The volume fraction of the dispersed phase (v_2) was varied between 0 and 0.45 for the circles, and between, 0 and 0.4 for the squares and rectangles.

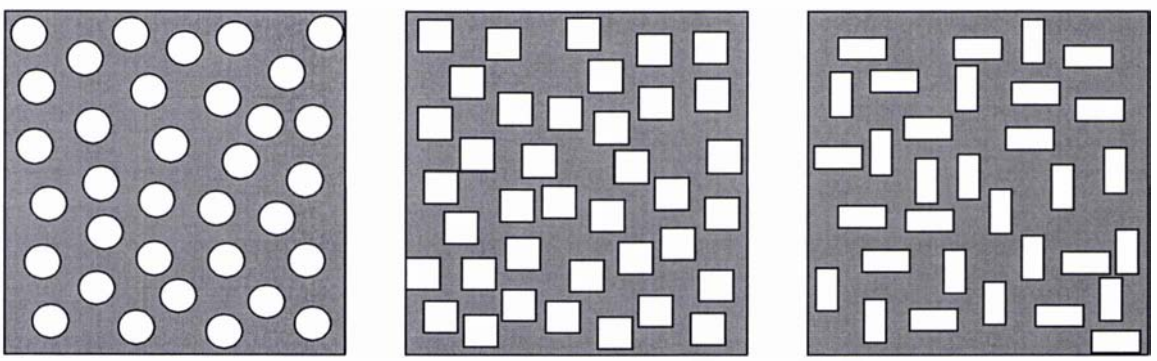

Figure 5.7: Diagrams of FE grids containing different shaped inclusions (not to scale)

5.2.3.3 ***Simulation 3****: Relative Influences of Continuous and Dispersed Phases*

In order to examine the relative influences on the effective thermal conductivity of the continuous and dispersed phases, simulations were performed on two materials with the same component thermal conductivity ratio but with opposite continuous and dispersed phase conductivities (one material had a continuous-phase conductivity equal to k_1 and a

dispersed-phase conductivity equal to k_2, and vice versa for the other material, see Fig. 5.8).

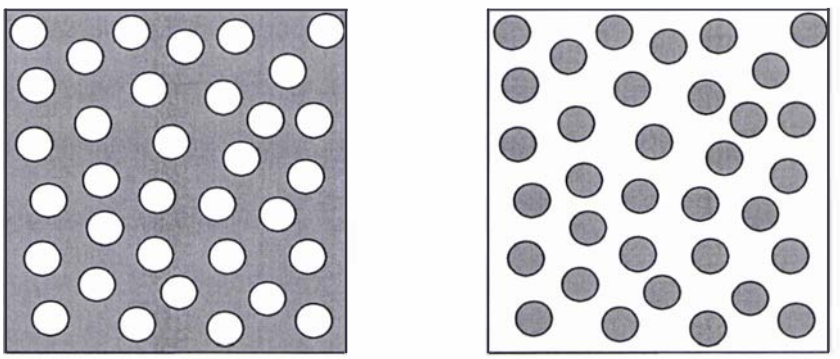

Figure 5.8: Diagrams of FE grids with identical structures but with opposite conductivities of the dispersed and continuous phases

5.2.3.4 ***Simulation 4****: Pore Interaction*

All of the systems considered above had a definite continuous phase and a definite dispersed phase since the inclusions were not allowed to come into contact with their neighbours. This constraint was one of the assumptions required in the derivation of Maxwell's effective thermal conductivity model (see Section 2.3.4 of Chapter 2), and so this type of pore interaction will be referred to as the Maxwell scenario. Two other pore interaction scenarios were also considered (see Figs. 5.9a to 5.9c).

For the arrangement shown in Fig. 5.9c, the finite element grid area was divided into 196 discrete cells (each cell occupied 5.1×10^{-3} of the total grid area). Each cell was assigned a random number between 0 and 1. The thermal conductivity of each cell was determined by whether the random number was greater than the required value of v_2. In this way a random distribution of the two materials over the grid in the desired amounts was

obtained. In this arrangement neither component was necessarily continuous or dispersed. This scenario is the sort of arrangement assumed by the effective medium theory (see Section 2.3.5 of Chapter 2) and will be referred to as the Kirkpatrick scenario (after Kirkpatrick, 1973).

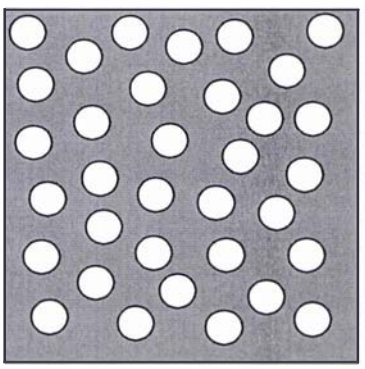

Figure 5.9a: Maxwell-type interaction

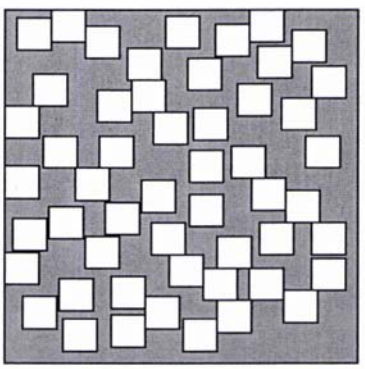

Figure 5.9b: Intermediate-type interaction

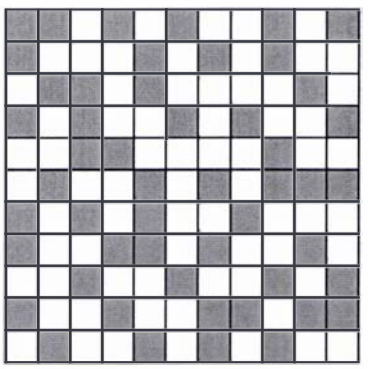

Figure 5.9c: Kirkpatrick-type interaction

A third model of pore interaction was also examined (see Fig. 5.9b). Individual pores of component 2 were positioned randomly in the FE grid area, with the remaining grid area occupied by component 1, similar to the Maxwell scenario. But unlike the Maxwell scenario the pores were allowed unconstrained contact with neighbouring pores, thus they had the potential to form larger conglomerate pores. Hence this type of interaction was an intermediate between the Maxwell and Kirkpatrick scenarios.

Both the Maxwell and Kirkpatrick scenarios are feasible physical models of real foods. For example, according to descriptions of microscopic structure (see Campbell *et al.*, 1999), ice cream might be thought of as a continuous/discontinuous (Maxwell) type structure, since the individual pores are totally isolated, while the structure of a sponge cake might be thought of as approximating a Kirkpatrick type structure, since the porous phase may be as continuous as the condensed phase.

5.2.3.5 ***Simulation 5****: Effect of Component Thermal Conductivity Ratio*

In Simulations 1 to 4, the component thermal conductivity ratio (k_1/k_2) was maintained at a value of 20, which was similar to the component thermal conductivity of the EPS/gel food analogues used in the experiments described in Chapter 4. In Simulation 5 k_1/k_2 was varied for the Maxwell-type and Kirkpatrick-type grids (see Figs. 5.9a and 5.9c) at selected volume fractions in order to examine how the trends in the k_e/k_1 vs. v_2 data for the different grid types were affected by the component thermal conductivity ratio.

5.3 Results

Due to the limited number of lines of input text allowed by the software, the number of inclusions of the dispersed phase was relatively small, and therefore, since the distribution of the components was determined randomly, there was no guarantee that the distribution of components 1 and 2 on an individual grid was uniform. For this reason simulations were performed on six different grids at a certain volume fraction, with each grid having a different random distribution of the components. The mean of the k_e/k_1 results from the six grids was used as a final result for the model evaluations performed in Chapter 6. Since the component distributions were random, the 'average' distribution of a sufficient number of grids would be expected to approximate a uniform distribution. Six replicates per volume fraction was regarded as a sufficient number to achieve uniformity since the discrepancy between the mean k_e/k_1 value for five replicates and the mean k_e/k_1 value for six replicates was less than 1%.

In Simulations 1 to 4, the thermal conductivities of components 1 and 2 were k_1 = 0.6 W m^{-1} K^{-1} and k_2 = 0.03 W m^{-1} K^{-1} respectively, giving a component thermal conductivity ratio of 20. The standard deviation of the k_e/k_1 values of the six replicates was typically between 0.5% and 8% of the mean, and generally increased as v_2 increased. For Simulation 5, where k_1/k_2 was as high as 200, the standard deviation of the replicates was as high as 20% of the mean. The standard deviation of the replicates was used as an

estimate of the uncertainty in the results, since it was significantly higher than the *PDEase2D™* calculation error limit and the estimated uncertainty in the individual effective thermal conductivity calculations. Contact resistance and heat transfer by convection or radiation were not considered in the simulations.

5.3.1 Effect of Pore size (Simulation 1)

Due to their similarity in structure and component thermal conductivity ratio, the FE grids involved in Simulation 1 could be thought of as two-dimensional equivalents of the EPS/guar gel food analogues described in Chapter 4. The individual k_e/k_1 values for three different 'pore' sizes at each v_2 are plotted in Fig. 5.10. The mean values are shown in Fig. 5.11.

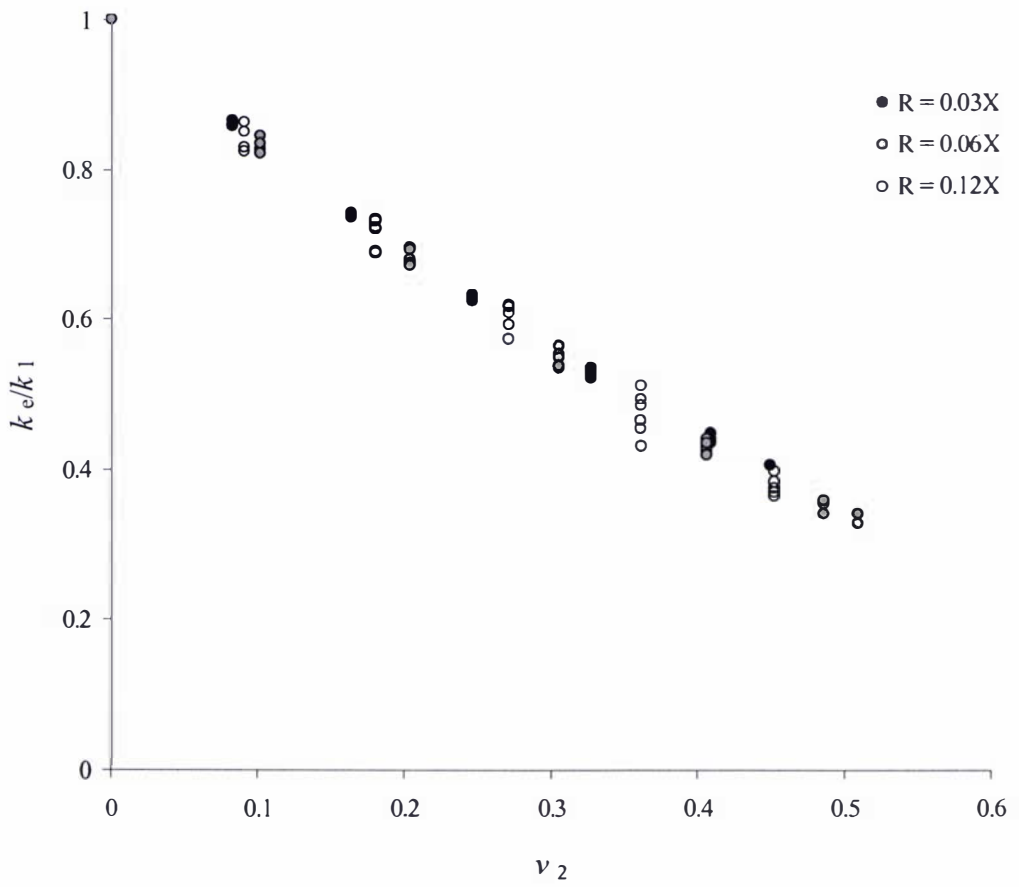

Figure 5.10: Individual k_e/k_1 results over a range of v_2 for three different 'pore' sizes (results from Simulation 1)

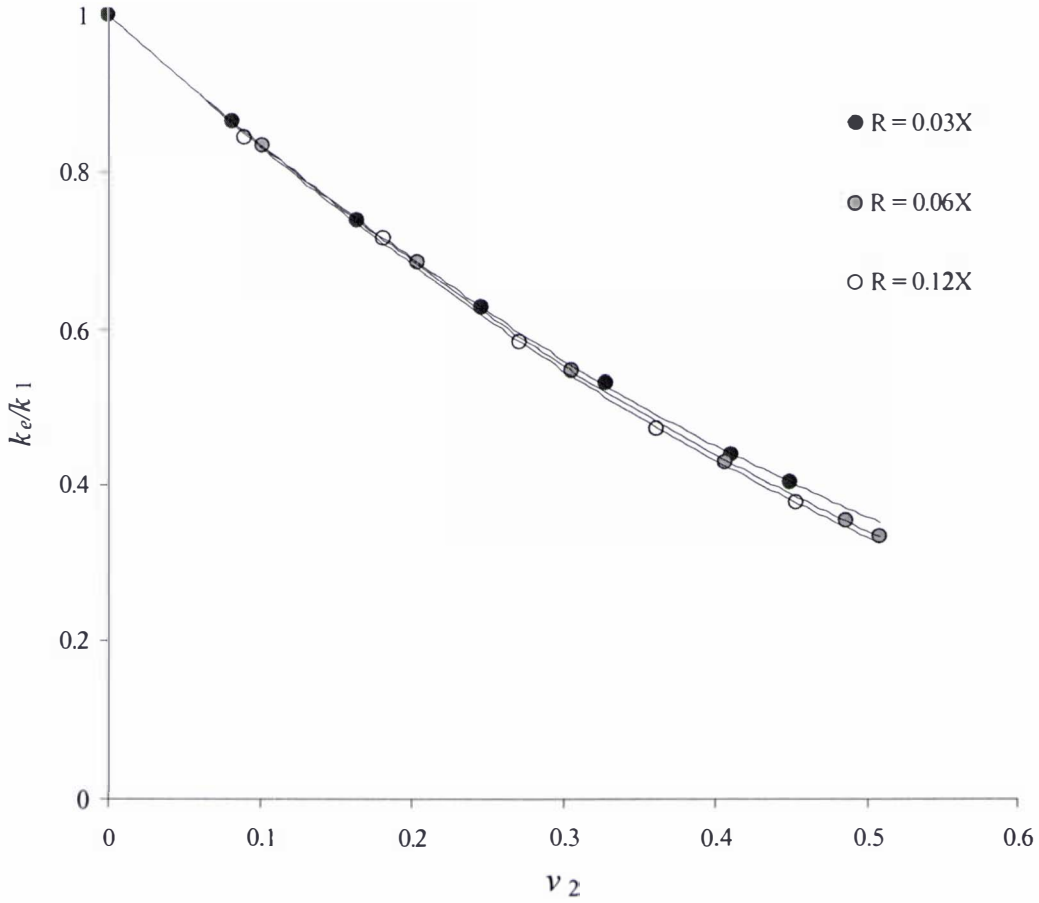

Figure 5.11: Mean k_e/k_1 results over a range of v_2 for three different 'pore' sizes (results from Simulation 1)

The similarity in appearance between Fig. 5.10 and Fig 4.8 of Chapter 4 is obvious, which might suggest that the numerical approach used in this chapter does indeed model the physical situation, albeit in two dimensions. Because the simulations were performed in two dimensions, a direct comparison between the numerical values of the results displayed in Fig. 5.10 and Fig 4.8 of Chapter 4 could not be made. However, as discussed in Section 6.3.1 of Chapter 6, a modified two-dimensional form of the Maxwell-Eucken effective thermal conductivity model may be used to confirm the agreement between the numerical results from Simulation 1 and the experimental results of the EPS/guar gel food analogues.

Similarly to the EPS/guar gel results, there was the suggestion of a minor dependence of k_e/k_1 on pore size, with k_e/k_1 decreasing as the pore size is increased.

5.3.2 The Effect of Pore Shape (Simulation 2)

The individual k_e/k_1 values for three different pore shapes at each v_2 are plotted in Fig. 5.12. The mean values are shown in Fig. 5.13.

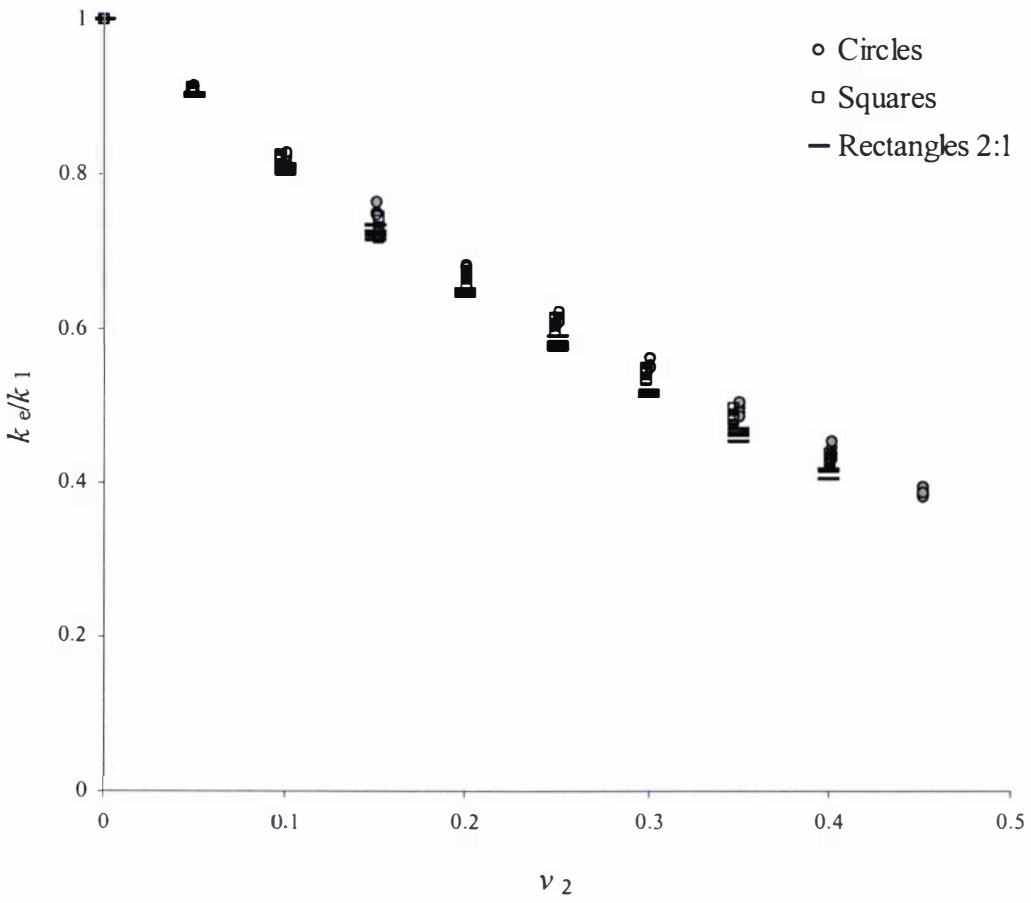

Figure 5.12: Individual k_e/k_1 results over a range of v_2 for three different 'pore' shapes (results from Simulation 2)

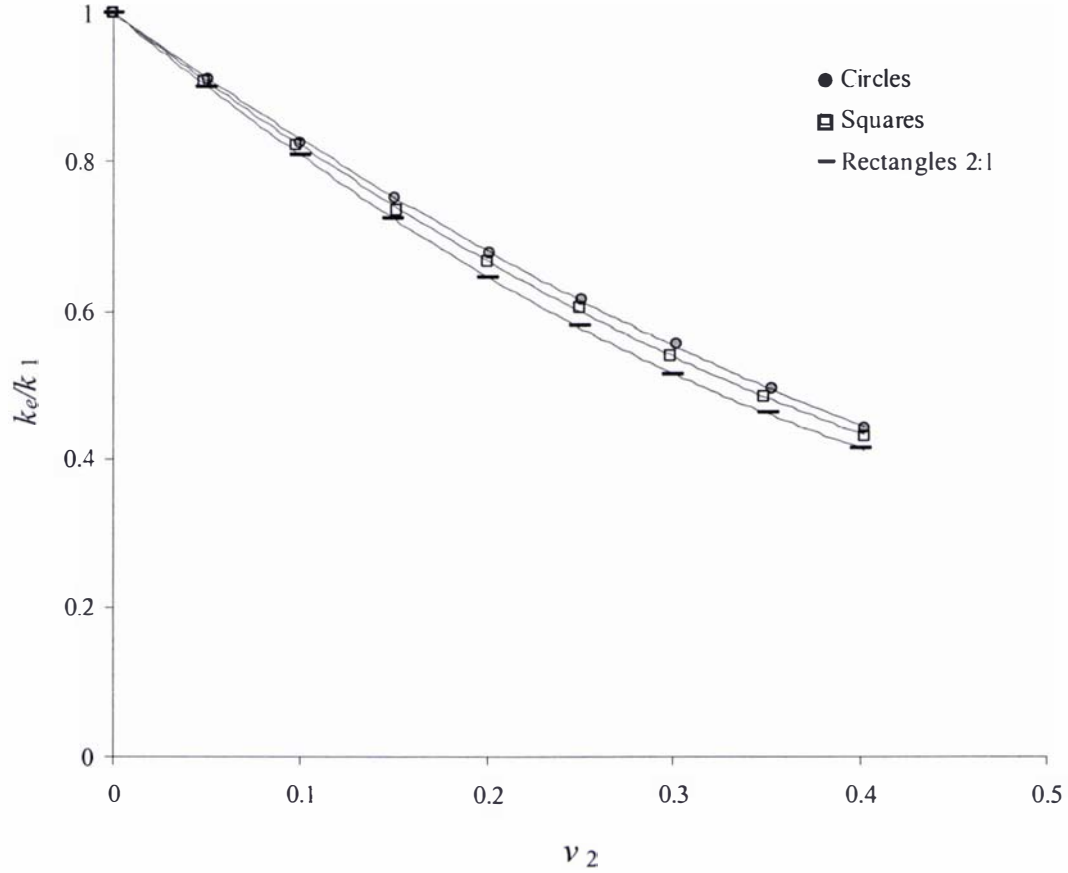

Figure 5.13: Mean k_e/k_1 results over a range of v_2 for three different 'pore' shapes (results from Simulation 2)

The results for the circles and squares were similar, with a maximum difference between the mean k_e/k_1 values of the two shapes of 2.6% (at $v_2 = 0.4$), which was similar to the 3% uncertainty (standard deviation) in that result. Beyond a porosity of 0.15, the discrepancy between the results for the circles and rectangles was greater than the uncertainties of the results, suggesting a minor dependence of the effective thermal conductivity on pore shape.

5.3.3 Relative Influences of the Continuous and Dispersed Phases (Simulation 3)

Figure 5.14 shows the results of simulations for two Maxwell-type materials (see Fig. 5.8) with opposite continuous and dispersed phase conductivities:

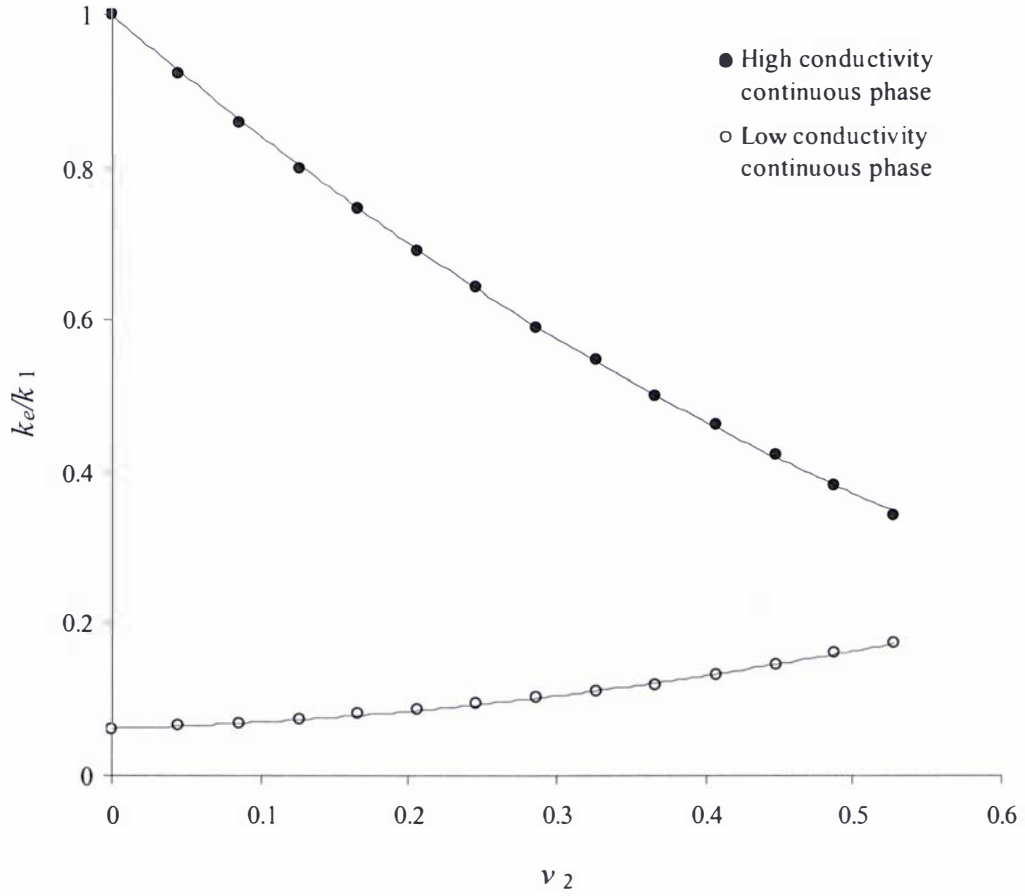

Figure 5.14: Comparison of the roles of the continuous and dispersed phases on the effective thermal conductivity (results from Simulation 3)

Figure 5.14 clearly confirms assertions (see Sections 2.4.1.1 and 2.4.1.4 of Chapter 2) that a continuous phase has a more dominant influence on the effective thermal conductivity than a dispersed phase.

5.3.4 The Effect of Pore Interaction (Simulation 4)

The individual k_e/k_1 values for three different inclusion interaction scenarios at each v_2 are plotted in Fig. 5.15. The mean values are shown in Fig. 5.16.

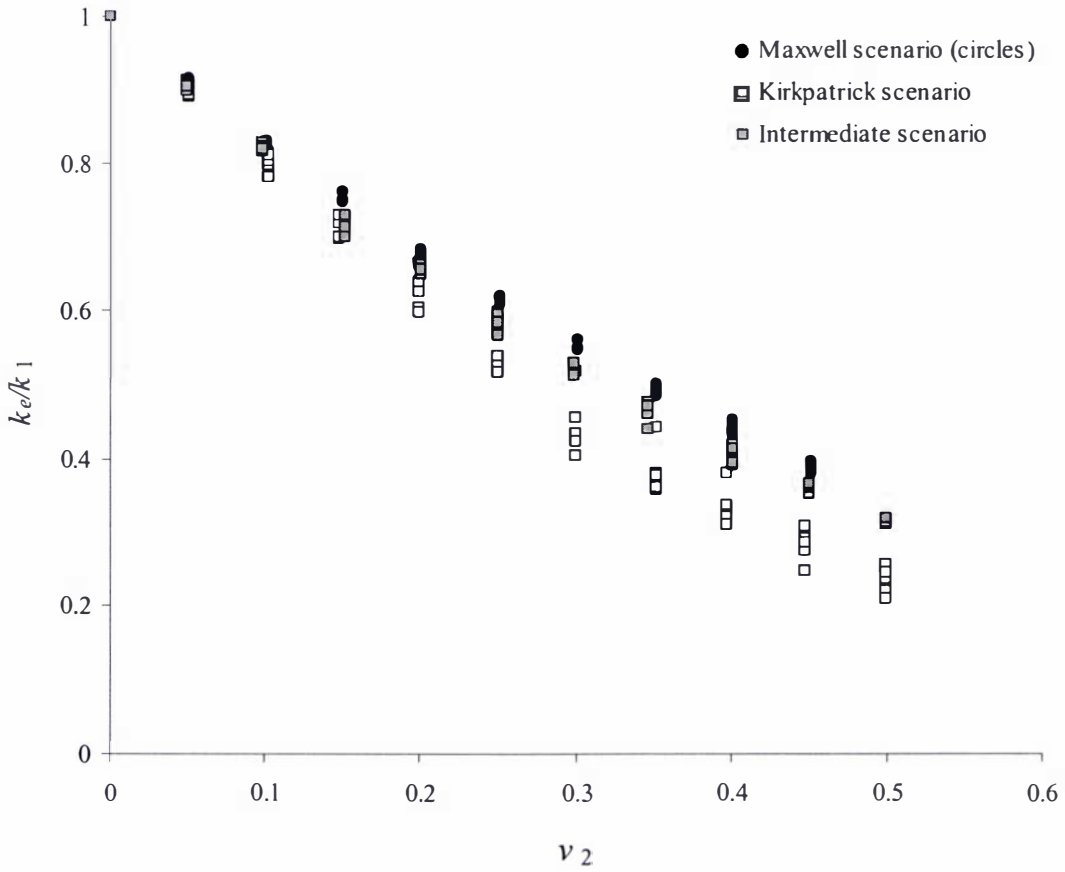

Figure 5.15: Individual k_e/k_1 results over a range of v_2 for three different 'pore' interaction scenarios (results from Simulation 4)

Figures 5.15 and 5.16 suggest a clear dependence of the effective thermal conductivity on the extent of contact between inclusions (as much as 40% difference between the Maxwell and Kirkpatrick scenarios). As expected, the results for the intermediate scenario lay between the results for the Maxwell and Kirkpatrick scenarios.

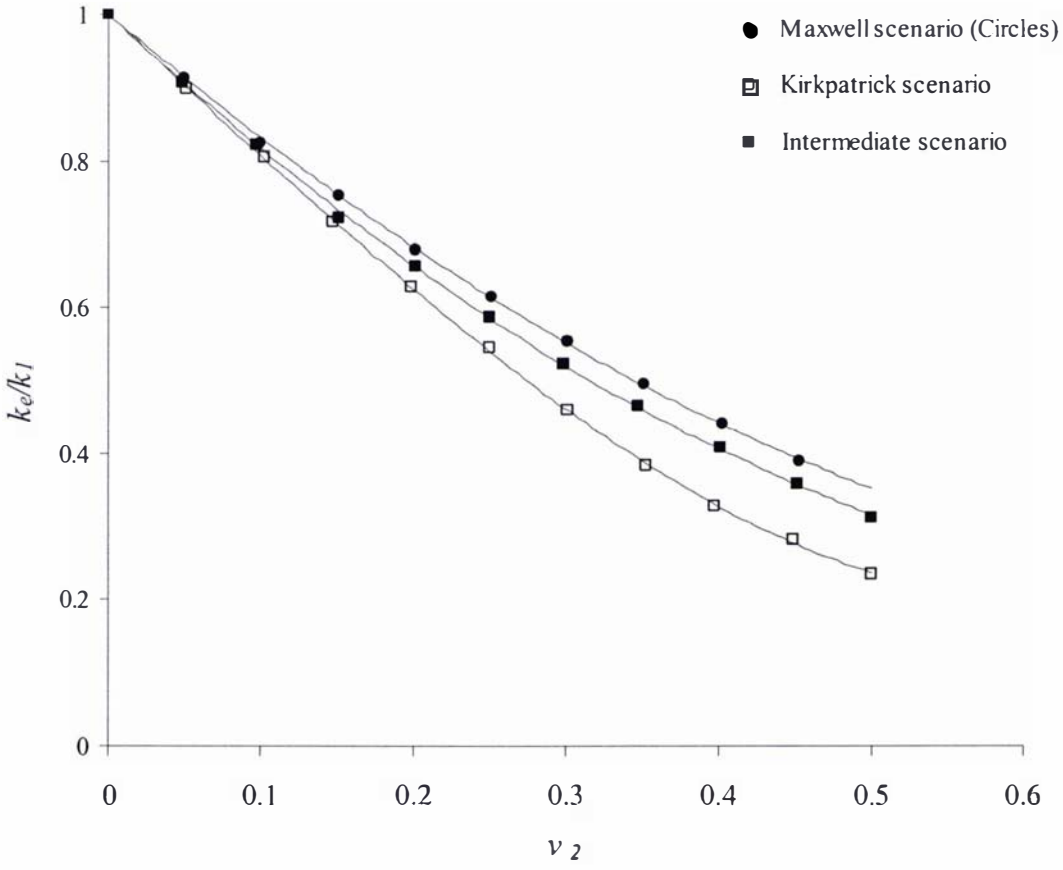

Figure 5.16: Mean k_e/k_1 results over a range of v_2 for three different 'pore' interaction scenarios (results from Simulation 4)

5.3.5 Effect of Component Thermal Conductivity Ratio (Simulation 5)

Figure 5.17 shows the mean k_e/k_1 results for a range of k_1/k_2 values between 0.005 and 200 for the Maxwell-type grids shown in Fig. 5.9a.

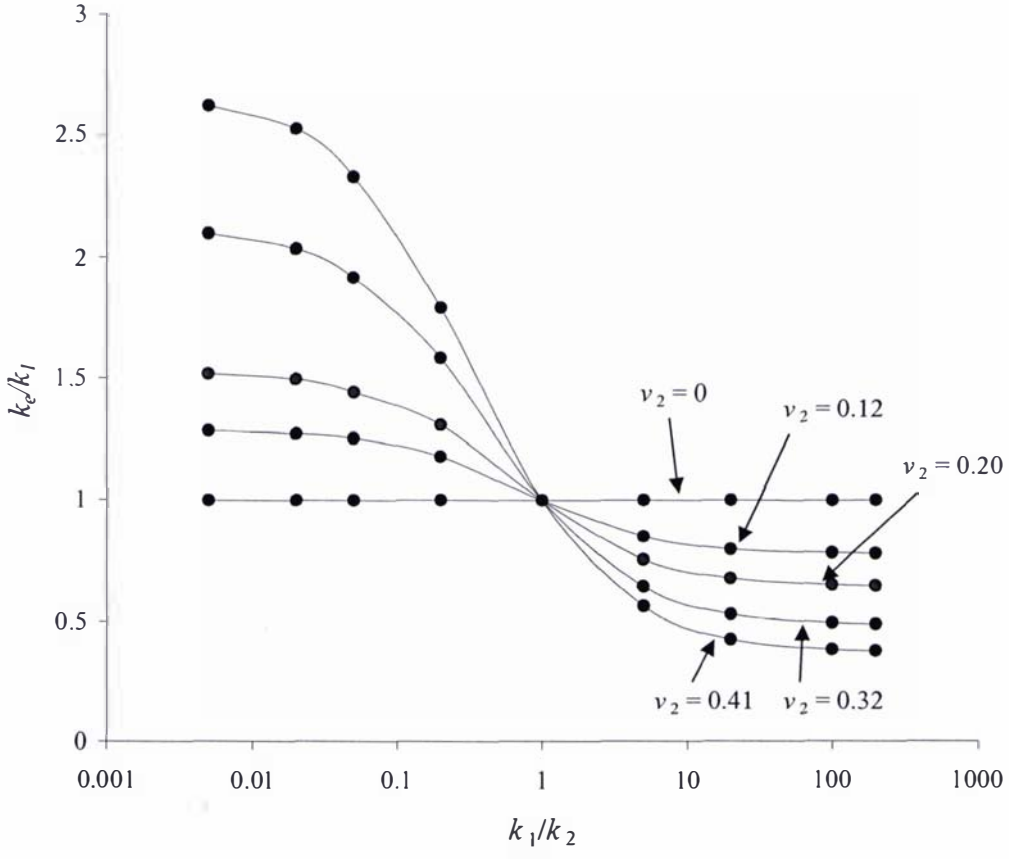

Figure 5.17: Mean k_e/k_1 results over a range of k_1/k_2 for Maxwell type FE grids (results from Simulation 5)

Figure 5.18 shows the mean k_e/k_1 results for a range of k_1/k_2 values between 1 and 200 for the Kirkpatrick-type grids shown in Fig. 5.9c (k_1/k_2 values below unity were not included since the EMT does not make a distinction between the continuous and dispersed phases).

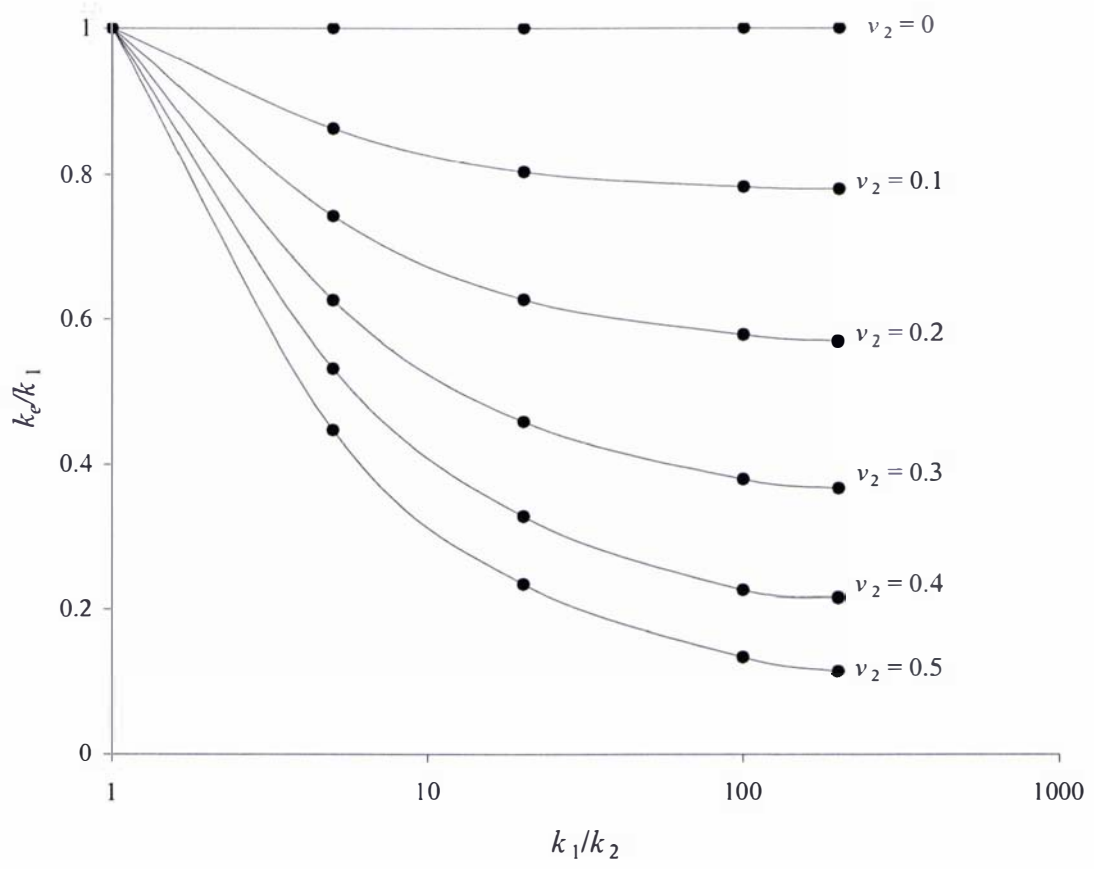

Figure 5.18: Mean k_e/k_1 results over a range of k_1/k_2 for Kirkpatrick type FE grids (results from Simulation 5)

5.4 Discussion

5.4.1 Limitations of Two-dimensional Simulations

The simulations were performed in two dimensions (2-D) which was sufficient for examining relative influences of structure-related variables, if not their absolute effects. There was uncertainty surrounding the issue of whether the influences of any variables were likely to be more pronounced, the same, or less pronounced in 2-D than in 3-D. However, it was reasonable to assume in the analysis of the results that if one variable showed a greater influence on the effective thermal conductivity than another in 2-D, then the same would be true in 3-D.

As has been mentioned previously, the fact that the simulations were not performed in three dimensions meant that direct comparisons between numerical results of the simulations and physical experiments could not be made, and it also provided difficulties in comparing some effective thermal conductivity model predictions to the result, as is discussed in Chapter 6.

5.4.2 Effect of Pore Size

As mentioned above, the results from the numerical simulations that examined the effect of individual pore size on thermal conductivity were similar to the equivalent experimental results. Both suggested a minor dependence of the effective thermal conductivity on relative pore size, with the effective thermal conductivity decreasing as the pore size increased, but the dependence was of a similar magnitude to the uncertainty in the results and so was not considered significant.

As with the EPS/guar gel results, the scatter in the numerical results from Simulation 1 increased as the pore size increased, and hence as the number of 'pores' decreased. This was most likely an indication of the degree of uniformity of distribution for the different grids, being good for the smallest ($R = 0.03X$) pores, but poor for the largest ($R = 0.12X$) pores. The spread of the replicates may be a useful indicator of whether the number of pores is sufficiently large to allow for the assumption of uniformity. For the smallest pores, the maximum standard deviation of the k_e/k_1 results was 1.8% of the mean, and hence a single replicate may provide a sufficient approximation of a uniform distribution. For the largest pores the standard deviation in the results was as high as 8% of the mean value, and hence a single replicate could not be relied upon as an approximation of a uniform distribution. A single pore with the smallest diameter ($R = 0.03X$) occupied 2.8 x 10^{-3} of the total FE grid area. It is reasonable to assume that, so long as individual pores are this size or smaller, a random Maxwell-type distribution in two-dimensions will also be a sufficient approximation of a uniform distribution.

5.4.3 Effect of Pore Shape

Based on the findings of Hamilton and Crosser, the shape of the pores was not expected to influence the effective thermal conductivity, since the conductivity of the continuous phase was significantly greater than the conductivity of the dispersed phase. While the results for the rectangles were noticeably different from the results for the circles and squares it was not clear how much was due to the pore shape alone and how much could be attributed to anisotropy — the orientation of the rectangles was not truly random since they were either exactly parallel or exactly orthogonal to the direction of heat flow. Regardless of the cause of the difference in the results, this difference was relatively minor, and since the majority of pores in foods tend to be roughly isometric, pores having aspect ratios as great as 2:1 would be uncommon.

5.4.4 Relative Influences of the Continuous and Dispersed Phases

The results displayed in Fig. 5.14 were consistent with an intuitive analysis of the heat transfer pathways involved in materials where one component is definitely dispersed and the other is definitely continuous. The question of whether the gaseous phase within a product forms a continuous or dispersed phase (or whether either component is in fact a genuine dispersed phase) is therefore an important issue, since the status of each component phase has such a significant influence on the effective thermal conductivity.

5.4.5 Effect of Pore Interaction

The difference between the pore interaction scenarios was more significant than the effect of pore shape or pore size. The results from the intermediate pore-contact scenario described above suggested that there may be a continuum of pore interaction scenarios between the Kirkpatrick and Maxwell scenarios. The degree of pore interaction was also dependent, to some extent, on the volume fraction of pores. Intuitively, it would be

expected that pore interaction would be negligible at low porosity, as long as the pores are randomly and uniformly dispersed, and hence the effective thermal conductivities of both the Maxwell and Kirkpatrick scenarios would be expected to be very similar, as was indeed the case, as shown in Figs. 5.15 and 5.16. As the porosity was increased and the probability of pore contact increased, the Maxwell and Kirkpatrick results diverged.

5.4.6 Effect of Component Thermal Conductivity Ratio

Figures 5.17 and 5.18 show that, for both the Maxwell and Kirkpatrick type distributions, the k_e/k_1 vs. v_2 trends have a significant dependence on the component thermal conductivity ratio between k_1/k_2 values of 0.01 and 100, but k_e/k_1 appears to approach a limiting value for a given v_2 outside this region.

5.5 Conclusions

The numerical models of Simulation 1 were two-dimensional forms of the basic structural model of the EPS/guar-gel food analogues described in Chapter 4. In Chapter 6 it will be shown that the EPS/guar-gel results were modelled well by the three-dimensional form of the Maxwell-Eucken model, while the numerical results from Simulation 1 were modelled well by a two-dimensional form of the Maxwell-Eucken model. On this evidence, the numerical simulations appeared to be in good agreement with the physical experiments, allowing for the different numbers of dimensions involved.

The method proved effective for examining the significance of the variables that had the potential to influence the effective thermal conductivity, and hence fulfilled the third objective outlined in Chapter 3. The results indicated that in addition to the component thermal conductivity ratio and volume fractions, the identification of continuous and

dispersed phases and the degree of pore contact were both influential variables, whereas the individual size and shape of the pores had only minor significance, if any at all.

As well as identifying the significance of certain variables to the effective thermal conductivity, the simulations also provided additional data that could be used, along with the data from the physical experiments described in Chapter 4, for model evaluation purposes.

Chapter 6: Model Evaluation

6.1 Introduction

6.1.1 Objective

The objective of this chapter was to compare predictions from a selection of effective thermal conductivity models against the data from the physical experiments and numerical simulations described in Chapters 4 and 5 in order to determine which model(s) were most suitable for predicting the thermal conductivity of porous foods.

6.1.2 Models Considered in the Evaluation Exercise

As was identified in Chapter 2, an abundance of effective thermal conductivity models may be found in the literature. As well as being highly impractical, an attempt to evaluate every model that has ever been proposed would be unnecessary since many models may be ruled out before any comparisons are made. The following criteria were used to select models for this evaluation exercise:

1. general applicability
2. physical structures appropriate for food materials
3. appropriate degree of complexity.

The first criterion ruled out models that were purely empirical as well as many purely theoretical models that had been derived for a single application. The second criterion ruled out any models that were based on detailed and specific geometry, as well as any anisotropic models (with the exceptions of the Series and Parallel models and simple derivatives), since this study was only concerned with macroscopically isotropic materials. The third criterion was imposed because of the context of this study; since the variability in food properties is comparatively high, there is little value in using highly complex models containing numerous

parameters. While not a rigid criterion, preference was also given to those models that were familiar to the food engineering literature.

Based on these criteria the models that were selected for this evaluation exercise are listed below. They were divided into two classes: those that were dependent solely on the component thermal conductivities and volume fractions (referred to as Type A models), and those that also contained a single, adjustable parameter (referred to as Type B models). Each of the models was introduced briefly in Section 2.2 of Chapter 2.

Type A: *Models without adjustable parameters*
Series (Eq. 2.7), Parallel (Eq. 2.8), Geometric (Eq. 2.9), Cheng-Vachon (2.12), Russell (Eq. 2.13), Maxwell-Eucken (Eqs. 2.20 and 2.21), Landauer-EMT (Eq. 2.26), Levy (Eqs 2.23 and 2.20), Kopelman Isotropic (with k_1 much greater than k_2, Eq. 2.29)

Type B: *Models containing one adjustable parameter*
Krischer (Eq. 2.10), Chaudhary-Bhandari (Eq. 2.11), Maxwell-Hamilton (Eq. 2.22), Kirkpatrick-EMT (2.27)

Models containing more than one adjustable parameter were not considered, based on a recommendation made by Rahman (1995) that implied that semi-empirical models that contain a single adjustable parameter would suit applications in the food industry best.

Thirteen models were considered in the validation exercise, nine Type A models and four Type B models. This number might not seem very large even given the selection criteria, however this group did include the majority of the most commonly used models in the food industry (see lists in Rahman, 1995, *ASHRAE Handbook of Refrigeration*, 1998). In addition, since the Series/Parallel and Maxwell-Eucken models formed the bases of a large proportion of published models, the important basic physical structures were covered.

6.2 Comparisons of Model Predictions with Data from Physical Experiments

6.2.1 EPS/Guar-gel Data

Since the size of the pores did not appear to have a significant effect on the thermal conductivity of the EPS/gel datasets described in Chapter 4, the effective thermal conductivity models were compared to the combined data from Datasets 1 to 3.

6.2.1.1 Comparison of Type A Models with EPS/gel results

Figure 6.1 shows the results from EPS/guar gel samples plotted with the predictions from the Type A models. The mean absolute discrepancies (AD_M) between the data and the models, as defined by Eq. (6.1), are listed in Table 6.1.

$$AD_{\mathrm{M}} = \frac{\sum_{n} \sqrt{\left(k_{\text{experiment}} - k_{\text{predicted}}\right)^2}}{n_d} \tag{6.1}$$

AD_{M} = mean absolute discrepancy, n_d = number of data points

Model	*Mean Absolute Discrepancy*
Parallel	0.063
Series	0.45
Geometric	0.20
Maxwell-Eucken	0.015
Landauer-EMT	0.059
Levy	0.14
Russell	0.021
Kopelman	0.014
Cheng-Vachon	0.038

Table 6.1: Mean absolute discrepancies between Type A models and EPS/guar-gel data

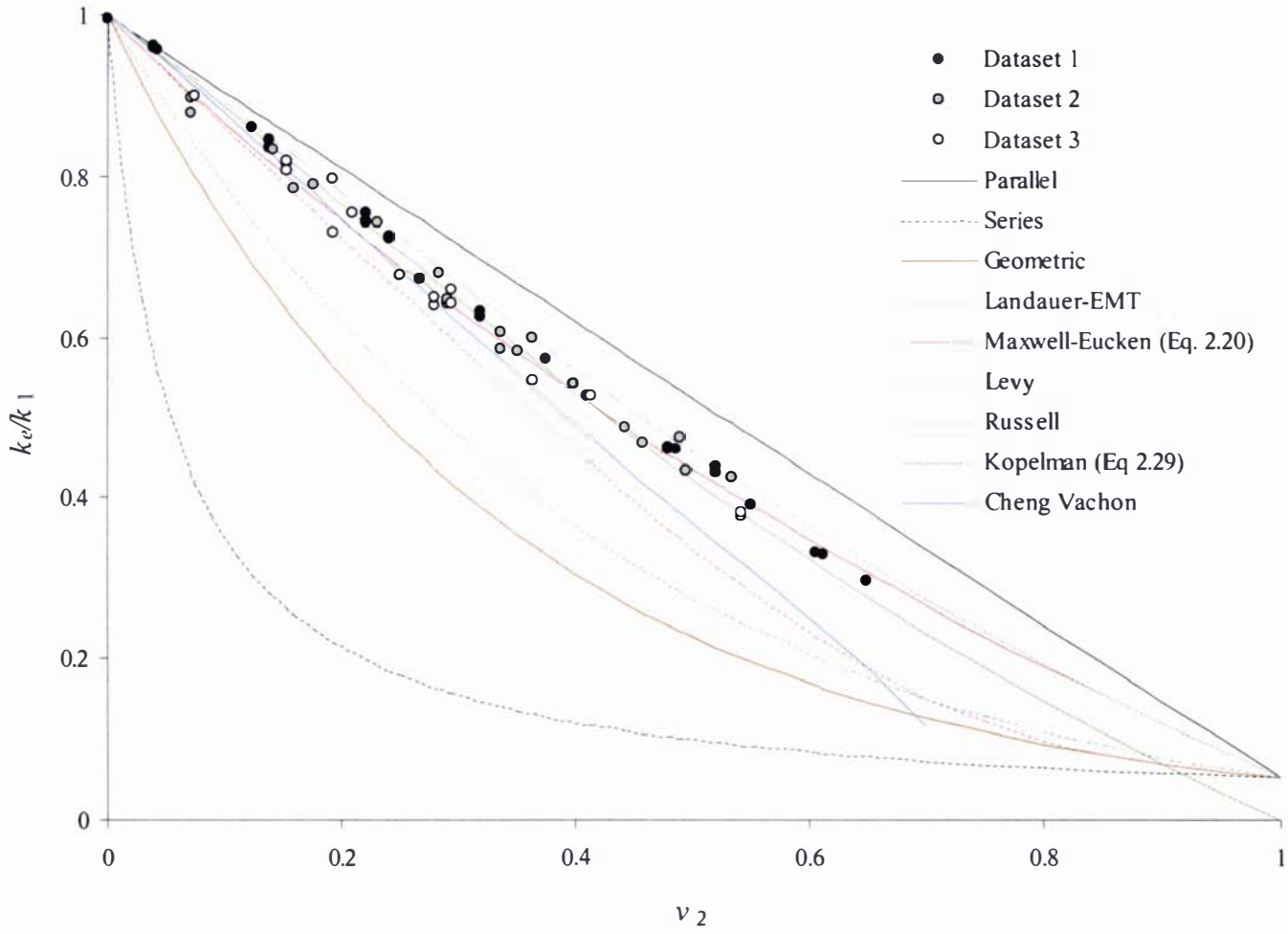

Figure 6.1: Comparison of model predictions from Type A models with EPS/guar-gel results

Figure 6.1 shows that three models - Russell's model (Eq. 2.13), the Maxwell-Eucken model (Eq. 2.20) and the Kopelman Isotropic model (Eq. 2.29) - provided good predictions of the thermal conductivity of the EPS/guar gel mixture over a range of volume fractions. At lower volume fractions ($v_2 < 0.2$) the Landauer-EMT (Eq. 2.26) and Cheng-Vachon (Eq. 2.12) models also provided reasonable predictions.

6.2.1.2 Comparison of Type B Models with EPS/guar-gel results

Figure 6.2 shows the results from EPS/guar-gel plotted with the Type B models which were fitted to the data by a least-squares method. The numerical values of the adjustable parameter as well as the mean absolute discrepancy values (see Eq. 6.1) are shown in Table 6.2.

Model	Mean Absolute Discrepancy	Best-Fit Parameter Value
Maxwell-Hamilton	0.014	3.3
Kirkpatrick-EMT	0.014	10.5
Krischer	0.019	0.034
Chaudhary-Bhandari	0.024	0.93

Table 6.2: Mean absolute discrepancy and best-fit parameter values from the least-squares curve fitting procedure for the results displayed in Figure 6.2

Figure 6.2 shows that all four models that were considered fit the data well over the range of volume fractions for which experiments were performed, although the AD_M values of the Maxwell-Hamilton and Kirkpatrick-EMT models were lower than the values of the other two models.

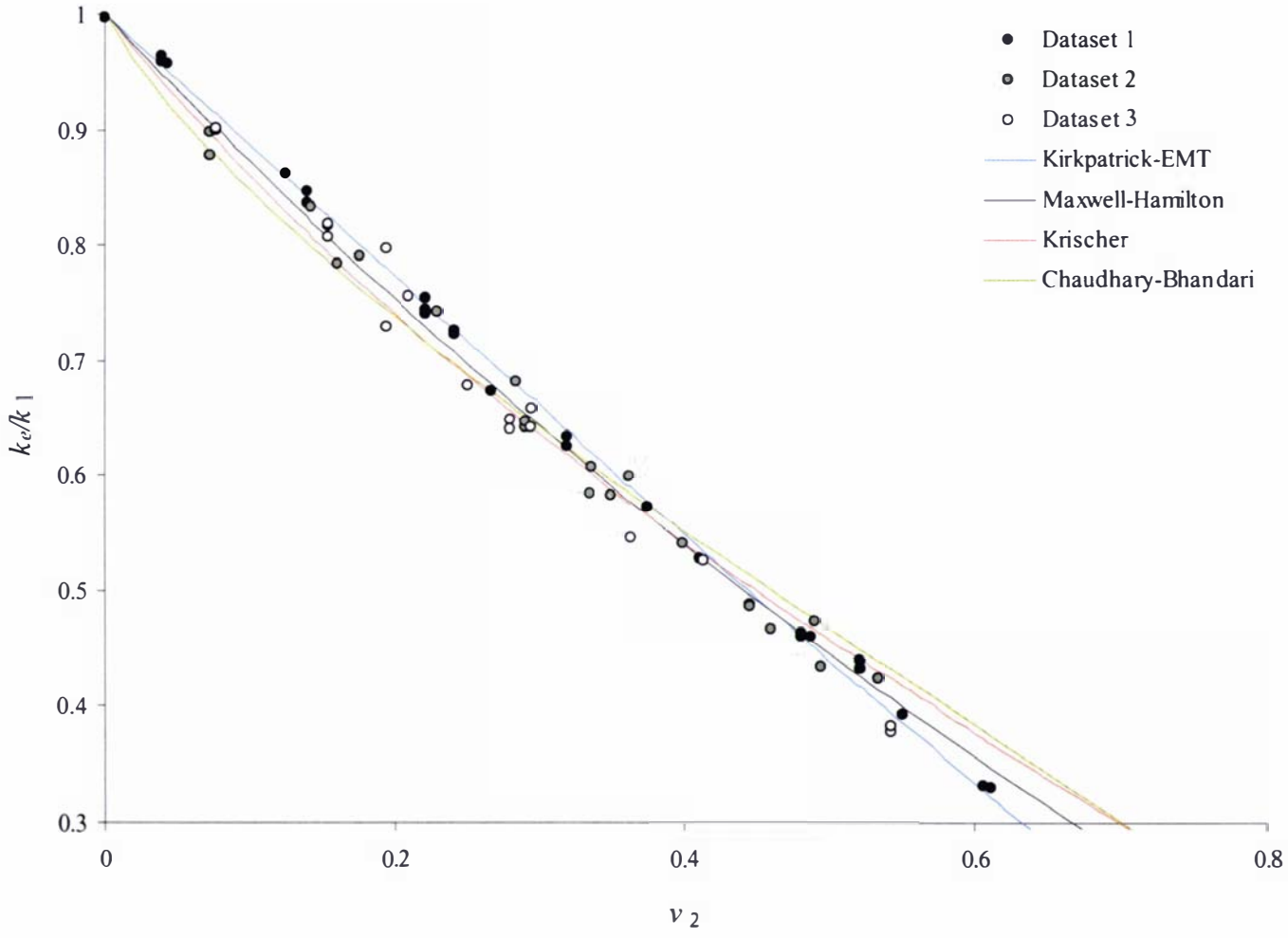

Figure 6.2: Comparison of Type B models that have been fitted to the results from EPS/guar gel results

Keey (1972) reported values for the *f*-parameter of Krischer's model of 0.2 to 0.25, while Lin recommended an average value of 0.16. Chaudhary & Bhandari (1968) recommended *f*-values between 0.8 and 0.9 for their model. Had these *f*-values been used in the prediction of the effective thermal conductivity of the EPS/guar-gel samples, the AD_M values would have been between 0.16 and 0.22 for Krischer's model and between 0.033 and 0.10 for the Chaudhary-Bhandari model. However, it was pointed out that the *f*-parameter in both models was dependent on the material under consideration, and hence variations in the numerical values of *f* were to be expected.

6.2.2 Aluminium/Guar-gel Data

6.2.2.1 Comparison of Type A Models with Aluminium/Guar-gel Results

Figure 6.3 shows the results from Dataset 4 plotted against the predictions of the Type A models. The mean absolute discrepancies between the data and the models are listed in Table 6.3.

Model	*Mean Absolute Discrepancy*
Parallel	105
Series	2.8
Geometric	33
Maxwell-Eucken (Eq. 2.20)	1.7
Maxwell-Eucken (Eq. 2.21)	81
Landauer-EMT	6.0
Cheng-Vachon	1.2

Table 6.3: Mean absolute discrepancies between Type A models and aluminium/guar-gel data

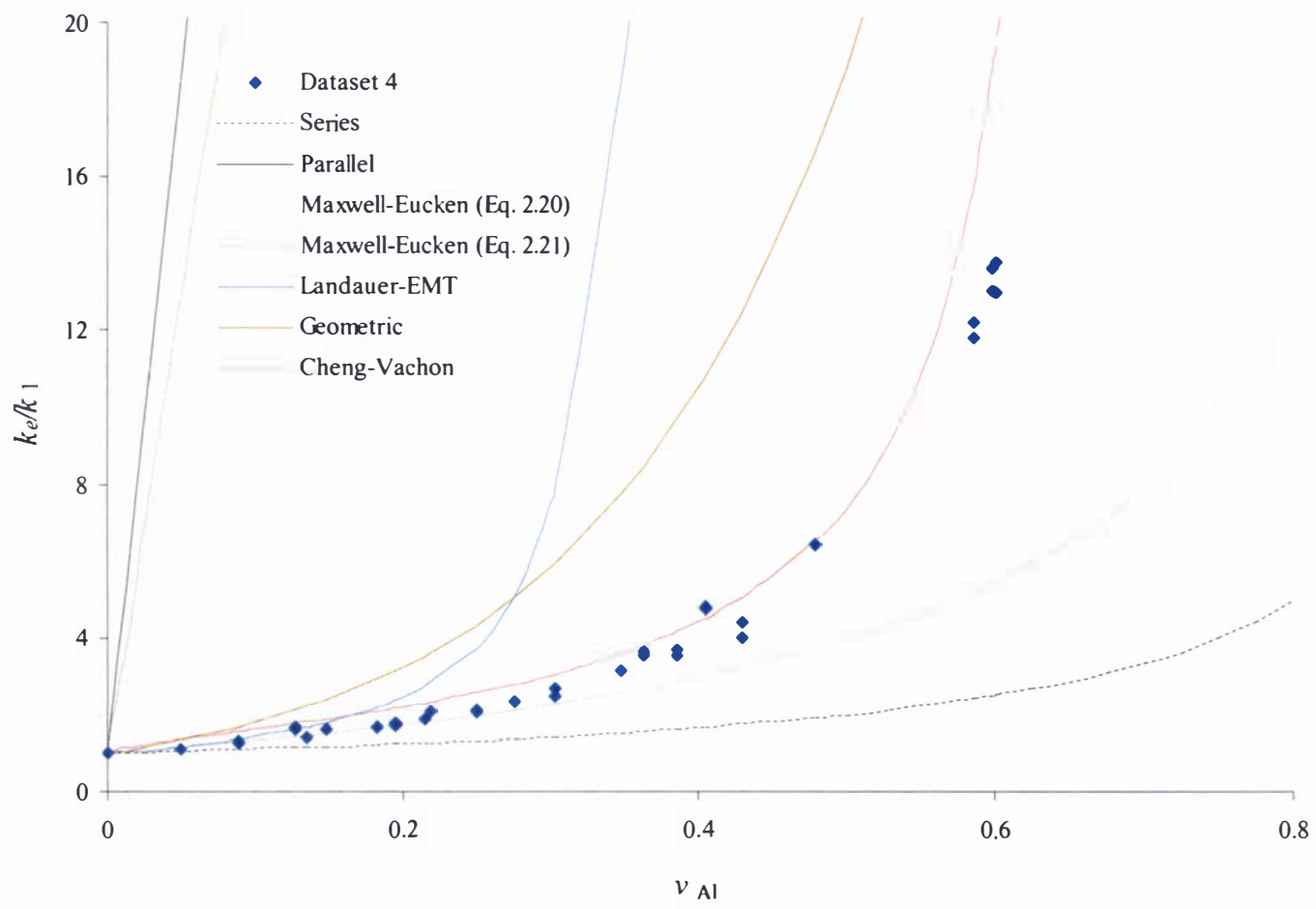

Figure 6.3: Comparison of model predictions from Type A models with aluminium/guar-gel results

Because of the extreme difference between the thermal conductivities of the components of the aluminium/guar-gel samples (see Table 4.1 of Chapter 4) the envelopes between the Wiener and Hashin-Shtrikman bounds were very wide, as is clearly shown by Fig 6.3. The Cheng-Vachon model provided the closest predictions to the experimental data, although for predictions above a volume fraction of aluminium of 0.5 the value of $d(k_e/k_1)/dv_2$ became very large and the accuracy of the prediction of effective thermal conductivity became extremely sensitive to the uncertainty in the value of v_2.

6.2.2.2 Comparison of Models Type B with Aluminium/Guar-gel Results

Figure 6.4 shows the results from Dataset 4 plotted with the Type B models which were fitted to the data by a least-squares method. The numerical values of the adjustable parameter as well as the mean absolute discrepancy values from the least-squares method are shown in Table 6.4.

Model	Mean Absolute Discrepancy	Best-Fit Parameter Value
Maxwell-Hamilton	1.1	7.2
Kirkpatrick-EMT	0.65	3.2
Krischer	2.2	0.29
Chaudhary-Bhandari	2.1	0.28

Table 6.4: Mean absolute discrepancy and best-fit parameter values from the least-squares curve fitting procedure for the results displayed in Figure 6.4

Table 6.4 shows that, of the four models that were considered, the Kirkpatrick-EMT model provided the best fit to the data according to the AD_M values.

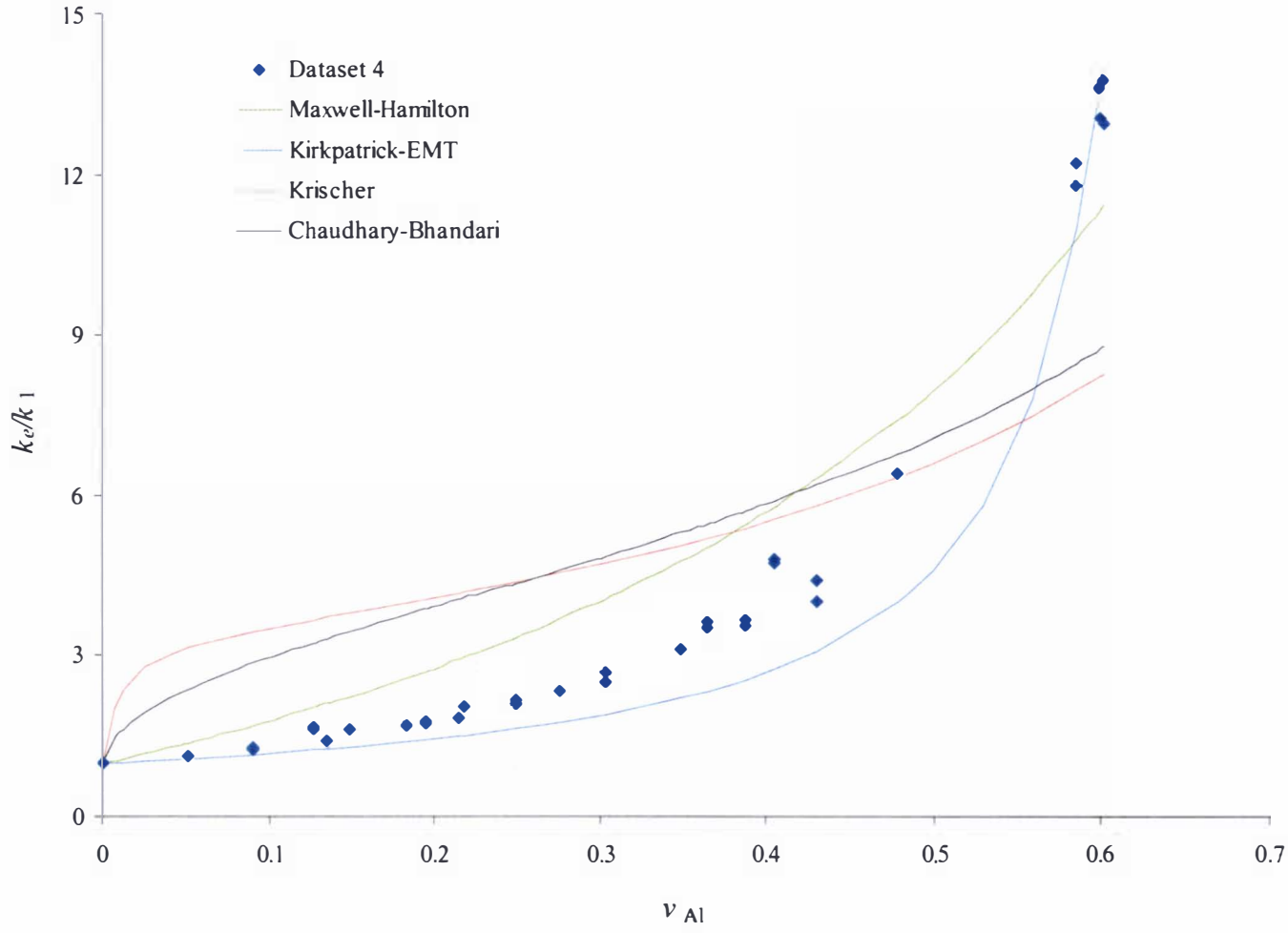

Figure 6.4: Comparison of Type B models that have been fitted to the results from Dataset 4

6.3 Comparison of Model Predictions with Numerical Simulation Data

6.3.1 Comparison of Selected Type A Models to Simulation Data

Apart from the Series, Parallel and Geometric models, most of the Type A models listed in Section 6.1.2 assumed three-dimensional geometries, which meant that direct comparisons with the results from the two-dimensional numerical simulations would have had little value. However, some of the models could be converted to two-dimensional form, as was shown by Kirkpatrick (1973) with the EMT equation (see Section 2.3.5.2 of Chapter 2). If a Z-value of 4 is substituted into Eq. (2.27), it is reduced to:

$$(1-v_2)\frac{k_1-k_e}{k_1+k_e}+v_2\frac{k_2-k_e}{k_2+k_e}=0 \qquad (6.2)$$

which may be thought of as a two-dimensional equivalent of Landauer's EMT model (Eq. 2.25). The conversion of the EMT from a three-dimensional form to a two-dimensional form resulted in the change of the coefficient of k_e in the denominator of Eq. (2.25) from a value of 2 to a value of 1 (compare Eq. 6.2 with Eq. 2.25) and since both the EMT and the Maxwell-Eucken models may be derived from Eq. (2.14);

$$T_m = br\cos\theta - bR^3\frac{k_s-k_m}{k_s+2k_m}\frac{\cos\theta}{r^2} \qquad (2.14)$$

it seemed reasonable to assume that the Maxwell-Eucken model could be reduced from a three-dimensional form to a two-dimensional form by the same process. Equations (6.3) and (6.4) were therefore proposed as two-dimensional forms of Eqs. (2.20) and (2.21):

$$k_e = k_1 \frac{k_1 + k_2 - (k_1 - k_2)v_2}{k_1 + k_2 + (k_1 - k_2)v_2} \tag{6.3}$$

$$k_e = k_2 \frac{k_2 + k_1 + (k_1 - k_2)(1 - v_2)}{k_2 + k_1 - (k_1 - k_2)(1 - v_2)} \tag{6.4}$$

Based on Kirkpatrick's results it was expected that Eq. (6.2) would provide good predictions of the simulation results from FE grids of the type shown in Fig 5.9c (Chapter 5). This proved to be the case, as shown in Fig. 6.5. The mean absolute discrepancy between the model and the simulation results was 0.046.

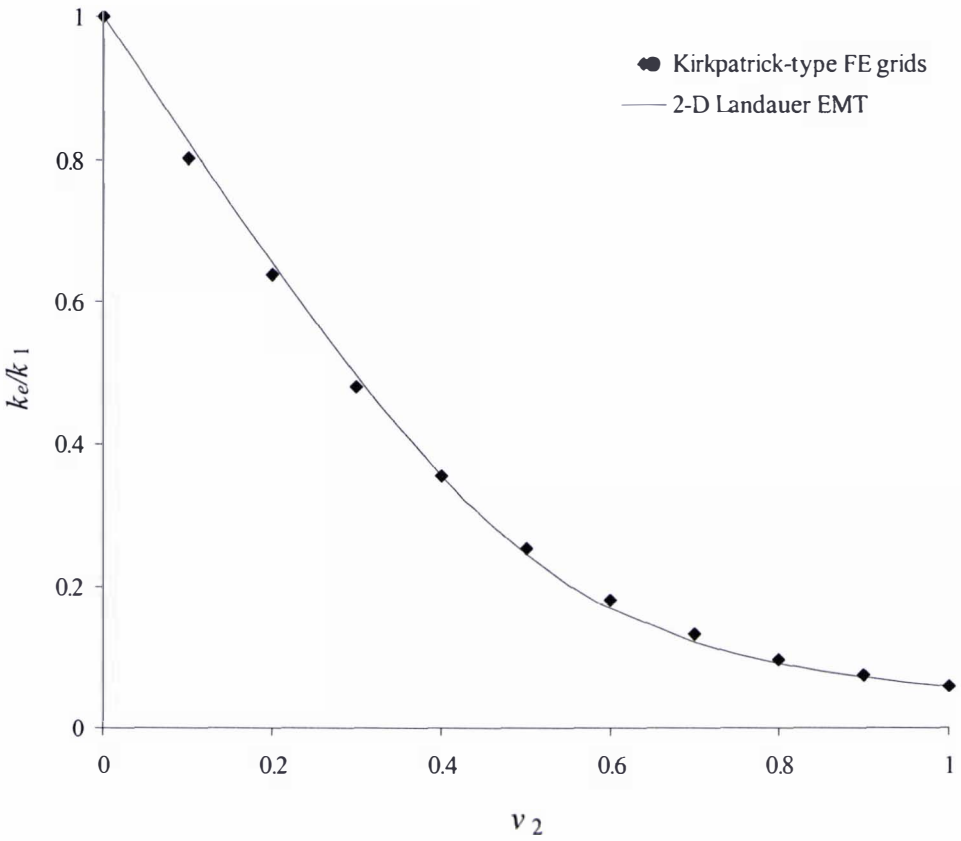

Figure 6.5: Comparison of numerical simulation results for 'Kirkpatrick'-type FE grids with two-dimensional EMT model (AD_M = 0.046)

If the reasoning used to derive Eqs. (6.3) and (6.4) was sound, then it would be expected that Eq. (6.3) would provide good predictions for the simulation results from FE grids of the type shown in Fig 5.9a (Chapter 5). This also proved to be the case, as shown in Fig. 6.6 (AD_M = 0.014):

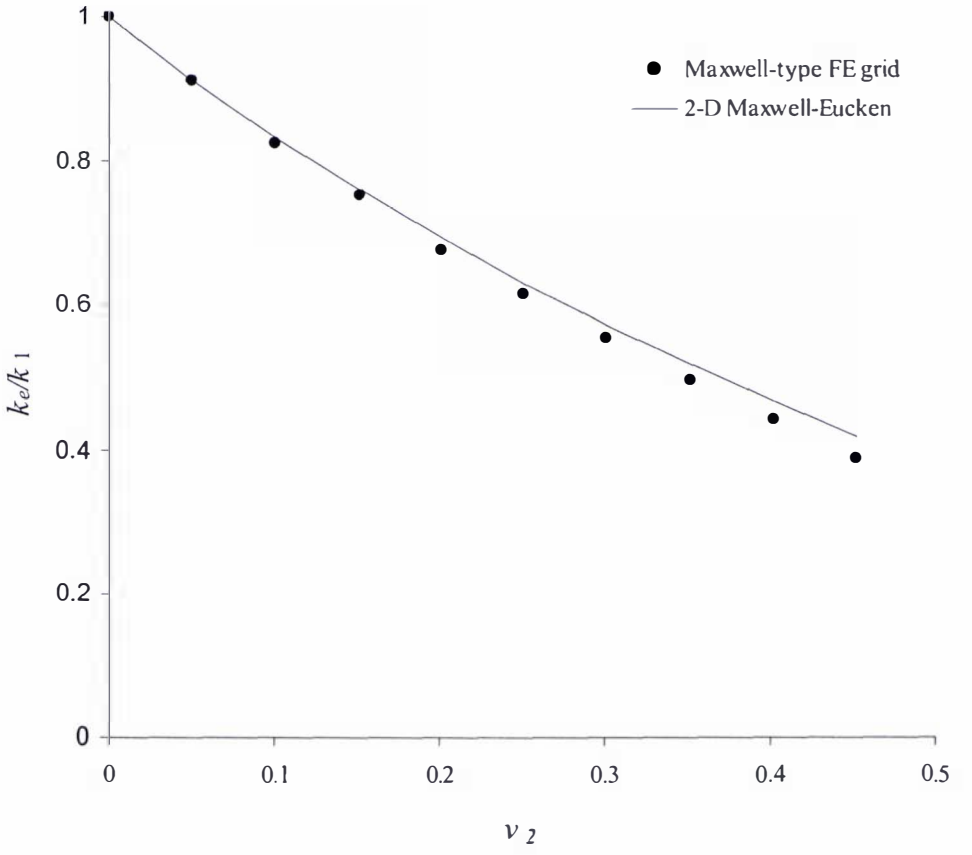

Figure 6.6: Comparison of numerical simulation results for 'Maxwell'-type FE grids with two-dimensional Maxwell-Eucken model (AD_M = 0.014)

Finally, it would be expected that the simulation results from FE grids of the type shown in Fig 5.9b would lie between the predictions of Eqs. (6.1) and (6.2), which was the case, as is shown in Fig. 6.7:

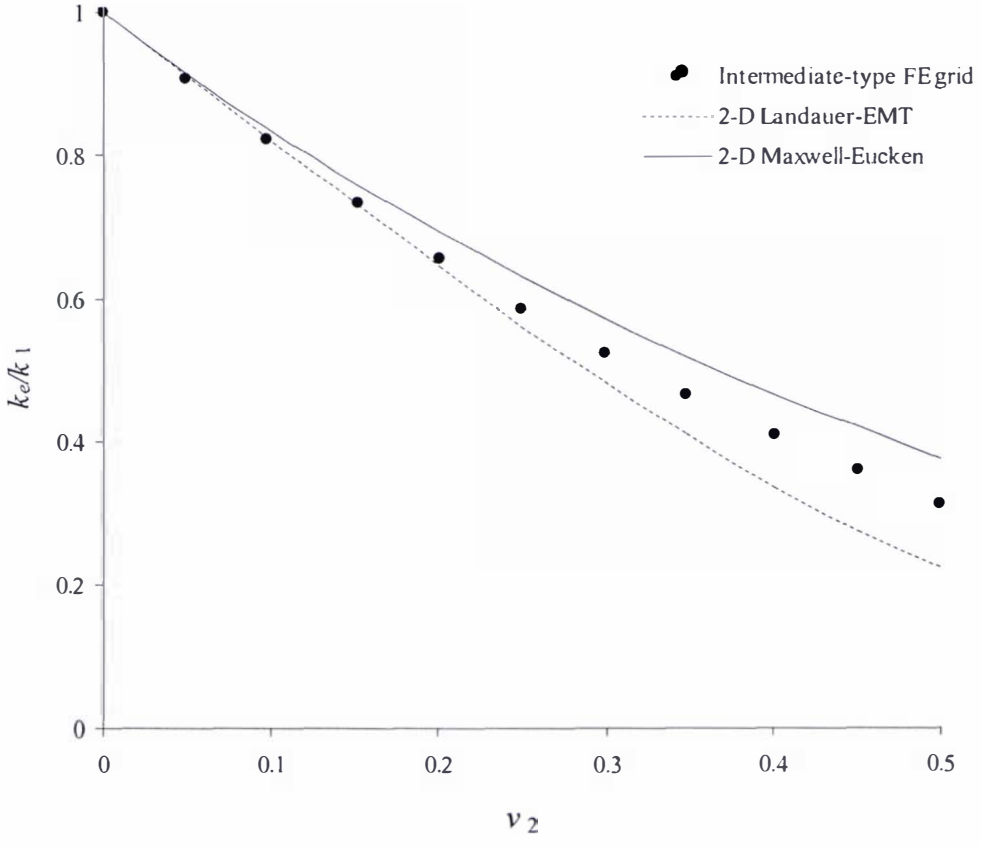

Figure 6.7: Comparison of numerical simulation results for 'Intermediate'-type grids with two-dimensional Maxwell-Eucken model and two-dimensional EMT model

6.3.2 Comparison of Type B Models to Simulation Data

Since the Type B models contained adjustable parameters, they were not restricted by the number of dimensions involved. Figure 6.8 shows the simulation results for the Maxwell-type FE grids plotted with the Type B models which were fitted to the data by a least-squares method. The numerical values of the adjustable parameters as well as the mean absolute discrepancy values from the least-squares method are shown in Table 6.5.

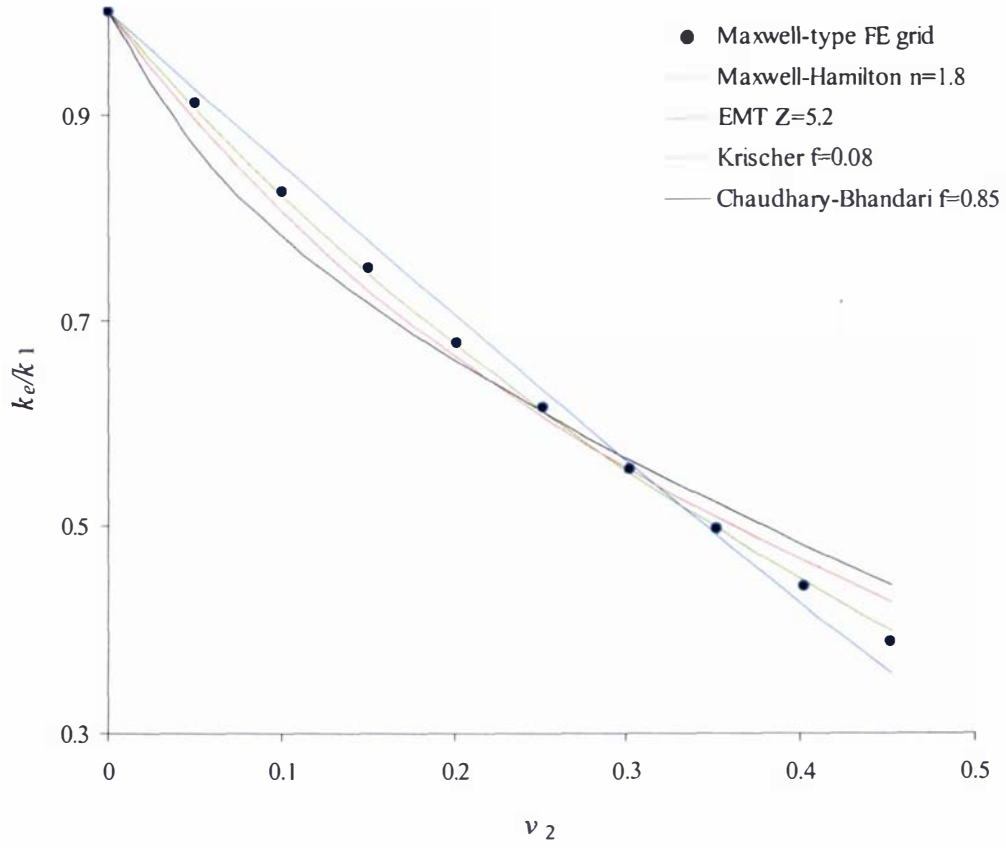

Figure 6.8: Comparison of Type B models that have been fitted to the simulation results from 'Maxwell'-type FE grids: **1** Krischer, **2** Chaudhary-Bhandari, **3** Maxwell-Hamilton, **4** Kirkpatrick-EMT

Model	Mean Absolute Discrepancy	Best-Fit Parameter Value
Maxwell-Hamilton	0.0047	1.8
Kirkpatrick-EMT	0.016	5.2
Krischer	0.016	0.076
Chaudhary-Bhandari	0.027	0.85

Table 6.5: Mean absolute discrepancy and best-fit parameter values from the least-squares curve fitting procedure for the results displayed in Figure 6.8

Similarly, the Type B models were fitted to the results for the Intermediate and Landauer type FE grids as well:

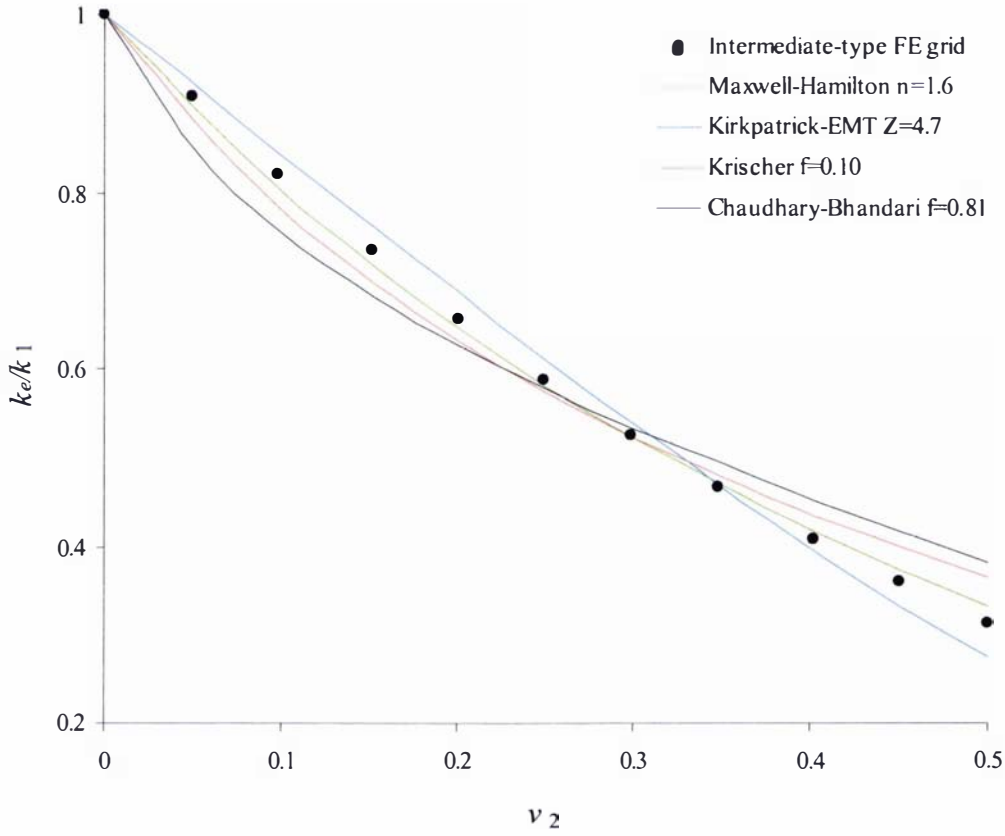

Figure 6.9: Comparison of Type B models that have been fitted to the simulation results from 'Intermediate'-type FE grids

Model	Mean Absolute Discrepancy	Best-Fit Parameter Value
Maxwell-Hamilton	0.010	1.6
Kirkpatrick-EMT	0.020	4.7
Krischer	0.024	0.098
Chaudhary-Bhandari	0.038	0.81

Table 6.6: Mean absolute discrepancy and best-fit parameter values from the least-squares curve fitting procedure for the results displayed in Figure 6.9

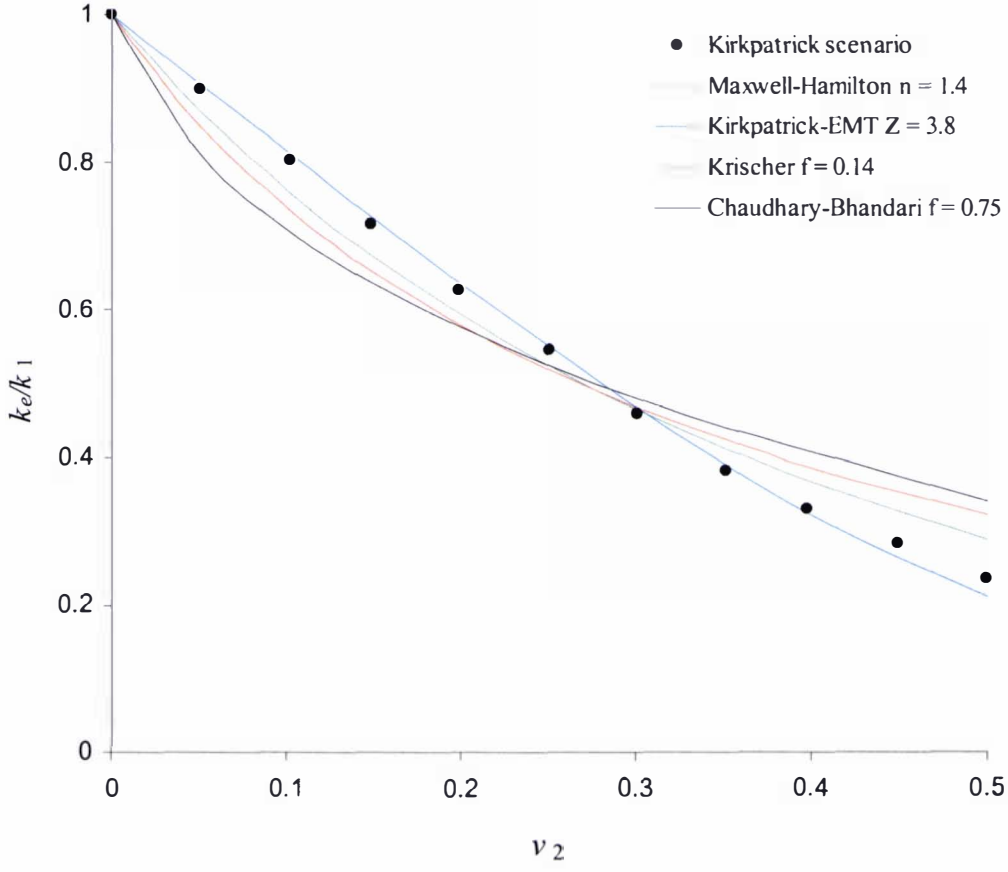

Figure 6.10: Comparison of Type B models that have been fitted to the simulation results from Kirkpatrick-type FE grids

Model	Mean Absolute Discrepancy	Best-Fit Parameter Value
Maxwell-Hamilton	0.031	1.4
Kirkpatrick-EMT	0.0087	3.8
Krischer	0.048	0.14
Chaudhary-Bhandari	0.063	0.75

Table 6.7: Mean absolute discrepancy and best-fit parameter values from the least-squares curve fitting procedure for the results displayed in Figure 6.10

6.3.3 Comparison between Model Predictions and Simulation Data for Extreme Values of k_1/k_2

Figures 6.5 and 6.6 showed that the two-dimensional forms of the Maxwell-Eucken and Landauer-EMT models provided good predictions for the Maxwell and Kirkpatrick type grids respectively, for a k_1/k_2 value of 20. In Section 5.4.6 it was suggested that the k_e/k_1 vs. k_1/k_2 plots for the Maxwell and Kirkpatrick-type grids (Figs. 5.17 and 5.18) approached limiting values for a given v_2. Equations 6.5 and 6.6 show forms of Eqs. (6.3) and (6.2) respectively, rearranged such that the component thermal conductivities are combined in a single term:

$$\frac{k_e}{k_1} = \frac{1 + k_2/k_1 - (1 - k_2/k_1)v_2}{1 + k_2/k_1 + (1 - k_2/k_1)v_2} \tag{6.5}$$

$$(1 - v_2)\frac{1 - k_e/k_1}{1 + k_e/k_1} + v_2\frac{k_2/k_1 - k_e/k_1}{k_2/k_1 + k_e/k_1} = 0 \tag{6.6}$$

In the limit as k_2/k_1 approaches zero (k_1/k_2 approaches ∞), Eqs. (6.5) and (6.6) may be reduced to Eqs. (6.7) and (6.8) respectively:

$$\frac{k_e}{k_1} = \frac{1 - v_2}{1 + v_2} \tag{6.7}$$

$$\frac{k_e}{k_1} = 1 - 2v_2 \tag{6.8}$$

(Eq. 6.8 provides predictions up to $v_2 = 0.5$ beyond which point $k_e/k_1 = 0$).

Figure 6.11 shows the portion of Fig. 5.17 ($k_1/k_2 > 1$) along with the limiting k_e/k_1 values at each v_2 as predicted by Eq. (6.7).

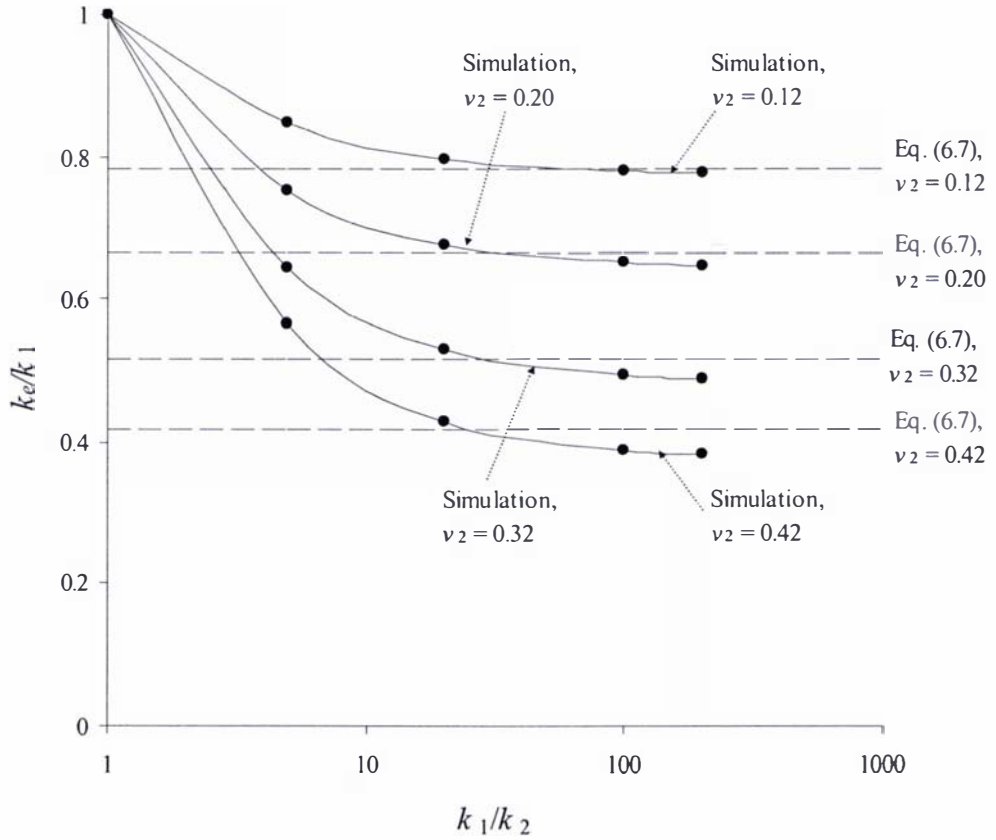

Figure 6.11: Comparison between simulation data and model predictions for limiting k_e/k_1 values for Maxwell-type FE grids

The mean absolute discrepancy between the predictions of the k_e/k_1 limits and simulation results for $k_1/k_2 = 200$ was 0.022.

Figure 6.12 shows a similar plot to Fig. 6.11 for the Kirkpatrick-type grids:

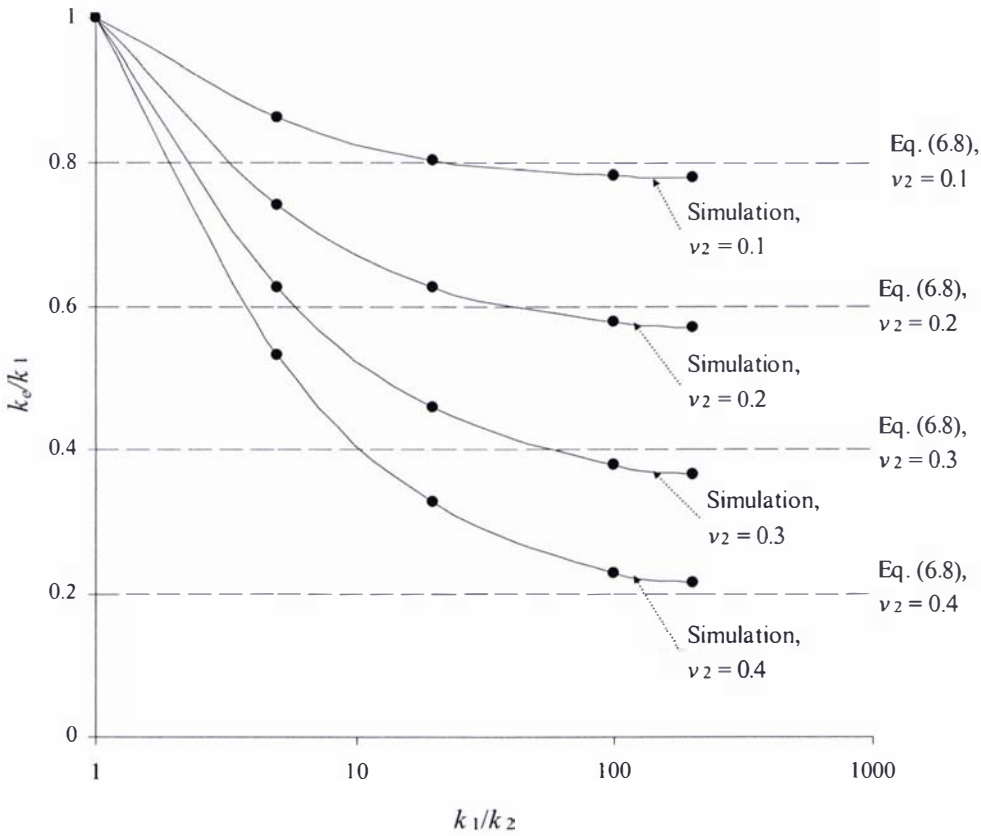

Figure 6.12: Comparison between simulation data and model predictions for limiting k_e/k_1 values for Kirkpatrick-type FE grids

The mean absolute discrepancy between the predictions of the k_e/k_1 limits and simulation results for $k_1/k_2 = 200$ was 0.025.

6.4 Discussion

6.4.1 Accuracy of Predictions for EPS/Guar-gel Food Analogue

6.4.1.1 Type A Models

Nesvadba (1981) suggested that uncertainties in thermal conductivity data of up to 10% were sufficient for calculations in engineering design. As mentioned in Section 6.2, the Russell, Maxwell-Eucken, and Kopelman Isotropic models all provided good predictions for the EPS/guar-gel samples over the range of porosity considered. The mean relative discrepancy between the measured and predicted thermal conductivity value was 2% for the Maxwell-Eucken and Kopelman models and 3% for Russell's model, which, using Nesvadba's guideline, would be quite acceptable for the food industry.

Given that the structure of the food analogue was very similar to the structure assumed by the Maxwell-Eucken model it was to be expected that this model would provide accurate predictions, although it wasn't expected to provide such good predictions at higher porosities (0.4 to 0.65). The form of Kopelman's model that was used (Eq. 2.29) relied on having the conductivity of the continuous phase significantly higher than the conductivity of the dispersed phase, and so the predictions might not have been as accurate if the continuous phase had not had such a high water content. Regardless of the component thermal conductivities involved, the numerical values of the predictions from the Russell and Maxwell-Eucken models are always similar to each other.

As was discussed in Section 4.5.2 of Chapter 4, this particular food analogue would by no means be representative of all porous foods, and, therefore, while the Maxwell-Eucken model fitted the EPS/guar-gel data well, on this evidence alone it cannot be concluded that it would provide accurate predictions for all porous foods.

6.4.1.2 Type B Models

As mentioned in Section 6.2, all four Type B models fitted the EPS/gel data reasonably well over the entire range of v_2 values considered, with the best fit, according to the AD_M values, being provided by the Kirkpatrick-EMT model. The f-value in Krischer's model of 0.034 was significantly different from the value of 0.16 recommended for a porous food material by Lin (Lin *et al.*, 1997 and Lin, 1994), although it should be pointed out that Lin noticed a dependence of f value on v_2, and an f value of 0.16 was quoted as an average value over a range of volume fractions. This discrepancy is discussed in Chapter 7.

6.4.2 Accuracy of Predictions for Aluminium/Guar-gel Samples

6.4.2.1 Type A Models

The Maxwell-Eucken model provided reasonable predictions (uncertainty <10%) at low volume fractions of aluminium, but above a v_2 value of 0.3 the discrepancy between the predictions and the experimental data increased rapidly. The Cheng-Vachon model provided good predictions over the range of v_2 considered, although, as mentioned above, for v_2 values above 0.5 the value of $d(k_e/k_1)/dv_2$ was so high that uncertainties in the predictions of k_e would be very large, regardless of the model used.

6.4.2.2 Type B Models

Of the type B Models, only the Kirkpatrick-EMT model could follow the basic trend in the k_e/k_1 vs. v_2 data for the aluminium/guar-gel samples. This observation highlighted the importance of choosing an appropriate model for a given application. Just because a model contains an adjustable fitting parameter does not necessarily mean it will provide acceptable predictions over a range of compositions, even if the parameter has been fitted to experimental data.

6.4.3 Accuracy of Predictions for Numerical Simulation Results

The two-dimensional forms of the Maxwell-Eucken and Landauer-EMT models (Eqs. 6.2 and 6.3) provided reasonable predictions for the Maxwell and Kirkpatrick type structures respectively, both at $k_1/k_2 = 20$ and as k_1/k_2 approached infinity. Given that the three-dimensional form of the Maxwell-Eucken model provided good predictions for a real Maxwell-type structure (the EPS/guar-gel food analogues), the agreement between the effective thermal conductivity models and the finite element models for their respective structure-types supported the numerical method used in the simulations described in Chapter 5.

As with the data from the physical experiments, the Maxwell-Hamilton and Kirkpatrick-EMT models consistently provided more accurate fits to the simulation data than the Krischer and Chaudhary-Bhandari models over the range of v_2 values involved. Since the Maxwell and EMT based models assumed isotropy, whereas the Krischer and Chaudhary-Bhandari models were weighted means of the highly anisotropic Series and Parallel models, this observation was not surprising because all the component distributions involved in the simulations were essentially isotropic. Again the point is emphasised that the plots of different models cannot necessarily be superimposed on each other simply by changing the value of the adjustable parameter (unless it is adjusted separately for each data point, which would largely defeat the purpose of the model).

6.5 Conclusion

The model evaluation was performed to meet the fourth objective listed in Chapter 3. The Maxwell-Eucken model provided good predictions (within 2%) of the effective thermal conductivity of the EPS/guar-gel food analogues, however this was expected since they were Maxwell-type structures. The Maxwell-Eucken model did not provide good predictions over the range of composition for the aluminium/guar-gel samples. In fact, none of the Type A models provided good predictions over a wide range of composition for all the applications considered (both physical experiments and numerical simulations).

The Maxwell and EMT based models consistently provided better predictions than the Series/Parallel based models (i.e. the Krischer and Chaudhary-Bhandari models), which highlighted the importance of choosing a model which assumed an appropriate structure, even if the models are to be fitted to experimental data. Of the Maxwell and EMT based models, the Maxwell based models provided the better predictions on average, with the notable exception of the aluminium/guar-gel samples.

Chapter 7: General Discussion

7.1 Introduction

7.1.1 Objective

The aim of this chapter was to propose guidelines for a general approach to the prediction of the effective thermal conductivity of isotropic materials based on the results and conclusions from Chapters 4 to 6. Particular emphasis was placed on porous foods in keeping with the project objectives.

7.1.2 Deficiencies in the Food Engineering Literature with regard to Effective Thermal Conductivity Prediction

Much of the literature concerned with the prediction of the thermal conductivity of foods may be fitted into two basic categories: food-engineering/food-properties handbooks, and model evaluation exercises. The typical approach of handbook-type literature has been to provide lists of effective thermal conductivity models that have been used for foods, but only a little commentary on the suitability and limitations of their applications (see for example Miles *et al.*, 1983, Rahman, 1995, *ASHRAE Handbook of Refrigeration*, 1998, and Rahman, 2001b). Typical examples of model-evaluation literature have compared predictions from selected models with experimental data for one class of foods (such as powders, Murakami & Okos, 1989, or meat/offal, Pham & Willix, 1989), but have not provided (or necessarily intended to provide) convincing evidence that models that were accurate for the foods considered in their evaluation would be equally accurate if applied to other food types.

A more attractive reference tool would be a general set of guidelines advising a food engineer how to go about the task of predicting the effective thermal conductivity of foods from start to finish, including the selection of an

appropriate model. However, aside from Kopelman's approach (see Section 2.3.6.2 of Chapter 2), the literature does not appear to contain any such guidelines. Some of the texts referred to above provided worked examples, but the reasons for their choice of model were not discussed in much detail. Kopelman, at least, made it clear which of his models should be used for which general types of foods; however, on the evidence of results from previous chapters, his equations for isotropic materials do not appear to be applicable for all isotropic foods.

The physical experiments and numerical simulations described in previous chapters have provided a substantial set of data that, along with theory and data from previous workers, were used to address this issue.

7.2 Comparison of Results from Physical Experiments with Previous Data

The experimental method described in Chapter 4 was similar to the approach used by Sakiyama & Yano (1990), although, with a model evaluation exercise in mind, a greater number of data points was produced in this study. The results from both methods were also similar in that the Maxwell-Eucken model (Eq. 2.20) was found to provide good predictions over the entire range of volume fractions considered. The uncertainty in the results reported in Sakiyama & Yano (1990) was not explicitly discussed; however, a visual assessment of the scatter in the results displayed in Fig. 3 of Sakiyama & Yano (1990) suggested a comparable degree of scatter to the results described in Chapter 4.

Direct comparisons with the results from Murakami & Okos (1989) and Lin (1994) were more difficult to make because of differences in focus of the investigations and the form in which results were displayed. Neither source produced k_e/k_1 vs. v_2 plots similar to Figs. 4.5 to 4.9 of Chapter 4 of this work, or

Figs. 1 to 4 of Sakiyama & Yano (1990). Instead, results were displayed as tables of discrepancies between the results and model predictions. Both Murakami & Okos and Lin recommended the use of Krischer's model (referred to as 'Keey's Model') in which the value of the adjustable parameter, f (referred to as the 'distribution factor'), was related to moisture content and porosity, in the case of Murakami & Okos, or simply porosity, in the case of Lin. Hence ranges of f-values rather than single values were recommended by both Murakami & Okos and Lin, although Lin also recommended that an average f-value of 0.16 was most suitable if a constant f-value was to be used.

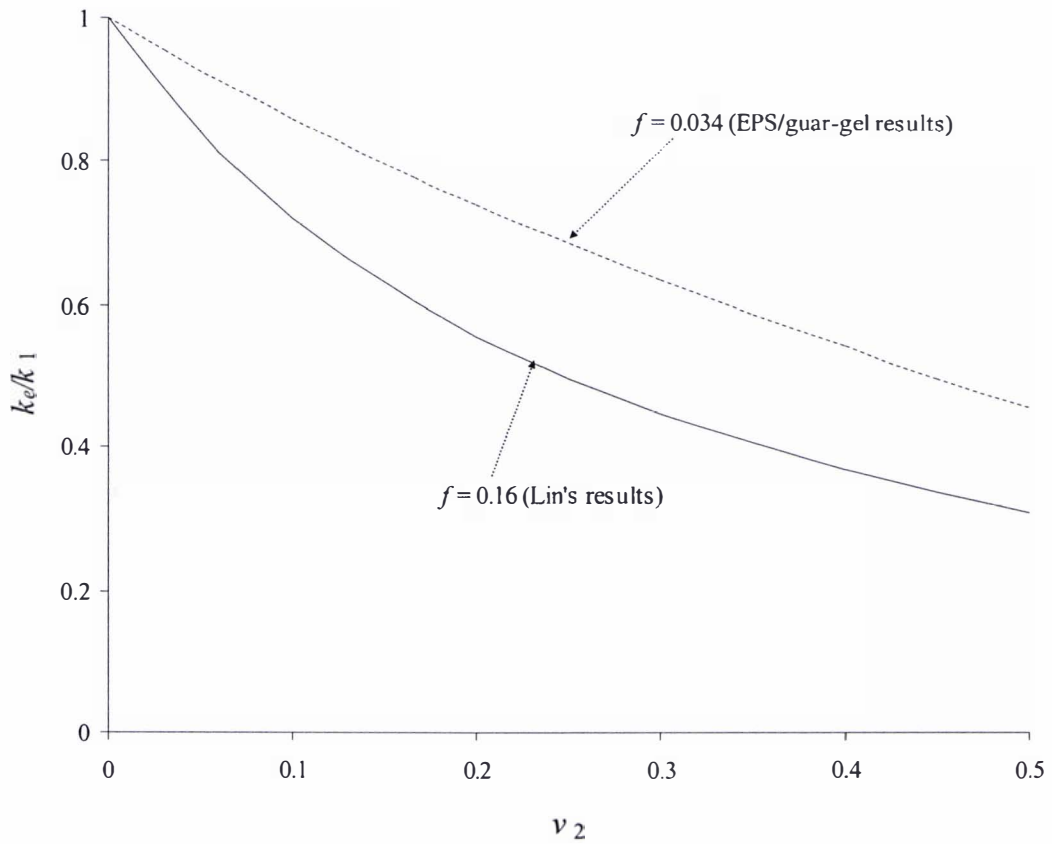

Figure 7.1: Comparison of results from Lin's experiments (Lin 1994) and results from this work as indicated by the different resultant f-values when Krischer's model was fitted to the data

It was shown in Fig. 6.2 of Chapter 6 that Krischer's model with an f-value of 0.034 fitted the experimental results from this work with reasonable accuracy. Figure 7.1 shows Krischer's model plotted with f-values of 0.16 and 0.034 for a

porosity (v_2) range of 0 to 0.5, representing the results from Lin's work and this work respectively.

Figure 7.1 shows a significant difference between the results from Lin's experiments and the results from the experiments described in Chapter 4. This difference may be due in part to the high degree of scatter in Lin's results (see Fig. 7.2), or the fact that the voids were not necessarily distributed uniformly in Lin's samples (see page 118 of Lin, 1994). (It should be noted that in addition to porosity, Bi and the ratio of the container size S to the particle size R, were also varied in the results displayed in Fig. 7.2. However, since no clear dependence of k_e on Bi or S/R was observed, all the results have been displayed on one graph.)

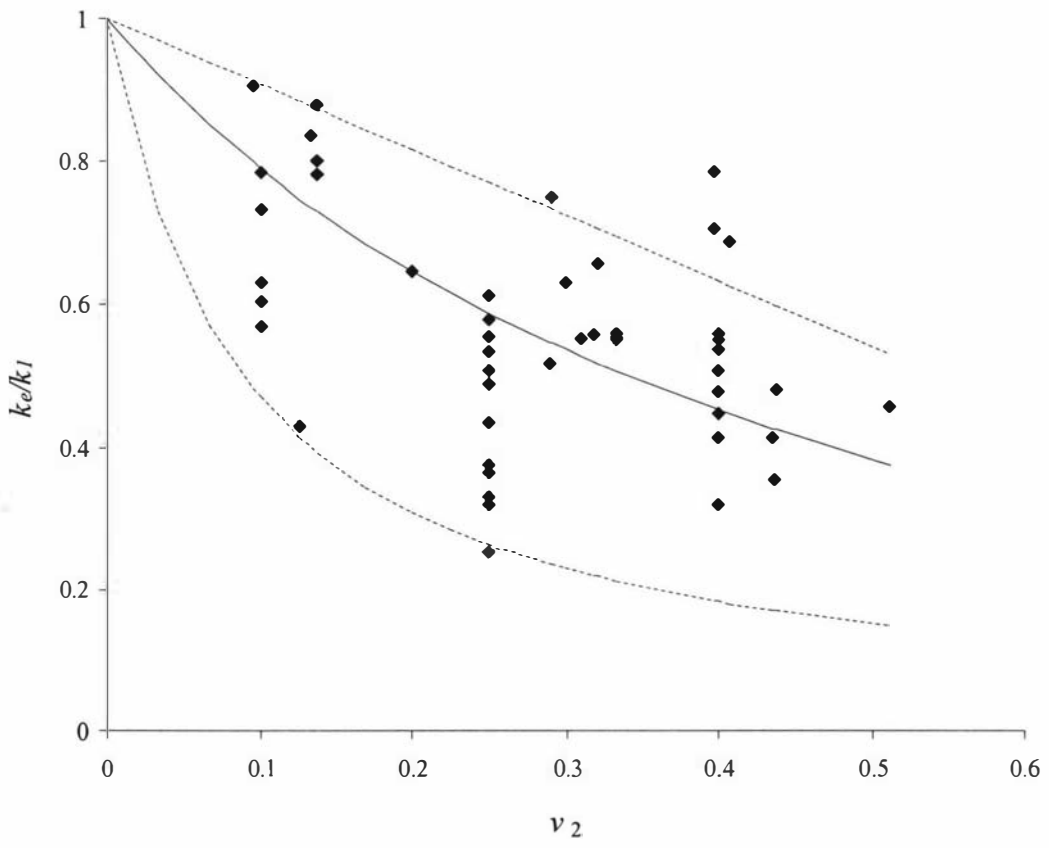

Figure 7.2: Results from Lin's experiments (points) taken from Table 7.3 of Lin (1994) plotted with the Wiener bounds (dashed lines) and Krischer's model with an *f*-value of 0.16 (solid line).

However, it was also probable that much of the difference between the results was due to the fact that Lin was experimenting on materials with external porosity, while the experiments described in Chapter 4 dealt with samples containing internal porosity. Just how significant this issue was cannot be determined by this comparison alone however, since the uncertainty in Lin's results was so high.

7.3 Heat Conduction Pathways

7.3.1 Internal or External Porosity

The question of whether porosity is internal (gaseous phase dispersed) or external (gaseous phase continuous) is of vital importance to the prediction of effective thermal conductivities since it relates to the determination of the 'path of least resistance' from a heat conduction perspective. As has been suggested previously (see Section 2.3 of Chapter 2 and Section 5.2.3.3 of Chapter 5), the continuous phase of a material has a greater influence on its effective thermal conductivity than the dispersed phase. This might not have been shown conclusively from a comparison of the results from Lin's work with the results described in Chapter 4, but it can be shown from thermal conductivity data in the literature of inorganic materials. Unfortunately, it was difficult to find thermal conductivity data in the literature for materials with similar component thermal conductivity ratios to each other that could be used to compare the different effects of external and internal porosity. However, meaningful comparisons between data of differing thermal conductivity ratios may be performed by noting their positions relative to thermal conductivity models on plots of k_e/k_1 vs. v_2. Figure 7.3 shows the measured effective thermal conductivity of samples of alumina (Al_2O_3) that contained varying numbers of 3.1mm diameter, isometric internal pores (taken from Fig. 8 of Francl & Kingery, 1954).

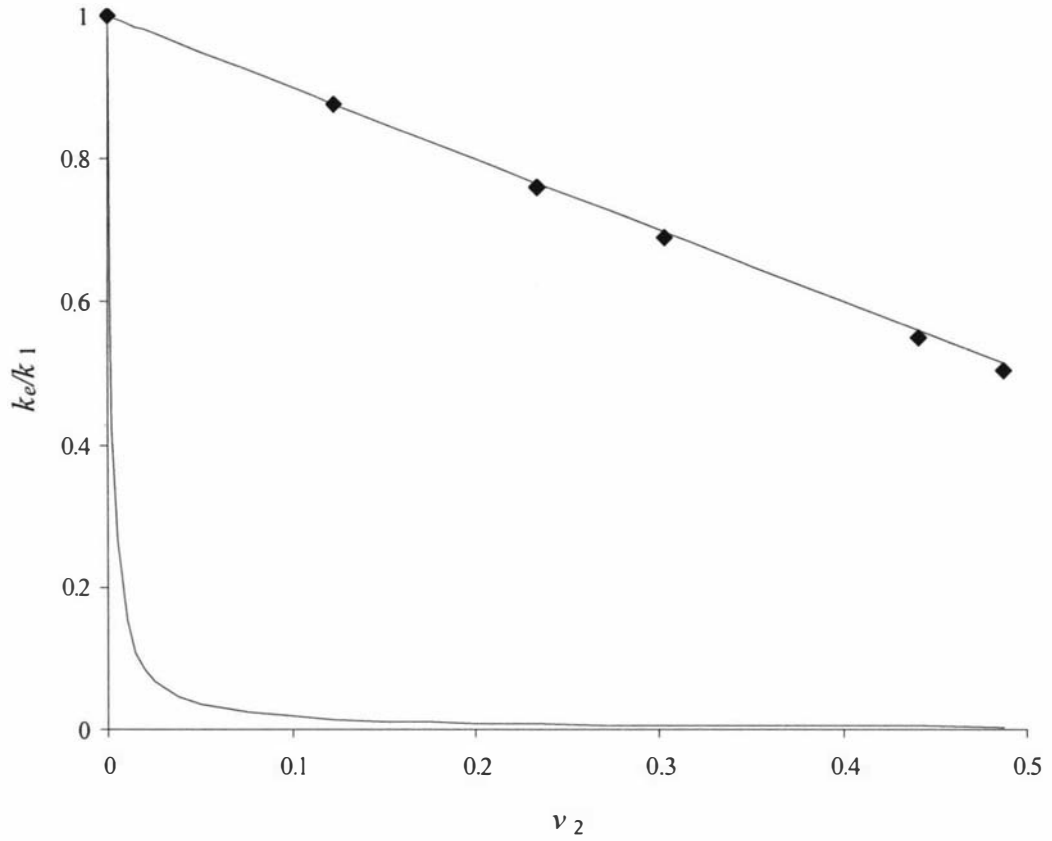

Figure 7.3: Effective thermal conductivity of alumina containing isometric internal pores (points) plotted with the Wiener bounds (lines), $k_1/k_2 \approx 550$

The ratio of the thermal conductivity of the alumina to the thermal conductivity of the air was approximately 550.

Figure 7.4 shows data of the effective thermal conductivity of samples of loose quartz-sand (taken from Fig. 3 of Woodside & Messmer, 1961b). The ratio of the thermal conductivity of the sand to the thermal conductivity of the air was approximately 330 (note that for the purpose of comparison the effective thermal conductivity, k_e, was plotted relative to k_2, the conductivity of the dispersed phase).

Figures 7.3 and 7.4 show clear experimental corroboration of the hypothesis that internal voids (i.e. gaseous phase dispersed) have less influence on the effective conductivity than external pores (i.e. gaseous phase continuous), and also support

the suggestion above, that the difference between the results from Lin's experiments and the experiments described in Chapter 4 was, at least in part, due to the fact that one set of experiments dealt with internal porosity while the other dealt with external porosity.

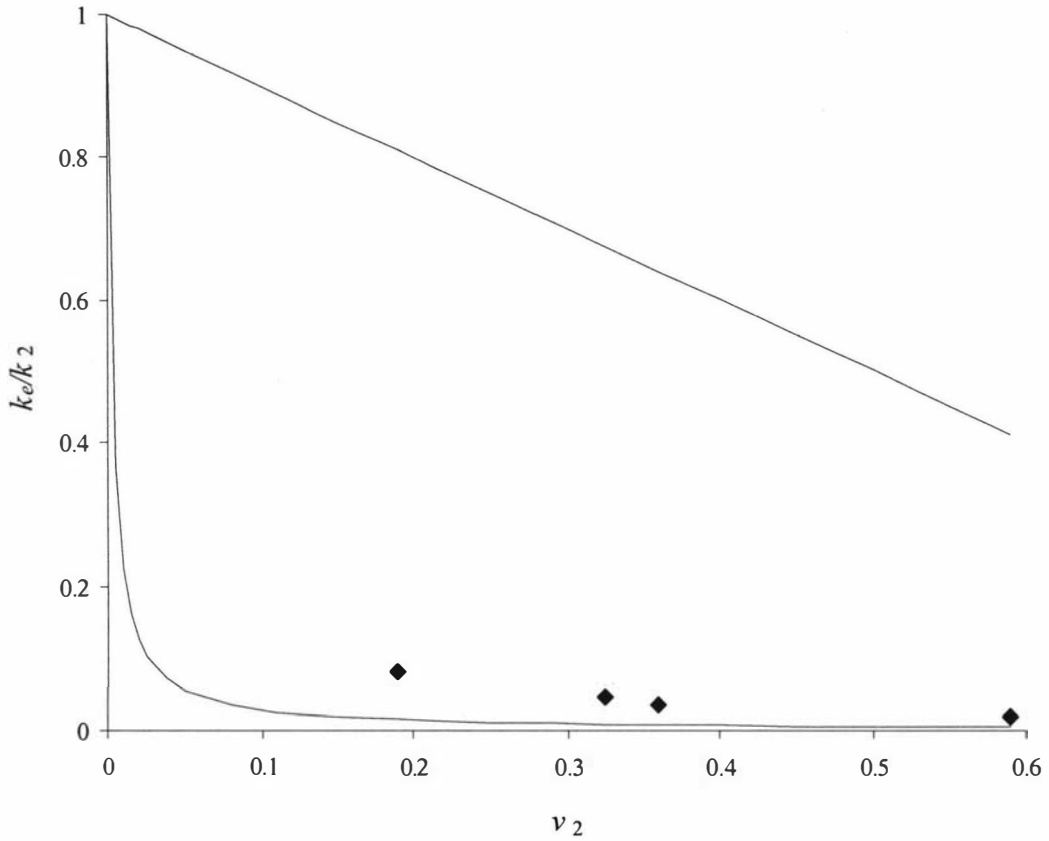

Figure 7.4: Effective thermal conductivity of loose sand (points) plotted with the Wiener bounds (lines)

7.3.2 Continuous and Dispersed (Discontinuous) Phases

7.3.2.1 Continuous and Dispersed Phases in Maxwell-type Materials

Section 7.3.1, and previous studies (e.g. Russell, 1935, Hamilton & Crosser, 1962, Chisaka & Tanaka, 1991), have shown that when one phase is definitely continuous and the other is definitely dispersed, the continuous phase has a

greater influence on the overall heat conduction. In the examples that were used (EPS beads dispersed in guar gel, containers of diced and grated cheese, alumina blocks with discrete holes, and grains of sand), it was easy to identify the continuous and dispersed phases. One of the phases was divided up into discrete parts (i.e. inclusions) that, while sometimes being in contact with other similar discrete parts, were not attached by physical bonds. Clearly this phase was dispersed (or discontinuous). The other phase formed a matrix around the dispersed phase, and was therefore clearly a continuous phase. These types of material could be approximated by the Maxwell-type finite element (FE) grids described in Chapter 5. Figure 7.5 shows that, in the case of genuine (i.e. non-contacting) Maxwell structures, the status of the continuous and discontinuous phases is independent of the volume fraction of the components:

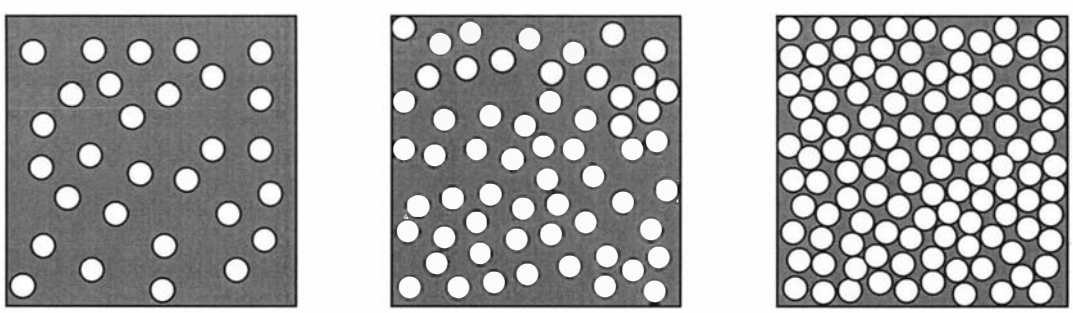

Figure 7.5: Maxwell-type structures with distinct continuous (grey component) and dispersed (white component) phases, regardless of the volume fractions

In Chapter 5 it was shown that these Maxwell-type grids were, as expected, modelled well by the Maxwell-based models. By precluding any contact between inclusions of the dispersed phase, the Maxwell model ensured that one phase always had continuous heat transfer pathways between the external boundaries, while the other component had no continuous heat transfer pathways between the external boundaries. This meant that the model assumed maximum influence of the continuous phase on the effective thermal conductivity, whether it acted to enhance conduction (as would be the case if the continuous phase had had a higher thermal conductivity than the dispersed phase), or obstruct conduction (as

would be the case if the continuous phase had had a lower thermal conductivity than the dispersed phase). Hence, since they assume extreme scenarios for isotropic materials, the two forms of this model will, theoretically, predict the upper and lower bounds for the conductivity of isotropic materials: the upper bound when the higher conductivity phase is continuous, the lower bound when the lower conductivity phase is continuous. Although this evaluation of the Maxwell-Eucken model is argued intuitively here, effectively the same conclusion was arrived at mathematically by Hashin & Shtrikman (1962).

If the continuous phase has the higher conductivity of the two components, then the greatest flow of heat will be through that phase, avoiding the inclusions of the dispersed phase which behave as heat flow obstacles, as shown schematically in Fig. 7.6.

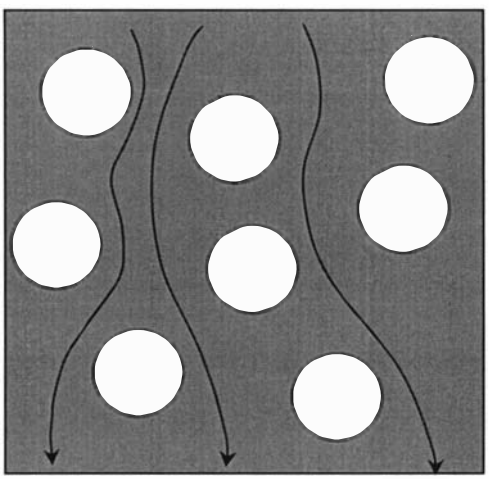

Figure 7.6: Schematic representation of optimum heat transfer pathways for material in which the continuous phase has a higher thermal conductivity than the dispersed phase, arrows indicating preferred heat transfer pathways

If the continuous phase has the lower thermal conductivity of the two components, the optimum heat transfer pathway is through as many inclusions of the dispersed phases as possible, as shown schematically in Fig. 7.7.

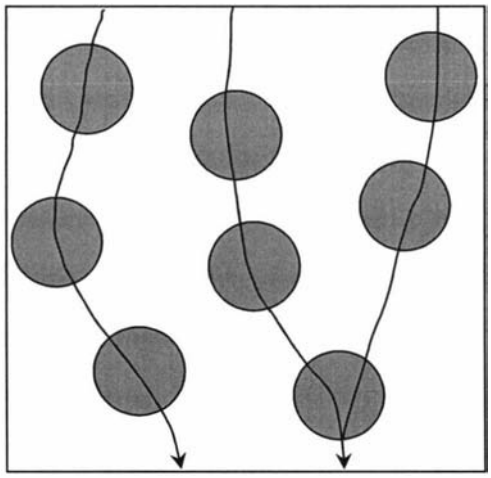

Figure 7.7: Schematic representation of optimum heat transfer pathways for material in which the continuous phase has a lower thermal conductivity than the dispersed phase, arrows indicating preferred heat transfer pathways

7.3.2.2 Continuous and Dispersed Phases in Kirkpatrick-type Materials

Consider the Kirkpatrick-type FE grids described in Chapter 5. Figure 7.8 shows Kirkpatrick-type grids with varying volume fractions. Unlike the Maxwell-type structures, the Kirkpatrick-type structures do not have distinctive continuous and dispersed phases. The grid on the left of Fig. 7.8 would appear to have a continuous grey component, while the grid on the right would appear to have a continuous white component.

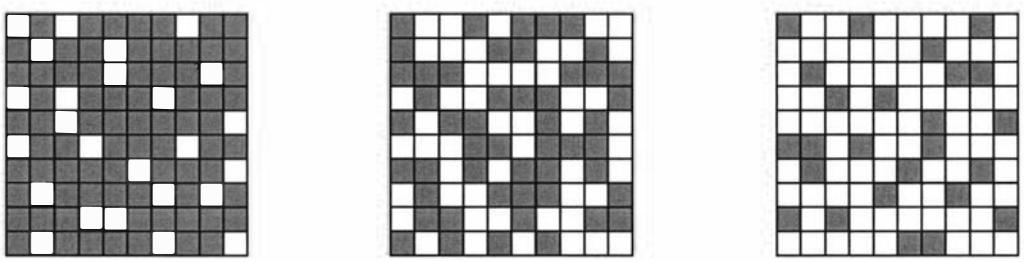

Figure 7.8: Kirkpatrick-type structures in which the distinction between continuous and dispersed phases is dependent on the volume fractions of the components

The components of the central grid appear to have equal status since it would be possible for either (or both) components to have continuous heat transfer pathways between the external boundaries. Any distinction between the components appears to be dependent on the relative amounts of the two components. The optimum heat transfer pathways of the Kirkpatrick-type structures are a lot more dependent on the volume fractions than for the Maxwell-type structures. If the grey component had a higher thermal conductivity than the white component, the optimum heat transfer pathways for the left hand FE grid of Fig. 7.8, would probably be similar to the scenario depicted in Fig. 7.6, while the optimum pathway for the right hand FE grid of Fig. 7.8 would probably be similar to the scenario depicted in Fig. 7.7. The central FE grid of Fig. 7.8 would probably contain a mixture of the two scenarios depicted in Figs. 7.6 and 7.7: in some regions the scenario in Fig. 7.6 might be the optimum pathway, while the scenario in Fig. 7.7 might be the optimum pathway in other regions, depending on the exact distribution of the components.

7.3.2.3 Significance of the Maxwell-Eucken and Landauer-EMT models

One form of the Maxwell-Eucken model has maximum bias to the component with higher thermal conductivity, the other form has maximum bias to the component with lower thermal conductivity, and together they may be thought of as enclosing the range of possible effective thermal conductivities of isotropic materials (referred to in Chapter 2 as the Hashin-Shtrikman bounds). The Landauer-EMT model, which may be derived from the same basic physical model as Maxwell's model, is completely unbiased with respect to the components, and therefore it is a neutral intermediate between the two forms of the Maxwell-Eucken equation. On this basis, it is proposed that the region bounded by the two forms of the Maxwell-Eucken model on a k_e/k_1 vs. v_2 plot (the Hashin-Shtrikman bounds), which, as discussed above, contains all plausible effective thermal conductivities of isotropic materials, may be divided into two sub-regions by the Landauer-EMT model, as illustrated in Figs. 7.9 to 7.11 for selected component thermal conductivity ratios.

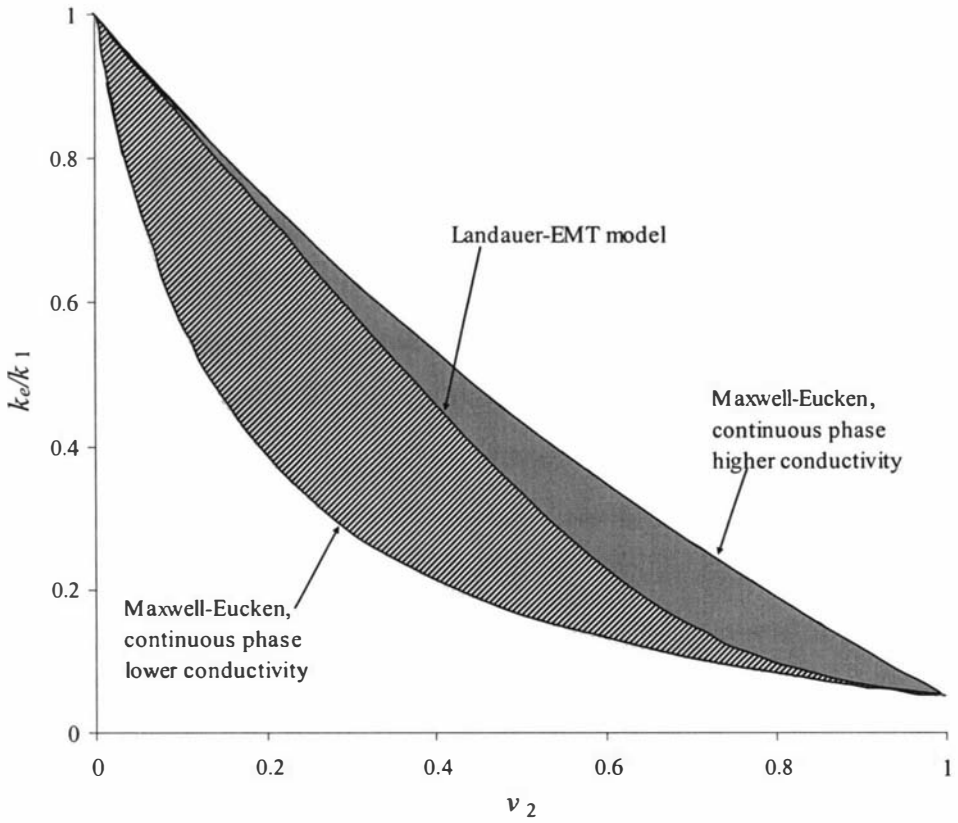

Figure 7.9: Predictions of Maxwell-Eucken and Landauer-EMT ($k_1/k_2 = 20$)

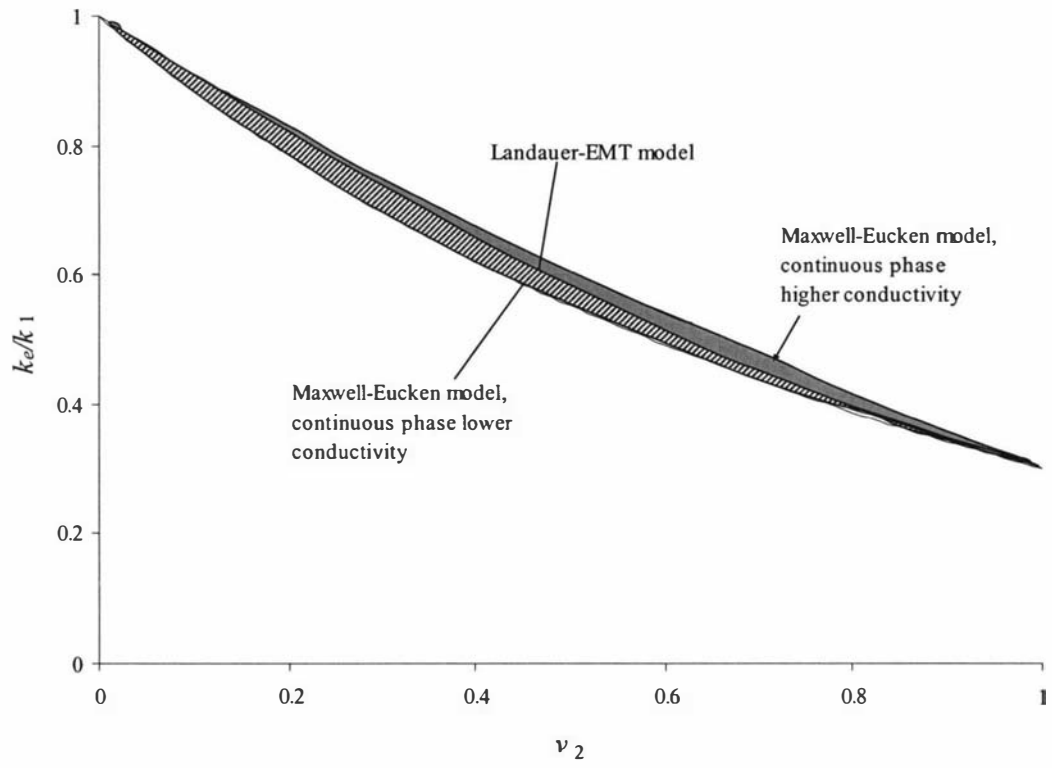

Figure 7.10: Predictions of Maxwell-Eucken and Landauer-EMT ($k_1/k_2 = 3$)

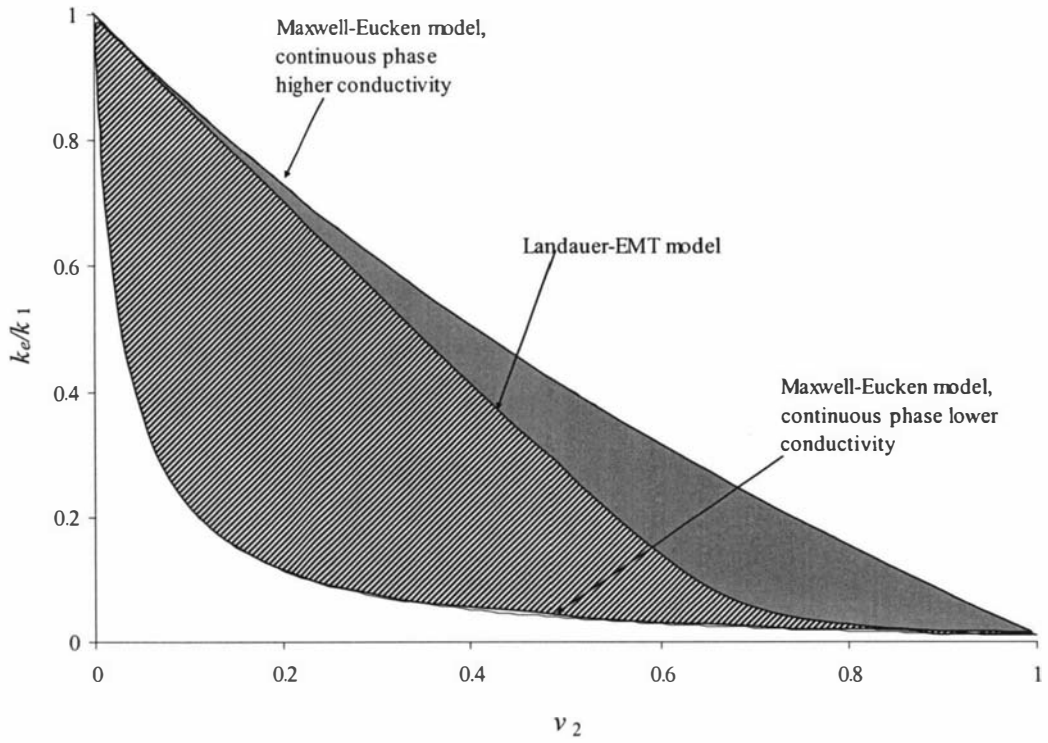

Figure 7.11: Predictions of Maxwell-Eucken and Landauer-EMT ($k_1/k_2 = 100$)

One would expect that materials in which the continuous phase had a higher thermal conductivity than the dispersed phase (i.e. having optimum heat transfer pathways according to Fig. 7.6) would lie in the shaded region, while materials in which the continuous phase had a lower thermal conductivity than the dispersed phase (i.e. having optimum heat transfer pathways according to Fig. 7.7) would lie in the cross-hatched region. Stating it a different way, the Landauer-EMT model might serve as a lower bound for effective thermal conductivities of materials in which the continuous phase has a higher thermal conductivity than the dispersed phase (with the Maxwell-Eucken model as the upper bound), and as an upper bound for effective thermal conductivities of materials in which the continuous phase has a higher thermal conductivity than the dispersed phase (with the Maxwell-Eucken model as the lower bound).

Figure 7.12 summarises the division of the region between the Hashin-Shtrikman bounds in terms of the optimum heat transfer pathways, as depicted in Figs. 7.6 and 7.7, that are proposed to exist in each sub-region:

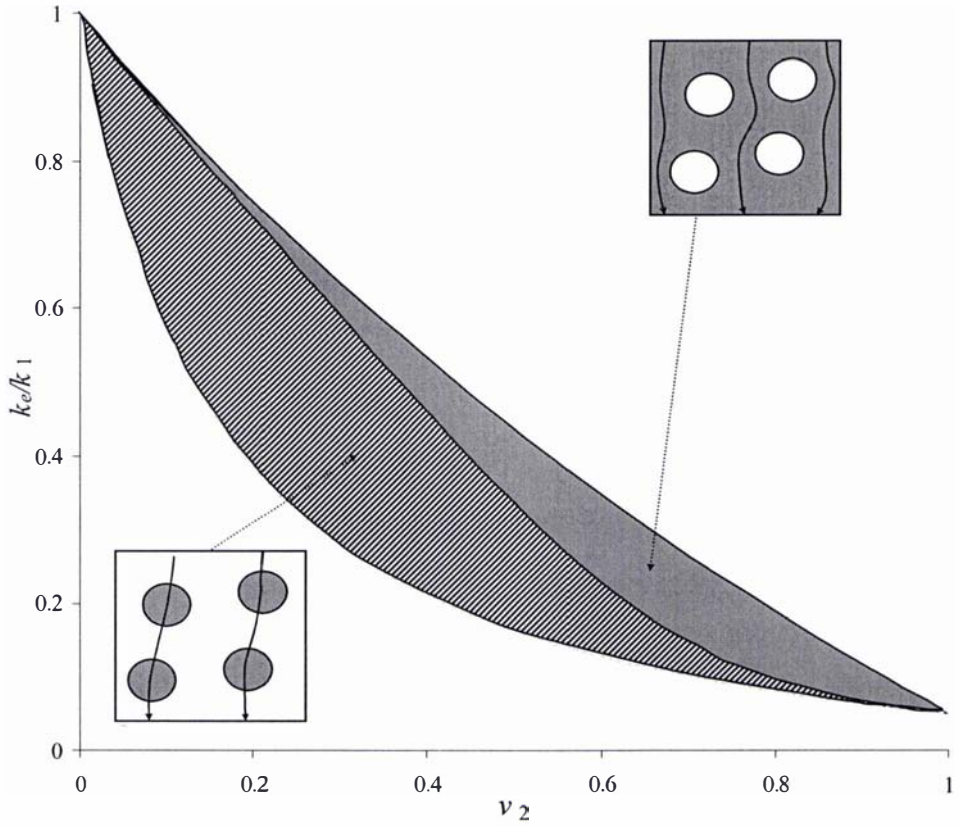

Figure 7.12: Division of the Hashin-Shtrikman region into two sub-regions according to the optimum heat transfer pathways of each region

The data from the physical experiments described in Chapter 4 supported the proposed division of the effective thermal conductivity region as described above. The EPS/guar-gel materials were examples of materials where the continuous phase had a higher thermal conductivity than the dispersed phase, and hence would be expected, within the limits of experimental uncertainty, to lie in the shaded region of Figs. 7.9 to 7.12. This was indeed the case, as shown in Fig. 7.13.

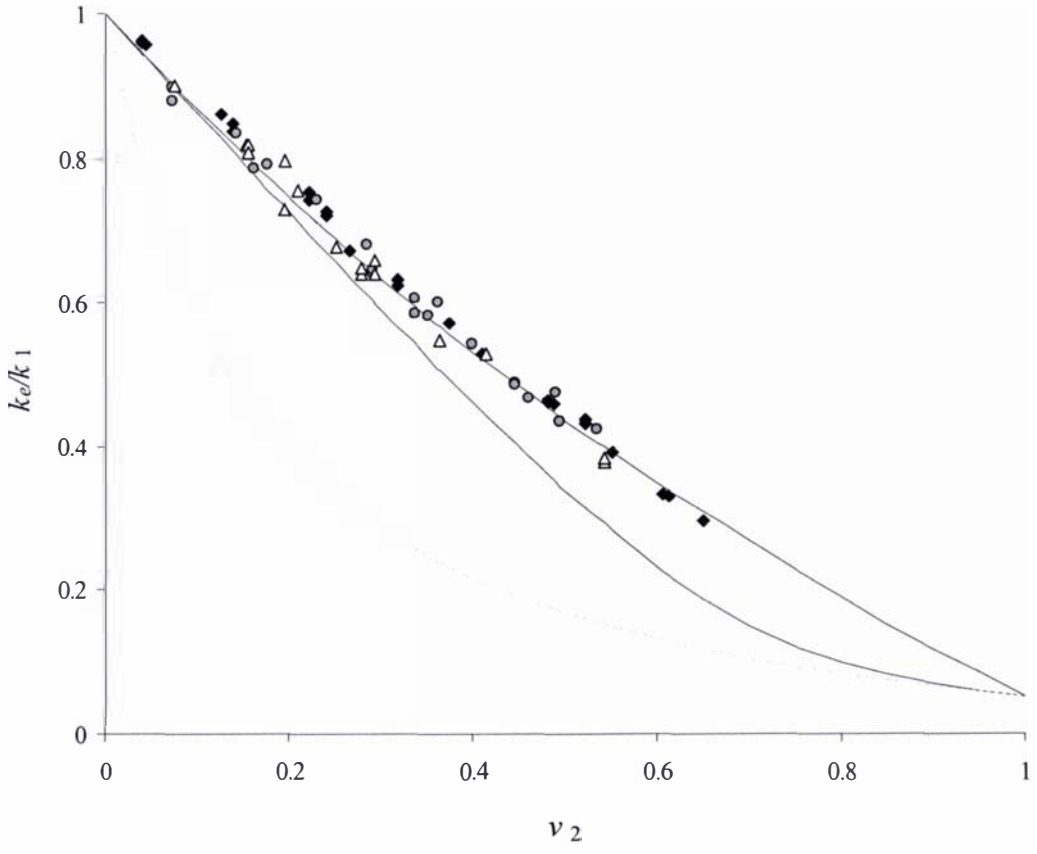

Figure 7.13: Expanded polystyrene (EPS)/guar-gel thermal conductivity results lie in the shaded sub-region of Figs. 7.9 to 7.12

Conversely, since the conductivity of the dispersed phase of the aluminium/guar-gel samples was higher than the continuous phase, it would be expected that the effective thermal conductivity would lie in the cross-hatched region of Figs. 7.9 to 7.12, as shown in Figure 7.14.

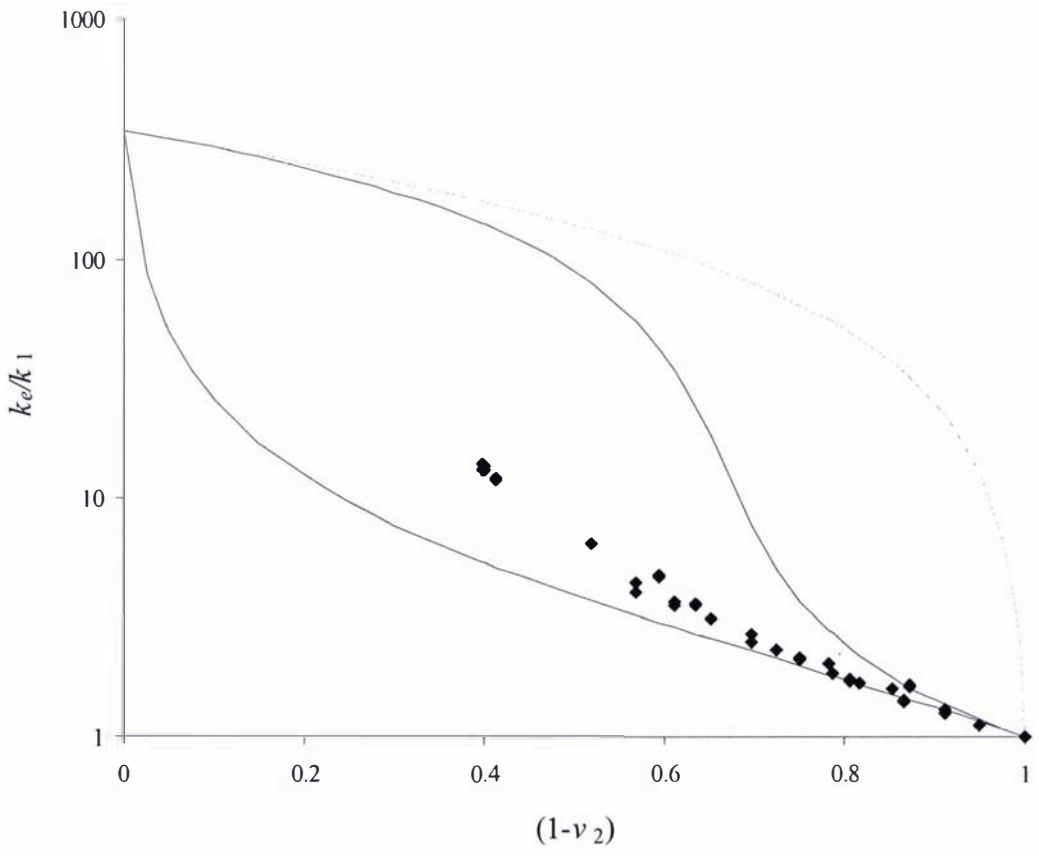

Figure 7.14: Aluminium cylinder/guar-gel thermal conductivity results lie in the cross-hatched region of Figs. 7.9 to 7.12 (note the use of logarithmic scale on the ordinate axis and the independent variable of $(1-v_2)$ rather than v_2 as plotted in Figs. 4.9 and 6.3)

Similar behaviour would be expected from the numerical simulations described in Chapter 5. Figure 6.7 of Chapter 6 showed that the thermal conductivities of the 'intermediate-type' FE grid (see Fig. 5.9b) in which the conductivity of the continuous phase was higher than the conductivity of the dispersed phase did indeed lie between the predictions of two-dimensional forms of the upper Maxwell-Eucken and Landauer-EMT models (shaded region of Figs. 9 to 12). Figure 7.15 shows the simulation results for the same type of grid but with the thermal conductivities of the phases reversed, and, as expected, the effective thermal conductivities lie between the predictions of the Landauer-EMT and the lower Maxwell-Eucken model (cross-hatched region of Figs. 9 to 12).

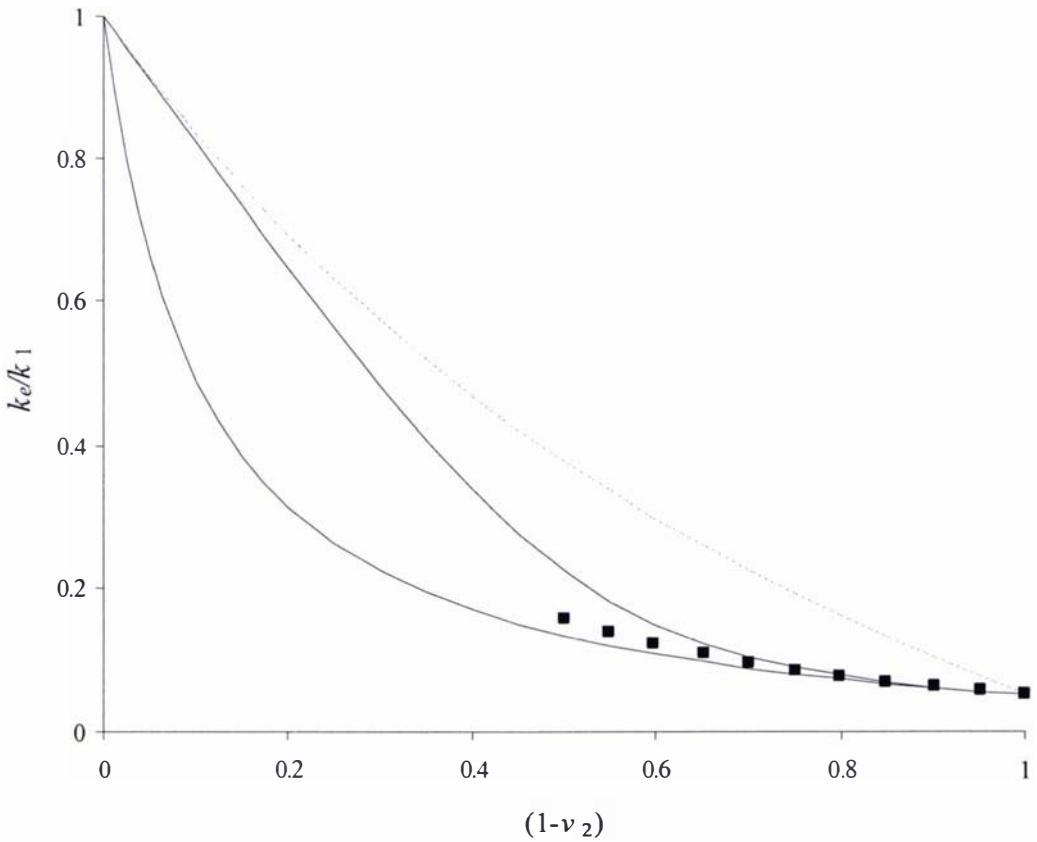

Figure 7.15: Numerical simulation results from 'intermediate-type' FE grids (see Fig 5.9b of Chapter 5), in which the continuous phase has a lower thermal conductivity than the dispersed phase (note the independent variable is $(1-v_2)$ rather than v_2 as was plotted in Fig 6.7)

Because the thermal conductivity of the continuous phase of materials with internal porosity is higher than the thermal conductivity of the dispersed phase, in future discussions the region bounded by the upper Hashin-Shtrikman bound and the Landauer-EMT model (shaded region in Figs. 7.9 to 7.12) will be referred to as the 'internal porosity region', since the majority of discussions are concerned with porous materials. Similarly, the region bounded by the Landauer-EMT model and the lower Hashin-Shtrikman bound (cross-hatched region in Figs. 7.9 to 7.12) will be referred to as the 'external porosity region'.

7.3.3 Problems with the Identification of Continuous and Dispersed (Discontinuous) Phases

Just as the Hashin-Shtrikman bounds (i.e. the two forms of the Maxwell-Eucken model) narrowed the envelope of possible effective thermal conductivities within the Wiener Bounds (see Section 2.3.9 of Chapter 2), the use of the Landauer-EMT model between the Hashin-Shtrikman bounds further narrows the range of expected effective thermal conductivities, if continuous and dispersed phases can be identified.

The discussion so far has considered materials as being made up of two components, each constituting a phase. Food products may contain more than two phases, but typically all chemical components may be included in one of four phases: gaseous, aqueous liquid, lipid, or solid. However, since the thermal conductivities of the major non-gaseous chemical components of food, other than ice, have relatively similar thermal conductivities (see Table 2.1 of Chapter 2), the error introduced by incorrectly identifying the continuous and dispersed phases would be minor. This is illustrated in Fig. 7.10 by the relatively narrow region between the Hashin-Shtrikman bounds when the thermal conductivity ratio is approximately 3.

This assertion was supported by Pham & Willix (1989) who noted that for a variety of *un*frozen meat products with widely varied chemical composition, a number of effective thermal conductivity models, including the Maxwell-Eucken model provided sufficiently accurate predictions. However, the discrepancy between the predictions of the models below the initial freezing point was significant. Hence serious consideration of the continuous and dispersed phases is only important for foods containing gaseous components and/or ice. Fortunately, the physical distinction between a gaseous phase and a condensed phase (solid/liquid) is often obvious from a visual assessment, especially with the aid of micrographs of food structures which are often readily available in the literature

(for examples see Campbell *et al.*, 1999, *Journal of Food Science* and *Food Structure* journal).

In some foods the identification of continuous and dispersed phases is obvious, especially if the gaseous phase forms discrete bubbles (for example, see scanning electron micrographs of whipped cream in Smith *et al.*, 1999). Certainly this would be the case in foods with structures that approximate the Maxwell structural model. In general, if a component of a food product is physically continuous this would suggest that it forms the 'continuous phase' in the sense that the term has been used so far in reference to effective thermal conductivity models. Similarly, if a food component is physically discontinuous this would suggest that it forms the 'dispersed phase'. This summation formed the basis of the definitions of internal and external porosity outlined in Section 2.2.4.2 of Chapter 2, and provides the rough guideline that food products such as powders, grains, flakes, shavings etc. may be thought of as having the gaseous component as the continuous phase (external porosity), and that most others may be thought of as having the gaseous component as the dispersed phase (internal porosity).

However, while the terms 'continuous phase' and 'dispersed phase' appear frequently in the effective thermal conductivity literature, ultimately the material structure may need to be analysed in terms of the optimum heat transfer pathways to avoid potential confusion, as explained in the following section.

7.3.4 Thermal Contact between Neighbouring Inclusions (i.e. Pores or Particles)

7.3.4.1 The Significance of Inclusion Contact

When bubbles coalesce significantly with neighbouring bubbles, the structure approaches the Kirkpatrick structural model, where either or both phases may be considered continuous. Hamilton & Crosser (1962), anticipated that the terms 'continuous' and 'discontinuous' might become ambiguous as the probability of

contact between inclusions (pores or particles) increased, and the issue of pore or particle contact was also identified in the numerical simulations of Chapter 5 as being an important variable in the prediction of effective thermal conductivities. Brailsford & Major (1964), who were concerned with the prediction of the thermal conductivity of porous sandstone, observed that the structure of the sandstone did not match the assumed physical structures of either the Maxwell-Eucken model or the Landauer-EMT model, but was somewhere in between. Figure 7.16 is a reproduction of Fig. 5 of Brailsford & Major (1964), who used data from Fig. 14 of Sugawara & Yoshizawa (1961).

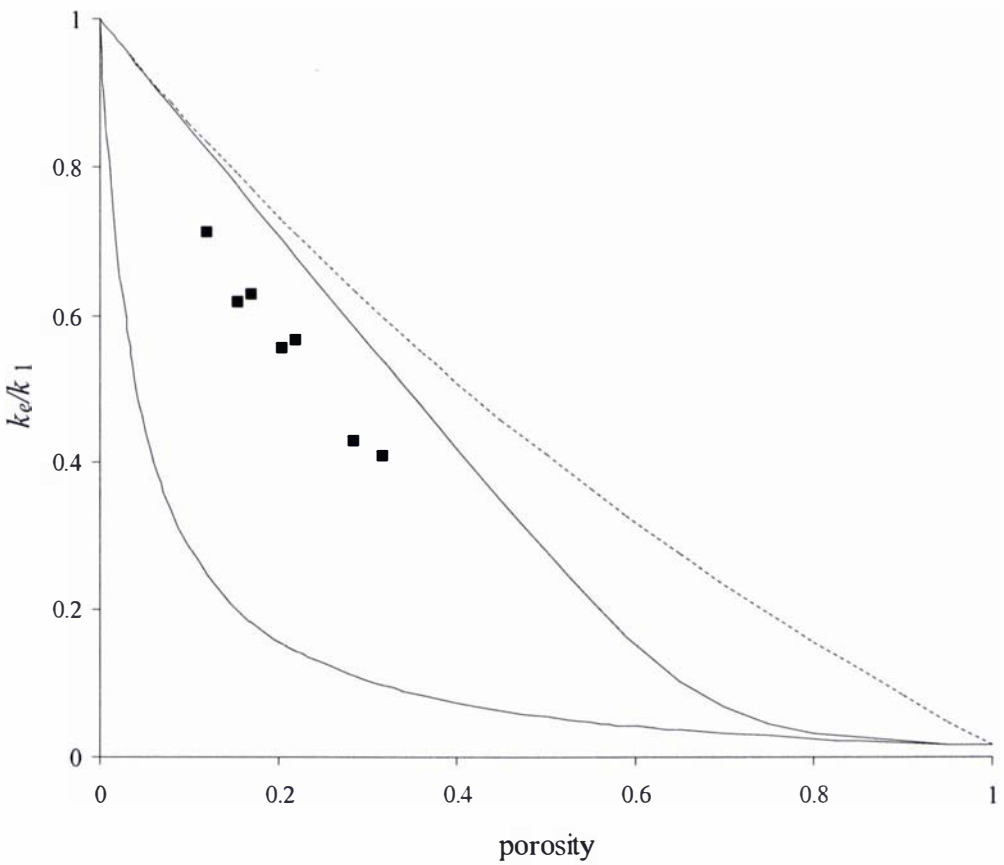

Figure 7.16: Relative effective thermal conductivities of porous sandstone, taken from Fig. 14 of Sugawara & Yoshizawa (1961), plotted with the two forms of the Maxwell-Eucken model and the Landauer-EMT model (compare with Fig. 7.11)

The relatively low porosities of the sandstone (between 0.12 and 0.317) might suggest that air was the dispersed phase and, since air has a lower thermal conductivity than sandstone, it would be expected that the thermal conductivity data would lie in the internal porosity region of a k_e/k_1 vs. v_2 plot. However, Fig. 7.16 shows that the data actually lie in the external porosity region. Hence, at face value the experimental data for the thermal conductivity of sandstone would appear to be in conflict with the discussion in Section 7.3.2.3 and the basis for the division of the region between the Hashin-Shtrikman bounds. However, an analysis of the optimum heat transfer pathways in porous sandstone can reveal consistency between this data and Section 7.3.2.3.

Figure 7.17 shows a schematic diagram of a theoretical lump of consolidated granular material (e.g. sandstone), which is made up of discrete particles that have been compacted to form a larger solid (compare with Fig. 11 of Sugawara & Yoshizawa, 1961).

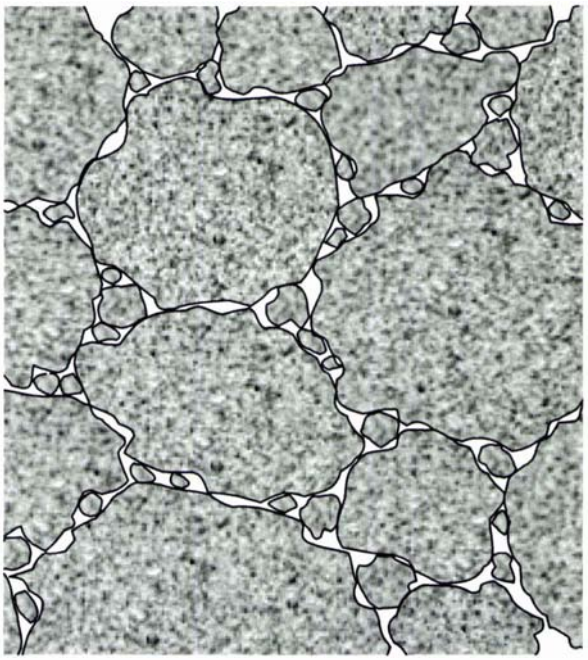

Figure 7.17: Schematic diagram of a consolidated granular material (sandstone)

Because the particles are packed tightly with smaller particles filling the interstices between larger particles, each individual particle is held in place and the overall mechanical properties are essentially those of a single solid. However, although the consolidated material does have physical continuity, Fig. 7.17 shows that the proportion of the surface of each particle that is in contact with neighbouring particles is small, and so while there is sufficient contact for each particle to be held in a fixed position relative to its neighbours, the heat conduction is inhibited by the low proportion of surface area that is in intimate contact with neighbouring particles. (The issue of the quality of thermal contact between different solids, commonly known as 'contact resistance', is not limited to porous materials. Since this type of porous material contains so many discontinuous surfaces, however, contact resistance has a very significant influence on its effective thermal conductivity.)

The heat flow mechanism within the sandstone is more like the one shown schematically in Fig 7.7 than the one shown in Fig 7.6. So although it occupies only a small proportion of the total space, the gaseous phase behaves as the 'continuous phase' from an effective thermal conductivity perspective. Therefore the thermal conductivity of the 'dispersed phase' is actually higher than that of the continuous phase, and hence it is not surprising that the data shown in Fig. 7.16 lie in the external porosity region. Hence the terms 'continuous phase' and 'dispersed phase' as they are used for effective thermal conductivity analyses should be defined from a thermal perspective rather than from a physical or mechanical perspective.

7.3.4.2 Determining the Extent/Quality of Contact between Inclusions

So long as the inclusions (pores or particles) of the dispersed phase are distributed randomly and uniformly, at low volume fractions of the dispersed phase the probability of individual inclusions coming into contact with neighbouring inclusions is low. In this situation, the difference between the Maxwell structures and the Kirkpatrick structures is minimal (compare the left hand FE grids shown in Figs. 7.5 and 7.8). This is demonstrated by the similarity between the

predictions of the Landauer-EMT model and the upper Maxwell-Eucken model for v_2 values below 0.2, and between the predictions of the Landauer-EMT model and the lower Maxwell-Eucken model for v_2 values above 0.8 (see Figs. 7.9 to 7.12). As the volume fraction of the dispersed phase is increased, the probability of interaction between inclusions also increases, and the difference between the Maxwell and Kirkpatrick structures becomes significant, as indicated by the divergence in the plots of the EMT and Maxwell-Eucken models.

In Chapter 5, the Maxwell and Kirkpatrick structures were used in the numerical simulations to examine the significance of inclusion contact, since they represented extreme scenarios: zero contact for the Maxwell-type structures, and unlimited contact for the Kirkpatrick-type structures. The 'intermediate' scenario represented an intermediate degree of inclusion contact, and, as expected, the effective thermal conductivities calculated from the intermediate-type grids lay between the results of the Kirkpatrick and Maxwell-type grids. There does not appear to be any reason why inclusion contact scenarios may not range anywhere between the Maxwell and Kirkpatrick extremes, therefore thermal conductivity data might be expected to lie anywhere between the Landauer-EMT and Maxwell-Eucken bounds. As identified in Chapter 5, in general, the extent of inclusion contact becomes more significant as the volume fraction of the dispersed phase is increased. From Figs. 7.9 to 7.12, a volume fraction of approximately 0.2 appears to be a critical point beyond which, based on the divergence of the Landauer-EMT and Maxwell-Eucken models, inclusion contact becomes significant.

Neither the Maxwell-Eucken nor the Landauer-EMT model provided accurate predictions for the Intermediate scenario over the range of porosities considered. The best predictions for all three pore-contact scenarios described in Chapter 5 were provided by models that contained adjustable parameters in addition to the component volume fractions and thermal conductivities (referred to in Chapter 6 as 'Type B' models). This suggests that, due to the variability associated with inclusion contact, in order for a model to have general applicability it must include some parameter that is related in some way to inclusion contact, the numerical

value of which will depend on the particular material being modelled. This conclusion is consistent with previous theoretical analyses of the effective thermal conductivity of porous systems, particularly granular materials. Kunii & Smith (1960) suggested that the degree of contact between neighbouring particles was a property specific to the material, but Nozad *et al.* (1985) found that the degree of particle-to-particle contact was difficult to determine other than by empirical means.

It might be possible to predict the value of the inclusion-contact parameter if the microstructure of the material of interest is known, but a detailed analysis of this issue was beyond the scope of this work.

7.3.4.3 Sensitivity of Materials to the Extent of Inclusion Contact

Conclusions drawn by Hamilton & Crosser (1962) and Cheng & Vachon (1969) suggested that the effective thermal conductivity of materials in which the conductivity of the dispersed phase was higher than the conductivity of the continuous phase, such as materials having external porosity, was inherently more variable than the reverse scenario, such as materials having internal porosity. This conclusion is supported by the observation that the internal porosity region covers a smaller area than the eternal porosity region regardless of the component thermal conductivity ratio (see Figs. 7.9 to 7.12). It is also consistent with an intuitive analysis of the different conduction pathway mechanisms. If heat flow is predominantly through the continuous phase, as is the case in internal porosity materials, then changes in variables associated with the dispersed phase, such as the size and shape of inclusions, will have minor effects. However, since the heat flow in the external porosity materials is through both continuous and dispersed phases, changes in variables related to the dispersed phase will have more significant effects, particularly, according to the results in Chapter 5, the degree of inclusion contact.

7.4 Selecting Suitable Effective Thermal Conductivity Models for Foods

7.4.1 The Appeal of the Maxwell and EMT based Models

In Chapter 6 several criteria were used to select effective thermal conductivity models for the model evaluation exercise. One criterion was that the number of material-specific parameters involved was no greater than one. Models containing no material-specific parameters were preferable because they required less information. Figures 7.9 to 7.12 showed that for low volume fractions of the dispersed phase (<0.2) the plots of the Maxwell-Eucken and Landauer-EMT models were almost superimposed on each other. In Section 7.3, it was argued that these models form the bounds of effective thermal conductivity, and since these bounds are so close together at low volume fractions of the dispersed phase, either model might be expected to provide accurate predictions at low volume fractions, without the need for a material-specific parameter. As was shown in Fig. 6.1 of Chapter 6, several other Type A models also provided similar predictions to the Maxwell-Eucken and Landauer-EMT models at low v_2 values, including the Cheng-Vachon model (Eq. 2.12), Russell's model (Eq. 2.13) and Kopelman's isotropic model (Eq. 2.29).

Above a dispersed-phase volume fraction of approximately 0.2 the plots of the Maxwell-Eucken and Landauer-EMT models diverged. Type B models must therefore be used beyond this point to account for the effects of inclusion contact. All four Type B models considered in the validation exercise in Chapter 6 could be fitted to any single point within the Wiener bounds simply by adjusting the material specific parameters f, n or Z. However, when a range of points was to be fitted by a Type B model with a constant parameter then, due to the characteristic shapes of the models, some models were shown to be better suited to a given application than others. Tables 6.1 to 6.5 of Chapter 6 showed that the

Maxwell-Hamilton and Kirkpatrick-EMT models consistently had lower mean absolute discrepancies than the Krischer and Chaudhary-Bhandari models. As mentioned in Chapter 6, this was not surprising, given that the materials under consideration in this study were isotropic, and that the former models assumed isotropic structures while the latter were simple weighted means of two highly anisotropic models (the Series and Parallel models).

Murakami & Okos (1989) and Lin (1994) both recommended the use of Krischer's model for porous food systems. However, neither study considered the Maxwell-Hamilton or Kirkpatrick-EMT models in their evaluation exercises. Krischer's model was the only Type B model that was considered by Lin, while Murakami & Okos considered both Krischer's model and the Chaudhary-Bhandari model, but preferred Krischer's model as it had received more use in the food industry.

It was difficult to select either the Maxwell-Hamilton model or the Kirkpatrick-EMT model ahead of the other on the evidence in Chapter 6 since neither model consistently provided better fits to the data than the other, according to the AD_M values displayed in Tables 6.1 to 6.5 of Chapter 6. The difference between the characteristic shapes of models becomes more obvious as the component thermal conductivity ratio is increased (compare model shapes from Fig. 6.4 with model shapes in Fig. 6.2), and as the range of volume fractions involved is increased. Figures 6.2, 6.8, 6.9, and 6.10 of Chapter 6 show that, when fitted to the data, the Maxwell-Hamilton and Kirkpatrick-EMT models tended to lie on either side of the data, usually crossing over at some point. Therefore, it is important to recall the physical structure assumed by each model in deciding which is the most appropriate for a given material. If the dispersed and continuous phases are easy to identify then the Maxwell-based models should be used. If it is unclear which phase is continuous, or if it appears that more than one of the phases is continuous, then the EMT-based models should be used. However, more experimental work would be required in order to provide clearer guidelines for selecting between the two types of model.

It is worthwhile observing that the Maxwell-Hamilton (Eq. 2.22) model can be fitted to either form of the Maxwell-Eucken model (Eq. 2.20 or Eq. 2.21), and so either Maxwell-Eucken equation may be modified to produce the Maxwell-Hamilton model. However the value of the *n*-parameter will depend on the form of the Maxwell-Eucken model used in the derivation. For example, Eq. (2.22) was derived from Eq. (2.20) by changing the coefficient "2" to "(*n*-1)":

$$k_e = k_1 \frac{2k_1 + k_2 - 2(k_1 - k_2)v_2}{2k_1 + k_2 + (k_1 - k_2)v_2} \qquad (2.20)$$

became:

$$k_e = k_1 \frac{(n-1)k_1 + k_2 - (n-1)(k_1 - k_2)v_2}{(n-1)k_1 + k_2 + (k_1 - k_2)v_2} \qquad (2.22)$$

The Maxwell-Hamilton model could equally have been derived from Eq. (2.21), changing:

$$k_e = k_2 \frac{2k_2 + k_1 - 2(k_1 - k_2)(1 - v_2)}{2k_2 + k_1 + (k_1 - k_2)(1 - v_2)} \qquad (2.21)$$

to give:

$$k_e = k_2 \frac{(n'-1)k_2 + k_1 + (n'-1)(k_1 - k_2)(1 - v_2)}{(n'-1)k_2 + k_1 - (k_1 - k_2)(1 - v_2)} \qquad (7.1)$$

Equations (7.1) and (2.22) will give identical results so long as their adjustable parameters are related by the following equation:

$$\frac{n'-1}{n-1} = \frac{k_1}{k_2} \qquad (7.2)$$

7.4.2 Difficulty with Non-linearity of Adjustable Parameters

The n and Z parameters of the Maxwell-Hamilton (Eq. 2.22) and Kirkpatrick-EMT (Eq. 2.27) models were related to specific physical variables in their derivations. In the case of the Maxwell-Hamilton model it was the sphericity of the pores (see Hamilton & Crosser, 1962), while in the case of the Kirkpatrick-EMT model it was the number of adjacent resistors (see Kirkpatrick, 1973). Mattea *et al.* (1989) related the Z-parameter of the Kirkpatrick-EMT model to the structure of cellular food tissues (potatoes, pears, apples), and used a Z-value of 6, but otherwise the literature does not appear to contain any studies connecting the n and Z parameters to the structure of foods. The Maxwell-Hamilton model does not appear to have been used for foods at all.

In previous discussions it was suggested that the most influential variable, other than the volume fractions and conductivities of the components, was the extent of contact between inclusions, and hence the adjustable parameter should, if possible, be related to this variable, as discussed in Section 7.3.5. If, however, the parameters are for more general purposes, such as fitting models to existing data, there is an incentive to modify Eqs. (2.22) and (2.27) in order that the values of this parameter may provide more information than is currently provided by the n and Z parameters.

The value of the n-parameter of the Maxwell-Hamilton model may vary between 1 and ∞ while the Z-parameter of the Kirkpatrick-EMT model may vary between 2 and ∞ (see Section 2.3 of Chapter 2). Figures 7.18 and 7.19 show plots of the two models with various n and Z values.

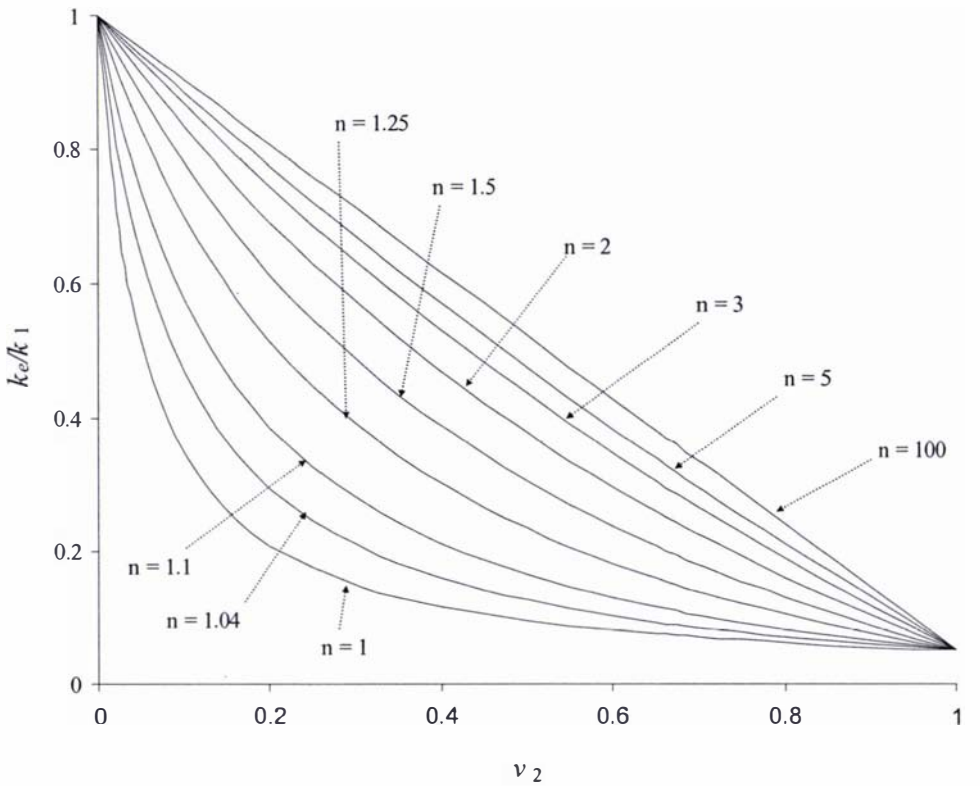

Figure 7.18: Plots of the Maxwell-Hamilton model with varying *n*-values (*n* as defined by Eq. 2.22)

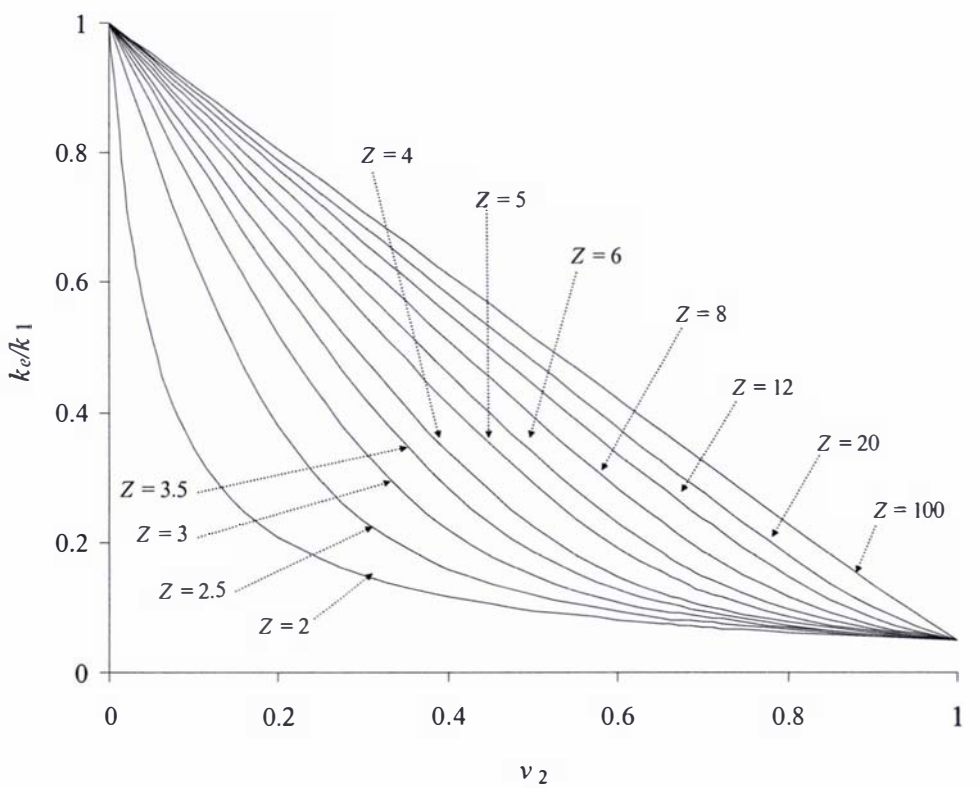

Figure 7.19 Plots of the Kirkpatrick-EMT model with varying *Z*-values

It is clear from Figs. 7.18 and 7.19 that the position of the model plots between the limiting values of the models (the Wiener bounds) had a non-linear dependence on the n and Z parameters (i.e. $dk_e / dn|_v$ and $dk_e / dZ|_v$ are not constant). It would be a lot more useful if the values of the parameters that best-fit the data could indicate how close to either of the Wiener bounds the data lie. Since it was possible for the plots of either model to lie anywhere between the Wiener bounds, it must also be possible for them to lie at approximately regular intervals. The difficulty is in determining a relationship between the adjustable parameter and the model that results in approximately linear variation in both the value of the parameter, and the position of the model's plot within the Wiener bounds.

Both the Maxwell-Hamilton and Kirkpatrick-EMT models were derived by modifying the coefficient of k_m in Eq. (2.14), the equation from which both the Maxwell-Eucken and Landauer-EMT models may be derived (see Sections 2.3.4 and 2.3.5 of Chapter 2, and Appendix B). Since the value of this coefficient controls the positions of the plot of the model between the Wiener bounds, the objective was to derive a function that nullified the non-linear behaviour caused by the (n - 1) and (Z/2 - 1) coefficients of Eqs. (2.22) and (2.27).

As shown in Figs. (7.20) and (7.21), this was achieved to a certain extent by Eqs. (7.3) and (7.4) which are modified forms of the basic Maxwell and EMT models with fitting parameters j_1 and j_2:

$$k_e = k_1 \frac{\left(\frac{j_1^2}{1-j_1^2}\right)k_1 + k_2 - \left(\frac{j_1^2}{1-j_1^2}\right)(k_1 - k_2)v_2}{\left(\frac{j_1^2}{1-j_1^2}\right)k_1 + k_2 + (k_1 - k_2)v_2} \qquad (7.3)$$

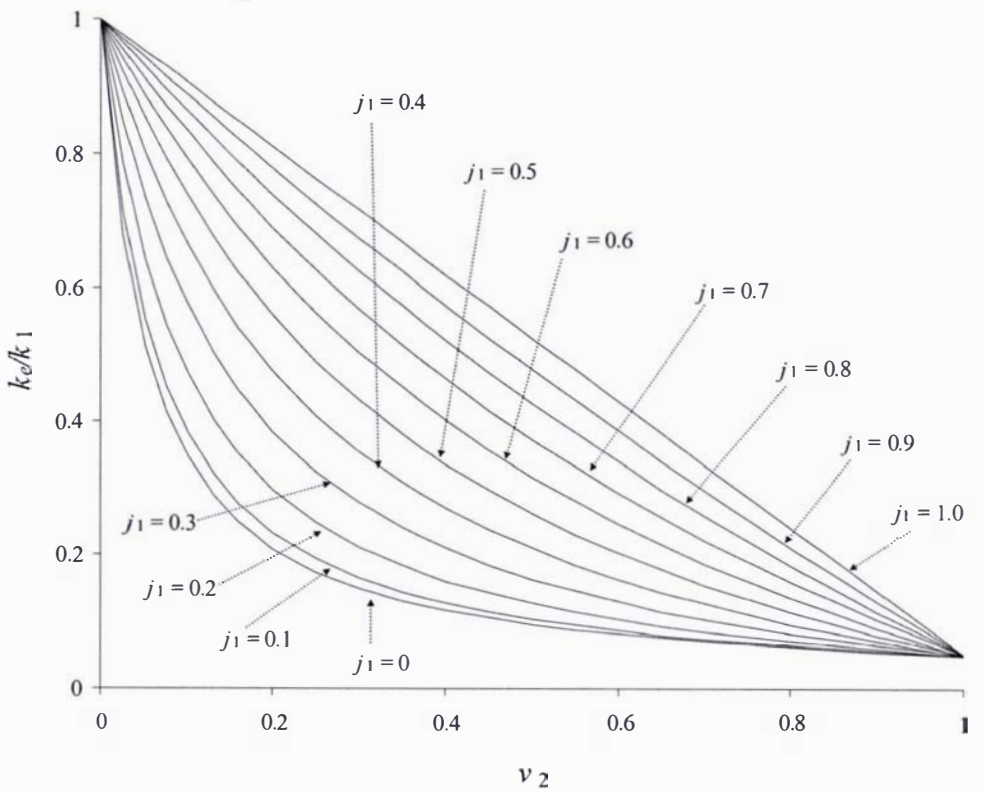

Figure 7.20: Plots of the Maxwell-Hamilton model with varying j_1-values (refer to Eq. 7.3)

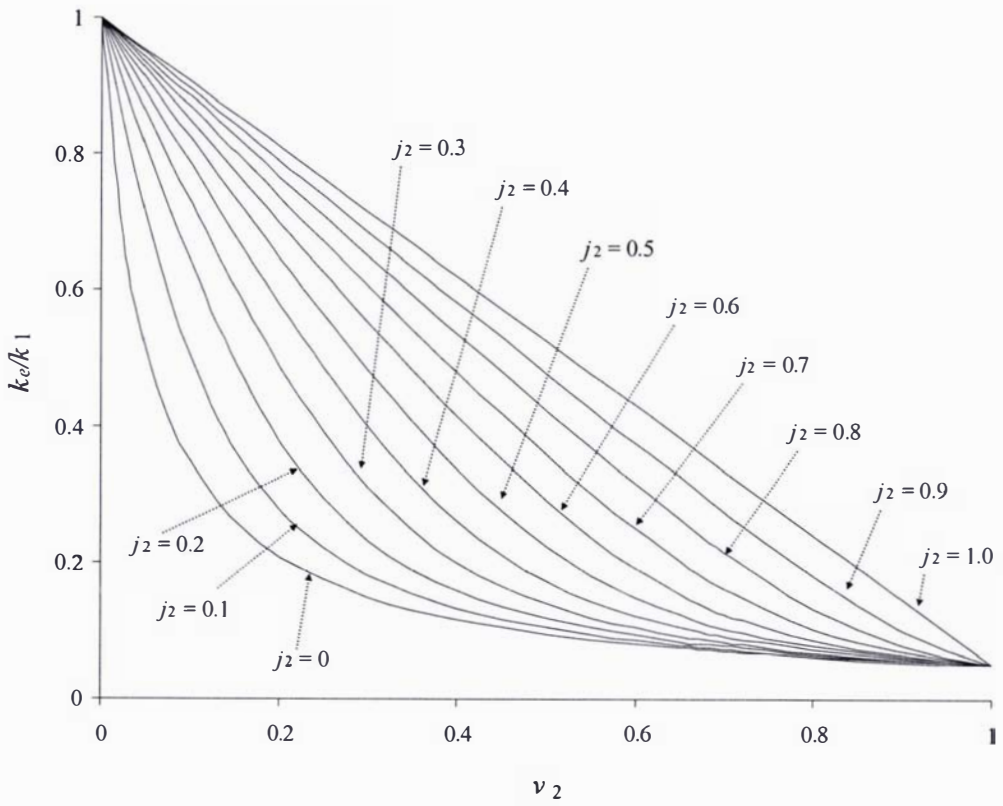

Figure 7.21: Plots of the Kirkpatrick-EMT model with varying j_2-values (refer to Eq. 7.4)

$$(1-v_2)\frac{k_1-k_e}{k_1+\left(\frac{j_2}{1-j_2}\right)k_e}+v_2\frac{k_2-k_e}{k_2+\left(\frac{j_2}{1-j_2}\right)k_e}=0 \qquad (7.4)$$

Equations (7.3) and (7.4) may be used for any component thermal conductivity ratio, however the variation of Eq. (7.3) is only linear with respect to j_1 when $k_1 > k_2$. Since it is based on the EMT model Eq. (7.4) makes no distinction between the components.

The linearised parameters, j_1, and j_2, may be related to the n and Z parameters of Eqs, (2.22) and (2.27) by Eqs. (7.5) and (7.6) respectively:

$$j_1=\sqrt{1-\frac{1}{n}} \qquad (7.5)$$

$$j_2=1-\frac{2}{Z} \qquad (7.6)$$

The greatest advantage of using linearly varying data-fitting parameters instead of the non-linearly varying n and Z parameters is that the numerical value of the parameter provides a clear indication of where experimental data lie within the k_e/k_1 vs. v_2 region. For example, when a comparison of the inorganic data displayed in Section 7.3.1 was made it could simply have been said that the data from Francl & Kingery (1954) had a j_1-value of 0.98 and the data from Woodside & Messmer (1961b) had a j_1-value 0.13, which would immediately have communicated, without the need for graphs, that the Francl & Kingery data lay very close to the upper Wiener bound (Parallel model), while the Woodside & Messmer data lay near the lower Wiener bound (Series model).

This feature may also be valuable for comparisons between other effective thermal conductivity models, particularly Type A models, whose positions are fixed relative to the Wiener bounds. For example, the Geometric model and Levy's model have best-fit j_1 values of 0.47 and 0.56 respectively. The j_1 values indicate that Levy's model lies slightly closer to the upper Wiener bound than the Geometric model does. With j-values close to 0.5, both lie fairly close to the middle of the k_e/k_1 vs v_2 region, whereas Russell's model, with a j_1 value of 0.87 lies much closer to the upper Wiener bound. Figure 7.22 displays this comparison:

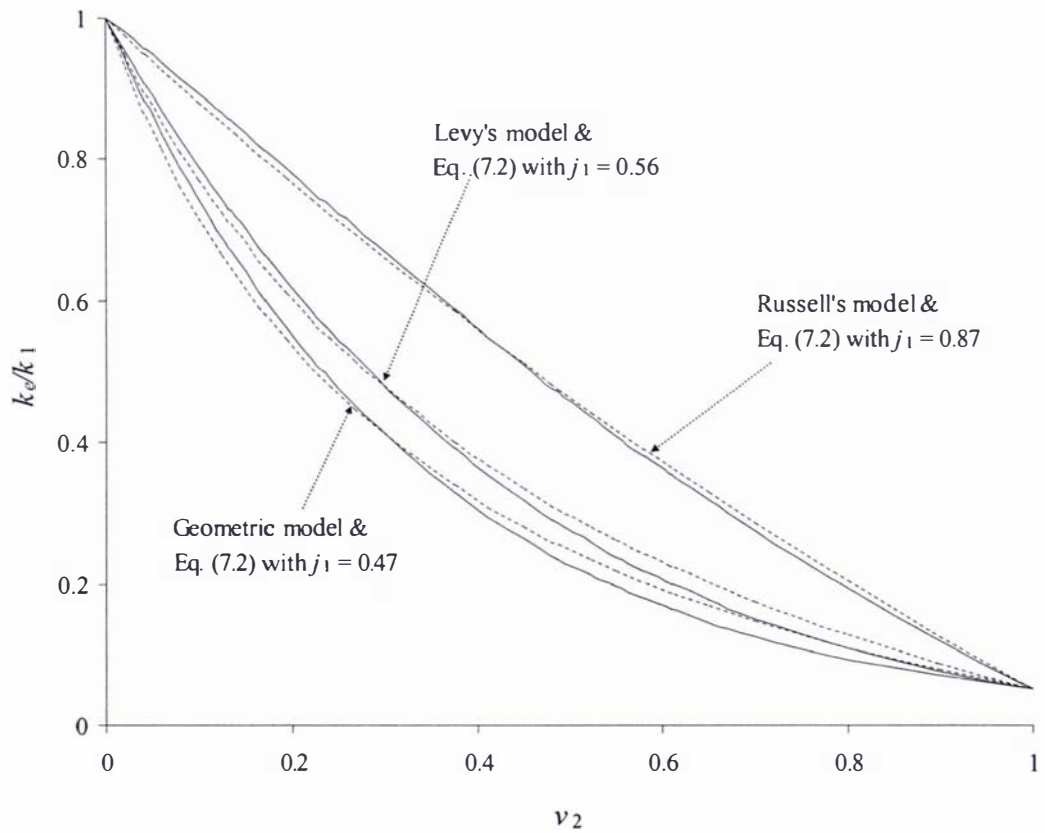

Figure 7.22: Comparison of three Type A models (solid lines) against Eq. (7.2) (dashed lines) with j_1 adjusted to fit the Type A models

The bounds defined in Section 7.3.2.3 may also be stated in terms of j-values. Table 7.1 shows that the j_1 and j_2 parameters, particularly for the upper Maxwell and Landauer-EMT bounds, are in surprisingly good agreement with each other, given that Maxwell-based models and EMT-based models have different

characteristic shapes. This observation highlights the value of Eqs. (7.3) and (7.4): it may be possible to perform a single thermal conductivity measurement on a material of unknown structure and, subject to the uncertainty in the measurement, determine the data-point's position relative to both the Wiener bounds and the bounds for porosity as defined above, based on its j-value alone.

	n (Eq. 2.22)	Z (Eq. 2.27)	j_1 (Eq. 7.3)	j_2 (Eq. 7.4)
Upper Maxwell bound	**3**	*12.8*	0.81	*0.84*
Landauer-EMT bound	*1.8*	**6**	*0.67*	0.67
Lower Maxwell bound	1.1	*2.5*	0.3	*0.2*

Table 7.1: Parameter values corresponding to the bounds proposed in Section 7.3.2 Numbers in bold indicate definition values, numbers in italics indicate that a parameter of a Maxwell-model has been fitted to an EMT plot or vice versa

7.4.3 Summary of Recommended Models for Isotropic non-Frozen Foods

In Section 7.3.3 it was pointed out that for non-porous, non-frozen foods the maximum component thermal conductivity ratio had a value of approximately 3, and in this case the discrepancies between the predictions of any of a number of models, including the Maxwell-Eucken and Landauer-EMT models, would be negligible compared with the uncertainty in the data used in the models.

For porous foods, the component thermal conductivity ratio may be as high as approximately 20. If the volume fraction of the dispersed phase, whether it be the gaseous phase or the condensed phase, is below 0.2 then either of the Maxwell-Eucken or Landauer-EMT models will be suitable. Above this volume fraction, a model containing a parameter related to the extent of inclusion contact is required. The linearly-varying parameter models (Eqs. 7.3 and 7.4) may be the

most convenient for this purpose. For volume fractions greater than 0.2, a micrograph of the food's structure will provide valuable assistance in determining which phase (gaseous or condensed) forms the continuous phase (from an effective thermal conductivity perspective), and may also be used to provide an estimate of the j-values of Eqs. (7.3) and (7.4) if no experimental data is available to determine its value empirically.

Figure 7.23 shows a diagrammatic summary of the recommended effective thermal conductivity models:

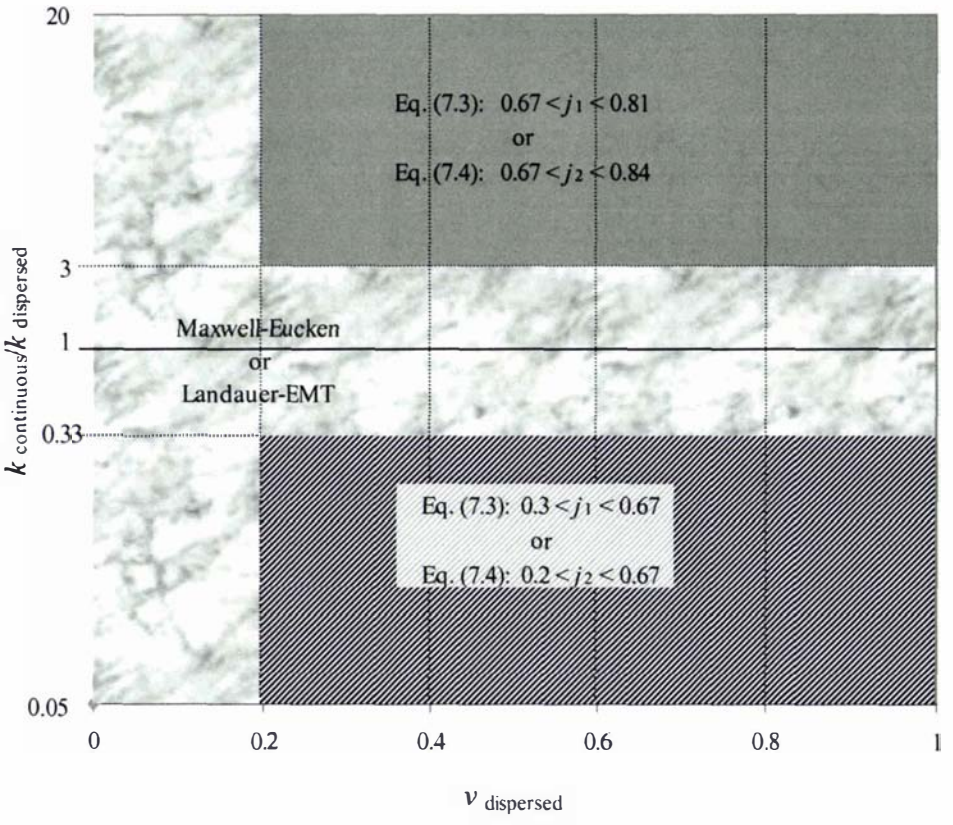

Figure 7.23: Summary of recommended effective thermal conductivity models

Frozen foods have not been considered so far in this investigation. As well as the relatively high thermal conductivity of ice (by comparison with other food components), the freezing characteristics and ice crystal formation mechanisms that are dependent on the structure of a specific food introduce complexities that

require separate analysis. The spatial distribution of ice-crystals in the product, which may well be non-uniform, and the possibility of contact and/or fusion between neighbouring ice crystals are particular issues that need consideration. However, it may be possible to use a similar analysis to that described here, although further investigation is required.

7.5 Possible Influences on Heat Transfer by Mechanisms other than Conduction

The discussion so far has been restricted to heat transfer by conduction, consistent with the scope of this study (see Chapter 3). However, porous foods may also be subjected to radiative, convective and evaporative heat transfer, depending on the particular food and the thermal process involved.

7.5.1 Radiation and Convection

Different aspects of the issue of radiation and convection in porous materials have been investigated by Russell (1934), Loeb (1954), Yagi & Kunii (1957), Progelhof *et al.* (1976) and North (2000). The size of the pores (or void spaces) was found to be influential for both radiation and convection, and the absolute temperature was significant for radiation. It is difficult to provide comprehensive thresholds of pore size and absolute temperature beyond which radiation and convection become significant, since physical properties of the material involved are also potentially influential. However, indicative values were provided by Russell, who stated that below a pore diameter of ¼ inch (6.35 mm) convection effects could be ignored, and Progelhof *et al.* who stated that for foamed polymers, radiation was significant above 200°F (93.3°C) and a pore diameter of 0.04 inch (≈1mm).

As mentioned in Section 2.3.1 of Chapter 2, several effective thermal conductivity models have been proposed that incorporate non-conduction heat transfer modes (see Appendix A for equations). Locb (1954) proposed a model that accounted for radiative heat transfer across pores. When radiation is negligible, at low temperatures for example, Loeb's model provides similar predictions to the Maxwell-Eucken model. Yagi & Kunii proposed models that took into account both radiative and convective heat transfer; however they involved several heat transfer coefficients and characteristic dimensions that must either be assumed or measured.

7.5.2 Evaporation

Sakiyama & Yano (1990) observed that moisture migration across vapour spaces in aerated gels was significant at 40°C for high water-content gels. Many food products have very high-water contents. The evaporative effect was found to have a strong dependence on temperature, so although the water activity might not be as high in many foods as it is in some gels, the fact that it was observed in the gels at temperatures as low as 40°C suggests that it might have a significant influence on other foods at slightly higher temperatures.

Sakiyama & Yano proposed a model (see Appendix A) that accounted for possible evaporative effects by replacing the k_2 term in Eq. (2.20) by ($k_2 + k_{evap}$). Essentially it was the same equation as the Maxwell-Eucken model with the exception that rather than using the true conductivity of air, an 'apparent air conductivity' was used that accounted for the increase in apparent conductivity due to the evaporative effects. When evaporation was negligible, the equation was reduced to the Maxwell-Eucken model. The model was found to predict the experimental data well.

7.5.3 Significance of non-Conduction Heat Transfer in the Prediction of Effective Thermal Conductivity

Clearly internal heat transfer by modes other than conduction has potential to influence many thermal processes involving porous foods. However, the situation is simplified by the fact that non-conduction heat transfer is likely to be significant only for the gaseous phase. Hence the simple approach taken by Sakiyama & Yano to account for evaporation by modifying the conductivity of the gaseous component, may be a suitable approach for all types of non-conduction heat transfer. The temperature dependence of the true thermal conductivities of the components of the food will often need to be accounted for regardless of other modes of heat transfer and, since radiation and evaporation in particular have strong dependences on temperature, incorporating them into the analysis may not involve much extra effort. However, since the focus of this study has been restricted to conduction, further work in this area, which would be needed before definite conclusions may be drawn, falls outside the scope of this research.

7.6 A General Procedure for the Prediction of the Effective Thermal Conductivity of Isotropic non-Frozen Food Products

Based on the results from the experimental work, and the discussion in this chapter, the following general procedure is proposed for the prediction of the effective thermal conductivity of isotropic non-frozen food products, firstly in the form of a step-by-step list, secondly in the form of a flow-chart.

7.6.1 Recommended Procedure in the form of a Step-by-Step List

Step 1: Determine composition of food in question.

In most cases it is probably sufficient simply to know the porosity and moisture content, since the thermal conductivities of the other components are very similar.

Step 2: Determine maximum component thermal conductivity ratio.

This step is important for determining how much uncertainty is involved in the prediction.

1. If the food is non-porous ($k_1/k_2 \approx 3$) then the region between the Hashin-Shtrikman bounds is narrow (see Fig. 7.10), hence the uncertainties involved are relatively minor. Use either the Maxwell-Eucken or one of several other models for the prediction of the effective thermal conductivity. Probably only need to consider food as made up of two components, water and remaining components combined.
2. If the food is porous then (k_1/k_2 = 10 to 20), and the region between Hashin-Shtrikman bounds is significant (see Fig. 7.9). Proceed to Step 3.

Step 3: Determine whether gaseous phase is continuous or dispersed (from a thermal perspective).

As a basic guide, internal pores (bubbles) are most likely to constitute a dispersed phase, while external voids, such as exist between interstices of granular materials, are likely to constitute the continuous phase. However, as was discussed in Section 7.3.4, the designation of phases is not always straightforward, and the analysis should determine the optimum heat transfer pathway within the material, either through the dispersed phase, or avoiding the dispersed phase (see Section 7.3). If possible, use a micrograph or some other image of the structure to assist.

Step 4: Determine volume fraction of dispersed phase.

This step should use results from Step 1 and Step 3.

1. If the volume fraction of the dispersed phase is less than 0.2, then use either the Maxwell-Eucken or Landauer-EMT models to predict the effective thermal conductivity. It is probably sufficient to calculate the thermal conductivity of the condensed (non-gaseous) phase as per option 1 of Step 2.
2. If the volume fraction of the dispersed phase is greater than 0.2 then proceed to Step 5.

Step 5: Use either Eq. (7.3) or Eq. (7.4) with appropriate *j*-values.

Beyond a volume fraction of 0.2 the issue of inclusion contact becomes significant, and a new parameter must be involved in the effective thermal conductivity prediction. At this point it is helpful to determine into which of the regions between the Hashin-Shtrikman bounds the effective thermal conductivity is likely to fall.

1. *Internal porosity region* ($k_{condensed} > k_{dispersed}$): In this region, j_1 values vary between 0.67 and 0.81, while j_2 values vary between 0.67 and 0.84 (see Table 7.1). As mentioned in Section 7.3.5, the extent of inclusion contact is a material-specific property, and, at this stage, there are no clear guidelines for relating the values of the *j* parameters to any measurable property. However, *j*-values may be estimated from a visual assessment of a food's structure. If the structure is a reasonable approximation to the Maxwell-type structure (i.e. if continuous and disperse phases are easy to identify) then Eq. (7.3) should be used, with a j_1-value between close to 0.81 If it appears that both the gaseous and condensed phases may be continuous, then Eq. (7.4) should be used with a j_2-value close to 0.67. In the absence of a means of estimating the *j*-values from an image of the food's structure, a mid-range *j*-value (≈0.73-0.76) might provide reasonable predictions, especially for volume fractions of 0.4 or lower (note size of region between Landauer-

EMT and upper Hashin-Shtrikman bound of Fig. 7.9, below v_2 = 0.4).

2. *External porosity region* ($k_{condensed} < k_{dispersed}$): In this region, j_1 values vary between 0.3 and 0.67, while j_2 values vary between 0.2 and 0.67 (see Table 7.1). Unfortunately the extent of pore contact is highly influential in this sub-region and estimates of j-values along the same lines as for the internal porosity foods would probably involve unacceptable levels of uncertainty. It is probable that the only satisfactory way to determine the values of the j-parameters is to fit Eq. (7.3) or Eq. (7.4) to measured data. Since with the majority of external porosity foods (particulate foods) it is easy to identify the continuous and dispersed phases, Eq. (7.3) will most often be the appropriate model and should therefore be the default choice.

7.6.2 Recommended Procedure in the form of a Flow-Chart

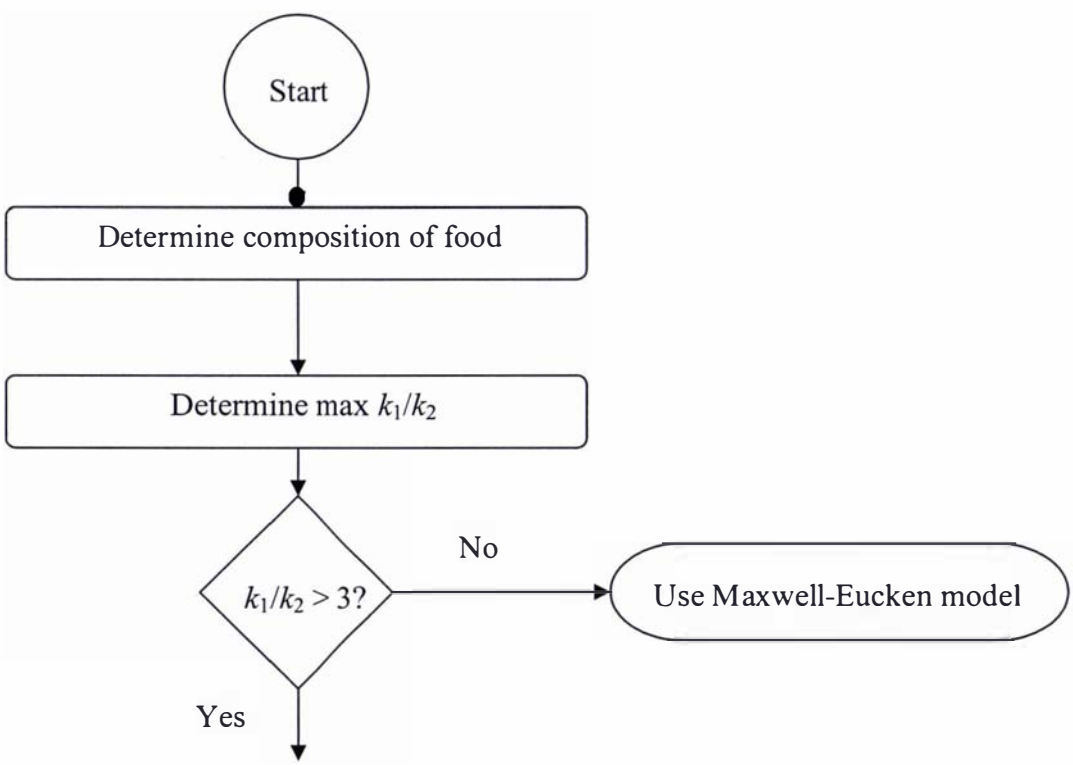

Figure 7.24a: Flow-chart for effective thermal conductivity model selection – Part 1

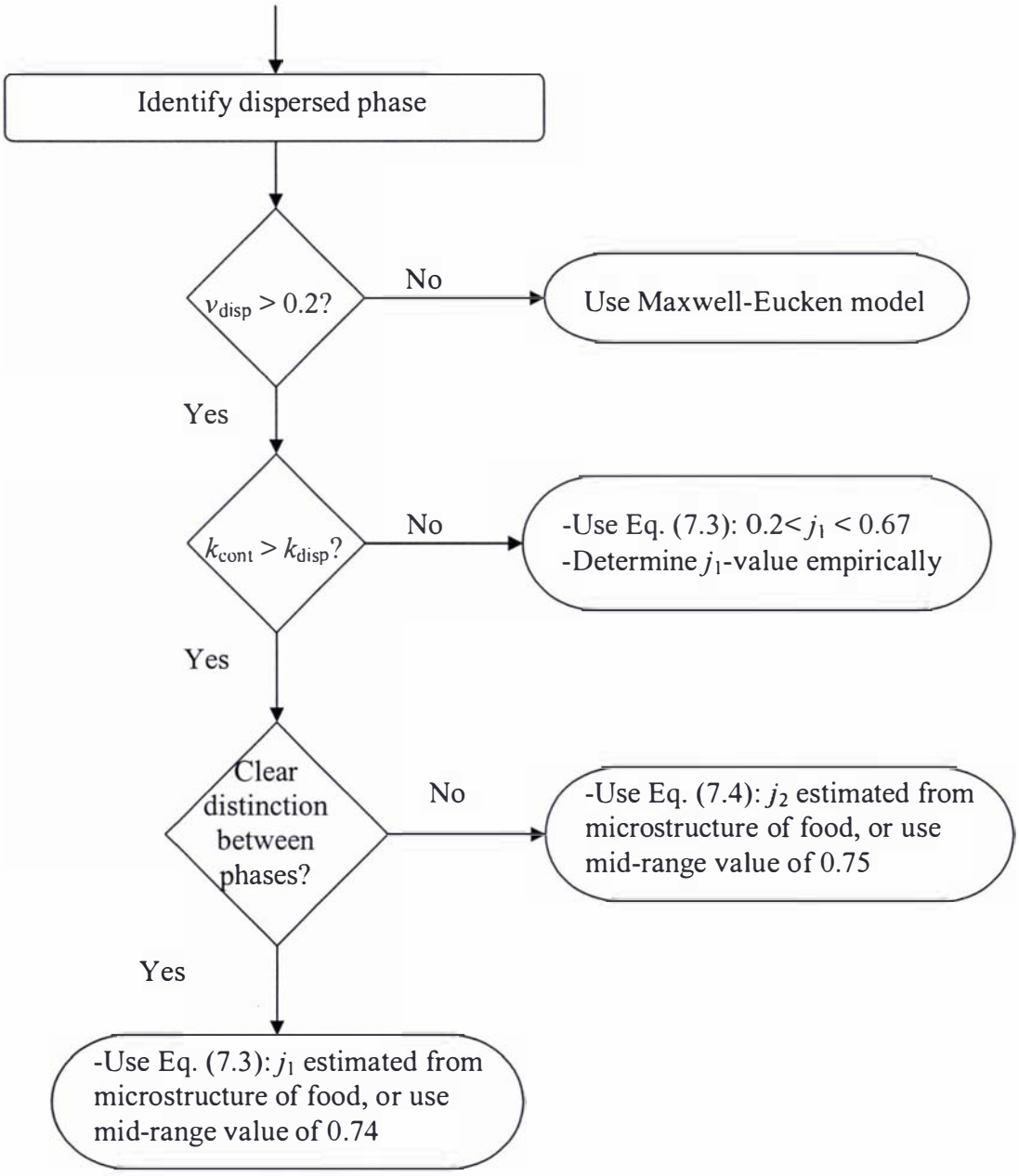

Figure 7.24b: Flow-chart for effective thermal conductivity model selection – Part 2

7.7 Conclusion

The recommendations outlined in Section 7.6 were intended to address a deficiency in the food engineering literature, as outlined in Section 7.1.2, in accordance with the fifth and sixth objectives listed in Chapter 3. This was achieved to a certain extent, in that a step-by-step procedure for the prediction of effective thermal conductivities has been proposed for isotropic, non-frozen foods. However, since it is a new procedure, it should be tested before it can be used with confidence. The determination of the j-values, particularly for external porosity materials, requires more work.

The materials that fell outside the scope of this procedure (frozen and anisotropic foods), along with non-conduction heat transfer effects, may potentially be dealt with in a similar manner to the materials and heat transfer modes that were considered, and hence it might be possible to develop a single procedure to cover all these possibilities. However further work would be required for this development.

Chapter 8: Practical Application

8.1 Introduction

8.1.1 Objective

The aim of this chapter was to test the conclusions and recommendations made in previous chapters by applying the procedure outlined in Section 7.6 of Chapter 7 to real porous foods.

8.1.2 Availability of Information Required by the Recommended Effective Thermal Conductivity Prediction Method

The use of the models recommended in Chapter 7 will only be feasible if the data that they require is readily available. The types of models recommended were functions of the composition of the food, component thermal conductivity, and, in some cases, a third parameter that was either empirically determined, or was related to the extent of inclusion contact of the material. It was also concluded that, if possible, continuous and dispersed phases should be identified, since the optimum heat conduction pathways are dependent on which phase has the higher thermal conductivity (see Section 7.3 of Chapter 7).

8.1.2.1 Availability of Composition Data

Methods of chemical analysis that may be used to determine the chemical composition of foods are well-known, and in most cases have been standardised (Lees, 1975, Osborne & Voogt, 1978, Williams, 1984). The methods range from simple proximate analyses to more accurate procedures involving chromatography and spectroscopy. The fact that most food products have basic composition data printed on the packaging is an indication that chemical composition data for foods is reasonably obtainable by food manufacturers. However, a complete chemical analysis is probably unnecessary, since, due to their similar thermal conductivities,

components other than water and air may be lumped together with the introduction of minimal error (see Section 7.3.3 of Chapter 7).

8.1.2.2 Measurement of Porosity in Food Products

Gaseous components of food (mainly air and carbon dioxide) are not usually included in the chemical analyses described in Section 8.1.2.1. Methods for the measurement and prediction of porosity are provided by Rahman (1995). Perhaps the most practical method of porosity measurement is the comparison of the true density to the apparent density, which was the method that was used in this study (see Section 4.3.5 of Chapter 4).

8.1.2.3 Thermal Conductivity Data of the Chemical Components of Food

Osborne & Voogt (1978) divided the chemical components of foods into two classes: macronutrients and micronutrients. (The division was made on the basis of the relative amounts within the food, as opposed to the molecular size of the components). The macronutrient class included proteins, carbohydrates, fats (lipids), and water, while the micronutrients included vitamins and minerals. Table 1 of Chapter 8 in *ASHRAE Handbook of Refrigeration* provides data for the thermal conductivities of the macronutrient food components as a function of temperature between -40°C and 150°C, and a similar table for the thermal conductivities of the basic food components at 0°C was shown in Chapter 2 (Table 2.1). Because the micronutrient components occur in such small amounts it was not necessary to consider them separately.

8.1.2.4 Designation of Continuous and Dispersed Phases

The problem of distinguishing between continuous and dispersed phases from a thermal perspective was discussed in Section 7.3 of Chapter 7. Unfortunately definitive guidelines were not established, since further investigations would be required. However, often an intuitive assessment will suffice. For non-porous foods, the issue is not critical, since the error introduced by the incorrect identification of the phases would be minimal.

For porous foods a distinction between the gaseous and condensed phase(s) is, at least, easy to make, especially with the benefit of micrograph images of the food in question. For external porosity foods the gaseous phase is continuous, while for internal porosity foods the condensed phase is continuous. Hence, as a rough guideline, the condensed phase will be continuous in the majority of foods other than grains, powders, flakes, shavings etc. However, an individual assessment of the food should be performed for each food in question, as per Section 7.3 of Chapter 7.

8.1.2.5 Extent of Contact between Inclusions: j- Parameter

For some porous foods Type A models are sufficient (see Figure 7.23 of Chapter 7). However, the evidence from previous chapters suggested that the use of Type B models was necessary for many foods. It was recommended that the third parameter (after the prerequisite component thermal conductivity and volume fraction) should be related to the degree of contact between inclusions of the dispersed phase.

This stage of the prediction method is the weakest, and until further investigations of the relationship between inclusion contact and thermal conductivity have been performed, the numerical value of this parameter must be estimated or determined empirically. Estimates may be made based on an intuitive analysis of the structure of the food, or alternatively, for internal pores, mid-range *j*-values may provide predictions of sufficient accuracy, particularly for porosities of 0.4 or less.

8.1.3 Case Studies

The method outlined in Section 7.6 of Chapter 7 was used to predict the effective thermal conductivity of two types of cake (sponge cake and yellow cake), and the predictions were compared to thermal conductivity measurements that were performed, as described in subsequent sections of this chapter.

Generic cake types such as sponge cake and yellow cake may be expected to have slightly different structures, due to the differing amounts of the basic ingredients (flour, sugar, eggs, fat and milk) used in each recipe. The relative amounts of flour, fat and eggs in particular have significant influences on the structure of the cake: a high proportion of eggs is used in lighter, fluffier cakes such as sponge cake, while high proportions of flour are used in tougher, denser cakes, such as yellow cake (Pyler, 1973). The cake's structure is also affected by changes in temperature, particularly during the baking process as the bubbles increase in size and come into contact with neighbours.

8.1.3.1 Sponge Cake

Steps 1 and 2 of the procedure are trivial, since it is known that cakes contain both air and water, and hence they will have component conductivity ratios greater than 3. Assuming that the condensed phase is the continuous phase, based on the rough guideline that this is the case other than for particulate foods (Step 3), and knowing that the porosity will be greater than 0.2 (Step 4), cakes may reasonably be assumed to be candidates for predictions from Eq. (7.3) or Eq. (7.4).

Hence a more detailed consideration of the cake's structure is required. Lostie *et al.* (2002) studied the baking process of a sponge cake. Figure 8.1 is taken from Lostie *et al.* (2002) and shows images of the cross-section of the cake at different stages of the baking process. Near the beginning of the process the bubbles are small and the majority are completely isolated (left hand image of Fig. 8.1), which is the basic structure assumed by Maxwell's model. After a significant baking period the bubbles have increased greatly in size and there is a significant degree of coalescence between bubbles (right hand image of Fig. 8.1). The condensed phase is continuous both after 1 hour and after 2½ hours, however, due to the substantial coalescence of the bubbles after 2½ hours, continuous gaseous pathways may be observed (this feature is even more obvious in Fig. 5 of Lostie *et al.*, 2002). Hence, while at the start of the baking process the cake's structure is a Maxwell-type, it becomes more Kirkpatrick-like as the baking progresses.

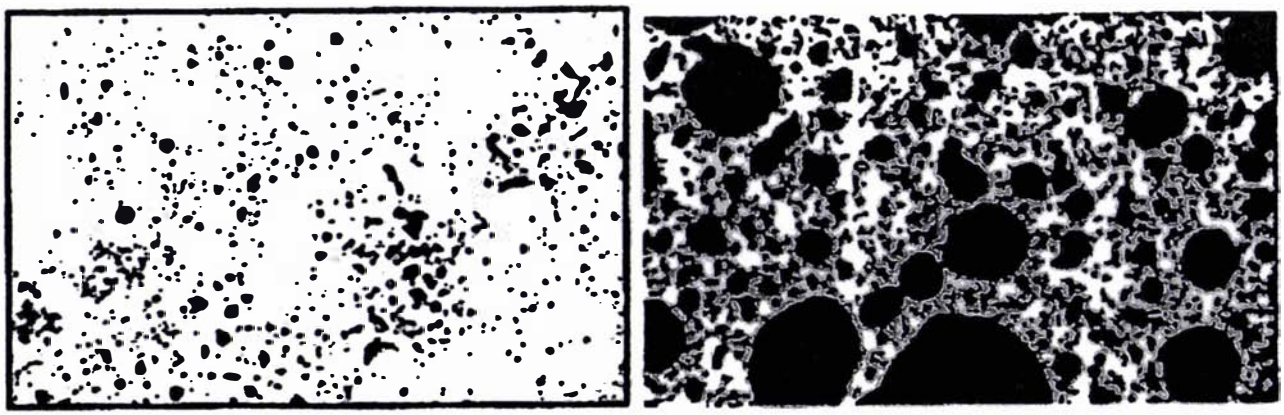

Figure 8.1: Magnified photographic images of cross-sections of sponge cake at different stages of the baking process, 1 hour (left), and 2 ½ hours (right) (taken from Lostie *et al.*, 2002)

Since the condensed phase of the cake is continuous throughout the baking process, and has a higher thermal conductivity than the gaseous phase, the *j*-values would be expected to lie between 0.67 and 0.84 (refer to Table 7.1 of Chapter 7) regardless of the stage of the baking process.

The thermal conductivity measurements (described in Section 8.2) were performed on the fully baked cakes. Since the structure of a sponge cake at the completion of the baking process would be expected to be closer to the Kirkpatrick limit than the Maxwell limit, Eq. (7.4) would be more applicable than Eq. (7.3), since it is based on the EMT, and a j_2 value between 0.67 and 0.75 might be expected (since a j_2 value of 0.75 bisects the internal porosity region of Fig. 7.9).

8.1.3.2 Yellow Cake

Without the benefit of an image of the structure of yellow cake, a mid-range *j*-value (0.74-0.75) should be used, as recommended in Section 7.6 of Chapter 7. Yellow cakes have significantly higher flour contents than sponge cakes (compare ingredient amounts in Table 8.2 to amounts in Table 8.1) and, according to Pyler (1973), the starch in the flour has the effect of toughening the cake, and so it might be expected that yellow-cake batters would pose greater resistance to

bubble coalescence than sponge-cake batters. However, if the bubbles cannot coalesce to the same extent in the yellow cakes as they can in sponge cakes then they have less potential to interrupt the continuous heat transfer pathways through the higher conductivity condensed phase. On this basis it would be expected that yellow cakes would have structures closer to the Maxwell limit than sponge cakes, and hence it would be expected that yellow cakes might have slightly higher j-values than sponge cakes.

8.2 Method

8.2.1 General Approach

The emphasis of this study of effective thermal conductivity has been on the effect of porosity specifically, and, other than in selected discussion sections, all non-gaseous components have been lumped together as a single condensed phase. The foods under investigation in this chapter were, like most foods, multi-component materials, but since the emphasis has been on porosity, it was more convenient to treat them as two-component materials, consistent with the rest of the study. This approach also had a practical advantage in that it allowed the use of the same thermal conductivity measurement method that was used for the food analogues described in Chapter 4. This method involved the comparison of the cooling rates of a test sample and a control sample with the test sample simply being an aerated version of the control sample.

Since this method provided relative thermal conductivity measurements rather than absolute measurements, predictions of absolute effective thermal conductivity could not be verified by these results. However, relative thermal conductivity measurements were sufficient for comparisons with the expected

values outlined in Section 8.1.3, and hence this method provided a means of testing the recommendations made in Chapter 7.

8.2.2 Sample Preparation

8.2.2.1 Cake: Test samples

The compositions of the sponge and yellow cakes were based on guidelines found in Pyler (1973) and are listed in Tables 8.1 and 8.2.

Ingredient	Mass %
egg	34.5
sugar	34.7
milk (full cream)	8.8
flour	13.5
canola oil	7.5
baking powder*	1

* the amount of baking powder added was varied in order to vary the porosity of the cakes

Table 8.1: Relative amounts of ingredients of sponge cakes

Ingredient	Mass %
egg	15
sugar	25.8
milk (full cream)	15
flour	30
canola oil	13.5
baking powder*	0.7

* the amount of baking powder added was varied in order to vary the porosity of the cakes

Table 8.2: Relative amounts of ingredients of yellow cakes

The ingredients for the cakes were obtained from general retail outlets. The batter for the sponge cakes was mixed using the 'creaming' method in which the oil and sugar are mixed first, followed by the eggs, and finally the milk and the flour (sieved) in alternate small portions (Pyler, 1973). The baking soda was added at the same time as the flour and the amount was varied in order to vary the final porosity of the cake. The cake batter was then poured into the 75mm radius hemispherical aluminium sample containers.

The cakes were baked in the sample containers at 170°C for as long as was required for the centre of the cake to cook (typically between 1 and 1½ hours). At the completion of the baking process the cakes were allowed to cool overnight. The next day the excess cake was cut from the tops of the containers in order that the two hemispheres could be attached together after the thermocouple had been placed at the centre of the sphere. The moisture content of a sample taken from the off-cut was determined by drying at 104°C.

8.2.2.2 Cake: control samples

The preparation of the control samples for the cakes was not straightforward, since it was almost impossible to bake a cake that did not contain air. In fact, it was also difficult to prepare a batter that did not contain a significant amount of air. Because of the difficulty in preparing air-free cake or cake batter, a pseudo-cake mixture was used as a control sample. The pseudo-cakes did not contain eggs or baking powder, which are the ingredients responsible for the majority of the air entrainment. Also, the pseudo-cakes were not baked, so if a small amount of air was entrained in the mixing process, the bubbles would not expand.

A fundamental requirement of the control samples was that they had the same composition as the condensed phase of the cakes, in particular the moisture content. Since the removal of egg from the ingredient lists in Tables 8.1 and 8.2 would affect the relative amounts of the major chemical components in the control samples, the amounts of the remaining ingredients in the control samples

were altered to compensate. Tables 8.3 and 8.4 show the relative amounts of the ingredients of the pseudo-cake control samples, and Tables 8.5 and 8.6 show comparisons of the relative amounts of the basic chemical components of the cakes and the control samples. The basic chemical compositions of the cake ingredients were determined from Table 3 in Chapter 8 of the *ASHRAE Handbook of Refrigeration*.

Ingredient	Mass %
egg	0
sugar	40.4
milk (full cream)	38.4
flour	9.1
canola oil	12.1
baking powder	0

Table 8.3: Relative amounts of ingredients of pseudo-sponge cake control sample

Ingredient	Mass %
egg	0
sugar	38.3
milk (full cream)	29.7
flour	15.4
canola oil	16.6
baking powder	0

Table 8.4: Relative amounts of ingredients of pseudo-yellow cake control sample

Component	Sponge Cake	Control Sample
Water	35.5	35.3
Protein	6.0	2.5
Fat	11.8	10.9
Carbohydrate	46.7	51.3

Table 8.5: Comparison of the relative amounts of basic chemical components in the sponge cakes and the control samples

Component	Yellow Cake	Control Sample
Water	28.2	28.2
Protein	5.4	2.7
Fat	16.6	17.1
Carbohydrate	49.8	52.0

Table 8.6: Comparison of the relative amounts of basic chemical components in the yellow cakes and the control samples

The pseudo-cakes were prepared by dissolving the sugar in the milk by mixing at the low speed. Once the sugar had dissolved, the oil was added and then the flour. One third of the amount of flour listed in Tables 8.3 and 8.4 was replaced by guar powder to prevent the possibility of convection. The chemical composition of the guar (mostly carbohydrate) was assumed to be the same as that of flour.

8.2.3 General Procedure

Other than the measurement of the moisture contents of the cakes, the general procedure was the same as the procedure described in Section 4.3.4 of Chapter 4. The apparatus was the same as that used in Chapter 4 (see figure 4.2).

The thermal conductivity of the pseudo-cake control samples was measured using a thermal conductivity probe, and the specific heat capacity was calculated from the amounts of the components using Eq. (4.10) and data from Table 1 in Chapter 8 of the *ASHRAE Handbook of Refrigeration*.

8.3 Results

8.3.1 Uncertainty Analysis

Potential sources of error associated with the apparatus and procedure were discussed in Section 4.4.1 of Chapter 4. The only significant differences between the methods described in this chapter and those described in Chapter 4 were associated with the compositions of the test and control samples.

It was assumed that the only difference in composition between the test and control samples was the presence of air, and that the relative amounts of the other chemical components were the same. The relative amounts of the components listed in Tables 8.5 and 8.6 were predicted based on composition data in the literature, and, apart from the moisture content, the true amounts of the chemical components were not measured. However, the measured moisture contents of the cakes (test samples) were in reasonable agreement with the values listed in Tables

8.5 and 8.6 (for example, the sponge cakes had an average moisture content of 34%, mass basis, compared to 35.3% listed in Table 8.5).

The agreement between replicate measurements was good, being typically less than 2%, but the k_e/k_1 vs. v_2 plots did not appear to follow as clear a trend as was seen with the EPS/guar gel results in Chapter 4. The cakes were a lot more complex chemically than the EPS/gel samples, and it was expected that the real foods would have greater inherent variability than the food analogues, but it was difficult to estimate a numerical value for the random error of the data since the number of data points was small.

Since the experiments described in this chapter would be expected to have, on average, greater random and systematic error than those described in Chapter 4, the uncertainties involved in these experiments could not be expected to be less than 10%, which was the highest estimated uncertainty for the measurements described in Chapter 4.

8.3.2 Results for Sponge Cakes

Figure 8.2 shows the data points for sponge cakes in relation to the Maxwell-Eucken and Landauer-EMT bounds. Figure 8.3 shows an enlarged portion of the graph along with a plot of Eq. (7.4) with a j_2 value of 0.71 (the midpoint value of the 0.67-0.75 range recommended in Section 8.3.1). Figure 8.4 shows the results plotted along with the predictions of several Type A models (see Section 6.1.2), and Figure 8.5 shows the results plotted with the predictions of the Krischer and Chaudhary-Bhandari whose f-parameters have values recommended in the literature.

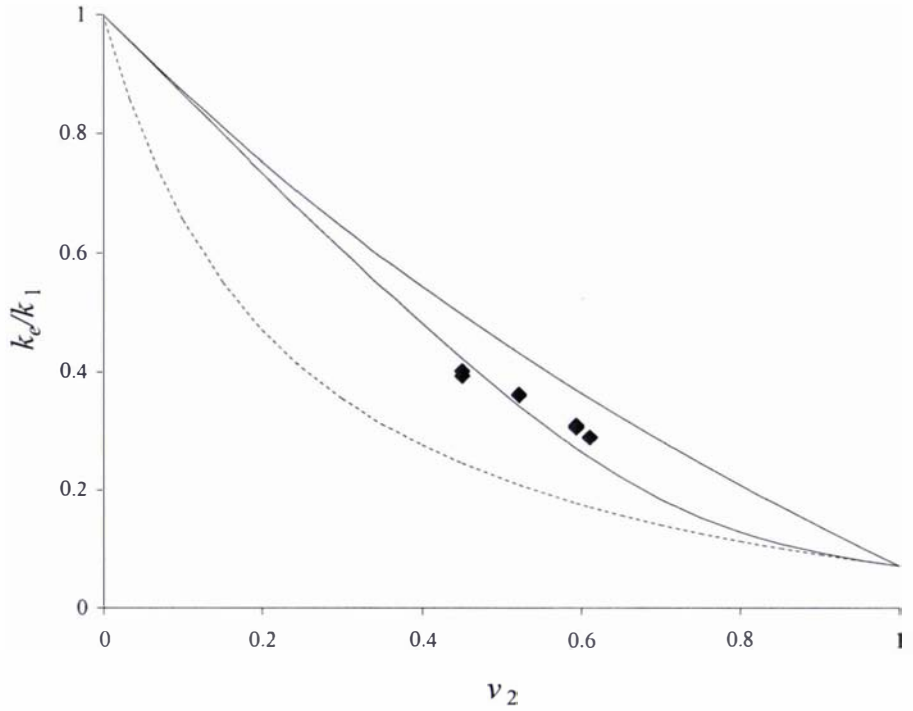

Figure 8.2: Effective thermal conductivity of sponge cakes (points), plotted with Upper Maxwell-Eucken and Landauer-EMT bounds (solid lines) and Lower Maxwell-Eucken bound (dashed line)

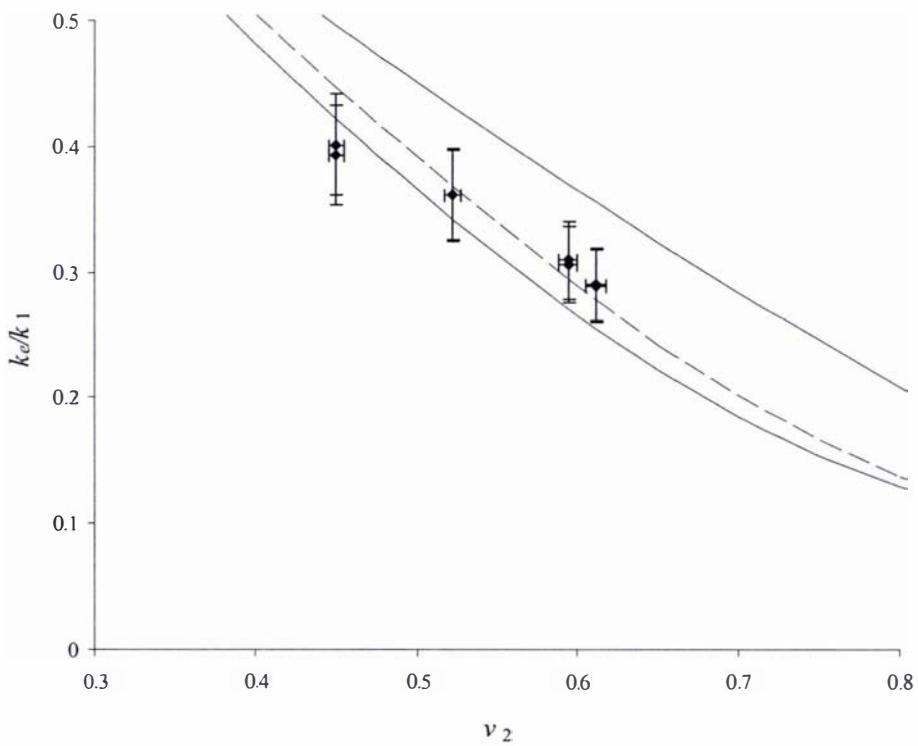

Figure 8.3: Effective thermal conductivity measurements for sponge cakes (points), plotted with the Maxwell-Eucken and Landauer-EMT bounds (solid lines), and Eq. (7.4) with a j_2 value of 0.71 (dashed line)

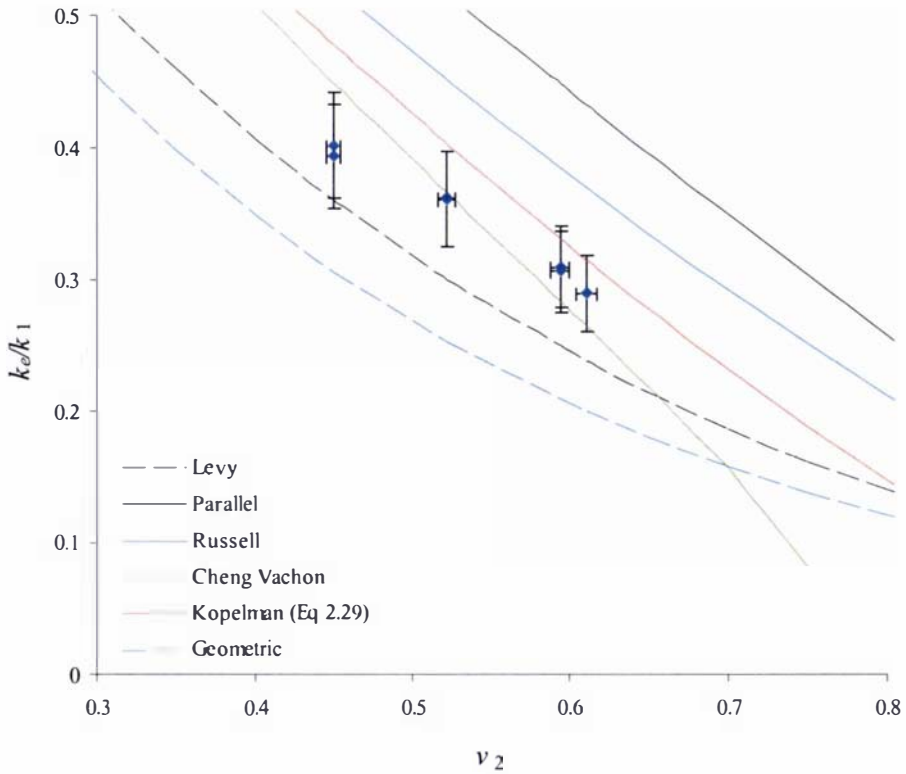

Figure 8.4: Effective thermal conductivity measurements for sponge cakes (points), plotted with predictions from selected Type A models

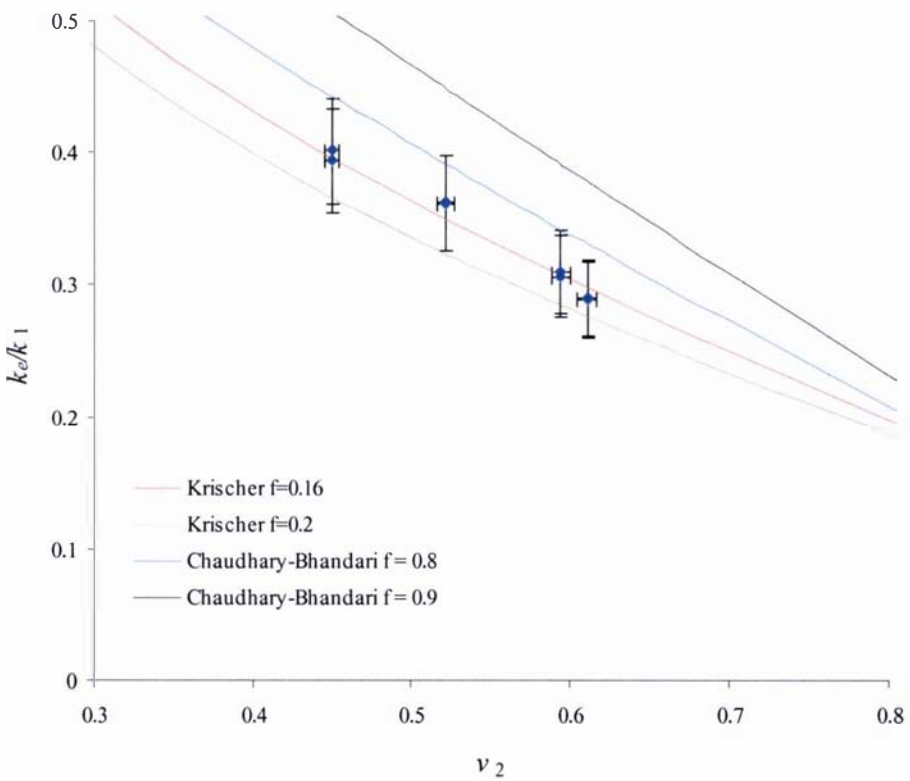

Figure 8.5: Effective thermal conductivity measurements for sponge cakes (points), plotted with predictions from the Krischer and Chaudhary-Bhandari models

8.3.3 Results for Yellow Cakes

Figure 8.6 shows the data points for yellow cakes in relation to the Maxwell-Eucken and Landauer-EMT bounds. Figure 8.7 shows an enlarged portion of the graph along with plots of Eq. (7.3) a j_1 value of 0.74 and Eq. (7.4) with a j_2 value of 0.75 (the midpoint j-values as recommended in Section 8.1.3). Figure 8.8 shows the results plotted along with the predictions of several Type A models (see Section 6.1.2), and Fig. 8.9 shows the results plotted with the predictions of the Krischer and Chaudhary-Bhandari models whose f-parameters have values recommended in the literature.

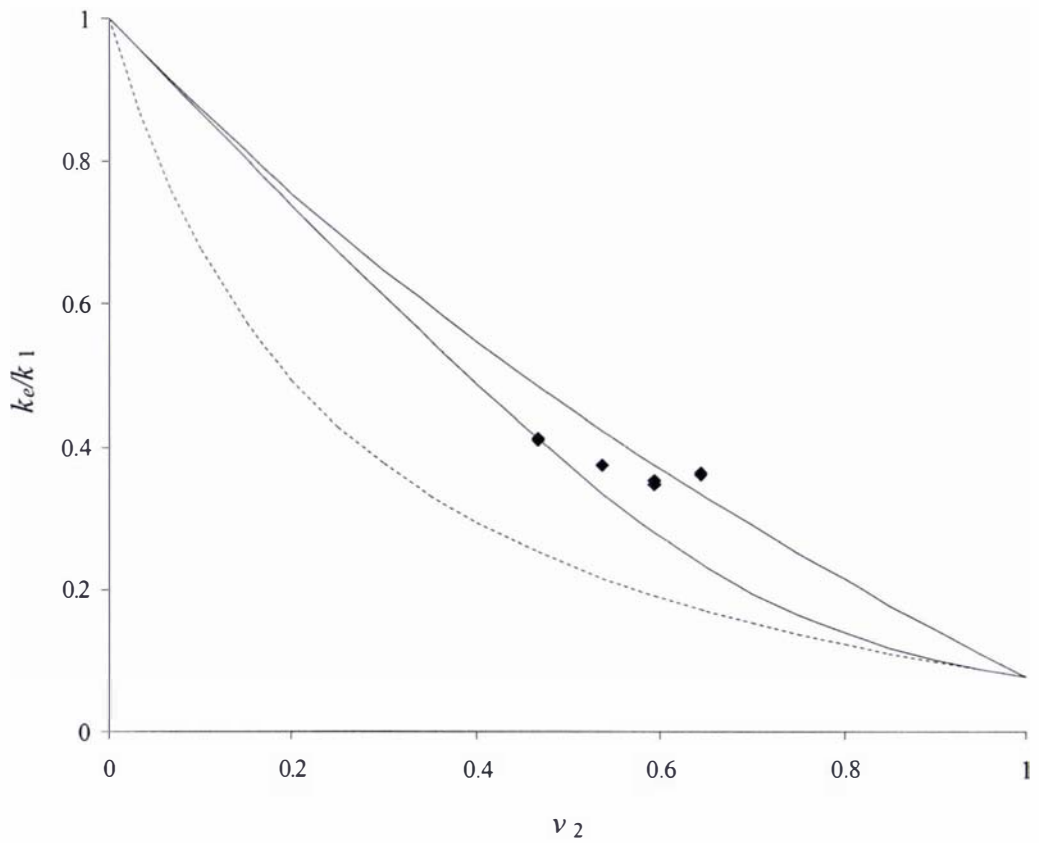

Figure 8.6: Effective thermal conductivity measurements for yellow cakes (points), plotted with the Upper Maxwell-Eucken and Landauer-EMT bounds (solid lines) and the Lower Maxwell-Eucken bound (dashed line)

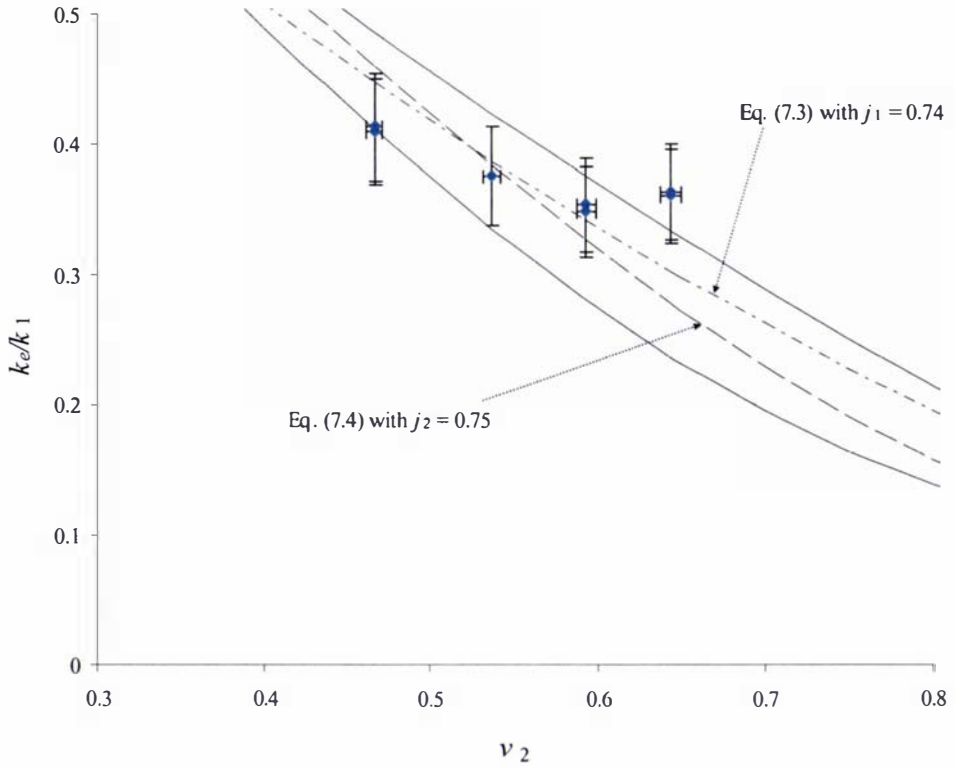

Figure 8.7: Effective thermal conductivity measurements for sponge cakes (points), plotted with the Maxwell-Eucken and Landauer-EMT bounds (solid lines), and Eqs. (7.3) and (7.4) (as indicated)

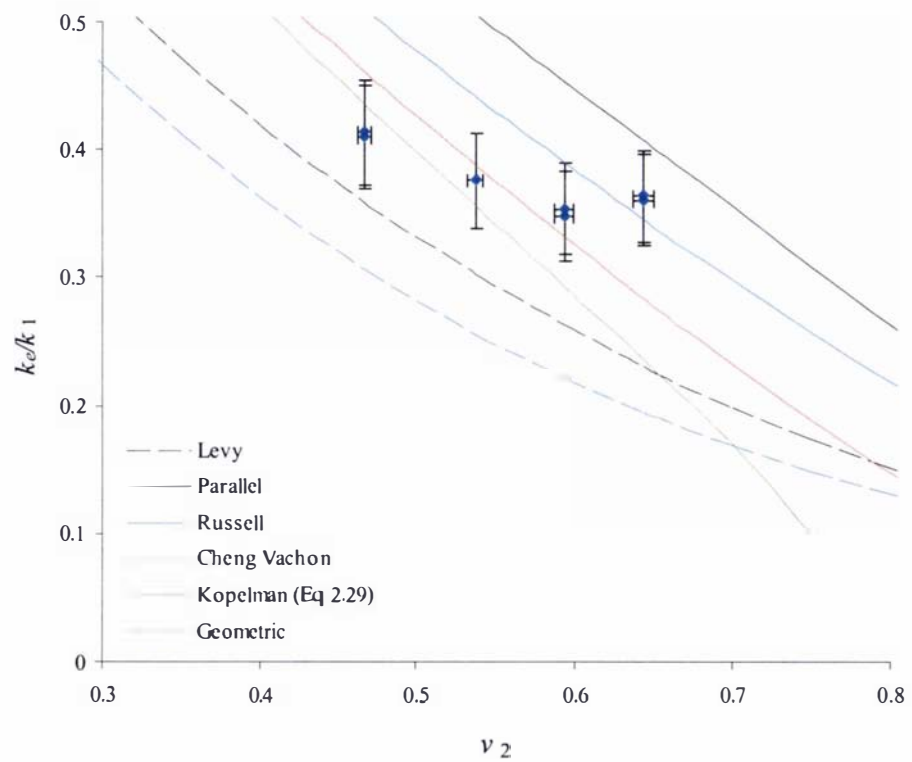

Figure 8.8: Effective thermal conductivity measurements for sponge cakes (points), plotted with predictions from selected Type A models

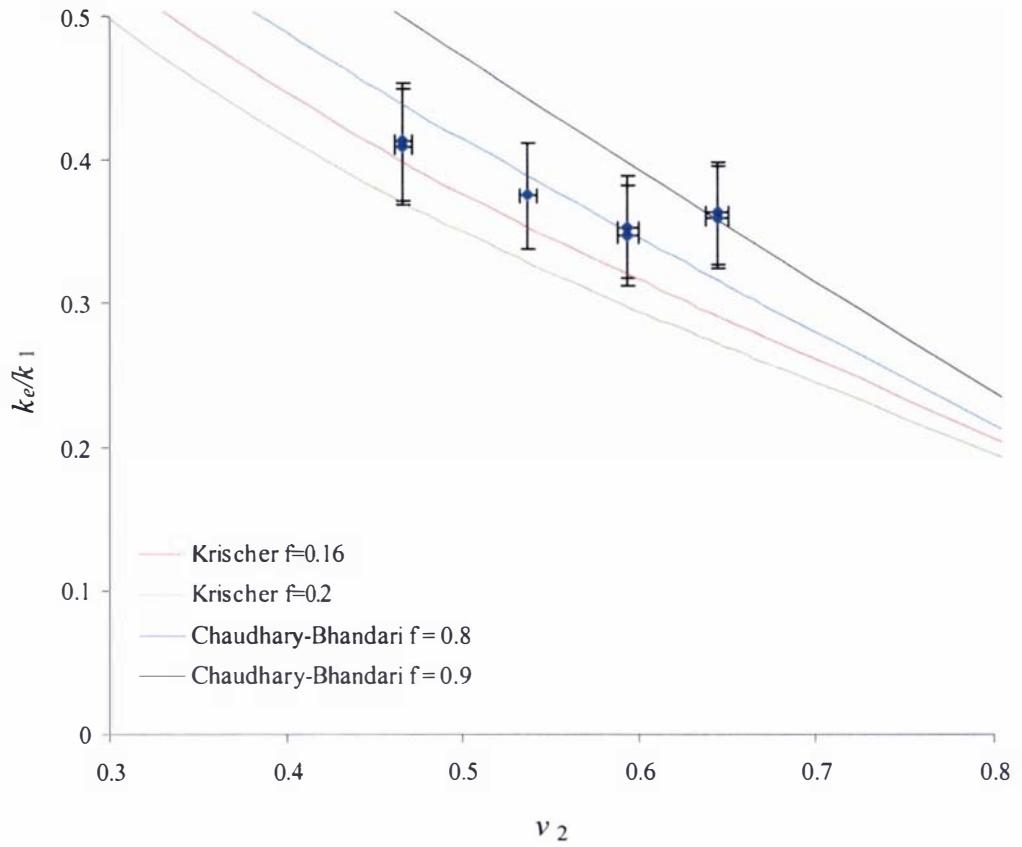

Figure 8.9: Effective thermal conductivity measurements for sponge cakes (points), plotted with predictions from the Krischer and Chaudhary-Bhandari models

8.4 Discussion

8.4.1 Validity of the Proposed Thermal Conductivity Bounds

The Maxwell-Eucken and Landauer-EMT models were plotted in Figs. 8.2, 8.3, 8.6 and 8.7 since the data from all the measurements were expected to lie on or between the plots of these equations. The majority of the data points did in fact lie between these bounds, with the exception of the lowest porosity sponge cakes, which were 7% less than the Landauer-EMT bound, and the highest porosity yellow cakes, which were 8% higher than the upper Maxwell-Eucken bound.

However, in both instances the difference could be reconciled given the estimated experimental uncertainty of 10%.

8.4.2 Accuracy of Predictions from Equations (7.3) and (7.4)

8.4.2.1 Sponge Cakes

Other than at the lowest porosity (v_2 = 0.45), the measurements of the thermal conductivity of the sponge cakes were close to the values predicted by Eq. (7.4) with j_2 = 0.71 (see Fig. 8.5). The two measurements at v_2 = 0.45 were respectively 13% and 11% lower than the prediction from Eq. (7.4), and 7% and 5% lower than the Landauer-EMT bound, but with an estimated uncertainty of approximately 10% this may be explained by experimental error, especially since the j_2 value was estimated rather than measured.

8.4.2.2 Yellow Cakes

The predictions of the thermal conductivity of the yellow cakes were not as close to the measured data as the predictions for the sponge cakes (see Fig. 8.7), and the data points did not appear to follow the basic trend of either Eq. (7.3) or Eq. (7.4) as closely as the sponge cake data although, of the two, Eq. (7.3) was better. The point at the highest porosity (v_2 = 0.64) appeared as though it might be an outlier, but a check of the calculations and procedure did not identify any evidence of a mistake, and there did not appear to be any justification for ignoring this point. The yellow cakes were better fitted by models with higher j-values than for the sponge cake data, as anticipated (see in Section 8.1.3.2).

8.4.3 Performance of other Effective Thermal Conductivity Models

8.4.3.1 Type A models

None of the Type A models provided predictions consistently within the error bars for both types of cakes. The Cheng-Vachon model performed reasonably

well for the sponge cakes, providing predictions that were close to, if not within, the error bars for all porosities, but it did not perform as well for the yellow cakes. The only other model to provide predictions within the error bars on more than one instance was Kopelman's Eq. (2.29). Ironically, the Cheng-Vachon model was the only one of these models that has not been suggested for use in food applications. Since Russell's model (which is mathematically equivalent to Kopelman's Eq. 2.28), Levy's model and the Parallel model have all provided reasonable predictions for some foods, these results highlight the inadequacy of Type A models for general purposes: they do not provide the flexibility to account for different structures.

8.4.3.2 Series/Parallel-based Type-B Models

Krischer's model with an f-value of 0.16 (as recommended by Lin *et al.*, 1997) provided acceptable predictions for all but the highest porosity yellow cake, which may have been an outlier in any case. The predictions for the sponge cakes in particular were very good. However, with an f-value of 0.2 (as recommended by Keey, 1972), the predictions were outside the error bars for the yellow cakes. The Chaudhary-Bhandari model with an f-value of 0.8 provided better predictions than Krischer's model for the yellow cakes. Clearly, both models could be made to fit the data for both types of cake by adjusting the f-values appropriately, but since there were no guidelines for relating the f-parameter to material structure, the empirical values in the literature were all that were available.

8.4.4 Effectiveness of the Prediction Method

In Section 8.1.3 the effective thermal conductivities of the sponge cakes and yellow cakes were predicted based on thermal conductivity data of the foods' chemical components, which was available in the literature, the volume fractions of the foods' components, and the j-parameter, estimated from a visual assessment of the foods' structures according to guidelines from previous chapters. No experimentation was required by this prediction method. Given that

the majority of the measured thermal conductivities agreed with the predictions within ±10%, which was the estimated uncertainty of the measurements, this general method appeared to provide predictions for specific foods with accuracy that would be sufficient for the food industry. However, the uncertainty involved in the measurements of the thermal conductivities of the cakes was relatively high and further testing of the method on more precise data would be desirable.

8.5 Conclusion

The general method for predicting the effective thermal conductivity of isotropic materials described in Section 7.6 of Chapter 7 was tested on real foods in order to meet the final objective listed in Chapter 3. The application of the procedure to sponge cakes and yellow cakes was relatively straight-forward, and did not require any information that was not available in the literature. The experimental results appeared to support the use of the prediction method, since the majority of the predictions agreed with the measured thermal conductivities within the estimated experimental uncertainty of 10%.

Chapter 9: Conclusions and Recommendations

Conclusions and Recommendations

9.1 Conclusions

The results and analysis of the physical experiments and numerical simulations, along with the model evaluation exercise, provided a basis for a proposed general procedure for the prediction of effective thermal conductivity. The procedure required only basic information related to the material which would be readily available to a food engineer. When applied to the prediction of the thermal conductivity of sponge and yellow cakes, the procedure provided predictions that, other than for a few points, agreed with experimental measurements to within ±10%, which would be of sufficient accuracy for industrial purposes. Hence the objectives of this study have largely been achieved (see Chapters 1 and 3).

However, the procedure is a lot more useful for materials with internal porosity (i.e. materials in which gas bubbles are suspended in a solid/liquid matrix) than for materials with external porosity (i.e. particulate and granular materials), and a large degree of uncertainty still remains over the prediction of effective thermal conductivities of the latter group. This was attributed mainly to the strong dependence of effective thermal conductivity on the extent or quality of thermal contact between particles, which has a high degree of variability between different types of granular material. It appears that the determination of the extent of thermal contact between particles, other than by empirical means, is an issue that requires more research.

Due to practical constraints, the study was limited to isotropic, non-frozen foods, and only heat transfer by conduction was considered. However, it is quite possible that the procedure may be developed to cater for other modes of heat transfer and for foods that fell outside the scope of this study (isotropic frozen foods in particular).

9.2 Recommendations for Future Work

1. Since only limited testing of the proposed effective thermal conductivity prediction procedure outlined in Chapter 7 was preformed, it would be valuable to perform more trials on different foods in order to evaluate the accuracy and expediency of the procedure
2. Investigate possible improvements to the determination/estimation of numerical values of the j-parameters of Eqs. (7.3) and (7.4), particularly for granular materials
3. Investigate the feasibility of incorporating radiation/convection/ evaporation effects into the model, using the approach of Sakiyama &Yano (1990)
4. Investigate the suitability of the procedure for frozen foods, and determine what modifications are required.

References

ASHRAE Handbook of Refrigeration (1998), American Society of Heating, Refrigeration and Air-conditioning Engineers, Atlanta GA

Baik, O. D., Sabiani, S. S., Marcotte, M., Castaigne, F. (1999) "Modeling the Thermal Properties of a Cup Cake During Baking", *Journal of Food Science*, Vol. 64, No. 2, pp295-299

Baltz, B. A., Ingber, M. S. (1997) "A parallel implementation of the boundary element method for heat conduction analysis in heterogeneous media", *Engineering Analysis with Boundary Elements*, Vol. 19, pp3-11

Bart, G. C. J. (1994) *Thermal Conduction in Non Homogeneous and Phase Change Media*, Thesis, Delft University of Technology (Netherlands)

Brailsford, A. D., Major, K. G. (1964) "The thermal conductivity of aggregates of several phases including porous materials", *British Journal of Applied Physics*, Vol. 15, pp313-319

Brennan, J. G., Butters, J. R., Cowell, N. D., Lilley, A. E. V. (1990) *Food Engineering Operations* 3rd Edition, Elsevier Applied Science, London

Bruggeman, D. A. G. (1935) "Berechnung verschiedener physikalischer Konstanten von heterogenen Substanzen: I. Dielektrizitätskonstanten und Leitfähigkeiten der Mischkörper aus isotropen Substanzen", *Annalen der Physik*, Vol. 24, pp636-664

Campbell, G. M., Webb, C., Pandiella, S. S., Niranjan K. (Eds.) (1999) *Bubbles in Food*, Eagan Press, St. Paul

Carslaw, H. S., Jaeger, J. C. (1959) *Conduction of Heat in Solids* 2nd Ed., Clarendon Press, Oxford

Chaudhary, D. R., Bhandari, R. C. (1968) "Heat transfer through a three-phase porous medium", *Journal of Physics D* (British Journal of Applied Physics), series 2, Vol. 1, pp815-817

Cheng, P., Chin-Tsau, H. (1998) "Heat Conduction", in: Ingham, D. B., Pop, I., (Eds.), *Transport Phenomena in Porous Media*, Pergamon Press, pp57-76

Cheng, S. C., Vachon, R. I. (1969) "Prediction of Thermal Conductivity of Two and Three Phase Solid Heterogeneous Mixtures", *International Journal of Heat and Mass Transfer*, Vol. 12, pp249-264

Chuntranuluck, S. (1995) *Prediction of Chilling Times of Foods Subject to both Convective and Evaporative Cooling at the Product Surface*, PhD Thesis, Massey University

Clarke, R. J. (1957) *Process Engineering in the Food Industries*, Heywood & Co. Ltd., London

Cleland, A. C. (1990) *Food Refrigeration Processes — Analysis, Design and Simulation, Elsevier* Applied Science, London

Cleland, A. C., Earle, R. L. (1977) "A comparison of analytical and numerical methods of predicting the freezing times of foods", *Journal of Food Science*, Vol. 42, No. 5, pp1390-1395

Cleland, A. C., Earle, R. L. (1982a) "A simple method for prediction of heating and cooling rates in solids of various shapes", *International Journal of Refrigeration*, Vol. 5, No. 2, pp98-106

Cleland, A. C., Earle, R. L. (1982b) "Freezing time prediction for foods—A simplified procedure", *International Journal of Refrigeration*, Vol. 5, No. 3, pp134-140

Crank, J. (1975) *The Mathematics of Diffusion* 2nd Edition, Oxford University Press, Oxford

Crane, R. A., Vachon, R. I. (1977) "A Prediction of the Bounds on the Effective Thermal Conductivity of Granular Materials", *International Journal of Heat and Mass Transfer*, Vol. 20, pp711-723

Davies, L. J., Fryer, P. J. (2001) "Effective Electrical Conductivity of Foods", in: J. Welti-Chanes, G. V. Barbosa-Canovas, J. M. Aguilera (Eds) *Proceedings of the Eighth International Congress on Engineering and Food*, Technomic Publishing Co., Lancaster, PA, Vol. 1, pp146-150

Davis, H. T., Valencourt, L. R., Johnson, C. E. (1975) "Transport Processes in Composite Media", *Journal of the American Ceramic Society*, Vol. 58, pp446-452

Earle, R. L. (1966) *Unit Operations in Food Processing*, Pergamon Press, London

Eucken, A. (1940) "Allgemeine Gesetzmäßigkeiten für das Wärmeleitvermögen verschiedener Stoffarten und Aggregatzustände", *Forschung Gabiete Ingenieur*, Vol. 11, No 1, pp6-20

Every, A. G., Tzou, D. P., Hasselman, D. P. H., Raj, R. (1992) "The Effect of Particle Size on the Thermal Conductivity of ZnS/Diamond Composites", *Acta Metallurgica et Materialia* Vol. 40, No. 1, pp123-129

Farouki, O. T. (1986) *Thermal Properties of Soils*, Series on Rock and Soil Mechanics Vol II, Trans Tech Publications

Fellows, P. J. (2000) *Food Processing Technology: Principles and Practice*, 2nd Edition, Woodhead Publishing Company, Cambridge

Fidelle, T. P., Kirk, R. S. (1971) "A Study of Unidirectional Versus Tridirectional Heat Flux Models and the Effect of Particle Size on Heat Conduction in Composite Solids", *AIChE Journal*, Vol. 17, No. 6, pp1427-1434

Fleming, A. K., Earle, R. L. (1967) "Cooling and freezing of lamb and mutton carcasses – 1. Cooling and Freezing rates in legs.", *Food Technology*, Vol. 21, No. 1, 79-84

Francl, J., Kingery, W. D. (1954) "Thermal Conductivity: IX, Experimental Investigation of Effect of Porosity on Thermal Conductivity", *Journal of the American Ceramic Society*, Vol. 37, No. 2, pp99-107

Fricke, H. (1924) "The Electrical Conductivity of Two-Phase Materials", *Physics Review*, Vol. 24, pp575-587

Fryer, P. J., Pyle, D. L., Rielly, C. D. (1997) *Chemical Engineering for the Food Industry*, Blackie Academic and Professional, London

Hallström, B., Skjöldebrand, C., Trägårdh, C. (1988) *Heat Transfer and Food Products*, Elsevier Applied Science, London and New York

Hamilton ,R. L., Crosser, O. K. (1962) "Thermal Conductivity of Heterogeneous Two-Component Systems", *Industrial and Engineering Chemistry Fundamentals*, Vol. 1, No. 3, pp187-191

Hammersley, J. M. (1983) "Origins of Percolation Theory", in: Deutscher, G., Zallen, R., Adler, J. (Eds.), *Percolation Structures and Processes*, Annals of the Israel Physical Society, Vol. 5

Han, L. S., Cosner, A. A. (1981) "Effective Thermal Conductivities of Fibrous Composites", *Journal of Heat Transfer*, Vol. 103, pp387-392

Hashin, Z., Shtrikman, S. (1962) "A Variational Approach to the Theory of the Effective Magnetic Permeability of Multiphase Materials", *Journal of Applied Physics*, Vol. 33, No. 10, pp3125-3131

Hicsasmaz, Z., Clayton, J. T. (1992) "Characterization of the pore structure of starch based food materials", *Food Structure*, Vol. 11, pp115-132

Hill, J. E., Leitman, J. D., Sunderland, J. E. (1967) "Thermal Conductivity of Various Meats", *Food Technology*, Vol. 21, pp1143-1148

Holman, J. P. (1992) *Heat Transfer*, McGraw-Hill Book Company, Singapore

Jefferson, T. B., Witzell, O. W., Sibbitt, W. L. (1958) "Thermal Conductivity of Graphite-Silicone Oil and Graphite-Water Suspensions", *Industrial and Engineering Chemistry*, Vol. 50, No. 10, pp1589-1592

Keey, R. B. (1972) *Drying Principles and Practice,* Pergamon Press, New York

Keey, R. B. (1992) *Drying of Loose and Particulate Materials*, Hemisphere Publishing Corporation, New York

Kirk-Othmer (1994) *Encyclopedia of Chemical Technology*, Vol. 12, John Wiley & Sons, New York

Kirkpatrick, S. (1973) "Percolation and Conduction", *Reviews of Modern Physics*, Vol 45, pp574-588

Krach, A., Advani, S. G., (1996) "Influence of Void Shape, Void Volume and Matrix Anisotropy on the Effective Thermal Conductivity of a Three-Phase Composite", *Journal of Composite Materials,* Vol. 30, No. 8, pp933-946

Krischer, O. (1963) *Die wissenschaftlichen Grundlagen der Trocknungstechnik* (The Scientific Fundamentals of Drying Technology), Springer-Verlag, Berlin, cited in English in Chapter 7 of Keey, (1992)

Kunii, D., Smith, J. M. (1960) "Heat Transfer in Porous Rocks", *AIChE Journal*, Vol. 3, No. 3, pp373-381

Landauer, R. (1952) "The Electrical Resistance of Binary Metallic Mixtures", *Journal of Applied Physics*, Vol. 23, No. 7, pp779-784

Lees, R. (1975) *Food Analysis: Analytical and Quality Control Methods for the Food Manufacturer and Buyer*, Leonard Hill Books, London

Levy, F. L. (1981) "A modified Maxwell-Eucken equation for calculating the thermal conductivity of two-component solutions or mixtures", *International Journal of Refrigeration*, Vol. 4, No. 4, pp223-225

Lewis, T. B., Nielsen, L. E. (1970) "Dynamic Mechanical Properties of Particulate filled Composites", *Journal of Applied Polymer Science*, Vol. 14, pp1449-1471

Lin, Z. (1994) *Prediction of Chilling Times*, PhD thesis, Massey University

Lin, Z., Cleland, A. C., Serrallach, G. F., Cleland, D. J. (1996a) "A simple method for prediction of chilling times for objects of two-dimensional irregular shape", *International Journal of Refrigeration*, Vol. 19, No. 2, pp95-106

Lin, Z., Cleland, A. C., Serrallach, G. F., Cleland, D. J. (1996b) "A simple method for prediction of chilling times: Extension to three-dimensional irregular shape", *International Journal of Refrigeration*, Vol. 19, No. 2, pp107-114

Lin, Z., Cleland, A. C., Serrallach, G. F., Cleland, D. J. (1997) "Models of the thermal conductivity of a food (cheese) with voids during chilling", in: *Proceedings of the Seventh International Congress on Engineering and Food*, Academic Press, UK

Loeb, A. J., (1954) "Thermal Conductivity: VIII, A Theory of Thermal Conductivity of Porous Materials", *Journal of the American Ceramic Society*, Vol. 37, No. 2, pp96-99

Lostie, M., Peczalski, R., Andrieu, J., Laurent, M. (2002) "Study of sponge cake batter baking process. Part I: Experimental data", *Journal of Food Engineering*, Vol. 51, No. 2, pp131-137

Lozano, J. E., Urbicain, M. J., Rotstein, E. (1979) "Thermal Conductivity of Apples as a Function of Moisture Content", *Journal of Food Science*, Vol. 44, No. 1 pp198-199

Lu, K-T., Keu, H-S. (1993) "The Effective Thermal Conductivity of Porous Materials with Spherical Inclusions in a Tetragonal or Simple Cubic Array", *International Communications in Heat and Mass Transfer*, Vol. 20, pp489-500

Mattea, M., Urbicain, M. J., Rotstein, E. (1986) "Prediction of Thermal Conductivity of Vegetable Foods by the Effective Medium Theory", *Journal of Food Science*, Vol. 51, No. 1, pp113-115, 134

Mattea, M., Urbicain, M. J., Rotstein, E. (1989) "Effective thermal conductivity of cellular tissues during drying: prediction by a computer assisted model", *Journal of Food Science*, Vol. 54, No. 1, pp194-197, 204

Maxwell, J. C. (1954) *A Treatise on Electricity and Magnetism* 3rd Ed., Dover Publications Inc., New York

Magee, T. R. A., McMinn, W. A. M (2001) "Heat and Mass Transfer during Cake Baking", in: J. Welti-Chanes, G. V. Barbosa-Canovas, J. M. Aguilera (Eds) *Proceedings of the Eighth International Congress on Engineering and Food*, Technomic Publishing Co., Lancaster, PA, Vol. 1, pp337-341

McDonald, K., Sun, D-W. (2001) "Pore Size Distribution and Structure of a Cooked Beef Product as Affected by Vacuum Cooling", *Journal of Food Process Engineering*, Vol. 24, pp381-403

Miles, C. A., van Beek, G., Veerkamp, C. H. (1983) "Calculation of thermophysical properties of foods", in: Jowitt, R., Escher, F., Hallström, B., Meffert, H. F. T., Spiess, W. E. L., Vos, G. (Eds) *Physical Properties of Foods*, Applied Science Publishers, London

Mohsenin, N. N. (1980) *Thermal Properties of Foods and Agricultural Materials*, Gordon and Breach Science Publishers, New York

Motz, H. (1946) *Quarterly Journal of Applied Mathematics*, Vol. 4, p371 (cited in Crank, 1973)

Murakami, E. G., Okos, M. R. (1989) "Measurement and prediction of thermal properties of foods" in: R. P. Singh, A. G. Medina (Eds.), *Food Properties and Computer Aided Engineering of food Processing Systems* (pp. 3-48). Kluwer Academic Publishers, New York

Murakami, E. G., Okos, M. R. *Predicting the Thermal Conductivity of Dry Porous Foods* ASAE Paper No. 86-6538.

Nesvadba, P. (1982) "Methods for the measurement of thermal conductivity and diffusivity of foodstuffs", *Journal of Food Engineering*, Vol. 1, pp93-113

Niranjan, K. (1999) "An introduction to bubble mechanics in foods", in: Campbell, G. M., Webb, C., Pandiella, S. S., Niranjan K. (Eds.) *Bubbles in Food*, Eagan Press, St. Paul, USA, pp1-9

North, M. F. (2000) *Prediction of Chilling Rates For food Product Packages*, PhD Thesis, Massey University

Nozad, I., Carbonell, R. G., Whitaker. S. (1985) "Heat Conduction in Multiphase Systems — I: Theory and Experiment for Two-Phase Systems", *Chemical Engineering Science*, Vol. 40, No. 5, pp843-855

Osborne, D. R., Voogt, P. (1978) *The Analysis of Nutrients in Food*, Academic Press, London

PDEase2D™(1996) Reference Manual Macsyma Inc, Arlington USA

Pham, Q. T., Willix, J. (1989) "Thermal Conductivity of Fresh Lamb Meat, Offals and Fat in the Range --40 to +30°C: Measurements and Correlations", *Journal of Food Science*, Vol. 54, No. 3, pp508-515

Phelan, P. E., Niemann, R. C. (1998) "Effective Thermal Conductivity of a Thin, Randomly Oriented Composite Material", *Journal of Heat Transfer*, Vol. 120, pp971-976

Pongsawatmanit, R., Miyawaki, O., Yano, T. (1993) "Measurement of the Thermal Conductivity of Frozen and Unfrozen Food Materials by a Steady State Method with a Coaxial Dual-cylinder Apparatus", *Bioscience-Biotechnology-Biochemistry*, Vol. 57, No. 7, pp1072-1076

Progelhof, R. C., Throne, J. L., Reutsch, R. R. (1976) "Methods for Predicting the Thermal Conductivity of Composite Systems: A Review", *Polymer Engineering and Science*, Vol. 16, No. 9, pp615-625

Pugh, E. M., Pugh, E. W. (1970) *Principles of Electricity and Magnetism, 2nd Ed.*, Addison-Wesley, Reading MA

Pyler., E. J. (1973) *Baking Science and Technology*, Siebel Publishing Co., Chicago

Rahman, M. S., Potluri, P.L. (1990) "Thermal conductivities of fresh and dried squid meat by line source thermal conductivity probe", *Journal of Food Science*, Vol. 56, No. 2, pp582-583

Rahman, M. S., Potluri, P. L., Varamit, A. (1991) "Thermal Conductivities of Fresh and Dried Seafood Powders", *Transactions of the ASAE*, Vol. 34, No. 1, p217

Rahman, M. S. (1992) "Thermal Conductivity of four Food Materials as a Single Function of Porosity and Water Content", *Journal of Food Engineering*, Vol. 15, pp261-268

Rahman, M. S. (1995) *Food Properties Handbook*, CRC Press, Boca Raton FL

Rahman, M. S., Chen, X. D., Perera, C. O. (1997) "An Improved Thermal Conductivity Prediction Model for Fruits and Vegetables as a function of Temperature, Water Content and Porosity", *Journal of Food Engineering*, Vol. 31, pp163-170

Rahman, M. S. (2001a) "Mechanism of Pore Formation in Foods during Drying: Present Status", in: J. Welti-Chanes, G. V. Barbosa-Canovas, J. M. Aguilera (Eds) *Proceedings of the Eighth International Congress on Engineering and Food*, Technomic Publishing Co., Lancaster, PA, Vol. 2, pp1111-1116

Rahman, M. S. (2001b) "Thermophysical Properties of Foods", in: Sun, D.-W. (Ed.) *Advances in Food Refrigeration*, Leatherhead Publishing, Surrey, England

Rayleigh, Lord (1964) "On the Influence of Obstacles Arranged in Rectangular Order Upon the Properties of a Medium", *Scientific Papers by Lord Rayleigh (John William Strutt)*, Dover Publications, New York, Vol. 4, pp19-38

Renaud, T. Briery, P., Andrieu, J., Laurent, M. (1992) "Thermal Properties of Model Foods in the Frozen State", *Journal of Food Engineering*, Vol. 15, No. 2, pp83-97

Russell, H. W. (1935) "Principles of Heat Flow in Porous Insulation", *Journal of the American Ceramic Society*, Vol. 18, pp1-5

Sakiyama, T., Masanori, A., Miyawaki, O., Yano, T. (1999) "Effective thermal diffusivity of food gels impregnated with air bubbles", *Journal of Food Engineerings*, Vol. 39, No. 3, pp323-328

Sakiyama, T., Yano, T. (1990) "Effects of Air and Water Contents on the Effective Thermal Conductivity of Air-impregnated Gels", *Agricultural and Biological Chemistry*, Vol. 54, No 6, 1375-1380

Sakiyama, T., Yano, T. (1994) Finite Element Analysis on the Effective Thermal Conductivity of Dispersed Systems, *Proceedings of the 6th International congress on Engineering and Food*, Vol. 1, pp146-148

Schwartzberg, H. G. (1976) "Effective Heat Capacities for the Freezing and Thawing of Food", *Journal of Food Science*, Vol. 41, pp152-156

Slavin, A. J., Londry, F. A., Harrison, J. (2000) "A new model for the effective thermal conductivity of packed beds of solid spheroids: alumin in helium between 100 and 500°C", *International Journal of Heat and Mass Transfer*, Vol. 43, pp2059-2073

Smith, A. K, Goff, H. D., Kukuda, Y. (1999) "Quantitative Stereology Used to Measure the Effect of Heat Treatment and Stabilizer on Whipped Cream Structure", in: G. M. Campbell, C. Webb, S. S. Pandiella, K. Niranjan (Eds.), *Bubbles in Food*, Eagan Press, St. Paul, USA, pp197-205

Smith, G. D. (1986) *Numerical Solution of Partial Differential Equations: Finite Difference Methods,* 3rd Edition, Oxford University Press, Oxford

Spiess, W. E. L., Schubert, H. (1990) *Engineering and Food Vol. 1*, Elsevier Applied Science, pp408-423

Sugawara, A., Yoshizawa, Y. (1961) "An Experimental Investigation on the Thermal Conductivity of Consolidated Porous Materials and its Application to Porous Rock", *Australian Journal of Physics*, Vol. 14, No. 4, p469

Tanaka, M., Chisaka, F. (1991) "Effective Thermal Conductivities of Discontinuous and Continuous Solid Systems", *Heat Transfer*, Vol. 20, No. 5, pp418-428

Thorne, S. (1992) *Mathematical Modelling of Food Processing Operations*, Elsevier Applied Science, London

Tsao, G. T-N. (1961) "Thermal Conductivity of Two Phase Materials", *Industrial and Engineering Chemistry*, Vol. 53, No. 5, pp395-397

Unklesbay, N., Unklesbay, K., Nahaisi, M., Krause, G. (1981) "Thermal Conductivity of White Bread During Convective Heat Processing", *Journal of Food Science*, Vol. 47, pp249-253, 259

Vagenas, G. K., Marinos-Kouris, D., Saravacos, G. D. (1990) "Thermal properties of raisins", *Journal of Food Engineering*, Vol. 11, pp147-

Valentas, K. J., Rotstein, E., Singh, R. P. (1997) *Handbook of Food Engineering Practice*, CRC Press, Boca Raton FL

Vélez-Ruiz, J. F., Sosa-Morales, M. E. (2001) "Study on the Frying Process of Donuts", in: Welti-Chanes, J., Barbosa-Canovas, G. V., Aguilera, J. M. (Eds) *Proceedings of the Eighth International Congress on Engineering and Food*, Technomic Publishing Co., Lancaster, PA, Vol. 1, pp353-357

Williams, D. J. (1971) *Polymer Science and Engineering*, Prentice Hall, Inglewood, NJ

Williams, S. (Ed.) (1984) *Methods of Analysis – Association of Official Agricultural Chemists – 14th Edition*, AOAC Inc., Arlington, Virginia

Woodside, W., Messmer, J. H. (1961a) "Thermal Conductivity of Porous Media I: Unconsolidated Sands", *Journal of Applied Physics*, Vol. 32, No. 9, p1688-1699

Woodside, W., Messmer, J. H. (1961b) "Thermal Conductivity of Porous Media II: Consolidated Rocks", *Journal of Applied Physics*, Vol. 32, No. 9, p1699-1706

Yagi, S., Kunii, D. (1957) "Studies on Effective Thermal Conductivities in Packed Beds", *AIChE Journal*, Vol. 3, No. 3, pp373-381

Zallen, R. (1983) "Introduction to Percolation: A Model for All Seasons", in: Deutscher, G., Zallen, R., Adler, J. (Eds.), *Percolation Structures and Processes*, Annals of the Israel Physical Society, Vol. 5

Zanoni, B., C. Peri and R. Gianotti (1995) "Determination of the Thermal Diffusivity of Bread as a Function of Porosity", *Journal of Food Engineering*, Vol. 26, pp497-510

Zienkiewicz, O. C. (1983) *The Finite Element Method*, 3rd Ed., McGraw-Hill Book Company, Maidenhead

Nomenclature

		Units (if applicable)
A	cross sectional area of heat flow (Eqs. 2.1, 2.2)	(m^2)
A	surface area (Eq.4.10)	(m^2)
AD_M	mean absolute discrepancy (Eq. 6.1)	
b	temperature gradient (Eqs. 2.14, 2.15, Appendix B)	($K\ m^{-1}$)
B	regression constant (Eq. 2.32)	
B	ordinate intercept (Eq. 4.4)	
c	specific heat capacity	($J\ kg^{-1}\ K^{-1}$)
C	volumetric heat capacity	($J\ m^{-3}\ K$)
f	distribution factor (Krischer and Chaudhary-Bhandari models)	
h	heat transfer coefficient	($W\ m^{-2}\ K^{-1}$)
F	function from Levy's model (Eq. 2.21)	
j_1	structure-related parameter (Eq. 7.3)	
j_2	structure-related parameter (Eq. 7.4)	
k	thermal conductivity	($W\ m^{-1}\ K^{-1}$)
l	length	(m)
m	mass	(kg)
n	number of small spheres (Eq. 2.16, Appendix B)	
n	parameter in Eq. (2.22)	
n	number of data points (Eq. 6.1)	
n'	parameter in Eqs. (7.1), (7.2)	
q	heat flow	(W)
Q	heat flow	(W)
r	coordinate axis label/radial distance	(m)
R	radius	(m)
t	time	(s)
T	temperature	(°C)
v	volume fraction of component	

V	volume	(m^3)
x, y, z	coordinate axis labels/rectangular dimensions	(m)
X	width of finite element grid area (Chapter 5)	(m)
Y	fractional unaccomplished temperature change	
Y	total length of finite element grid area (Chapter 5)	(m)
Z	coordination number (Eq. 2.27)	

Greek

β	root of transcendental equation (Eq. 4.2)	
Γ	model parameter (Eq. 2.32)	
φ	proportion of EPS to guar-gel in samples (Eqs. 4.17 to 4.20)	
θ	coordinate-axis label/angular distance	(rad)
ρ	density	($kg\ m^{-3}$)
σ	slope of linear portion of cooling curve	(s^{-1})
Ψ	see Eq. 2.11	

Dimensionless Groups

Bi	Biot number
Fo	Fourier Number

Subscripts

0	initial (temperature)
1, 2	specific component labels
∞	bulk/infinite (temperature)
a	finite element grid occupied by theoretical material (Fig. 5.1, Chapter 5)

b	finite element grid occupied by end zones (Fig. 5.1, Chapter 5)
e	effective property
e	property of test sample (Chapter 4)
c	conduction heat transfer (Eqs. 2.1, 2.2)
c	control sample (Chapter 4)
i	generalised component label
m	property of matrix (Eqs. 2.14, 2.15, Appendix B)
s	property of sphere (Eqs. 2.14, 2.15, Appendix B)
y	end zones of finite element grids (Chapter 5)

List of Tables

Page #

List of Figures

Page #

Appendix A: A Selection of Theoretically Based Effective Thermal Conductivity Models, Listed Alphabetically

Unless otherwise stated k_1 refers to the continuous phase, k_2 refers to the dispersed (discontinuous) phase and v_2 to the volume fraction of the dispersed phase.

Behren's Models:

Parallel with fibres:

$$\frac{k_e}{k_1} = 1 + (k_2/k_1 - 1)v_2 - (k_2/k_1 - 1)^2 \frac{\Psi_{25} - \frac{\Psi_{26}^2}{2}}{1 - \Psi_{26}^2} \left[\frac{(1 - \Psi_{26}^2)v_2 - \left(\Psi_{25} - \frac{\Psi_{26}^2}{2} \right)}{(k_2/k_1 - 1)\frac{\Psi_{26}^2}{2} - (k_2/k_1 - 1)(v_2 - \Psi_{25})} \right]$$

Perpendicular to fibres:

$$\frac{k_e}{k_1} = 1 + \frac{(k_2/k_1 - 1)v_2\Psi_{26}^2}{(k_2/k_1 - 1)\frac{\Psi_{26}^2}{2} - (k_2/k_1 - 1)(v_2 - \Psi_{25})}$$

where:

$$\Psi_{25} = \sqrt{\frac{\Psi_{26}^4}{4} + (1 - \Psi_{26}^2)v_2^2}$$

and:

Ψ_{26} = (Major axis of ellipsoid)/(Focal distance)

For cylindrical rods:

$$k_e = k_1 \frac{[(k_2/k_1 + 1) + v_2(k_2/k_1 - 1)]}{[(k_2/k_1 + 1) - v_2(k_2/k_1 - 1)]}$$

Application: fibrous composites

Reference: Han & Cosner (1981), Progelhof *et al.* (1976)

Related Model(s): Maxwell-Eucken model

Böttcher Model: see Landauer's Effective Medium Theory

Bruggeman Model:

$$(1-v_2)=\frac{k_2-k_e}{k_2-k_1}\left(\frac{k_1}{k_e}\right)^{\frac{1}{3}}$$

Application: spheres dispersed in a continuous medium

Reference: Bruggeman (1935)

Budiansky Model:

$$\sum\frac{v_i}{\frac{2}{3}+\frac{1}{3}\frac{k_i}{k_e}}=1$$

Application: isotropic composite materials

Reference: Progelhof *et al.* (1976)

Chaudary-Bhandari Model:

$$k_e=[(1-v_2)k_1+v_2k_2]^{f_{CB}}\left(\frac{1-v_2}{k_1}+\frac{v_2}{k_2}\right)^{(1-f_{CB})}$$

f_{CB} is an empirical weighting parameter

Application: calcerous sandstone

Reference: Chaudhary & Bhandari (1968)

Related Model(s): Series, Parallel and Geometric models

Cheng-Vachon Model:

$$k_e = \left[\frac{2\tan^{-1}\left(\frac{\varpi_1}{2}\sqrt{\frac{\varpi_2(k_1-k_2)}{k_1+\varpi_1(k_2-k_1)}} \right)}{\sqrt{\varpi_1(k_2-k_1)\left[k_1+\varpi_1(k_2-k_1)\right]}} + \frac{1-\varpi_1}{k_1} \right]^{-1}$$

where:

$$\varpi_1 = \sqrt{3v_2/2} \qquad \text{and} \qquad \varpi_2 = -4\sqrt{2/(3v_2)}$$

Application: Materials for which the conductivity of the dispersed phase is much higher than that of the continuous phase

Reference: Cheng & Vachon (1969)

Related Model(s): Tsao's model

Chisaka and Tanaka Model:

For a continuous solid phase:

$$\frac{k_e}{k_1} = \frac{2(1-v_2)}{2+v_2} + \left(1-\frac{2(1-v_2)}{2+v_2}\right)\frac{\log\left[1+\frac{2(1-v_2)}{3}(k_2/k_1-1)\right]}{\frac{2(1-v_2)}{3}(1-k_1/k_2)}$$

For a discontinuous solid phase:

$$\frac{k_e}{k_2} = \frac{2v_2}{3-v_2} + \left(1-\frac{2v_2}{3-v_2}\right)\frac{\log\left[1+\frac{2v_2}{3}(k_1/k_2-1)\right]}{\frac{2v_2}{3}(1-k_2/k_1)}$$

Applications: packed beds, stacked wire nets, stacked cloth

Reference: Tanaka & Chisaka (1991)

Clayton's Model:

$$(1-v_2)=\left[\frac{k_2-k_e}{k_2-k_1}\right]\left[\frac{k_1}{k_e}\right]^{1/(f_C+1)}$$

where f_C is an adjustable parameter

Application: inorganic composites
Reference: Krach & Advani (1996)
Related Model(s): Bruggeman's model

de Vries' Model:

$$k_e=\frac{v_{air}k_{air}+(1-v_{air})\varpi_3 k_{solid}}{v_{air}+(1-v_{air})\varpi_3}$$

where:

$$\varpi_3=\frac{1}{3}\sum_{i=3}^{3}\left[1+(k_{solid}/k_{air}-1)g_i\right]^{-1}$$

and:

$$\sum_{i=1}^{3}g_i=1$$

The g_i are shape factors. For spherical particles $g_1 = g_2 = g_3$ and the equation reduces to the Maxwell-Eucken equation. de Vries recommended values of $g_1 = g_2 = 1/8$ and $g_3 = 3/4$ for ellipsoid particles.

Applications: unconsolidated soils
Reference: Woodside & Messmer (1961)
Related Model: Maxwell-Eucken model

Fricke's Model:

$$\frac{(k_e/k_1-1)}{(k_e/k_1+f_F)}=v_2\frac{(k_2/k_1-1)}{(k_2/k_1+f_F)}$$

where f_F is a shape factor

Application: ellipsoids within a continuous medium (red blood cells)

Reference: Fricke (1924)

Related Model(s): Maxwell's model

Effective Medium Theory:

1) *Landauer's EMT*:

$$\sum_i v_i\frac{k_i-k_e}{k_i+2k_e}=0$$

Explicit 2-component form:

$$k_e=¼\left((3v_2-1)k_2+[3(1-v_2)-1]k_1+\sqrt{[(3v_2-1)k_2+(3\{1-v_2\}-1)k_1]^2+8k_1k_2}\right)$$

2) *Kirkpatrick's EMT*:

$$\sum_i v_i\frac{k_i-k_e}{k_i+(Z/2-1)k_e}=0$$

Explicit 2-component form:

$$k_e=\Psi+\sqrt{\Psi^2+\frac{2k_1}{k_2(Z-2)}}$$

where:

$$\Psi=\frac{(Zv_2/2)-1+(k_1/k_2)[Z/2(1-v_2)-1]}{Z-2}$$

The Z factor was related by Kirkpatrick to the number of dimensions of the system, Z = 4 for square systems, $Z = 6$ for cubic systems. Landauer's equation may be obtained when $Z = 6$.

Application: general (assumes completely random distribution of components)
References: Landauer (1952), Kirkpatrick (1973), Davis *et al.* (1975), Mattea *et al.* (1986)

Fluid-Phase Continuous Model: see Maxwell-Eucken model (Brailsford & Major, 1963)

Francl's Model:

$$k_e = k_1(1 - v_2)$$

Application: porous inorganic materials
Reference: Francl & Kingery (1954)

Geometric Model:

$$k_e = k_1^{(1-v_2)} k_2^{v_2}$$

Application: general
Reference: Woodside & Messmer (1961)

Hamilton's Model: see Maxwell-Hamilton model

Halpin-Tsai Model:

$$k_e = \frac{1+\varpi_4 v_2\left(\dfrac{k_2-k_1}{k_2+\varpi_4 k_1}\right)}{1-v_2\left(\dfrac{k_2-k_1}{k_2+\varpi_4 k_1}\right)}$$

For spheres and cubes $\varpi_4 = 1.0$,

For plates of width x_1 and length x_2: $\varpi_4 = \sqrt{3}\log(x_1/x_2)$

Application: general

Reference: Progelhof *et al.* (1976)

Han and Cosner's Model:

$$k_e = k_1\left[(k_2/k_1)v_2/2 + (1-v_2/2)\right]$$

for $k_2/k_1>20$

Application: fibrous composites

Reference: Han & Cosner (1981)

Hashin-Shtrikman Model:

$$k_e = k_1 + \frac{v_2}{\dfrac{1}{k_2-k_1} + \dfrac{(1-v_2)}{3k_1}}$$

$$k_e = k_2 + \frac{(1-v_2)}{\dfrac{1}{k_1-k_2} + \dfrac{v_2}{3k_2}}$$

The Hashim-Shtrikman equations give identical results to the Maxwell-Eucken equations.

Application: determining effective conductivity bounds for isotropic materials
Reference: Hashin & Shtrikman (1962)

Herminge's Model:

$$k_e = \frac{1}{\left[\frac{\varpi_5}{(1-v_2)k_1 + v_2 k_2} + \varpi_6\left(\frac{1-v_2}{k_1} + \frac{v_2}{k_2}\right)\right]}$$

ϖ_5 and ϖ_6 are model parameters dependent on the geometry of the material

Application: moist, porous materials
Reference: Rahman (1995)
Related Model(s): Series and Parallel models

Hill, Leitman and Sunderland Model:

$$k_e = k_2(2\Phi - \Phi^2) + k_1(1 - 4\Phi + 3\Phi^2) + \frac{8k_1k_2(\Phi - \Phi^2)}{k_1\Phi + k_2(4 - \Phi)}$$

where: $\Phi = 2 - \sqrt{4 - 2v_2}$

Application: meat
Reference: Hill *et al.* (1967)

Jefferson's Model:

$$\frac{k_e}{k_1} = \left[1 - \frac{\pi}{4(1+2\varpi_7)^2}\right] + \frac{\pi}{4(1+2\varpi_8)^2}\left[\frac{(1/2+\varpi_7)\varpi_8 k_1}{k_1/2+\varpi_7\varpi_8}\right]$$

where:

$$\varpi_7 = \frac{\left(\frac{\pi}{6v_2}\right)^{1/3} - 1}{2}$$

and:

$$\varpi_8 = k_1 k_2\left[\frac{2k_2}{(k_2-k_1)^2}\ln(k_2/k_1) - \frac{2}{k_2-k_1}\right]$$

Applications: liquid suspensions

Reference: Jefferson *et al.* (1958)

Keey's Model: see Krischer's Model

Kirkpatrick's Model: see Effective Medium Theory

Kopelman's Models:

Isotropic (mathematically equivalent to Russell's model):

$$k_e = k_1\left[\frac{1-v_2^{2/3}(1-k_2/k_1)}{1-v_2^{2/3}(1-k_2/k_1)(1-v_2^{1/3})}\right]$$

Isotropic with k_1 significantly greater than k_2: (i.e. $k_2/k_1 \rightarrow 0$):

$$k_e = k_1\left[\frac{1-v_2^{2/3}}{1-v_2^{2/3}(1-v_2^{1/3})}\right]$$

Anisotropic parallel to fibres:

$$k_e = k_1\left[1 - v_2\left(1 - \frac{k_2}{k_1}\right)\right]$$

Anisotropic in series with fibres:

$$k_e = k_1\left[\frac{1 - \left(\frac{v_2^{1/2}}{1 - k_2/k_1}\right)}{1 - \left(\frac{v_2^{1/2}}{1 - k_2/k_1}\right)(1 - v_2^{1/2})}\right]$$

Application: foods

Reference: ASHRAE Handbook of Refrigeration (1998)

Related Model: isotropic model is mathematically equivalent to Russell's model

Krischer's Model:

$$k_e = \frac{1}{\left[\frac{1 - f_K}{(1 - v_2)k_1 + v_2 k_2} + f_K\left(\frac{1 - v_2}{k_1} + \frac{v_2}{k_2}\right)\right]}$$

f_K is the proportion of material in series with the heat flow

Application: dry, porous materials

Reference: Keey (1972) (in English), Krischer (1963) (in German)

Related Model(s): Series and Parallel models

Kunii and Smith:

$$\frac{k_e}{k_1} = v_2 + \frac{1 - v_2}{\varpi_9 + \frac{2k_1}{3k_2}}$$

ϖ_9 is related to the packing factor of the granular material

Application: stagnant thermal conductivity of a packed sphere bed

Reference: Kunii & Smith (1960)

Related Model(s): Series and Parallel Models

Landauer's Model: see Effective Medium Theory

Levy's model:

Levy's model is based on Maxwell's with v_2 replaced by F, where F is given by:

$$F = \frac{2/\Lambda - 1 + 2v - \sqrt{(2/\Lambda - 1 + 2v)^2 - 8v/\Lambda}}{2}$$

and:

$$\Lambda = \frac{(k_1 - k_2)^2}{(k_1 + k_2)^2 + k_1 k_2 / 2}$$

Application: foods

Reference: Levy (1981)

Related Model(s): Maxwell-Eucken model

Lewis-Nielsen Model:

$$k_e = k_1 \frac{1 + \varpi_{10}\varpi_{11}v_2}{1 - \varpi_{11}v_2\xi}$$

$$\varpi_{11} = \frac{k_2 - k_1}{k_2 + \varpi_{10}k_1}$$

ϖ_{10} depends on particle shape and ξ depends on distribution.

Application: particulate-filled polymers

Reference: Lewis & Nielsen (1970)

Loeb's Model:

$$\frac{k_e}{k_{solid}} = 1 - v_{cross} \frac{1 - \dfrac{4\varpi_{12}\varepsilon\sigma\Delta\overline{T}^3}{k_{solid}}}{1 + \dfrac{4\varpi_{12}\varepsilon\sigma\Delta\overline{T}^3}{k_{solid}} \left(\dfrac{1 - v_{long}}{v_{long}} \right)}$$

v_{cross} and v_{long} or the cross-sectional and longitudinal porosities respectively, ε is the emissivity of the porous phase, σ is the Stefan-Boltzmann constant, ϖ_{12} is a shape factor

Application: porous ceramics at elevated temperatures

Reference: Loeb (1954)

Maxwell's Model: see Maxwell-Eucken model

Maxwell-Eucken Model:

Component 1 as continuous phase:

$$k_e = k_1 \frac{2k_1 + k_2 - 2(k_1 - k_2)v_2}{2k_1 + k_2 + (k_1 - k_2)v_2}$$

Component 2 as continuous phase:

$$k_e = k_2 \frac{2k_2 + k_1 + 2(k_1 - k_2)(1 - v_2)}{2k_2 + k_1 - (k_1 - k_2)(1 - v_2)}$$

Application: general

References: Maxwell (1954), Eucken (1940)

Maxwell-Hamilton Model:

2-Component, component 1 continuous

$$k_e = k_1 \frac{(n-1)k_1 + k_2 - (n-1)(k_1 - k_2)v_2}{(n-1)k_1 + k_2 + (k_1 - k_2)v_2}$$

Multi-component, component 1 continuous:

$$k_e = k_1 \left[\frac{1 - \sum_{i=2}^{m} \frac{v_i (n_i - 1)(k_1 - k_i)}{k_i + (n_i - 1)k_i}}{1 + \sum_{i=2}^{m} \frac{v_i (k_1 - k_i)}{k_i + (n_i - 1)k_i}} \right]$$

Application: general

Reference: Hamilton & Crosser (1962), Cheng & Vachon (1969)

Related Model(s): Maxwell-Eucken model

Murakami-Okos Models:

Porous foods, use Krischer's model substituting f_K for f_{MO}:

$$f_{MO} = \sum_{j=0}^{3} \left[\left(\sum_{l=0}^{3} B_{jl} \Gamma_j^l \right) (v_2 - 0.4)^j \right]$$

Non-porous foods

$$k_e = \frac{1}{\frac{1 - v_{water}}{\sum v_i k_i / \sum v_i} + \frac{v_{water}}{k_{water}}}$$

Application: foods

Reference: Murakami and Okos (1989)

Related Model(s): Krischer's model, Series and Parallel models

Parallel Model:

$$k_e = (1 - v_2)k_1 + v_2 k_2$$

Application: general

Related Model(s): Series model

Paterson and Hermans Model:

$$k_e = k_1\left[1 + 3\varpi_{13}v_2 + 3\varpi_{13}^2\left(1 + \frac{\varpi_{13}}{4} + \frac{\varpi_{13}^2}{256} + \ldots\ldots\right)v_2^2 \ldots\ldots\right]$$

where:

$$\varpi_{13} = \frac{k_2 - k_1}{2k_1 + k_2}$$

Application: general

Reference: Progelhof *et al.* (1976)

Perpendicular Model: see Series model

Progelhof and Throne Model:

$$k_e = k_2\left[1 + \frac{k_1}{k_2}(1 - v_2)^{\varpi_{14}}\right]$$

where ϖ_{14} is and empirical parameter

Application: foamed plastics

Reference: Progelhof *et al.* (1976)

Rayleigh's Model:

$$\frac{k_e}{k_1} = 1 - \frac{3v_2}{\frac{2+k_2/k_1}{1-k_2/k_1} + v_2 - \left(\frac{1-k_2/k_1}{4/3+k_2/k_1}\right)\Psi_{25}v^{10/3} + ...}$$

neglecting higher terms:

$$\frac{k_e}{k_1} = \frac{\frac{2+k_2/k_1}{1-k_2/k_1} - 2v_2}{\frac{2+k_2/k_1}{1-k_2/k_1} + v_2}$$

Application: spheres arranged in a cubic array within a continuous medium

Reference: Lu & Kou (1993)

Related Models: The abbreviated form of Rayleigh's form is equivalent to the Maxwell-Eucken model

Renaud's Model:

$$k_e = (1-f_R)[(1-v_2)k_1 + v_2k_2] + f_R\left(\frac{1-v_2}{k_1} + \frac{v_2}{k_2}\right)$$

f_R is the proportion of material in series with the heat flow

Application: frozen foods

Reference: Renaud *et al.* (1960)

Related Model(s): Series and Parallel Models

Ribaud's Model:

$$k_e = k_2v_2^{1/3} + (1-v_2^{2/3})k_1$$

Application: porous materials

Reference: Sugawara & Yoshizawa (1961)

Russell's Model:

$$k_e = k_1 \left[\frac{v_2^{2/3} + \frac{k_1}{k_2}(1 - v_2^{2/3})}{v_2^{2/3} - v_2 + \frac{k_1}{k_2}(1 + v_2 - v_2^{2/3})} \right]$$

Application: porous materials

Reference: Russell (1935)

Related Model(s): Series and Parallel models, mathematically equivalent to Kopelman's isotropic model

Sakiyama and Yano Model:

$$k_e = k_1 \frac{2k_1 + (k_2 + k_{vap}) - 2\left[k_1 - (k_2 + k_{vap})\right]v_2}{2k_1 + (k_2 + k_{vap}) + \left[k_1 - (k_2 + k_{vap})\right]v_2}$$

k_{vap} is the equivalent thermal conductivity due to latent heat transfer across pores:

$$k_{vap} = \frac{D}{\Re T} \frac{P}{P - P_{vap}} L \frac{dP_{vap}}{dT}$$

where: D is the diffusivity of water in air, $\Re$ is the universal gas constant T is the temperature, P is the total pressure, P_{vap} is the vapour pressure and L is the latent heat of evaporation of water.

Application: moist, porous materials

Reference: Sakiyama & Yano (1990)

Related Model: Maxwell-Eucken model

Series Model:

$$k_e = \frac{1}{[(1-v_2)/k_1 + v_2/k_2]}$$

Application: general

Related Model(s): Parallel model

Solid-Phase Continuous Model: see Maxwell-Eucken model (Brailsford & Major, 1963)

Sugwara & Yoshizawa Model:

$$k_e = (1-\varpi_{15})k_1 + \varpi_{15}k_2$$

where:

$$\varpi_{15} = \frac{2^{f_{SY}}}{2^{f_{SY}}-1}\left(1-\frac{1}{(1+v_2)^{f_{SY}}}\right)$$

f_{SY} is an empirical weighting parameter

Application: porous rock

Reference: Sugwara & Yoshizawa (1961)

Tsao's Model:

$$k_e = \frac{1}{\int_0^1 \frac{dv_2}{k_1 + (k_2-k_1)\int_{v_2}^1 \frac{1}{\sigma\sqrt{2\pi}} e^{-1/2\left(\frac{v_2-\mu}{\sigma}\right)} dv_2}}$$

where μ and σ are the mean and standard deviation respectively, of the porosity distribution

Application: general

Reference: Tsao (1961)

Related Model(s): Series and Parallel models, Cheng-Vachon model

Woodside and Messmer:

$$k_e = \frac{\varpi_{16} k_1 k_2}{k_2(1-\varpi_{19}) + \varpi_{19} k_1} + \varpi_{17} k_2 + \varpi_{18} k_1$$

ϖ_{16} ϖ_{17} ϖ_{18} are the dimensions of certain phases in the unit-cube model (see Woodside & Messmer, 1961, for diagram)

Application: porous materials

Reference: Woodside & Messmer (1961)

Related Model(s): Series and Parallel models

Yagi and Kunii:

$$k_e = k_2 \frac{\varpi_{20}(1-v_2)}{(l_s / D_p)\left(\frac{k_2}{k_1}\right) + \frac{1}{\varpi_{21} + D_p h_{rs} / k_2} + v_2 \varpi_{20} \frac{D_p h_{rv}}{k_2}}$$

Without radiation the above equation reduces to:

$$k_e = k_2 \varpi_{20} \frac{1-v_2}{k_2 / k_1 + \varpi_{21}}$$

D_p is the average particle diameter, h_{rv} and h_{rs} are radiation heat transfer coefficients, l_s is the effective length of the solid affected by conductivity (see reference for more specific description).

ϖ_{20} and ϖ_{21} depend on mean particle diameter, mean distance between particle centres and mean diameter of void space. For practical purposes they may be assumed to be equal to unity.

Application: particulate materials saturated with motionless gas
Reference: Yagi & Kunii (1957)
Related Model(s): Series and Parallel models

Zehner & Schlunder:

$$\frac{k_e}{k_1} = 1 - \sqrt{1-v_2} + \frac{2\sqrt{1-v_2}}{1-k_1/k_2\varpi_{22}}\left[\frac{(1-k_1/k_2)\varpi_{22}}{(1-k_1/k_2\varpi_{22})^2}\ln\frac{1}{k_1/k_2\varpi_{22}} - \frac{\varpi_{22}+1}{2} - \frac{\varpi_{22}-1}{1-k_1/k_2\varpi_{22}}\right]$$

$$\varpi_{22} = \varpi_{23}\left(\frac{1-v_2}{v_2}\right)^{10/9}$$

ϖ_{23} is a shape factor, 1.25 for spheres, 1.4 for broken particles, 2.5 for cylinders

Application: particulate materials
Reference: Cheng & Chin-Tsau (1998)

Appendix B: Derivation of Equations (2.14) and (2.15)

Consider the situation shown in Figure B.1. A steady-state temperature gradient is imposed across the medium setting up a temperature field ∇T_0.

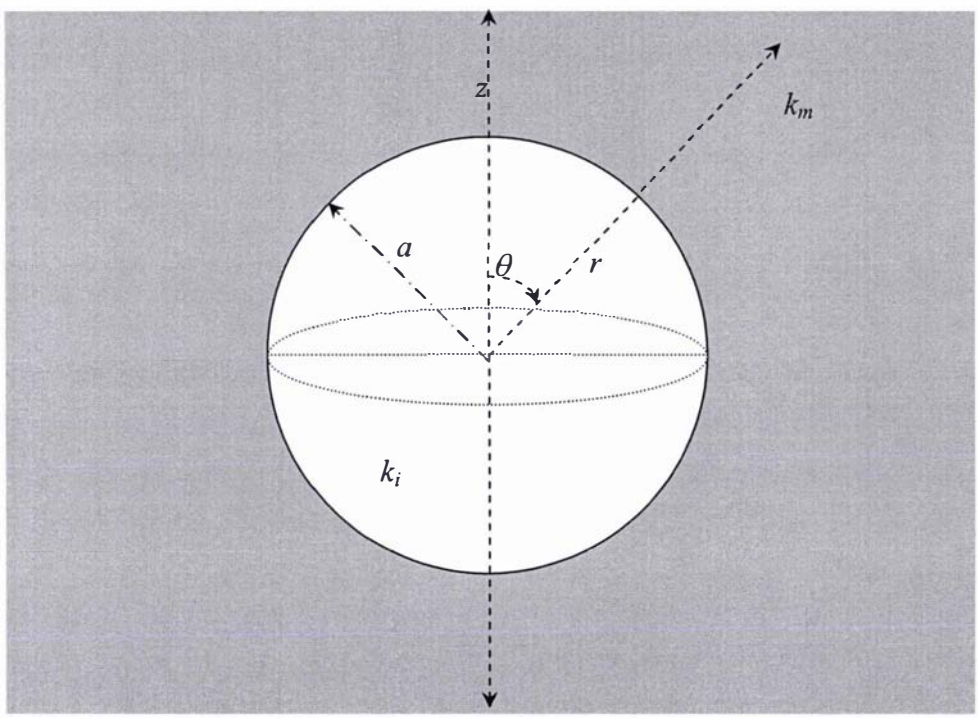

Figure B.1

The sphere of thermal conductivity k_i and radius a is placed in an infinite medium of thermal conductivity k_m which has a constant thermal gradient imposed on it in the z-axis direction (*i.e.* $\partial T/\partial z$ = const). The origin of the spherical coordinates is at the centre of the sphere. Under steady state conditions:

$$\nabla^2 T_i = 0 \qquad \text{for} \quad 0 < r < a \qquad \text{(B1)}$$

$$\nabla^2 T_m = 0 \qquad \text{for} \quad a < r < \infty \qquad \text{(B2)}$$

Where T_i is the temperature at any point within the sphere and T_m is the temperature at any point outside the sphere. It can be shown (Pugh & Pugh, 1970) that:

$$T = A + \frac{B}{r} + Cr\cos\theta + \frac{D}{r^2}\cos\theta \tag{B3}$$

is a solution of

$$\nabla^2 T = \frac{1}{r^2}\frac{\partial}{\partial r}\left(r^2\frac{\partial T}{\partial r}\right) + \frac{1}{r^2\sin\theta}\frac{\partial}{\partial\theta}\left(\sin\theta\frac{\partial T}{\partial\theta}\right) = 0$$

where A, B, C and D are constants that must be determined from the boundary conditions.

At the boundary when $r = a$ continuity of the temperature gradient requires that:

$$k_i\frac{\partial T_i}{\partial r} = k_m\frac{\partial T_m}{\partial r} \tag{B4}$$

which is the first boundary condition.

Since:

$$\oint \nabla T \cdot dr = 0$$

it implies that at $r = a$:

$$\frac{\partial T_i}{\partial\theta} = \frac{\partial T_m}{\partial\theta} \tag{B5}$$

which is the second boundary condition. To avoid infinite values of temperature a third boundary condition must be specified:

$$T_i(r = 0) \neq \infty \tag{B6}$$

The fourth boundary condition occurs at a boundary sufficiently far from the sphere such that $r >> a$ and the inhomogeneity of the sphere is negligible:

$$T_m = bz = br\cos\theta \tag{B7}$$

where b is a constant equal to $\partial T/\partial z$.

In deriving the equation for T_i from Eq. (B3) the third boundary condition, Eq. (B6), requires that any term with r in the denominator is zero, hence:

$$T_i = A_i + C_i r\cos\theta \tag{B8}$$

When r is very large, terms in Eq. (B3) with r in the denominator become negligible:

$$T_m \approx A_m + C_m r\cos\theta \tag{B9}$$

Comparing Eq. (B9) with the fourth boundary condition:

$$A_m + C_m r\cos\theta = br\cos\theta \tag{B10}$$

which implies that $A_m = 0$ and $C_m = b$. Hence:

$$T_m = \frac{B_m}{r} + br\cos\theta + \frac{D_m}{r^2}\cos\theta \tag{B11}$$

Differentiating Eqs. (B8) and (B11) with respect to r gives:

$$\frac{\partial T_i}{\partial r} = C_i\cos\theta \tag{B12}$$

and

$$\frac{\partial T_m}{\partial r} = \frac{-B_m}{r^2} + b\cos\theta - \frac{2D_m}{r^3}\cos\theta \tag{B13}$$

From the first boundary condition Eqs. (B12) and (B13) are equal when $r = a$:

$$\frac{-B_m}{a^2} + b\cos\theta - \frac{2D_m}{a^3}\cos\theta = \frac{k_i}{k_m}C_i\cos\theta \tag{B14}$$

Because Eq. (B14) must be valid for all values of θ, B_m must be equal to 0.

Differentiating Eqs. (B8) and (B11) with respect to θ gives:

$$\frac{\partial T_i}{\partial \theta} = -C_i r\sin\theta \tag{B15}$$

and

$$\frac{\partial T_m}{\partial \theta} = -br\sin\theta - \frac{D_m}{r^2}\sin\theta \tag{B16}$$

From the second boundary condition, Eqs. (B15) and (B16) are equal when $r = a$:

$$-ba\sin\theta - \frac{D_m}{a^2}\sin\theta = -C_i a\sin\theta \tag{B17}$$

Dividing Eqs. (B14) and (B17) by $\cos\theta$ and $-\sin\theta$ respectively gives:

$$b - \frac{2D_m}{a^3} = \frac{k_i}{k_m}C_i \tag{B18}$$

and

$$ba + \frac{D_m}{a^2} = C_i a \tag{B19}$$

Solving Eqs. (B18) and (B19) simultaneously for D_m and C_i gives:

$$D_m = -ba^3 \frac{k_i - k_m}{k_i + 2k_m} \tag{B20}$$

and

$$C_i = b\frac{3k_m}{k_i + k_m} \tag{B21}$$

Substituting Eqs. (B20) and (B21) back into Eqs. (B8) and (B11):

$$T_i = A_i + b\frac{3k_m}{k_i + k_m} r\cos\theta \tag{B22}/(2.15)$$

and

$$T_m = br\cos\theta - ba^3 \frac{k_i - k_m}{k_i + 2k_m}\frac{\cos\theta}{r^2} \tag{B23}/(2.14)$$

Equations (B23) and (B22) are the same as Eqs. (2.14) and (2.15) of Chaptcr 2 respectively.

QED.

Appendix C: Physical Property Data

C.1 Volumes and Radii of Aluminium Sample Containers

The volumes of the sample containers were determined by comparing the mass of the empty container to the mass of the container when filled with water. The internal radii were then calculated from the measured volumes, assuming the containers were perfect spheres. The thickness of the aluminium for all the spheres was 2mm. The volumes and radii of the containers are shown in Table C.1.

Container	Volume (dm^3)	±	Radius (mm)	±
"W"	4.637	0.2%	103.6	0.05%
"X"	4.614	0.2%	103.4	0.05%
"Y"	4.340	0.2%	101.2	0.05%
"Z"	4.308	0.2%	100.9	0.05%
"M"	1.847	0.5%	76.11	0.1%
"N"	1.816	0.5%	75.69	0.1%
"Q"	1.712	0.5%	74.21	0.1%
"R"	1.703	0.5%	74.09	0.1%
"S"	1.624	0.5%	72.91	0.1%
"T"	1.792	0.5%	75.35	0.1%

Table C.1: Dimensions of Aluminium Sample Containers

Care was taken to ensure the containers involved in a given experimental run had as similar dimensions as possible, i.e. Container "W" was used with Container "X", Container "Y" with Container "Z" etc.

C.2 Densities of Guar-gel, EPS, Air and Aluminium

Other than air, the densities of the materials used in the samples were measured by water displacement in volumetric flasks. The density of air was taken from Holman (1992).

Material	Density $kg\ m^{-3}$	±
Guar gel	1010	1%
Air	1.24	-
2 mm EPS	35.4	0.60%
6.5 mm EPS	16.7	1%
25 mm EPS	33.2	3%
Aluminium	2678	0.40%

Table C.2: Densities of materials used in experimental samples

C.3 Specific Heat Capacities of Guar-gel, EPS, Air and Aluminium

The specific heat capacity of the guar-gel was measured by differential scanning calorimetry. The specific heat of gels having 4% guar powder by mass was 4154 J kg^{-1} K^{-1} ± 0.5% at 10°C.

The specific heat capacities of the remaining experimental materials were obtained from the literature. The specific heat capacity of polystyrene was extrapolated from Fig. 2.16 of Williams (1971). At 10°C the specific heat capacity of polystyrene was 1210 J kg^{-1} K^{-1} ± 2% (the estimated extrapolation uncertainty). It was assumed that the specific heat capacity of expanded polystyrene was the same as that of polystyrene. Given the similarity between the specific heat capacities of air and polystyrene this was not an unreasonable assumption.

The specific heat capacities of aluminium and air were extrapolated from Tables A-2 and A-5 respectively, of Holman (1992). At 10°C the specific heat capacities of aluminium and air were 896 J kg^{-1} K^{-1} and 1006 J kg^{-1} K^{-1} respectively. The specific heat capacities of the experimental materials are summarised in Table C.3.

Material	Specific Heat Capacity $J\ kg^{-1}\ K^{-1}$	±
Guar-gel	4150	0.50%
Air	1006	negligible
Polystyrene	1210	2%
Aluminium	896	N/A

Table C.3: Specific heat capacities of materials used in experimental samples

C.4 Thermal Conductivities of Guar-gel, EPS, Air and Aluminium

The thermal conductivity was measured with a *Hukseflux™ TP08* thermal conductivity probe that had been calibrated with agar gel. At 10°C the thermal conductivity of the guar gels was 0.601 $W\ m^{-1}\ K^{-1} \pm 2\%$.

The thermal conductivity of air was taken from Table A-5 of Holman (1992). At 10°C the thermal conductivity of air was 0.0249 $W\ m^{-1}\ K^{-1} \pm 0.5\ \%$.

The thermal conductivity of EPS has a strong dependence on density, as well as temperature. Using the densities measured for the different sizes of EPS (Table C.2), the thermal conductivity of the EPS was extrapolated from a table in information supplied by the Plastics Institute of New Zealand and Fig. 5.15 of Williams (1971). Table C.4 shows the thermal conductivities at 10°C.

The thermal conductivity of the aluminium was obtained from the supplier (*Ullrich Aluminium Company Limited*), although no value for the uncertainty in the measurement was provided. However, since the thermal conductivity of aluminium is much higher than the thermal conductivities of the other components, even a relatively large uncertainty (±10%) would not have much bearing on the conclusions drawn from the results involving aluminium.

Material	Thermal Conductivity $W\ m^{-1}\ K^{-1}$	±
Guar-gel	0.601	2%
Air	0.0249	0.50%
2mm EPS	35	3%
6.5mm EPS	37	3%
25mm EPS	35	3%
Aluminium	209	N/A

Table C.4: Thermal conductivities at 10°C of materials used in experimental samples

C.5 Linear Temperature Dependencies of Materials Involved in Experiments

In Section 4.2.2, the use of average-temperature thermal conductivity values in the calculations was justified by the argument that the linear temperature variations of the thermal conductivities of the sample components cancelled each other out. Figure C.1 shows the thermal conductivity of air as a function of temperature between 0 and 20°C, and a similar plot for water is shown in Fig. C.2.

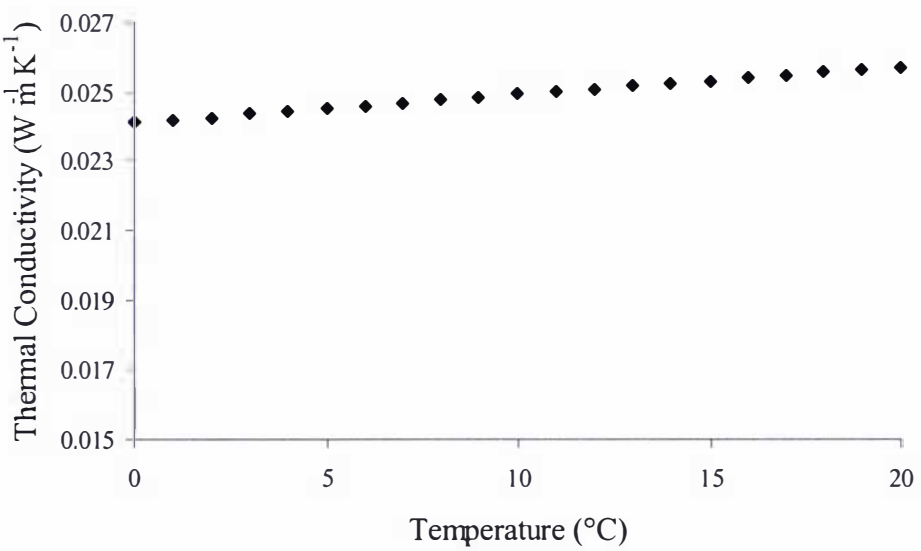

Figure C.1: Thermal conductivity of air as a function of temperature

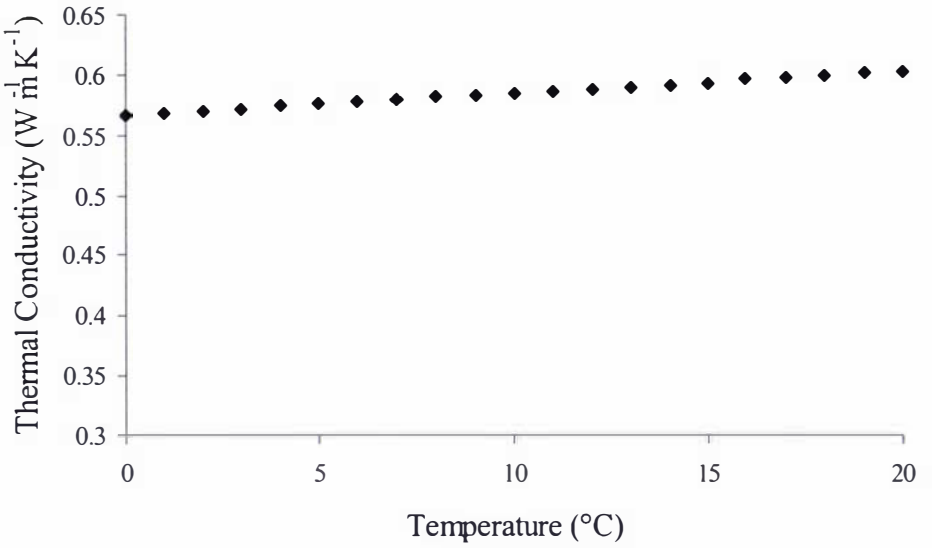

Figure C.2: Thermal conductivity of water as a function of temperature

Figures C.1 and C.2 clearly show that the temperature dependence of thermal conductivity in both air and water is linear, and that the thermal conductivities of both increases with temperature. On a volume basis, the guar-gels were largely composed of water and the EPS was largely composed of air, hence the temperature dependencies shown in Figs. C.1 and C.2 were likely to have been similar for guar-gel and air respectively.

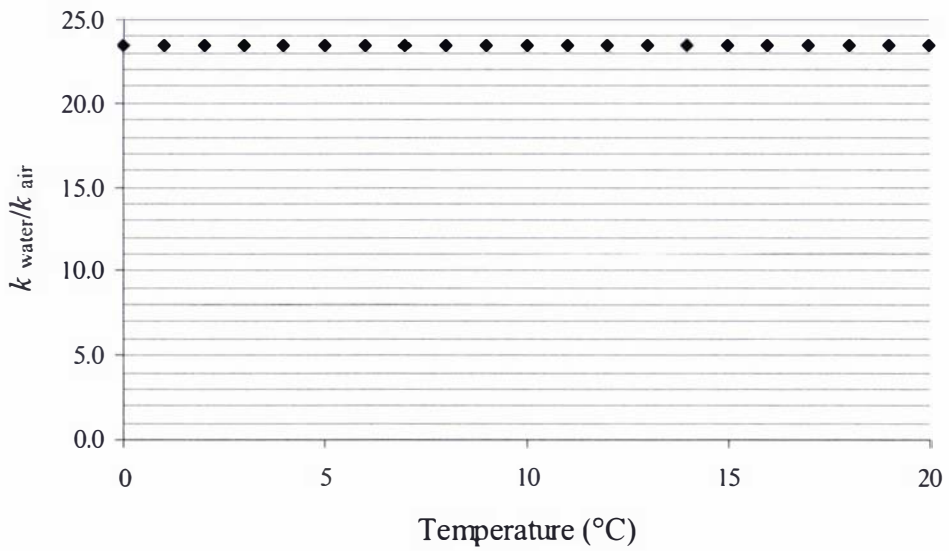

Figure C.3: Ratio of thermal conductivities of water and air as a function of temperature

Figure C.3 shows the ratio of the thermal conductivities of water to the thermal conductivity of air over the same temperature range. The ratio of thermal conductivities shows very little variation over the temperature range between 0 and 20°C. Therefore, the use of the mid-range temperature (10°C) as an average value in the calculations was unlikely to have contributed significant error to the results.

Appendix D: Single Factor ANOVA Test Results

The analysis of variance (ANOVA) tests were performed automatically by the statistical tool in the *Microsoft Excel*™ software package. The variable that was tested was the deviation of the thermal conductivity data from a linear best-fit model.

D.1 ANOVA Test for Difference between Results from Datasets 1 and 2

SUMMARY

Groups	*n*	*Sum*	*Average*	*Variance*
Dataset 1	27	0.244653	0.009061	0.000133
Dataset 2	20	-0.08925	-0.00446	0.000256

ANOVA α=0.05

Source of Variation	*Sum of Squares*	*Degrees of freedom*	*Mean Square*	F_{test}	*P-value*	F_{crit}
Between Groups	0.002101	1	0.002101	**11.374**	0.00154	*4.0566022*
Within Groups	0.008314	45	0.000185			
Total	0.010415	46				

$F_{test} > F_{crit}$, hence the ANOVA test suggests that, at the 5% level of significance, there was a difference between the results of Dataset 1 and Dataset 2.

D.2 ANOVA Test for Difference between Results from Datasets 1 and 3

SUMMARY

Groups	*n*	*Sum*	*Average*	*Variance*
Dataset 3	17	-0.17673	-0.0104	0.000354
Dataset 1	27	0.244653	0.009061	0.000133

ANOVA α=0.05

Source of Variation	*Sum of Squares*	*Degrees of freedom*	*Mean Square*	F_{test}	*P-value*	F_{crit}
Between Groups	0.003949	1	0.003949	**18.19945**	0.000111	*4.0726604*
Within Groups	0.009114	42	0.000217			
Total	0.013063	43				

$F_{test} > F_{crit}$, hence the ANOVA test suggests that, at the 5% level of significance, there was a difference between the results of Dataset 1 and Dataset 3.

D.3 ANOVA Test for Difference between Results from Datasets 2 and 3

SUMMARY

Groups	n	Sum	Average	Variance
Dataset 2	20	-0.08925	-0.00446	0.000256
Dataset 3	17	-0.17673	-0.0104	0.000354

ANOVA α=0.05

Source of Variation	Sum of Squares	Degrees of freedom	Mean Square	F_{test}	P-value	F_{crit}
Between Groups	0.000323	1	0.000323	**1.076699**	0.306553	*4.1213468*
Within Groups	0.010515	35	0.0003			
Total	0.010839	36				

$F_{test} < F_{crit}$, hence the ANOVA test suggests that, at the 5% level of significance, there was no difference between the results of Dataset 2 and Dataset 3.

D.4 ANOVA Test for Difference between Results from Datasets 1, 2 and 3

SUMMARY

Groups	n	Sum	Average	Variance
Dataset 1	27	0.244653	0.009061	0.000133
Dataset 2	20	-0.08925	-0.00446	0.000256
Dataset 3	17	-0.17673	-0.0104	0.000354

ANOVA α=0.05

Source of Variation	Sum of Squares	Degrees of freedom	Mean Square	F_{test}	P-value	F_{crit}
Between Groups	0.004445	2	0.002223	**9.70422**	0.000219	*3.1477896*
Within Groups	0.013971	61	0.000229			
Total	0.018417	63				

$F_{test} > F_{crit}$, hence the ANOVA test suggests that, at the 5% level of significance, there was a difference between the results of Datasets 1, 2 and Dataset 3.

Appendix E: Some Limitations of Finite Difference Methods when Used to Calculate the Effective Thermal Conductivity of a Random Resistor Network

E.1 Introduction

A numerical approach that has been used in the study of the prediction of the thermal or electrical conductivities (including Kirkpatrick, 1973, Phelan & Niemann, 1998, Davies & Fryer, 2001) is to model a material as a network of resistors. Each individual resistor in the network is randomly assigned the conductivity of one of the components of the material. In this way, a conceptual material can be made up from a random distribution of its components. If the number of resistors in the network is sufficiently large that each resistor represents only a small fraction of the overall network, and if the components are distributed randomly then, by a statistical argument, the overall conductivity of the material will be approximately uniform and hence may be represented by a single conductivity known as the effective conductivity.

Finite difference methods have often been used to solve the steady-state heat transfer problems associated with random resistor networks. A feature of some of these studies is that only one temperature node was used for each resistor in the network. The implicit assumption is that the temperature gradients across the resistors are flat enough that one finite temperature step in each direction sufficiently models the temperature profile over that resistor. The aim of the work reported here was to discover the sensitivity of the results obtained from these types of resistor network analyses to the fineness of the temperature grid.

E.2 Method

Finite difference (FD) models were constructed to simulate a thermal conductivity measurement apparatus similar to the finite element models described in Chapter 5 (see

Fig. 5.1 and Eqs. 5.1 to 5.9 of Chapter 5). Simulations were performed on Kirkpatrick type grids (refer to Fig. 5.9b of Chapter 5).

E.2.1 Finite Difference Method

The FD method used was similar to that described by Phelan & Niemann (1998). The finite difference form of Laplace's equation in two dimensions was rearranged so that it could be expressed in the form shown in equation E1:

$$\sum_j \frac{T_i - T_j}{R_{ij}} = 0 \qquad \text{(E1)}$$

where T_i was a given temperature node and T_j referred to any temperature node adjacent to T_i. The R_{ij} term was the resistance to heat flow between nodes i and j. Temperature nodes were positioned in a square arrangement with each temperature node a unit spacing apart from the adjacent nodes along the coordinate axes. The R_{ij} terms that were used were the same as those found in Table 3-4 of Holman (1992) with the exception of the interior nodes. The equations in Holman (1992) assumed uniform thermal conductivity and so it was necessary to derive an appropriate term for the internal nodes that allowed for variable conductivity:

$$R_{ij} = \frac{0.5}{k_i} + \frac{0.5}{k_j} \qquad \text{(E2)}$$

where k_i and k_j referred to the conductivities at the nodes T_i and T_j.

The FD grid area was divided into conductivity *sites* (k_α) according to a random number string, and each site contained thermal conductivity *nodes* (k_i.) The number of conductivity nodes was the same as the number of temperature nodes because it was convenient when writing the nodal equations for each temperature node to have its own conductivity node. The distinction between conductivity sites and conductivity nodes was necessary because the number of temperature nodes was not necessarily the same as the number of

conductivity sites. Within a conductivity site, all the conductivity nodes had the same value.

When the nodes T_i and T_j were in regions with similar thermal conductivity then:

$$k_i = k_j \tag{E3}$$

and Eq. (E2) was reduced to:

$$R_{ij} = \frac{1}{k_i} = \frac{1}{k_j} \tag{E4}$$

which was the same as the term found in Table 3-4 of Holman (1992).

The calculations were performed using *Microsoft Excel™ 2000* (Microsoft Corporation, Redmond, WA). Equation E1 was rearranged to be explicit for each T_i:

$$T_i = \frac{\sum_j T_j / R_{ij}}{\sum_j 1 / R_{ij}} \tag{E5}$$

and then solved iteratively using *Excel™*'s iteration function. Iterations were continued until the maximum change in a nodal temperature was less than 10^{-7} °C and the discrepancy between the heat flows Q_h and Q_c was less than 0.5% (see Eqs. 5.6 and 5.7 of Chapter 5). An advantage of using *Excel™* was that the temperature surface could be graphed, which made it easy to identify and correct any nodes with erroneous formulae.

The key difference between this work and the work of Phelan & Niemann (1998) and that of other previous workers was in the number of nodes per conductivity site (n_T/n_k). Phelan & Niemann specified exactly one temperature node per site, whereas in this work the number was varied. Three different sizes of temperature grids were constructed: 25 x

25 nodes, 100 x 100 nodes and 250 x 250 nodes. Simulations were performed over a range of volume fractions. The first set of simulations was run with one temperature node per site for each of the three grid sizes (i.e. $n_T/n_k = 1$). In the second set of simulations, the 100 x 100 and 250 x 250 node grids were divided into the same number of conductivity sites as the 25 x 25 node grid and had the same thermal conductivity distribution. Thus n_T/n_k was increased from 1 to 16, to 100. A summary of the finite difference simulations that were performed is given in Table 1.

Model	Number of temperature nodes (n_T)	Number of conductivity sites (n_k)	n_T/n_k
1	625	625	1
2	10000	10000	1
3	62500	62500	1
4	10000	625	16
5	62500	625	100

Table E.1: Description of finite difference models

E.2.2 Testing of Numerical Models against Series and Parallel models

The numerical models were tested against the predictions of the Series and Parallel. The models were set up so that the two materials lay in parallel strips lying either orthogonally or parallel to the direction of heat flow. The k_e values calculated from the simulation results of the numerical models were compared to the predictions of the Series and Parallel models. The numerical model results agreed with the predictions of the effective thermal conductivity models within the limits of precision, 0.5%, for both the series and parallel scenarios for all three grid sizes.

E.3 Results

Since the k_e measurements were performed over a range of volume fractions it was useful to display the results as plots of relative effective thermal conductivity (k_e/k_1) against the volume fraction of one of the components (v_2).

With random resistor networks it is important to determine whether the number of resistors (sites) involved is sufficiently large that the assumption of uniform distribution of the two components is valid. Figure E.1 shows a graph of the simulation results from models 1, 2 and 3 (refer to Table E.1). The results of the three simulations were very similar, even though the simulations were performed on different conductivity site arrangements and with the number of sites varied by two orders of magnitude. The closeness in the results suggested that 625 conductivity sites were sufficient to model a randomly distributed two-component material.

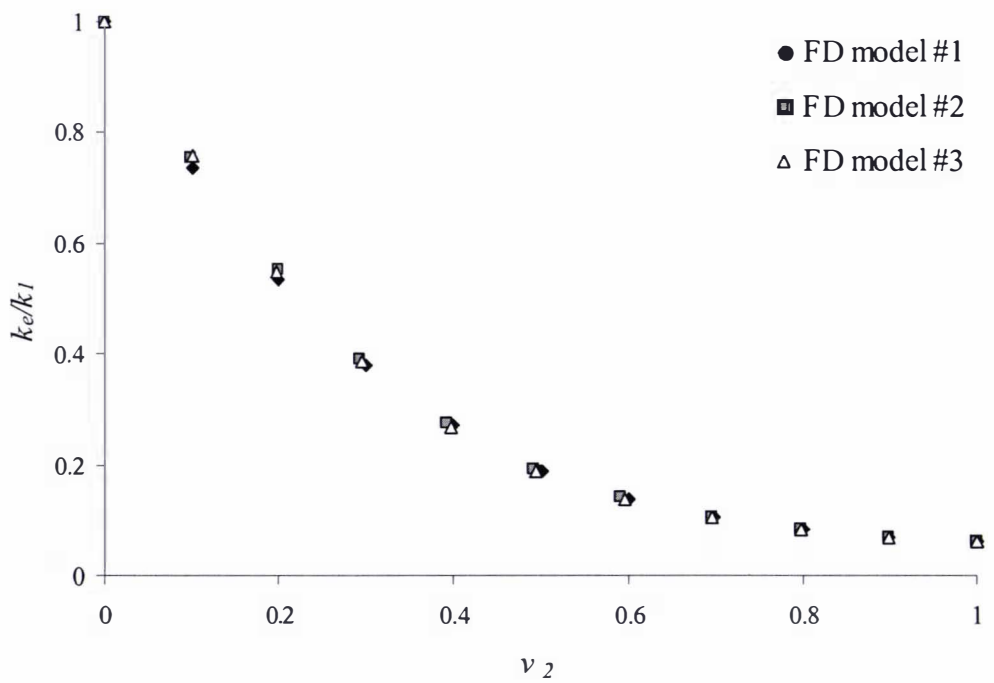

Figure E.1: Effective thermal conductivity results from models with one temperature node per conductivity site but different numbers of conductivity sites (refer to Table E.1)

Figure E.2 shows a graph of the simulation results from models 1, 4, and 5. There were clear discrepancies between the results from each model, as much as 26% between the results from model 1 and model 5. All three models were simulating identical thermal conductivity distributions and all three models had the same nodal equations, so if the finite difference method was accurate the results from the three models should have been in agreement.

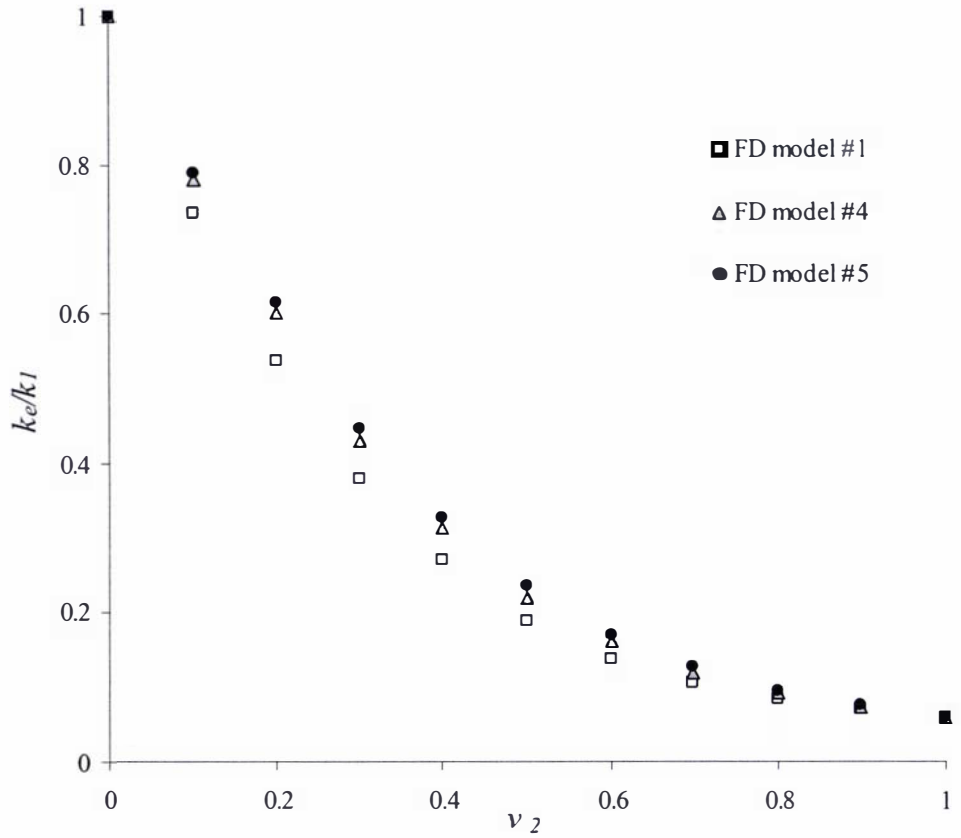

Figure E.2: Effective thermal conductivity results from models with different numbers of temperature nodes per conductivity site but with the same number of conductivity sites (refer to Table 1)

The only difference between the models was the number of temperature nodes per conductivity site (n_T/n_k), and Fig. E.2 clearly demonstrates that the results were sensitive to this ratio. This point is further demonstrated by Fig. E.3 which is a plot of the k_e/k_1 results as a function of the logarithm of n_T/n_k for a v_2 value of 0.5008, including points from models with n_T/n_k values of 4, 9, 25 and 36.

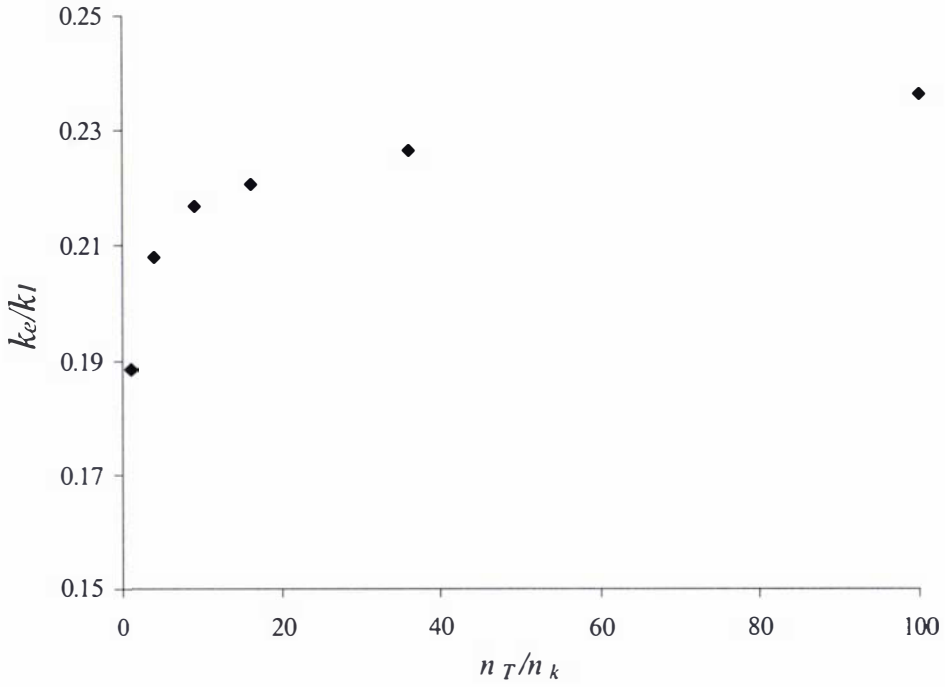

Figure E.3: Effective Thermal conductivity results as a function of the number of temperature nodes per conductivity site (n_T/n_k)

Figures E.4a to 4c show the temperature profiles of the region of nine adjacent thermal conductivity sites in the grid for $v_2 = 0.5008$ (as shown in Fig. 1). The differences between the temperature surfaces shown in Figs. E.4a and E.4c highlighted the effect of approximating a smooth curve with a limited number of straight lines, especially for the sites with low thermal conductivity where the temperature gradients changed rapidly. The fineness of the grid affects two important sources of error inherent with finite difference simulations: truncation error and discretisation error (refer to chapter 8 of Crank, 1973 and chapter 5 of Smith, 1986). In general, both sources of error are reduced as the fineness of the grid is increased (i.e. n_T/n_k is increased). These results suggest that random resistor network models with $n_T/n_k = 1$ have unacceptable levels of truncation and/or discretisation error.

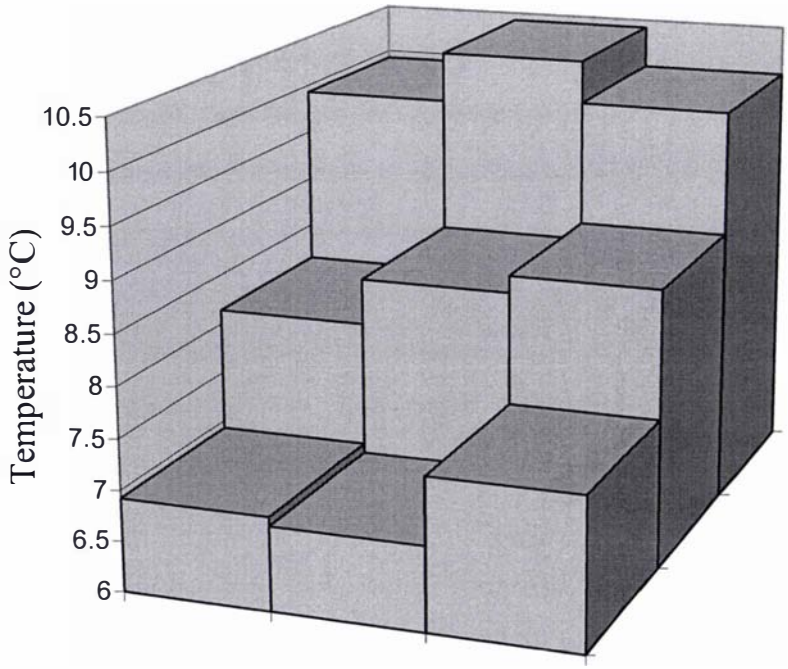

Figure E.4a: Nodal temperatures for the selected portion of the grid of the finite difference model with 1 temperature node per conductivity site (model 1)

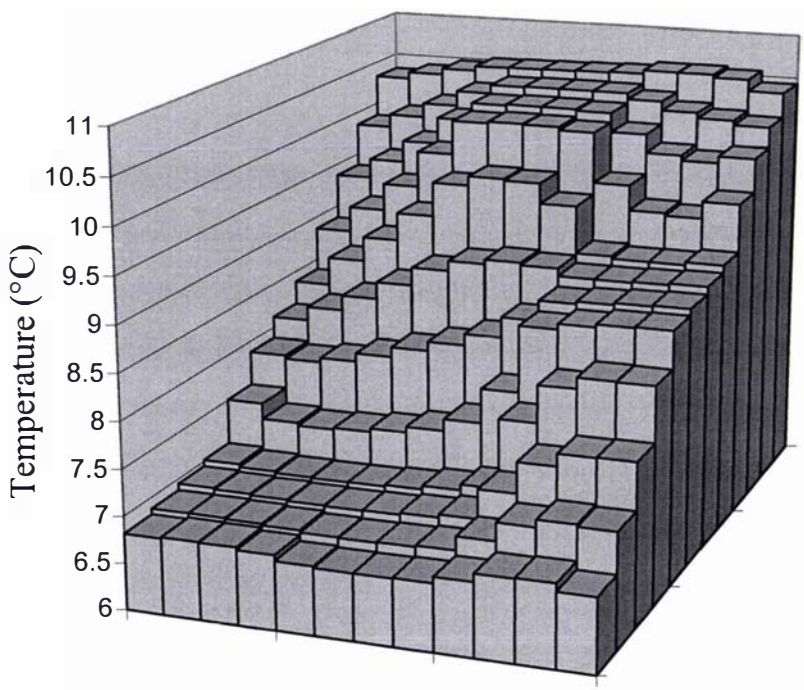

Figure E.4b: Nodal temperatures for the selected portion of the grid of the finite difference model with 16 temperature nodes per conductivity site (model 4)

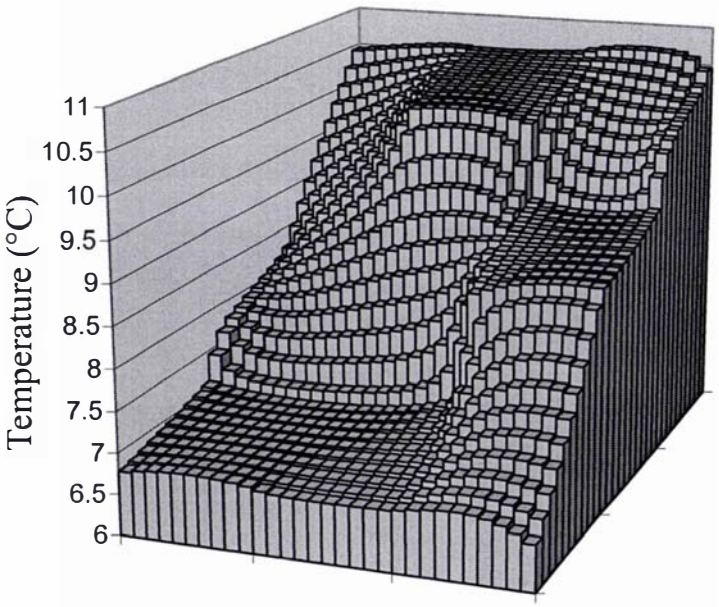

Figure E.4c: Nodal temperatures for the selected portion of the grid of the finite difference model with 100 temperature nodes per conductivity site (model 5)

There is another limitation to the use of simple finite difference methods such as the one described above. Since the temperature grid is divided into regions of different thermal conductivity, problems may occur at thermal conductivity boundary corners because of the discontinuity. Crank (1973) describes techniques that may be used to avoid these problems including one by Motz (1946) specifically for steady state problems, but these cannot be incorporated into a regular grid lattice.

The finite difference method used in this work performed well for the Series and Parallel model scenarios, but in those situations the heat transfer was essentially one-dimensional and without internal boundary corners, and hence the problems described above were avoided. The Series and Parallel models are clearly limited in their usefulness for testing the accuracy of numerical heat transfer models.

Although the regular geometric arrangement of resistor network models means that they appear well suited to being solved by simple finite difference methods the results obtained

in this work have shown that models with $n_T/n_k = 1$ should not be relied upon as being accurate, although they may provide useful insights when used to study relative phenomena.

E.4 Conclusion

Although random resistor networks appear to be ideally suited to finite difference modelling, the simulations performed in this study have shown a clear dependence of the calculated effective thermal conductivity on the number of temperature nodes per site. This dependence suggests that the discretisation of the temperature profile by one temperature step per site is not sufficient to give accurate results. In addition, internal boundary corners require special attention. Results from random resistor network studies should be viewed with caution if it is unclear how the finite difference calculations were performed.

Appendix F: Printouts of BASIC Programs and Input Scripts for *PDEase2D™* Finite Element Models

F.1 Plotc.BAS (Circle plotting program)

```
REM circle plotter
CLS
PRINT "n"; : INPUT n: PRINT "n1"; : INPUT n1:  PRINT "r"; : INPUT r: PRINT
"e="; : INPUT e
r1 = e + r
RANDOMIZE
DIM x(n), y(n)
OPEN "Xcoord.dat" FOR OUTPUT AS #1: OPEN "Ycoord.dat" FOR OUTPUT AS #2
c = 0
WHILE c < n + 1
  x(c) = RND: y(c) = RND
  IF x(c) > 0 + r1 AND y(c) > 0 + r1 THEN
     IF x(c) < 1 - r1 AND y(c) < 1 - r1 THEN
     PRINT #1, x(c): PRINT #2, y(c): c = c + 1
     END IF
  END IF
WEND
CLOSE #1: CLOSE #2
OPEN "Xcoord.dat" FOR INPUT AS #1: OPEN "Ycoord.dat" FOR INPUT AS #2
FOR s = 1 TO n
     INPUT #1, x(s): INPUT #2, y(s)
NEXT s
DIM x1(n1), y1(n1)
x1(1) = x(1): y1(1) = y(1)
x1(2) = x(2): y1(2) = y(2)
p = 2
FOR i = 3 TO n1
    k = 0
     FOR j = 1 TO p
      IF j < i THEN
        IF ((x1(j) - x(i)) ^ 2 + (y1(j) - y(i)) ^ 2) ^ .5 < 2 * r1 THEN
          k = k + 1
        END IF
      END IF
     NEXT j
    IF k = 0 THEN
     x1(p + 1) = x(i): y1(p + 1) = y(i)
     p = p + 1
     PRINT "i="; i, "p="; p
    END IF
NEXT i
fraction = 3.14159269# * r * r * p
PRINT "fraction="; fraction
OPEN "circles.dat" FOR OUTPUT AS #3
FOR f = 1 TO p
   PRINT #3, "Start("; x1(f) - r; ","; y1(f); ")              {"; f; "}"
   PRINT #3, "arc(center="; x1(f); ","; y1(f); ")angle=360"
   PRINT #3, "Finish"
NEXT f
CLOSE #3
```

```
END
```

F.2 PlotSq.BAS (Square plotting program)

```
REM square plotter
CLS
PRINT "n"; : INPUT n: PRINT "n1"; : INPUT n1:  PRINT "l"; : INPUT l
RANDOMIZE
DIM x(n), y(n)
OPEN "Xcoord.dat" FOR OUTPUT AS #1: OPEN "Ycoord.dat" FOR OUTPUT AS #2
c = 0
WHILE c < n + 1
  x(c) = RND: y(c) = RND
  IF x(c) < 1 - l + r AND y(c) < 1 - l THEN
    PRINT #1, x(c): PRINT #2, y(c): c = c + 1
  END IF
WEND
CLOSE #1: CLOSE #2
INPUT pause
OPEN "Xcoord.dat" FOR INPUT AS #1: OPEN "Ycoord.dat" FOR INPUT AS #2
FOR s = 1 TO n
     INPUT #1, x(s): INPUT #2, y(s)
NEXT s
DIM x1(n1), y1(n1)
x1(1) = x(1): y1(1) = y(1)
x1(2) = x(2): y1(2) = y(2)
p = 2
FOR i = 3 TO n1
    k = 0
     FOR j = 1 TO p
      IF j < i THEN
        IF ABS(x1(j) - x(i)) < l AND ABS(y1(j) - y(i)) < l THEN
          k = k + 1
        END IF
      END IF
     NEXT j
    IF k = 0 THEN
     x1(p + 1) = x(i): y1(p + 1) = y(i)
     p = p + 1
     PRINT "i="; i, "p="; p
    END IF
NEXT i
e = l * l * p
PRINT "e="; e
OPEN "squares.dat" FOR OUTPUT AS #3
FOR f = 1 TO p
   PRINT #3, "Start("; x1(f); ","; y1(f); ")                {"; f; "}"
   PRINT #3, "line to ("; x1(f); ","; y1(f) + l; ")"
   PRINT #3, "line to ("; x1(f) + l; ","; y1(f) + l; ")"
   PRINT #3, "line to ("; x1(f) + l; ","; y1(f); ")"
   PRINT #3, "line to ("; x1(f); ","; y1(f); ")"
   PRINT #3, "Finish"
NEXT f
CLOSE #3
END
```

F.3 Example of a *PDEase2D™* Input Script for a Maxwell-type Structure

```
Title
        "Two Material Heat flow"
Select
    errlim=1e-4
Variables
    Temp(range=0,20)
Definitions
     k
     h
     h2
     Ta
     Tc
Equations
      dx(-k*dx(temp))+dy(-k*dy(temp))=0
Boundaries
 region 1
    k=1
    h=0.0000001
    Ta=1
    h2=1000000
    Tc=1
    natural(temp)=h2*(temp-Ta)
    start (0,1.05)
    line to (1,1.05)
    natural(temp)=h*(temp-Ta)
    line to (1,1)
    line to (0,1)
    natural(temp)=h*(temp-Ta)
    line to (0,1.05)
    finish
  Region 2
    k=0.6
    h2=0.00000001
    Ta=0
    start (0,1)
    line to (1,1)
    natural(temp)=h2*(temp-Ta)
    line to (1,0)
    line to (0,0)
    natural(temp)=h2*(temp-Ta)
    line to (0,1)
    finish
  Region 3
    k=0.03
    Start( .5924589 , .2663325 )          { 1 }
arc(center= .6224589 , .2663325 )angle=360
Finish
Start( .1498654 , .3413053 )          { 2 }
```

```
arc(center= .1798654 , .3413053 )angle=360
Finish
Start( .8083701 , .3405229 )            { 3 }
arc(center= .83837 , .3405229 )angle=360
Finish
                    .
                    .
                    .
Start( .6330221 , .2145891 )            { 143 }
arc(center= .6630221 , .2145891 )angle=360
Finish
Start( .4029656 , 3.390908E-02 )            { 144 }
arc(center= .4329656 , 3.390908E-02 )angle=360
Finish
Start( .3836377 , .6478009 )            { 145 }
arc(center= .4136377 , .6478009 )angle=360
Finish


Region 4
    k=1
    h=1000000
    h2=0.000001
    Ta=0
    Tc=20
     start (0,0)
     line to (1,0)
     natural(temp)=h2*(temp-Ta)
     line to (1,-0.05)
     natural(temp)=h*(temp-Tc)
     line to (0,-0.05)
     natural(temp)=h2*(temp-Ta)
     line to (0,0)
     finish


Plots
     grid(x,y)
     contour(temp)
     contour(temp) zoom (0,0.5,0.5,0.5)
     contour(temp) zoom (0,0,0.5,0.5)
     contour(temp) zoom (0.35,0.1,0.25,0.25)
     contour(temp) zoom (0.5,0.5,0.5,0.5)
     contour(temp) zoom (0.5,0,0.5,0.5)
     contour(temp) zoom (0,0,1,1)
     surface(temp)
     elevation(temp) from (0,1.05) to (1,1.05) file(100)
     elevation(temp) from (0,1.04) to (1,1.04) file(100)
     elevation(temp) from (0,-0.05) to (1,-0.05) file(100)
     elevation(temp) from (0,-0.04) to (1,-0.04) file(100)
```